STRUCTURES AND MECHANICS REPORT
SM84-1

RESPONSE OF FLAT PLATE CONCRETE STRUCTURES TO SEISMIC AND WIND FORCES

by

Haruki Akiyama and Neil M. Hawkins

A Report to the National Science Foundation
Earthquake Hazards Mitigation Program
Grant No. ENV 72-03585

Any opinions, findings, and conclusions or recommendations expressed in this publication are those of the authors and do not necessarily reflect the views of the National Science Foundations.

Structural and Geotechnical Engineering and Mechanics
Department of Civil Engineering
University of Washington
Seattle, WA, 98195
July, 1984

ABSTRACT

This report utilizes the results of the comprehensive series of tests conducted at the University of Washington, on slab-column sub-assemblages and frames subjected to inelastic reversed cyclic lateral loads, to develop a general beam analogy model for predictions of the strength, stiffness, ductility, energy absorption, and energy dissipation characteristics of flat plate concrete structures subjected to lateral loads.

In that model the slab is taken as attached to the column by short beams that frame into each column face. Each short beam is assigned the stiffness, strength and hysteretic characteristics normally associated with the combinations of shear, moment, and torsional forces acting on those beams according to accepted reinforced concrete theory. Procedures are developed for incorporating the effects of bond slip and torsional actions into that model and for interconnecting the torsion and flexural elements so that compatability conditions are satisfied at their connections to the surrounding slab. A computerized form of the model is developed, incorporated into the Drain 2-D program developed at the University of California, Berkeley, and its use shown to predict accurately the strength, stiffness and hysteretic characteristics measured in the University of Washington sub-assemblage and frame tests.

A method is developed for devolving that relatively complicated beam-analogy model into a more simplistic model suitable for inelastic dynamic analyses of buildings. It is shown that with that simplistic model, and the modified Drain 2-D program, the response of the Holiday Inn, Orion Avenue, in the 1971 San Fernando Earthquake can be predicted. The measured and predicted time history responses for the upper floors of the building are shown to be in reasonable agreement with predictions utilizing the earthquake ground motions

recorded at the site, and the predictions for the change in period of the structure with ground shaking, and the magnitude of the relative displacements between floors are shown to be in good agreement with observed effects.

PREFACE

This report is the final technical report on an investigation into the strength and behavior of reinforced concrete slab-to-column and wall connections under simulated seismic loadings. During that investigation tests were made on slab-column subassemblages representing interior, exterior, and corner connections with and without shear reinforcement, with varying column dimensions, and with varying amounts of flexural reinforcement in the slab. In addition, simulated seismic loading tests were made on two slab-column frames representative to half and full-scale, respectively, of the interior and exterior bays of a flat plate structure. The results of those tests are summarized in Appendix A and the agreement between the strengths measured in those tests and the strengths predicted using the moment transfer provisions of ACI Code 318-77 are examined in Appendix D.

The attention of readers interested in simple design procedures is directed particularly to Sections 5.3.3 and Sections 2.3.1. In Section 5.3.3 a relatively simple analytical model is developed for the lateral load analysis of flat plate framing for both wind and seismic loading. In Section 2.3.1 a simple beam analogy model is developed for calculating the ultimate strength of interior, exterior and corner column connections.

The modified Drain 2D computer program described in this report in an IBM machine compatible form is available from the Earthquake Engineering Research Center, University of California, Berkeley, CA.

Copies of the theses and reports that detail the results of the sub-assemblage (3,4,5,6,7,8 and 9) and frame tests (10, 11) are available for cost of reproduction from the Literature Exchange Program Library, University of Washington, Seattle, WA, 98195 or the Department of Civil Engineering, FX-10, University of Washington, Seattle, WA 98195.

ACKNOWLEDGMENT

This report was prepared as a Ph.D. thesis by Dr. Akiyama working under the direction of Professor Hawkins. It is the final technical report on a seven year investigation sponsored by the National Science Foundation under Grants GI-38717, AEN 76-16702 and ENV 72-03585. The cognizant program managers for those grants was Dr. Charles C. Thiel and Dr. John B. Scalzi.

The assistance of Dr. Akiyama by Professors H. Okamura and K. Nishino of the University of Tokyo in carrying out the computer studies for this report is gratefully asknowledged. Also acknowledged are the contributions to the total knowledge represented by this report by former University of Washington graduate students, Dr. J. Yamazaki, Dr. M. S. Sheu, Dr. S. T. Chen, Dr. C. Georgiadis, S. N. Hanna, D. W. Symonds, E. Simpson, F. W. Wong, C. H. Yang, T. Chaichanavong, H. J. Chang, W. B. Hsiang, S. W. Yu, J. W. Broderick and G. H. Holdsworth, by former University of Washington faculty member Research Assistant Professor Denis Mitchell, and current faculty member Professor Ziad Elias.

TABLE OF CONTENTS

	Page
LIST OF TABLES	vi
LIST OF FIGURES	vii
NOMENCLATURE	xi
CHAPTER 1: INTRODUCTION	1
1.1 Nature of the Problem	1
1.2 Objective and Scope	4
CHAPTER 2: ANALYTICAL MODEL FOR SLAB-COLUMN CONNECTION	7
2.1 General Remarks	7
.1 Idealization of Connection	7
.2 Development of Procedure Suitable for Dynamic Analysis	13
2.2 Characteristics of Elements	15
2.2.1 Flexural Element	16
.1 General Configuration	16
.2 Monotonic Loading Response	18
.3 Cyclic Loading Response	24
2.2.2 Torsional Element	29
.1 General Configuration	29
.2 Distribution of Torsional Moment	30
.3 Monotonic Loading Response	37
.4 Cyclic Loading Response	46
2.2.3 Connecting Bar Element	47
2.2.4 Bond Slip Element	50
.1 General Configuration	50
.2 Monotonic Loading Response	50
.3 Cyclic Loading Response	55
2.3 Formulation of Model for Response of Slab-Column Connection	58

2.3.1 Strength of Connection 58

.1 Moments Caused by Gravity Loading 59
.2 Moment Transfer Strength 64

2.3.2 Stiffness of Connection 72

.1 Interior Column Connection 72
.2 Edge Column to Slab Connection Transferring Moment Parallel to Edge 76
.3 Edge Column to Slab Connection Transferring Moment Normal to Edge 77
.4 Corner Column to Slab Connection 78

CHAPTER 3: CYCLIC LOADING BEHAVIOR OF SLAB-COLUMN CONNECTIONS 78

3.1 General 78

3.2 Strength of Connections 79

3.3 Stiffness of Connections 88

3.4 Parameters Influencing Connection Behavior 110

3.4.1 Loading Conditions 110

3.4.2 Physical and Mechanical Conditions 118

CHAPTER 4: CYCLIC BEHAVIOR OF A FRAME 129

4.1 General 129

4.2 Test Frame 130

4.3 Strength of Connections 141

4.3.1 Moments Caused by Gravity Loading 141

4.3.2 Ultimate Strength of the Frame 141

4.4 Cyclic Response of Frame 146

4.4.1 Stiffness Model for Frame 146

4.4.2 Results and Discussion 148

CHAPTER 5: DYNAMIC RESPONSE OF A BUILDING 153

5.1 General 153

5.2 Holiday Inn, Orion Street 156

5.2.1 Description of Building 156

5.2.2 Earthquake Damage 163

5.2.3 Recorded Earthquake Response 163

5.3 Computer Modeling of Holiday Inn 165

5.3.1 Sectioning of Building 165

5.3.2 The Moment Caused by Gravity Load 166

5.3.3 Lateral Load Model 169

.1 General 169
.2 Simplified Column-Slab Connection Model 169

5.4 Dynamic Response of Holiday Inn 179

5.4.1 Behavior of Holiday Inn As-Built 179

5.4.2 Parametric Analyses 189

CHAPTER 6: CONCLUSIONS 195

REFERENCES 199

APPENDIX A: PREVIOUS RESEARCH 202

A.1 Previous Experimental Research 203

A.1.1 Interior Column-Slab Subassemblages 203

A.1.2 Exterior Column-Slab Subassembalges Transferring Moment Parallel to the Edge 218

A.1.3 Exterior Column-Slab Subassemblages Transferring Moment Normal to the Edge 218

A.1.4 Corner Column-Slab Subassemblages 218

A.1.5 One-Bay Frame with Interior and Exterior Column 219

A.1.6 One-Bay Fame with Two Interior Columns 219

A.2 Previous Analytical Research 219

A.2.1 Strength of Column-Slab Connections 220

.1 Linear Variation in Shear Stress Methods 220
.2 Thin Plate Methods 225
.3 Beam Analogy 226

A.2.2 Stiffness of Column-Slab Connections 231

APPENDIX B: COMPUTER PROGRAM FOR ESTIMATION OF THE PRIMARY CURVE (FOR INTERIOR COLUMN-SLAB CONNECTIONS) 234

APPENDIX C: DRAIN-2D PROGRAM 244

APPENDIX D: ULTIMATE CAPACITIES OF TEST SPECIMENS FOR MOMENT TRANSFER PROVISIONS OF ACI CODES 318-77 318-83 268

LIST OF TABLES

TABLE 3.1	STRENGTH OF CONNECTIONS	80
TABLE 3.2	LIMITING MOMENTS AND PARTIAL RIGIDITIES	91
TABLE 4.1	ULTIMATE CAPACITY OF LABORATORY TEST FRAME	144
TABLE 4.2	PARTIAL STIFFNESS AND LIMITING MOMENT VALUES FOR LABORATORY TEST FRAME	147
TABLE 5.1	PROPERTIES OF CONSTRUCTION MATERIAL FOR HOLIDAY INN	162
TABLE 5.2	REINFORCEMENT RATIOS FOR HOLIDAY INN	180
TABLE 5.3	LIMITING MOMENTS AND PARTIAL STIFFNESSES OF CONNECTIONS	182
TABLE A.1	PROPERTIES OF TEST SPECIMENS	205

LIST OF FIGURES

Figure		Page
2.1	IDEALIZATION FROM SPACE FRAME TO PLANE FRAME	8
2.2	STIFFNESS MODEL FOR INTERIOR COLUMN CONNECTION	10
2.3	TWO DIMENSIONAL MODEL FOR INTERIOR COLUMN-SLAB CONNECTION	11
2.4	M-θ RELATIONSHIP FOR INTERIOR CONNECTION	12
2.5	TYPICAL STRAIN DISTRIBUTIONS FOR REINFORCING BARS IN DIRECTION OF MOMENT TRANSFER	17
2.6	TYPICAL CRACKING FOR FLEXURAL ELEMENTS	19
2.7	TYPICAL DEFLECTION PROFILE FOR SLAB	19
2.8	FORCE-DEFORMATION RELATIONSHIP FOR FLEXURAL ELEMENT	20
2.9	RELATION BETWEEN ε_c AND ρ	22
2.10	MOMENT-STRAIN CURVES FOR A SINGLY REINFORCED CONCRETE BEAM BASED ON COMPRESSION TESTS ON CYLINDERS (42)	25
2.11	FORCE-DEFORMATION RELATIONSHIP FOR FLEXURAL ELEMENT FOR CYCLIC LOADING	25
2.12	MOMENT-ROTATION RELATIONSHIP FOR TAKEDA MODEL	26
2.13	TYPICAL CRACK PATTERN OF TORSIONAL ELEMENT	31
2.14	ANGLE OF TORSION OF SPECIMEN T-3	31
2.15	TENSILE STRAINS IN TOP REINFORCING BARS	32
2.16	DISTRIBUTION OF MOMENT IN TORSIONAL ELEMENT	34
2.17	FORCE-DEFORMATION RELATIONSHIP FOR TORSIONAL ELEMENT	38
2.18	TYPICAL FACE AND NOTATIONS	42
2.19(a)	RECTANGULAR SPACE TRUSS MODEL WITH 45 DEG-DIAGONALS	44
2.19(b)	TORQUE-TWIST CURVES OF HOLLOW AND SOLID CROSS-SECTIONS WITH DIFFERENT DISTRIBUTIONS OF LONGITUDINAL STEEL	45
2.20	STIFFNESS OF CONNECTING BAR	48

Figure		Page
2.21	FORCE-DEFORMATION RELATIONSHIP FOR BONDSLIP ELEMENT	51
2.22	STRESS AND ROTATION RELATIONSHIP WITH BONDSLIP	54
2.23	STRESS-STRAIN CURVES FOR REINFORCING BARS S1, S2, S3 S4, SS1 AND SS2	56
2.24	MOMENT DISTRIBUTION MODEL FOR GRAVITY LOAD CONDITION	61
2.25	TYPICAL EXAMPLES FOR STRAIN DISTRIBUTIONS IN REINFORCEMENT FOR GRAVITY LOAD CONDITION	62
2.26	TYPICAL EXAMPLES FOR STRAIN DISTRIBUTION IN REINFORCEMENT FOR GRAVITY LOAD CONDITION	65
2.27	FAILURE MODELS FOR INTERIOR COLUMN CONNECTIONS	68
2.28	GENERAL CONFIGURATION AND NOTATION FOR DEFORMED CONNECTION	73
3.1	STIFFNESS RELATIONSHIPS	90
3.2	LATERAL LOAD-SLAB DEFLECTION RELATIONSHIP (interior column connections)	96
3.3	CYCLIC BEHAVIOR PREDICTIONS FOR SS-3	104
3.4	LATERAL LOAD-SLAB DEFLECTION RELATIONSHIP (edge column connection transferring moment parallel to the edge)	106
3.5	LATERAL LOAD-SLAB DEFLECTION RELATIONSHIP (edge column connection transferring moment normal to the edge)	108
3.6	LATERAL LOAD-SLAB DEFLECTION RELATIONSHIP (corner column connection)	111
3.7	INFLUENCE OF GRAVITY LOAD	114
3.8	INFLUENCE OF GRAVITY LOAD ON MOMENT TRANSFER CAPACITY	116
3.9	INFLUENCE OF LOADING HISTORY ON STRAIN IN TOP REINFORCING BARS	118
3.10	INFLUENCE OF CONCRETE STRENGTH	120
3.11	INFLUENCE OF REINFORCEMENT RATIO	123

Figure		Page
3.12	INFLUENCE OF STIRRUPS	127
3.13	INFLUENCE OF EXTENT OF REGION REINFORCED WITH STIRRUPS	127
4.1	LATERAL LOAD-HORIZONTAL DEFLECTION-INTERIOR COLUMN	131
4.2	LATERAL LOAD-HORIZONTAL DEFLECTION-EXTERIOR COLUMN	132
4.3	TOTAL LATERAL LOAD-EXTERIOR COLUMN TIP DEFLECTION	133
4.4	DISTRIBUTION OF WEIGHT MODELING DEAD WEIGHT	136
4.5	REINFORCING MAT AND GAGES FOR EXTERIOR FRAME	137
4.6	INTERNAL FORCES CAUSED BY GRAVITY LOADING	142
4.7	INITIAL MOMENTS CAUSED BY GRAVITY LOADING	142
4.8	SCHEMATIC DIAGRAM OF FAILURE MODES IN TEST	145
4.9	IDEALIZATION OF THE FRAME FOR ANALYSIS	149
4.10	LATERAL LOAD HISTORY (SIMULATED)	150
5.1	DEFORMATIONS FOR HOLIDAY INN (OBSERVED AND PREDICTED)	155
5.2	HOLIDAY INN, ORION AVENUE. FIRST-FLOOR PLAN	157
5.3	HOLIDAY INN, ORION AVENUE. TYPICAL FLOOR FRAMING PLAN	158
5.4	HOLIDAY INN, ORION AVENUE. ROOF FRAMING PLAN	159
5.5	HOLIDAY INN, ORION AVENUE. SECTIONS AND DETAILS	160
5.6	HOLIDAY INN, ORION AVENUE. RECORDED ACCELERATION	164
5.7	EXTRACTED FRAME MODEL	167
5.8	MOMENTS CAUSED BY GRAVITY LOAD	168
5.9	BEAM ANALOGY MOMENTS DUE TO GRAVITY LOAD	168
5.10	SIMPLIFIED BEAM ANALOGY	170
5.11	EXCURSION AFTER FIRST BREAK UNTIL SECOND BREAK FOR SIMPLIFIED MODEL CYCLIC LOADING RESPONSE	171
5.12	IDEALIZED FRAME MODEL	172

Figure		Page
5.13	COMPARISON BETWEEN ORIGINAL STEP-BY-STEP AND SIMPLIFIED METHOD FOR ASSESSING COLUMN-SLAB CONNECTION RESPONSE	178
5.14	PREDICTED RELATIVE DEFORMATIONS BETWEEN FLOORS FOR HOLIDAY INN	185
5.15	TYPICAL PREDICTED FORCE DEFORMATION RELATIONSHIPS FOR SLAB-COLUMN CONNECTIONS OF HOLIDAY INN	186
5.16(a)	TYPICAL PREDICTED MOMENTS FOR SLAB-COLUMN CONNECTIONS OF HOLIDAY INN, NODES 5.13 AND 29-EXTERIOR COLUMN TO SLAB CONNECTIONS	187
5.16(b)	TYPICAL PREDICTED MOMENTS FOR SLAB-COLUMN CONNECTIONS OF HOLIDAY INN, NODES 6.14 AND 30 (INTERIOR COLUMN TO SLAB CONNECTIONS)	188
5.17	DEFORMATIONS WITH DIFFERENT MOMENT TRANSFER CHARACTERISTICS OF SLAB-COLUMN CONNECTIONS	191
5.18	THE INFLUENCE OF DAMPING RATIO ON THE DEFORMATIONS	193
A.1	SPECIMENS TESTED AT UNIVERSITY OF WASHINGTON	204
A.2	DEVELOPMENT OF TEST SPECIMEN FOR S AND SS SERIES	210
A.3	SCHEMATIC DIAGRAM OF TEST RIG	211
A.4	MODEL OF LINEAR VARIATION IN SHEAR STRESS BY DI STATIO AND VAN BUREN	221
A.5	LINEAR STRESS METHOD OF ANALYSIS	223
A.6	MOMENT-SHEAR INTERACTION RELATIONSHPS FOR INTERIOR COLUMN CONNECTION	224
A.7	STIFFNESS MODEL FOR INTERIOR COLUMN CONNECTION	228
A.8	LIMITING STRENGTH COMBINATIONS FOR BEAM ANALOGY FOR INTERIOR COLUMN CONNECTION	229
A.9	SLAB-COLUMN DEFORMATIONS	232
B.1	GENERAL CONFIGURATION OF CONNECTION AND NOTATION FOR STEP-BY-STEP PROCEDURE FOR DETERMINATION OF PRIMARY LATERAL LOAD RESPONSE RELATIONSHIP	236

NOMENCLATURE

A_c = area of concrete in the critical section

A_ℓ = total area of longitudinal reinforcement resisting torsion

A_s = area of tension reinforcement

A_h = area of transverse hoop reinforcement (one leg)

A_v = area of shear reinforcement within a distance s

a = distance between centers of column and flexural element

b_o = periphery of critical section for slabs or larger outer-to-outer dimension of longitudinal reinforcement resisting torsion

c_{AB} = distance from centroidal axis of critical section to front face of critical section

c_{CD} = distance from centroidal axis of critical section to front face of critical section

c_1 = size of rectangular column in direction of moment transfer

c_2 = size of rectangular column transverse to direction of moment transfer

c_m = width of cracked flexural element

c_t = width of cracked torsional element

d = effective depth to tensile reinforcement

d′ = effective depth to compression reinforcement

d* = distance between compression and tension bars

D_b = bar diameter

E_c = modulus of elasticity of concrete

E_s = modulus of elasticity of steel

EI_g = flexural stiffness of uncracked flexural element

EI_y = flexural stiffness of cracked but not yielded flexural element

EI_u = flexural stiffness of yielded flexural element

ET = flexural stiffness of connecting bar

EI_s = flexural stiffness of slab

f'_c = concrete cylinder compressive strength

f_y = yield strength of reinforcement

F_y = tension force

G_c = modulus of rigidity of concrete

GJ_o = torsional stiffness of concrete section uncracked in torsion

GJ_{cr} = torsional stiffness of concrete section cracked in torsion

h = overall depth of section

h_o = smaller outer-to-outer dimension of longitudinal reinforcement resisting torsion

J_c = polar moment of inertia of critical section

K = bond slip stiffness = bar force/loaded end slip

kd = neutral axis depth for cracked concrete section

KT = stiffness of torsional element

KB = stiffness of bond-slip element

ℓ = distance from column face to edge of slab in direction of moment transfer

ℓ_t = distance from column face to edge of slab transverse to direction of moment transfer

ℓ_c = column strip width

ℓ_b = length of connecting bar

L = distance between two lateral loads

MT = moment that can be transferred to column

M_{cr} = moment for flexural cracking

M_y = moment for flexural yielding

M_u = moment for flexural crushing

M_{yb} = moment for yielding of bondslip element

M_g = moment caused by gravity load

M_f = moment at front flexural element

M_b = moment at back flexural element

M_1 = moment transferred to column at yielding of flexural element and cracking of torsional element

M_2 = moment transferred to column at crushing of torsional element

n = Es / Ec

n_b = number of tension bars in region of flexural element of width c_2

s = reinforcement spacing

s_v = shear reinforcement spacing

s_h = transverse hoop reinforcement spacing

T = torque applied to section

T_{cr} = moment for torsional cracking

T_y = moment for torsional yielding

T_u = ultimate torsional capacity

T_g = torsion caused by gravity load

T_f = torsion acting on front half torsional element

T_b = torsion acting of back half torsional element

u = $2 (b_o + h_o)$

v_c = nominal permissible shear stress carried by concrete

v_g = shear stress caused by gravity load

V_f = shear force applied at front flexural element

V_o = shear capacity of any section

ρ = tension reinforcement ratio

ρ_h = $A_h u/b_o h_o s$

ρ_s = $A_\ell/b_o h_o$

$\phi(\phi_{cr}, \phi_y, \phi_u)$ = curvature (at cracking, yielding, crushing)

$\theta(\theta_{cr}, \theta_y, \theta_u)$ = rotation (at cracking, yielding, crushing)

$\psi(\psi_{cr}, \psi_y, \psi_u)$ = twist per unit length (at cracking, yielding, crushing)

δ = deflection at slab edge

β_o = damping coefficient dependent on elastic stiffness

CHAPTER 1

INTRODUCTION

1.1 Nature of the Problem

A flat plate concrete frame is a flat slab structure without drop panels or column capitals. From the architectural and constructional viewpoints, the flat plate frame is an ideal structural form. Flat plate framing requires relatively simple formwork. The overall depth of the flexural members is a minimum, columns can often be buried in walls, the framing provides minimum impediment to the location of mechanical and electrical services and it is relatively easy to make the final structure aesthetically pleasing.

Flat plate frames are widely used in the U.S.A. on the East Coast and in the Midwest. On the West Coast they are less frequently used because of serious doubts concerning their seismic behavior. Typically such frames are designed only to resist gravity loads and the lateral loads are taken by members with more reliable seismic behavior.

For seismic regions it is generally considered desirable to use a two-level earthquake concept to design important structures. For the lower level, moderate earthquake, the structure is designed to behave elastically. Typically, the moderate earthquake creates forces of the magnitude envisaged by the seismic provisions of the Uniform Building Code (1). Under those forces the resultant frame deformations should not cause significant damage to nonstructural

components. To achieve that objective, lateral drifts are commonly limited to 3/8 in. (9.5 mm) in 10 ft. (3 m). For the higher level, severe earthquake, the structure must be able to absorb, and ultimately dissipate, large amounts of energy. Damage to structural components, and especially to nonstructural components is to be expected, but the structure must not collapse. For flat plate frames, the severe inelastic deformations caused by higher order earthquake must not result in punching failures at slab-to-column connections. The Uniform Building Code addresses that problem by requiring that failure must not be predicted for moments corresponding to deformations three to four times greater than the deformations caused by the Code's specified lateral forces. Thus, for both moderate and severe earthquake conditions, accurate information is needed on the stiffness of the flat plate frame and its attachments in order to better determine how the lateral load is shared between the flat plate frame and the main resisting elements, and to better assess interstory drifts.

A wide range of experimental and theoretical investigations have been conducted on flat plate structures. When flat plates, designed in accordance with ACI 318-63, have been tested to destruction (2) it has been found that shear conditions at the slab-to-column connection, rather than flexural conditions, have generally controlled the system's ultimate strength. Further, tests of flat slab structures have shown that under gravity loads almost complete redistribution of moments can be achieved prior to collapse provided a premature punching failure is prevented at the slab-to-column connection (2).

Thus, a flat plate frame should inherently provide excellent energy dissipation if a punching failure can be prevented. There is, however, a decrease in the shear capacity of slab-to-column connections with increasing amounts of moment transfer. The amount of moment transferred depends on the stiffness of the slab relative to the column in the connection region. It appears that where moment is transferred between slab and column, either as a result of lateral loadings or unbalanced gravity loadings, conditions at the slab-to-column connection are critical for determining the strength and stiffness of flat plate construction.

The results of prior investigations demonstrate that it is difficult to resist significant seismic forces with flat plate framing alone. Interstory drifts exceed tolerable limits even under moderate earthquakes unless the structure is very limited in height or large columns are used in combination with deep slabs and small column spacings. For taller structures, the use of flat plate framing may only be possible in upper stories. At lower levels, such framing must be used in conjunction with shear walls or a primary moment resisting ductile frame. For low-rise structures and the upper levels of high rise structures, knowledge of the stiffness, strength and hysteretic characteristics of the slab-column connection is required if reasonably accurate determinations are to be made of the structure's likely response to lateral loading. For the lower levels of high-rise structures, the development of ductile shear wall construction seems to have become a realistic goal. Thus, even if flat plate framing is designed to carry gravity loads only, its

response for lateral loads becomes increasingly important for both strength and drift control as more of the major reinforced concrete lateral load resisting systems are designed to be ductile under severe earthquakes.

1.2 Object and Scope

The object of this study is to develop a general method for predicting the lateral load strength and stiffness characteristics of a flat plate concrete structure. The characteristics observed in laboratory tests to failure on flat plate subassemblage and frame specimens are used to develop, calibrate and test a model for the moment-rotation characteristics of flat plate to column connections. That model is then incorporated into an orderly scheme for analyzing the lateral load response of flat plate structures including the development of a procedure for inelastic dymanic analysis of such structures.

The study reported in this dissertation forms part of an eight year investigation at the University of Washington into the factors dictating the stiffness, strength and energy absorption characteristics of flat plate-to-column connections.

In Chapter 2, a general beam analogy model is developed for predicting moment-rotation characteristics, up to and including failure, for concrete flat plate to column connections. While that model was generated starting from previously existing beam analogy concepts, more general capabilites are built into the analogy by making the elements of the model satisfy accepted reinforced concrete

constitutive relationships, as well as equilibrium and compatibility constraints at the connection.

The model was developed by trial and error utilizing some eight interior column-plate subassemblage results and then adjusted so that it gave good agreement with both the envelope and hysteretic results for those specimens.

In Chapter 3 an examination is made of the agreement between the predictions of the model and the results of some 30 subassemblage tests conducted at the University of Washington and differing from the sub-assemblage results for which the model was originally developed. The sub-assemblage results against which the model was tested included interior column-plate connections with columns of differing size and shape, exterior column connections transferring moments both normal and parallel to the edge, and corner column connections. In Chapter 3 the model is also used to examine parametrically the influence of concrete strength, reinforcement ratio and gravity load on the strength and stiffness of connections.

In Chapter 4, as a third step, it is demonstrated how the models for an interior and an exterior connection can be linked in an orderly manner for predictions of the response of a one bay exterior frame specimen tested to failure at the University of Washington under reversed cyclic loading.

In Chapter 5, as a fourth and final step, a simplified form is developed of the beam analogy model utilized in Chapters 2 through 4. That simplified form is shown to give good agreement with the envelope data with which the model of Chapter 2 was originally

developed. That simplifeid model is then incorporated into the Drain 2-D program and used to predict the time history response of the Holiday Inn, Orion Avenue, in the 1971 San Fernando earthquake. It is demonstrated that with the model the observed changes in response of the real structure with time and displacements are predicted reasonably well.

The conclusions for this study are presented in Chapter 6. Previous experimental and analytical research relevant to this study are summarized in Appendix A, the computer program developed for predictions of the monotonic lateral load response of a column-slab connection is presented in Appendix B, and the modifications to the Drain 2-D program necessary for it to be used to predict the cyclic lateral load response of a connection and the time history response of a column-slab structure are presented in Appendix C.

CHAPTER 2

ANALYTICAL MODEL FOR SLAB-COLUMN CONNECTION

2.1 General Remarks

One common method for analyzing a building is to replace the three dimensional space structure by a series of two dimensional frames as shown in Fig. 2.1(a,b,c). Usually the idealization from the space frame to the column-slab subframe is made by imagining vertical cuts through the entire space frame along the line of zero shear which is usually taken as the center line of the panel between column rows. As there is no reason to contradict such cutting, the same approach is followed here. Because subframes with three dimensionsal properties are also very difficult to analyze, it is customary to seek some method for idealizing those subframes as equivalent plane frames, as shown in Fig. 2.1(d). The key to the accuracy of that idealization lies in the properties assigned to the connections since conditions at the column-slab connections are critical for determiing the strength and stiffness of the frame.

2.1.1 Idealization of Connection

From the previous research, it is apparent that to evaluate properly the behavior of connections, an analytical model is needed capable of taking into account the effects of torsion at the side faces of the column, bond slip of the reinforcing bars passing through the column, and shear deformations, particularly at the column corners. In this dissertation it is shown that the model

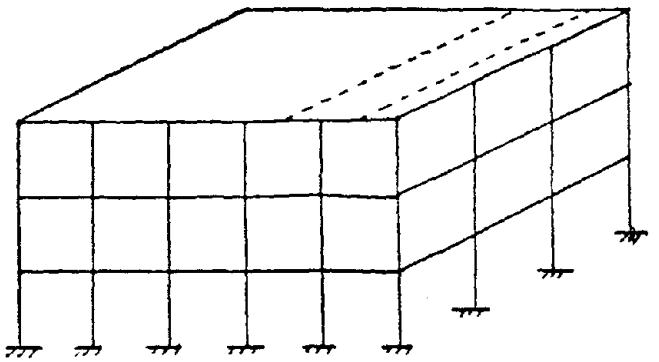

(a) Three Dimensional Space Frame

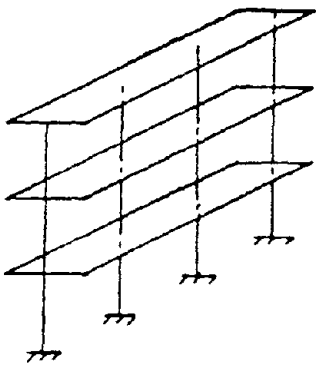

(b) Internal Column-Slab Subframe

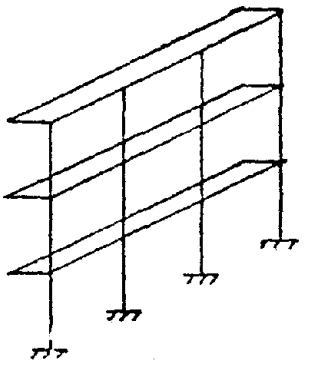

(c) External Column-Slab Subframe

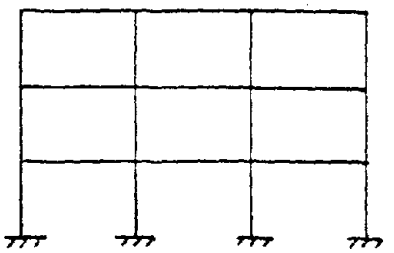

(d) Final Plane Frame

FIG. 2.1 IDEALIZATION FROM SPACE FRAME TO PLANE FRAME

illustrated schematically in Fig. 2.2 can provide for those actions and also be adjusted, in accordance with accepted reinforced concrete theory, so that it can be used to accurately predict the response of flat plate concrete slab to column connections transferring moments.

The slab is assumed to be attached to the column through a series of stub beam elements, that are the front and back face flexural elements F_1 and F_2 and the side face torsional elements T_1 and T_2. The torsional elements have in turn connecting elements C_1 and C_2 linking them to the slab at their ends remote from the column. At the interface between the column and the flexural elements F_1 and F_2, there are bondslip elements B_1 and B_2. The sharp deformations permitted by that model at the junction of the T and F elements implies that shear deformations at the column corners have little effect on the response of the connection. Once the rigidity and strength of the T, F, C, and B elements are defined, it is not difficult to assemble these elements into an equivalent two-dimensional connection model as shown in Fig. 2.3.

For unidirectional loading that model predicts a relationship between the moment transferred to the column and the deformation of the slab relative to the column with the six stages shown in Fig. 2.4. These six stages are terminated respectively by the gravity load condition, torsional cracking, back face cracking, front face yielding, back face yielding, and crushing of each of the elements. The order in which those actions occur can be changed or an action missed according to the loading conditions and the characteristics for each element.

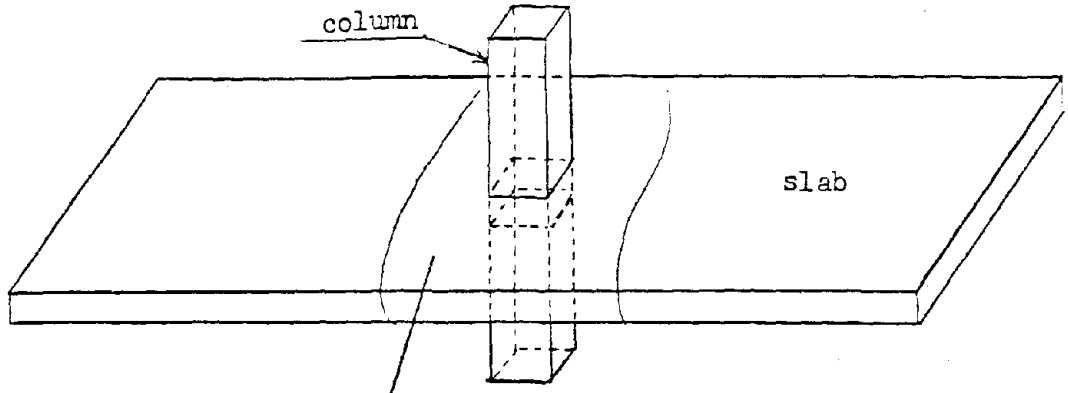

(a) general view

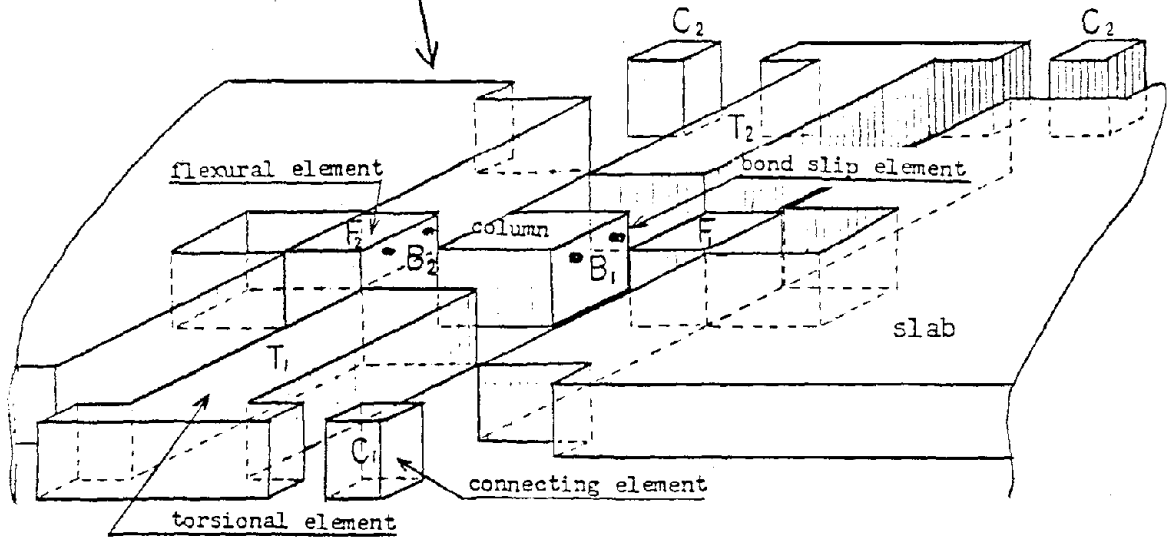

(b) stiffness model

FIG. 2.2 STIFFNESS MODEL FOR INTERIOR COLUMN CONNECTION

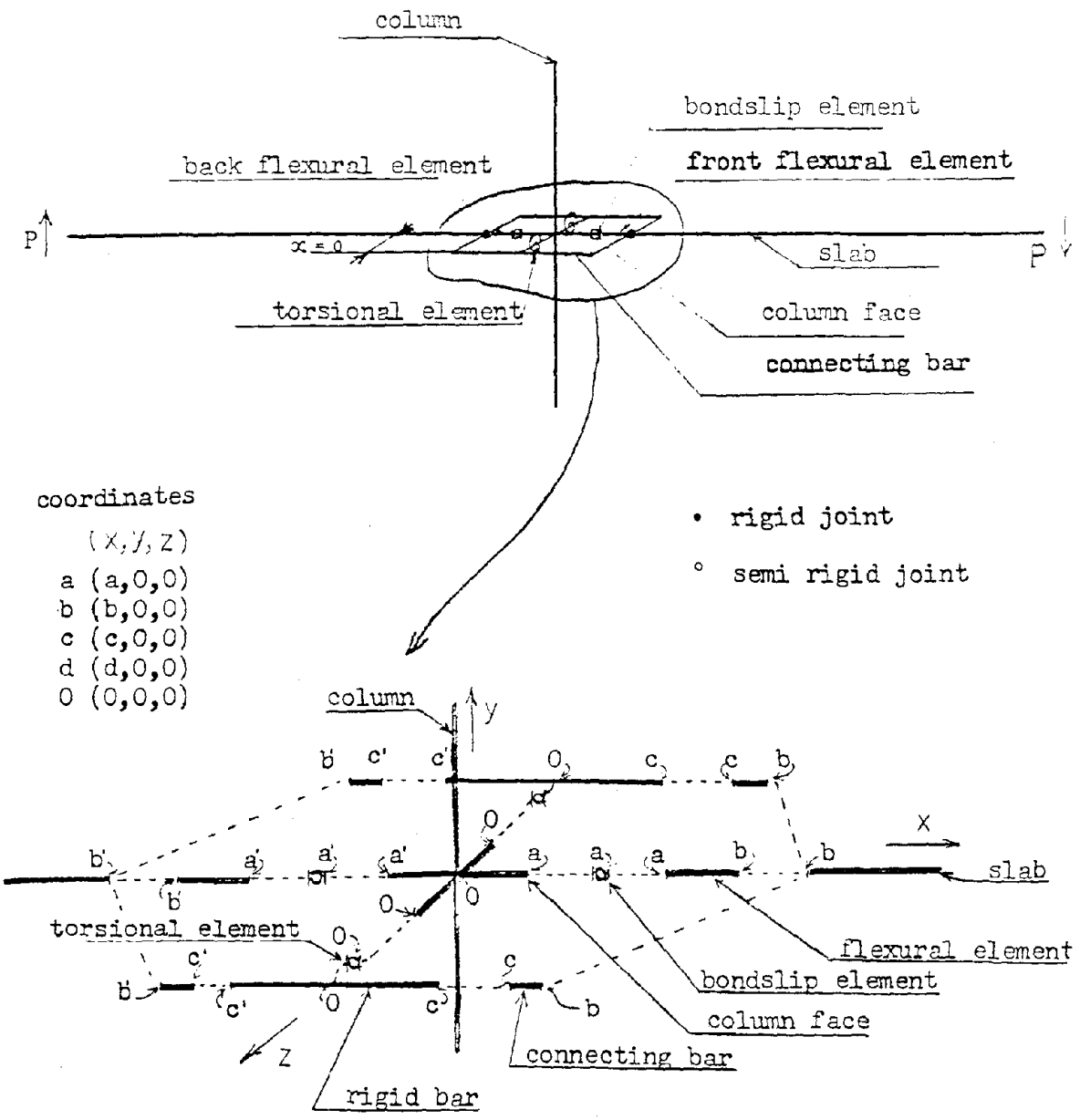

FIG. 2.3 TWO DIMENSIONAL MODEL FOR INTERIOR COLUMN-SLAB CONNECTION

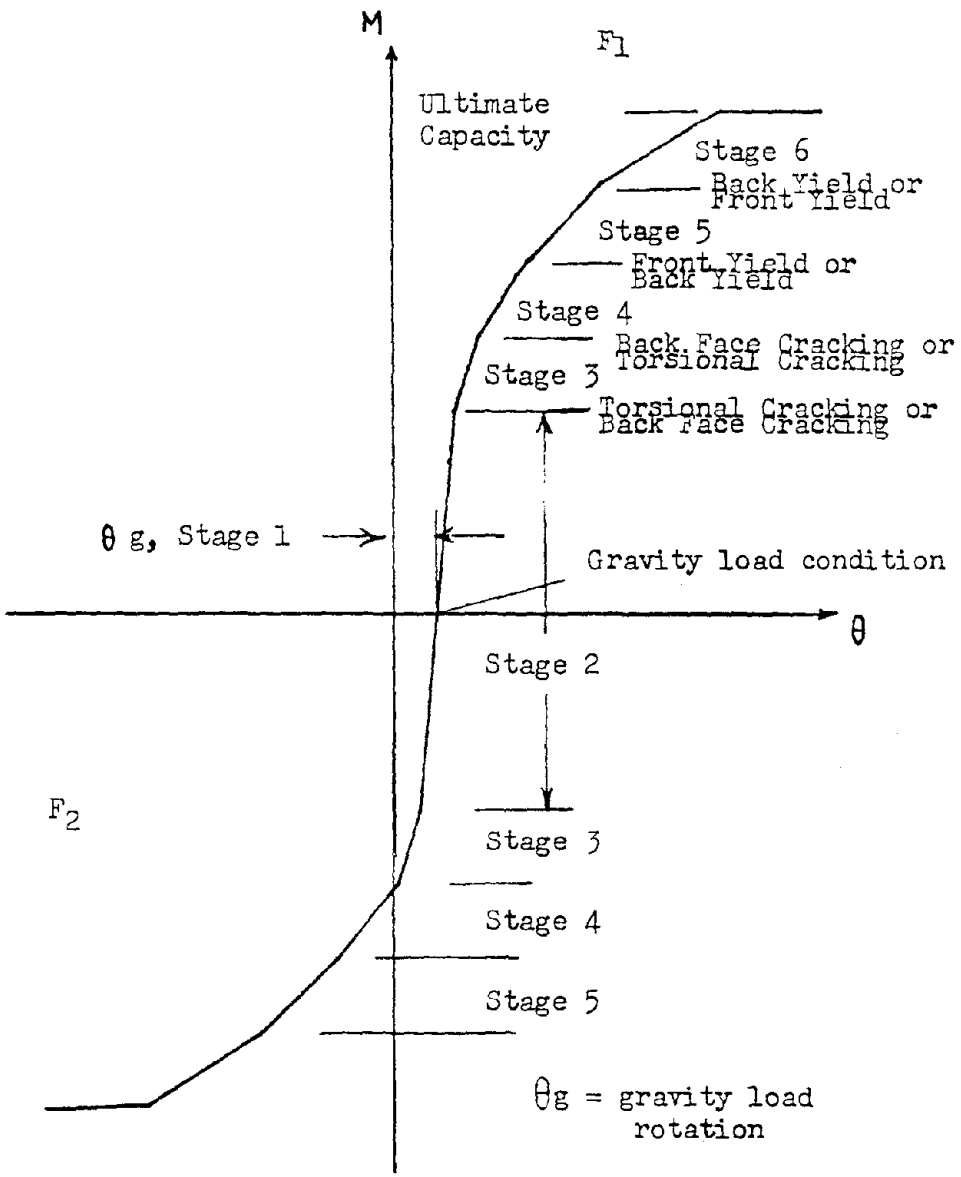

FIG. 2.4 M–θ RELATIONSHIP FOR INTERIOR CONNECTION

The model shown in Fig. 2.3 can be transformed into a form suitable for edge connections by imagining it split along one of the four faces of column so that the cutting line becomes the edge of the slab. It is then also obvious that the model is equally applicable to the corner connections. However, as presently constructed, this model has been verified only for structures with columns lying within the slab perimeter. The computer programs developed here require modeification and their predictions should be verified before being applied to structures with columns.

2.1.2 Development of Procedure Suitable for Dynamic Analysis

Once proper models of the column-slab connections are developed, it is relatively simple structural analysis to create an overall model suitable for lateral loading analysis by interconnecting the connection models by columns and by beams that represent the slab strips. However, for seismic analysis that overall model must also be adaptable to inelastic dynamic analysis. There are many computer programs available for the dynamic analysis but most are for the elastic range of behavior only. The number of inelastic dynamic programs are small, most are expensive to run, and with most it is difficult to represent adequately the inelastic behavior of connections. However, Drain-2D program is a dynamic anlaysis program that it is comparatively inexpensive to run and was found in calibration trials to produce answers in reasonable agreement with test data well into the non-linear range. Therefore, an overall procedure was

developed for monotonic and reversed cyclic lateral load analysis that was consistent with the use of Drain-2D.

The general procedure developed here for the lateral or dynamic load anlaysis of flat slab structures is then as follows:

1) Develop analytical models for column-slab connections.

.1 The slab-column connection is idealized into front and back face flexural elements, torsional elements, bond-slip elements, and connecting bar elements, as shown in Fig. 2.2.

.2 The capacities limiting each stage in Fig. 2.4 and the stiffness of each element for each stage are calculated. Suitable unloading and reloading stiffnesses are determined. Appropriate procedures are developed in Section 2.2.

.3 The ultimate strength of the connection is calculated based on the corresponding strength for each element. Appropriate procedures are developed in Section 2.3.1.

.4 The stiffnesses determined in Step 1.2 are used to calculate relationships between applied moments and connection rotations.

.5 The relationships of Step 1.4 are converted to simple tri-linear relationships and appropriate supplemental unloading and reloading stiffness added.

2) Establish the overall analytical model for the building.

.1 The stiffnesses of the inter-connection slabs and columns are determined according to customary procedures.

.2 An overall model is created for the building frame from the models of the connections, slabs and the columns.

3) Make the lateral load analysis

.1 Determine the initial forces acting on each element of the connections for gravity loading. Appropriate procedure are developed in Section 2.3

.2 With the forces determined in step 3.1 acting on the connections apply the lateral load to the overall analytical model. For dynamic analyses use the Drain-2D program.

If the structure being analyzed is small or the computer being used has a large capacity, then step 1.5 may be omitted and the relationship of step 1.4 used directly. However, for most practical structures step 1.5 is necessary and suitable short-cut procedures are developed in Chapter 5. The remainder of this chapter deals with defining the relationships described in steps 2.1, 1.3 and 1.4.

2.2 Characteristics of Elements

In this section, response characteristics are defined, in turn, for each basic element of the connection: the flexural F, torsional T, connecting bar C, and bond slip B elements. First, the proportions selected for the element and the reasons for that selection are described. Next, the analytical model for the response for monotonic loading is developed and finally the modification of that model for reversed cyclic loading is detailed.

2.2.1 Flexural Element

2.2.1.1 General Configuration

This element is assumed to have a depth equal to the slab depth h and a projection from that face also equal to h, as shown in Fig. 2.2. The effective width of this element is assumed to vary according to the distribution of reinforcing bars in the section and the loading intensity.

Before cracking, the effective width is taken as c_2, the width of the column face where the flexural moment is transferred. This value is appropriate because the gravity loading causes very high local slab stresses adjacent to the column corners and reduces the stiffness of the concrete on both sides of the element. However, after cracking at the column face, the stiffness of the slab becomes more uniform, there is moment redistribution, and the width is assumed to increase to $(c_2 + d)$, or $(c_2 + d/2)$ for edge connections transferring moment parallel to an edge or corner connections . This width then coincides with the width of the critical section for shear in ACI Code 318. Shown in Fig. 2.5 are typical strain distributions for reinforcing bars for specimens tested at the University of Washington. Those strains were measured on the line of the column face for bars at the locations shown. The broken lines paralleling the side column faces define the distance $(c_2 + 3h)$ which is the effective width specified in ACI Code 318 for the flexural element for transfer of the portion of the moment not transferred by shear.

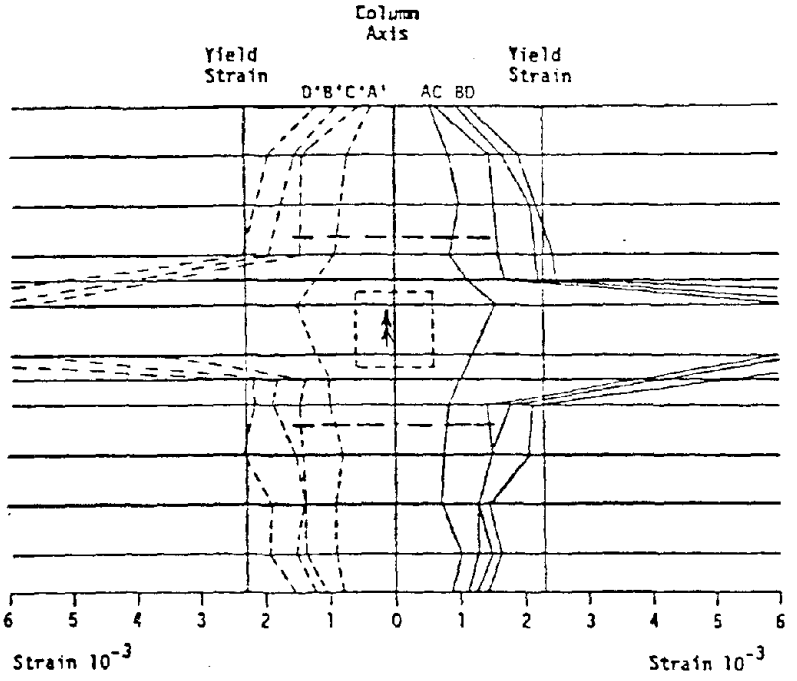

(a) SS-4

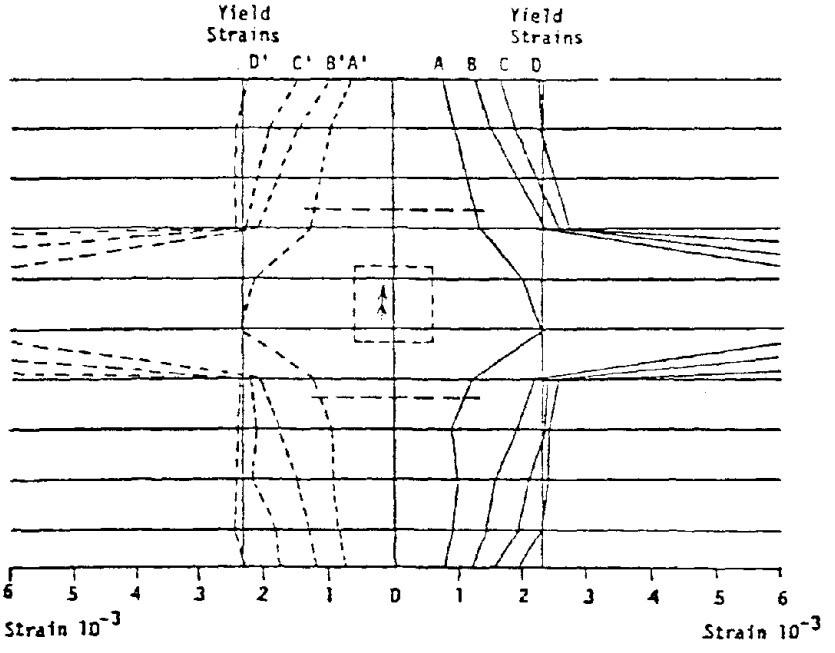

(b) SS-5

FIG. 2.5 TYPICAL STRAIN DISTRIBUTIONS FOR REINFORCING BARS IN DIRECTION OF MOMENT TRANSFER

It is apparent that there is a large strain within the width $(c_2 + d)$ adjacent to the column. However, by the width $(c_2 + 3h)$ that concentration has dissipated. Thus, $(c_2 + d)$ is a reasonable lower bound for the width of the flexural element.

The projection h is based on test data. The typical crack pattern for this element for cyclic shear and moment is shown in Fig. 2.6 and the deflected profile on the central, longitudinal, axis of a typical slab is shown in Fig. 2.7. Almost all test specimens showed a large deflection change at about a distance h from the face of the column. Because of the influence of shear, and of the resulting diagonal cracks, it can be assumed that as failure is approached, the yielding of the tension bars will spread over the whole length of the flexural element as a plastic hinge forms in that region (Reference 32).

2.2.1.2 Monotonic Loading Response

The hexa-linear curve of Fig. 2.8 defines the response for monotonic loading to failure and the envelope for cyclic loading. Critical moments and curvatures are calculated using the commonly accepted expressions shown in Fig. 2.8. The first break in the curves occurs at cracking for which the coordinates are obtained as follows:

$$M_{cr} = \frac{c_2 h^2}{6} \quad 7.5\sqrt{f'_c} \tag{2.1}$$

$$\phi_{cr} = M_{cr}/EI_g = 12\, M_{cr}/E_c c_2 h^3 \tag{2.2}$$

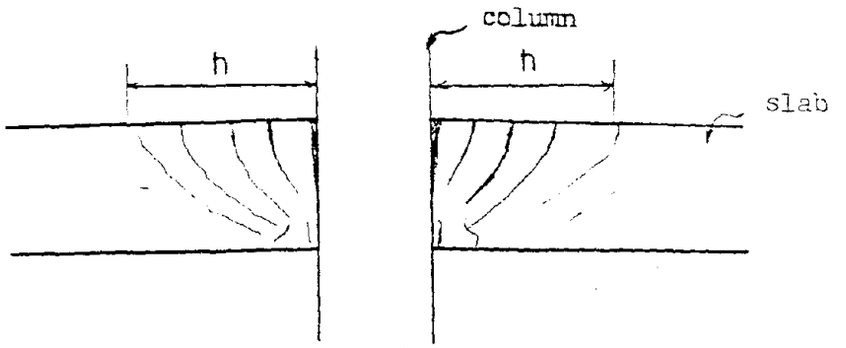

FIG. 2.6 TYPICAL CRACKING FOR FLEXURAL ELEMENTS

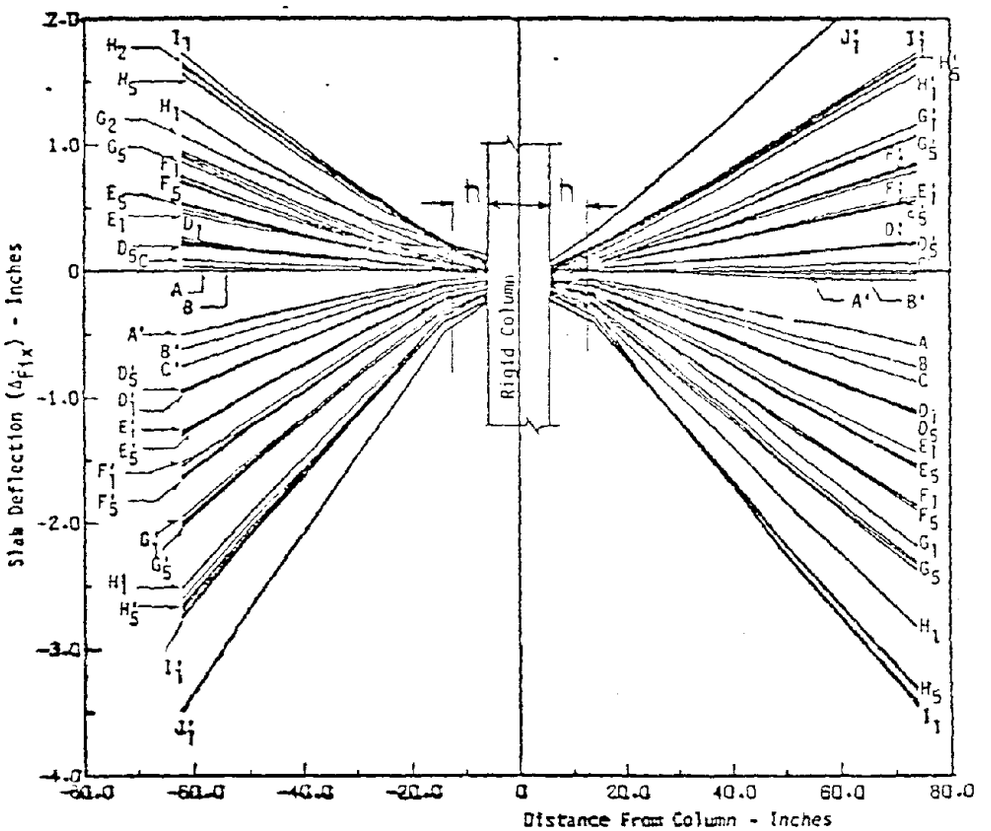

FIG. 2.7 TYPICAL DEFLECTION PROFILE FOR SLAB

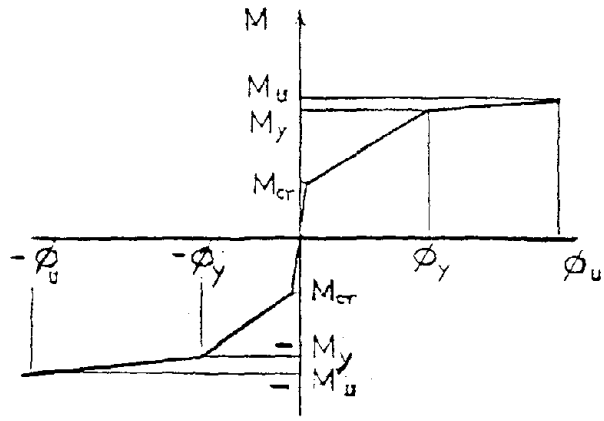

primary curve

$$M_{cr} = \frac{c_2 h^2}{6} \; 7.5\sqrt{f_c'} \tag{2.1}$$

$$\phi_{cr} = M_{cr}/EI_g \tag{2.2}$$

$$M_y = 0.95\rho_{c_m} d^2 f_y (1 - 0.6\rho f_y/f_c') \tag{2.4}$$

$$\phi_y = f_y/E_s(d - kd) \tag{2.5}$$

$$M_u = \rho_{c_m} d^2 f_y (1 - 0.6\rho f_y/f_c') \tag{2.7}$$

$$\phi_u = (0.004)(0.72f_c')/\rho d f_y \tag{2.8}$$

FIG. 2.8 FORCE-DEFORMATION RELATIONSHIP FOR FLEXURAL ELEMENT

where f'_c is the concrete strength (psi) EI_g is the uncracked stiffness and E_c is the modulus of elasticity of concrete ($E_c = 57{,}000\sqrt{f'_c}$, psi for dense aggregate concrete). Cracking moments are the same for positive or negative loading.

The second break in the curve occurs at yielding. For sections lightly reinforced in tension only, the yield moment can be calculated by the following equation:

$$M_y = \rho c_m d\, f_y\, (d-kd/3) \tag{2.3}$$

and

$kd = -\rho nd + \sqrt{(\rho nd)^2 + 2\rho nd}$, where ρ = tensile reinforcement ratio; d = distance from extreme compression fiber to centroid of tensile reinforcement; $c_m = c_2 + d$ or $c_2 + d/2$, as defined previously; $n = E_s/E_c$; E_s = modulus of elasticity of steel. However, if the section contains moderate or greater amounts of top reinforcement, Eq. 2.3 can yield values that are too large. Alternatively if the section contains relatively large amounts of bottom reinforcement Eq. 2.3 can yield values that are conservative.

For most slabs, the reinforcing ratio for the flexural element varies between 0.005 and 0.020 and for that range the compressive strain in the concrete for yielding of the steel varies from 0.006 to 0.015, respectively, as shown in Fig. 2.9. The relation between the ultimate strength and the extreme concrete strain ε_c was studied by Blume, Newmark and Corning (42). The result is shown in Fig. 2.10. The yield moment is generally 95% or more of the ultimate strength.

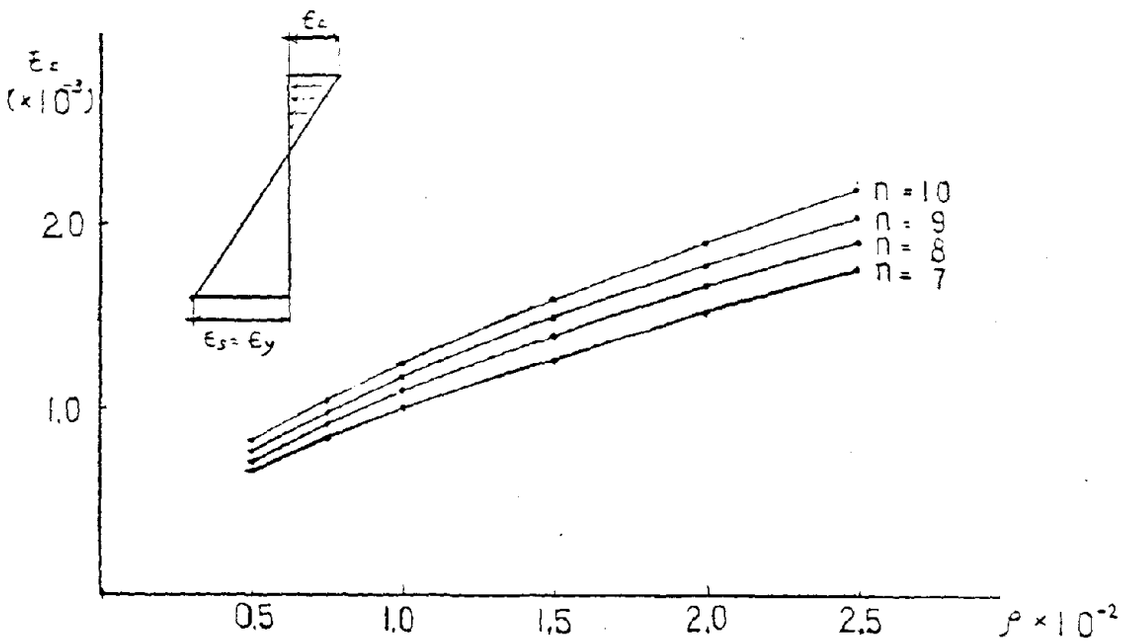

FIG. 2.9 RELATION BETWEEN ε_c AND ρ

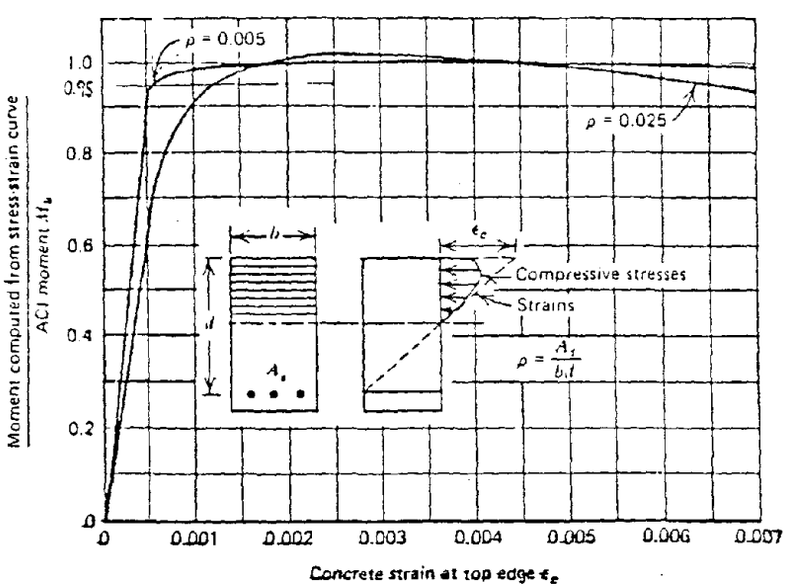

FIG. 2.10 MOMENT-STRAIN CURVES FOR A SINGLY REINFORCED CONCRETE BEAM BASED ON COMPRESSION TESTS ON CYLINDERS (42)

Therefore, for simplicity, the small increase in strength possible due to bottom reinforcement is ignored and calculated as follows:

$$M_y = 0.95\,\rho c_m d^2 f_y\,(1 - 0.6\rho f_y/f_c') \tag{2.4}$$

$$\phi_y = f_y/E_s\,(d - kd) \tag{2.5}$$

The stiffness between cracking and yielding (EI_y) is calculated as:

$$EI_y = (M_y - M_{cr}) \,/\, (\phi_y - \phi_{cr}) \tag{2.6}$$

The third break in the curve occurs at crushing, and the coordinates of that point (M_u, ϕ_u) are:

$$M_u = \rho\, c_m d^2 f_y\,(1 - 0.6\rho f_y/f_c') \tag{2.7}$$

$$\phi_u = (0.004)\,(0.72\, f_c')\,/\,\rho\, d\, f_y \tag{2.8}$$

Here, 0.004 instead of 0.003 is used as the crushing strain of the concrete because of the confining effect of the surrounding slab.

When $f_c' > 4{,}000$ psi, $0.85\,(0.85 - 0.05\,(\frac{f_c' - 4{,}000}{1{,}000}))$ should be used in place of 0.72 in Eq. 2.8. The stiffness between yielding and crushing (EI_u) is given by

$$EI_u = (M_u - M_y) \,/\, (\phi_u - \phi_y) \tag{2.9}$$

For the foregoing it is presumed that the shear force, V_n, acting on the flexural element does not exceed V_o, the shear capacity of the element, where $V_o = 4\, c_m d \sqrt{f_c'}$ for a connection without shear reinforcement and $V_o = 2c_m d \sqrt{f_c'} + 2A_v f_y d/s \leq 10\, c_m d \sqrt{f_c'}$ for a connection with shear reinforcement. If V_n exceeds V_o there is a redistribution of shear as discussed in Section 2.3.1.

Account could also be taken of the influence on M_u and ϕ_u of strain hardening of the tension bars, Bauschinger effects for the same bars for reversed cyclic loadings in the inelastic range,

confinement of the compressed concrete, and the presence of compression reinforcement. However, those influences are not large, can be offsetting, and are therefore ignored.

2.2.1.3 Cyclic Loading Response

To set up the model in a form appropriate for seismic analysis, the hysteresis loops must be defined for cyclic force-displacement relationships. The variations which occur in the relationship with load level and history must be considered in detail. Since there are many possible alternatives at each point in the loading history, it is not convenient to provide a continuous description of the moment-rotation curve. Therefore, a series of rules are developed for constructing the moment curvature curve for load reversals. The rules given for loading and unloading for different conditions are shown in Fig. 2.11. Those rules are basically the same as the rules proposed by Takeda et al., (33) and shown in Fig. 2.12.

The Takeda model has a bilinear envelope which allows for only one stiffness prior to yield. Further, the Takeda model assumes equal yield moments and stiffnesses for positive and negative moments. For this study, the Takeda model was modified so that the envelope could recognize both uncracked and cracked stiffnesses prior to yielding, as well as different yield moments and cracked section stiffnesses for positive and negative moments. Those modifications are appropriate because the Takeda rules were developed for beam sections. The change in stiffness with cracking is much less for beam sections of normal proportions than for slab sections. Further,

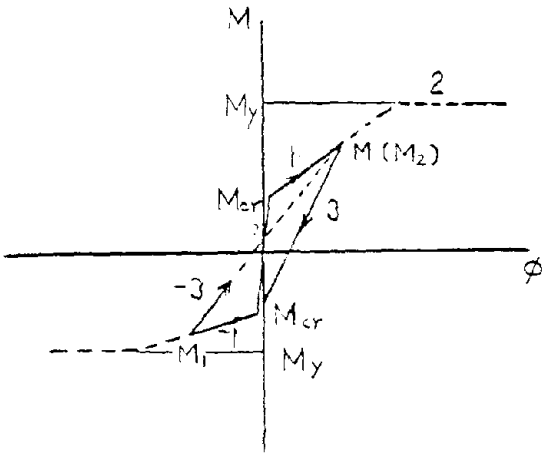

(a) after cracking until yield

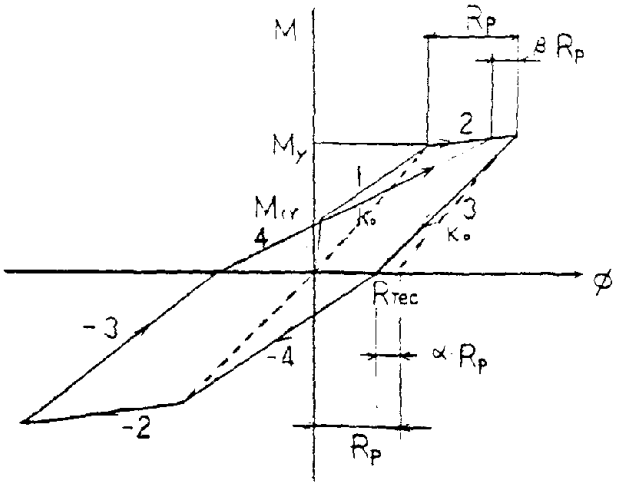

(b) after yield moment is exceeded

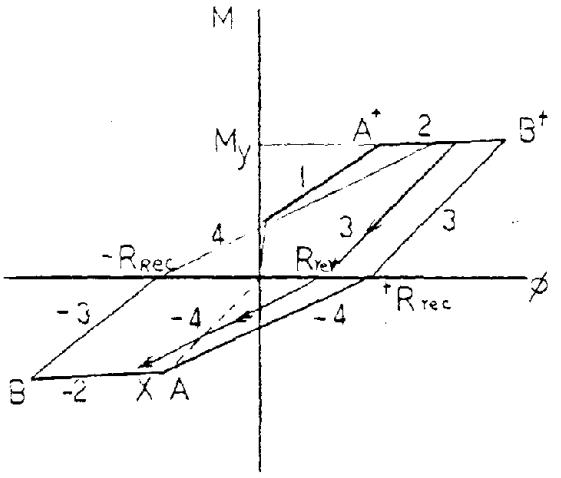

(c) after small yield excursion

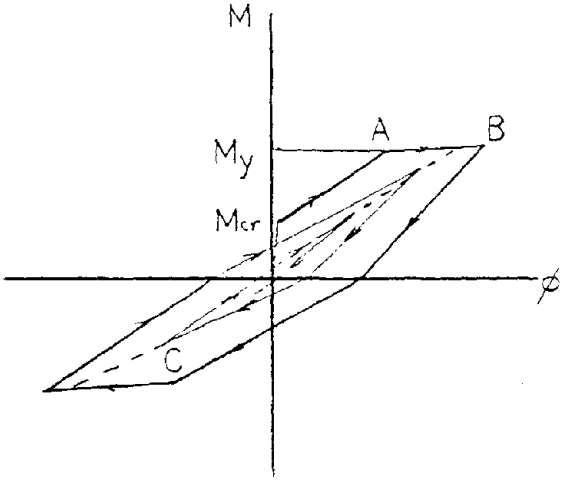

(d) small amplitude behavior

FIG. 2.11 FORCE-DEFORMATION RELATIONSHIP FOR FLEXURAL ELEMENT

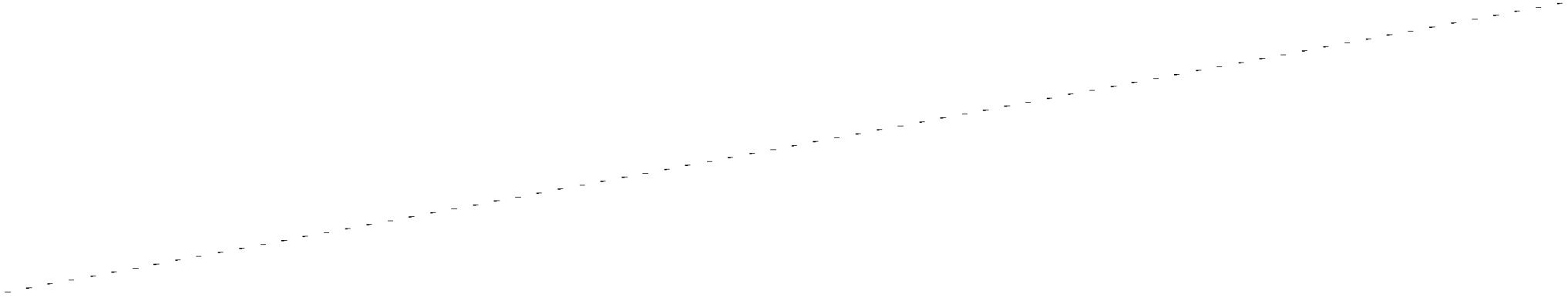

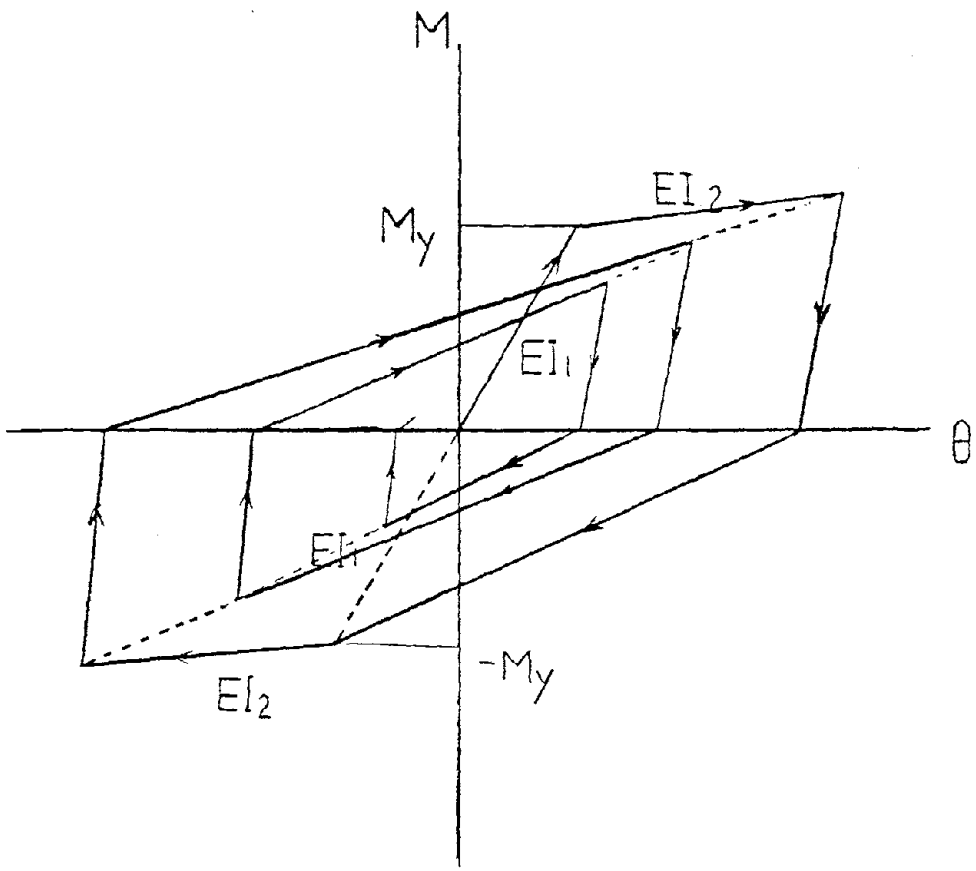

FIG. 2.12 MOMENT - ROTATION RELATIONSHIP FOR TAKEDA MODEL

while approximately equal top and bottom reinforcement ratios are likely in beams, the bottom reinforcement ratio in a slab for the width c_m is likely to be considerably less than the top reinforcement ratio. Further, since the Drain-2D program was to be used to predict cyclic loading results the unloading-reloading rules of the Takeda model were modified to a form consistent with the constraints of Drain-2D.

The cyclic loading rules are shown in Fig. 2.11, and are as follows:

Condition 1. The cracking moment, M_{cr}, has not been exceeded for one direction. The moment is reversed from a value M in the other direction. The moment $|M|$ is smaller than the yield moment $|M_y|$.

Rule - Unloading follows a straight line from conditions for the moment M to the conditions representing the cracking moment in the other direction.

Example - Segment 3 in Fig. 2.11(a). If unloading occurs before cracking, in the region near the origin, the rules provide no hysteresis loop.

Condition 2. The cracking moment has been exceeded in both directions. A moment M_1 is reached in one direction on the primary curve such that $|M_1|$ is larger than $|M_{cr}|$ but smaller than the yield moment $|M_y|$. The moment is then reversed to M_2 in the other direction such that $|M_2| < |M_1|$.

Rule - Unloading follows a straight line joining the position of return and the position at moment M_2.

Example - Segment (-3) in Fig. 2.11(a).

Condition 3. The yield moment, M_y is exceeded in one direction.

Rule - The unloading stiffness depends on the maximum deformation, and is controlled by the parameter α. This parameter dictates the unloading stiffness by locating the "recovery point," R_{rec}, as shown in Fig. 2.11(b)

The reloading stiffness also depends on the maximum deformation, and is controlled by the parameter β, shown in Fig. 2.11(b). According to Ref. (34), α typically ranges between zero and 0.4 and β between zero and 0.6 depending on the characteristics of the resisting sections. For these calculations α and β were taken as 0.2.

Example - Segments 3 and 4 in Fig. 2.11(b)

Condition 4. The yield moment M_y is exceeded in one direction but the cracking moment is not exceeded in the opposite direction.

Rule - Unloading follows Rule 3. Reloading heads to the yield moment - M_y in the other direction.

Example - Segment-4 in Fig. 2.11(b).

Condition 5. In the diagram shown in Fig. 2.11(c) the reversal point, R_{rev}, lies inside the positive recovery point, R_{rec}^{+}, because the inelastic excursion did not reach the previous maximum point B^{+}.

Rule - Reloading to a point X is assumed, where X lies between points A and B, at a location which depends on the location of R_{rev} between the limiting recovery points R_{rec}^{-} and

R_{rec}^{+}. The specific relationship which is assumed for negative reloading is:

$$\frac{AX}{AB} = \frac{R_{rec}^{+} - R_{rev}}{R_{rec}^{+} - R_{rec}} \qquad (2.10)$$

Example - Segment-4 in Fig. 2.11(c)

Condition 6. A series of small amplitude cycles, as illustrated in Fig. 2.11(d).

Rule - The assumed behavior is identical to that of the Takeda model, except that the reloading stiffness, from point C to line AB, is based on the position of the most recent reversal point.

Example - Fig. 2.11(d)

2.2.2 Torsional Element

2.2.2.1 General Configuration

The torsional element is assumed to project from the colum face towards the slab edge and to have a depth h, as shown in Fig. 2.2. The effective width of the element varies with cracking.

The width is taken as c_1 before cracking since most test results show cracks initiating at the column corners for the gravity load condition and a reduced stiffness is likely at the column corners. For the reasons discussed previously for the flexural element, after cracking the width is assumed to increase to $c_1 + d$; ($c_1 + d/2 - l_g$; in the case of an edge connection transferring moment normal to the edge of corner connection). That increase accounts for moment

redistribution and the stiffening effect of surrounding bars. That width also corresponds to the width of the critical section for shear at the torsion face in ACI Code 318.

The effective length of the torsional element varies with the crack pattern, the change in rotation along the length of the element, and the strain distirbution for the reinforcing bars within the element. As apparent from Figs. 2.13, 2.14 and Fig. 2.15, there is probably a small change in the effective length of the element with change in the rotation and with change in the strain in the reinforcing bars. Analysis of the test results showed that there were some variations in the length with bar size and distribution, concrete strength and loading conditions. However, to avoid modeling complexities, and because use of constant characteristics resulted in predictions in reasonable agreement with test data, the length of the torsional element was taken as the distance to the slab edge where the element was uncracked and as 1.5h where the element was cracked.

2.2.2.2 Distribution of Torsional Moment

Since the torsional element protrudes out of the 2-dimensional plane that is the idealized column and slab, it is appropriate to model that element as a spring as shown in Fig. 2.3. Some distribution must be assumed for the torsional moment in order to determine the proper stiffness for that spring. Once the distribution of moment and the rigidity of the torsional element are known, the stiffness of torsional spring can be readily calculated. The tests conducted at the University of Washington (Refs. 3 to 26) provide

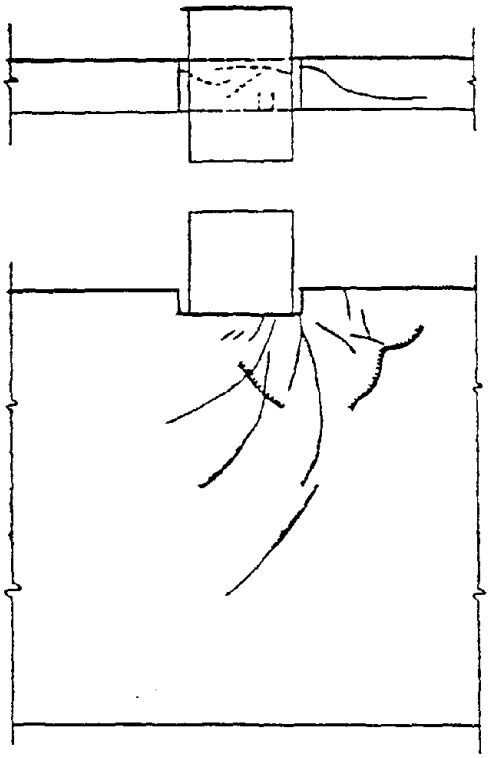

FIG. 2.13 TYPICAL CRACK PATTERN OF TORSIONAL ELEMENT REFERENCE(30)

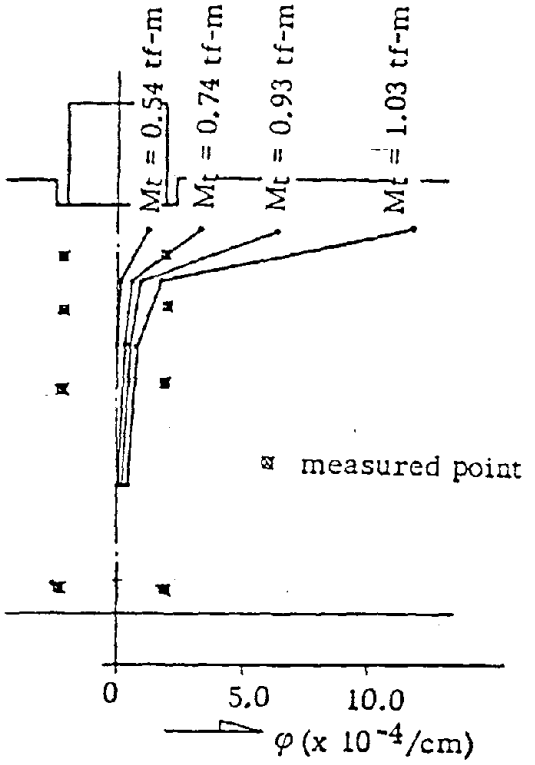

FIG. 2.14 ANGLE OF TORSION OF SPECIMEN T-3 REFERENCE (30)

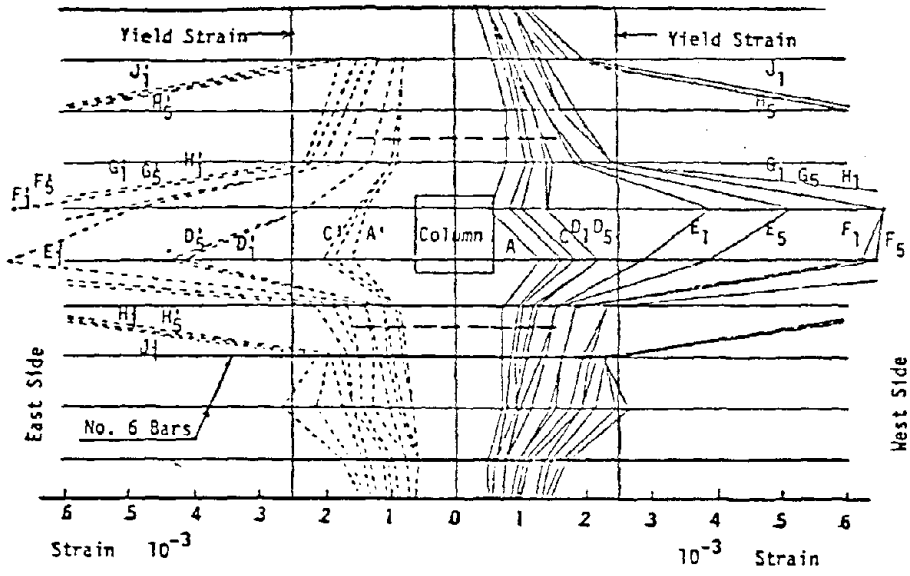

(a) SS-1

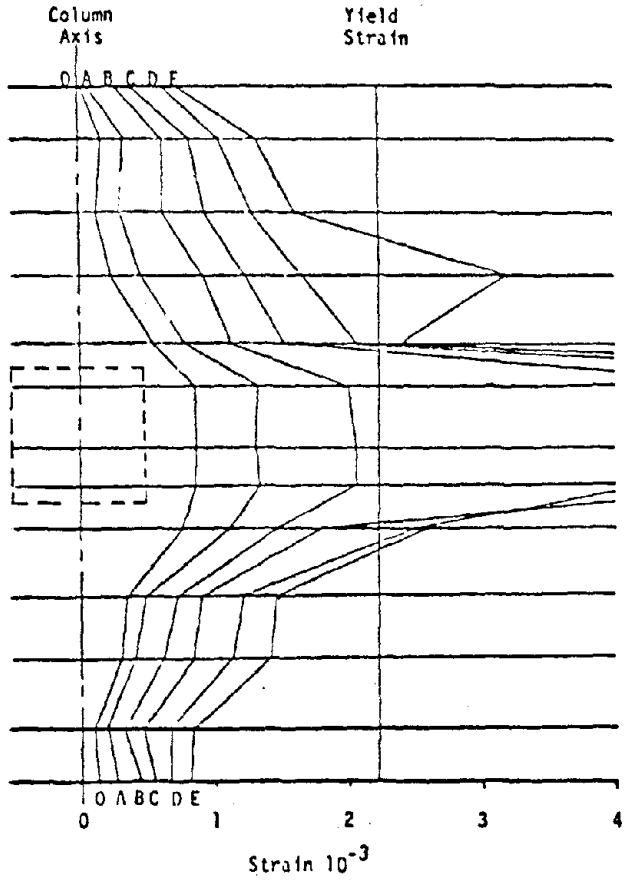

(b) E-2

FIG. 2.15 TENSILE STRAINS IN TOP REINFORCING BARS

data on the strain distribution in the reinforcing bars passing through the torsional element. Typical examples are shown in Fig. 2.15.

If the distribution of moments across the width of the slab induces torsional moment in the torsional element, then its unit torsional moment is probably directly proportional to the stress in the reinforcing bars passing through it. With that assumption, and with the strain distribution in the reinforcing bars simplified as shown in Fig. 2.16(a), the induced moment distribution becomes as shown in Fig. 2.16(b).

Yielding of the reinforcing bars in the flexural element quickly causes cracking of the torsional element or vice versa. Therefore, it is assumed that yielding of the reinforcing bars also means cracking of the torsional element. Then, two moment and stiffness conditions for the torsional element must be recognized: 1. Those before cracking; and 2. Those after cracking as shown in Figs. 2.16(c) and (d).

The distribution of the unit twisting moment and the resulting distribution for the rotation for conditions before cracking are the same as those implied in the ACI Code. The stiffness of the torsional spring for this stage is then as follows:

$$T = KT_1\theta \tag{2.11}$$

and

$$KT_1 = \frac{6GJ_o}{\ell_t} \quad \text{or} \quad \left(KT_1 = \frac{3GJ_o}{\ell_t} \text{ for one side only}\right) \tag{2.12}$$

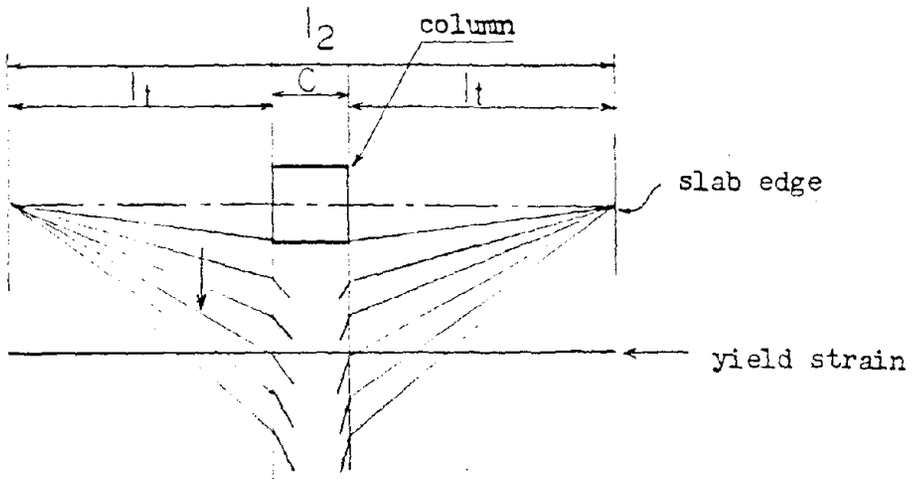

(a) distribution of strain in top reinforcing bars

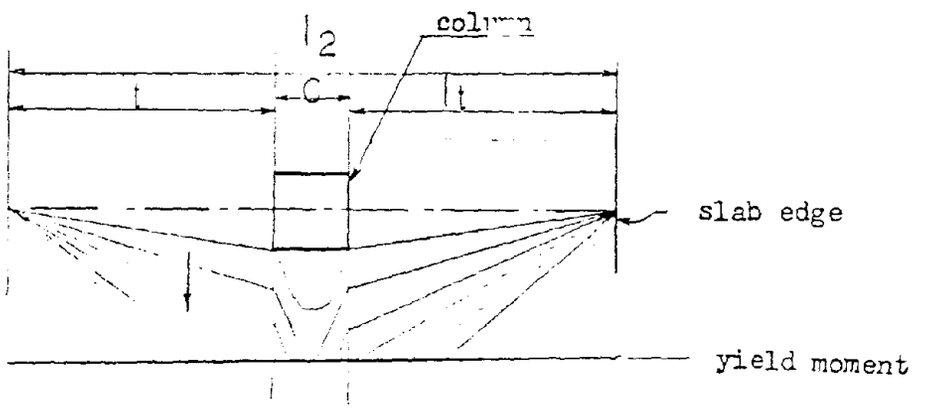

(b) distribution of induced unit moment in torsional element

FIG. 2.16 DISTRIBUTION OF MOMENT IN TORSIONAL ELEMENT

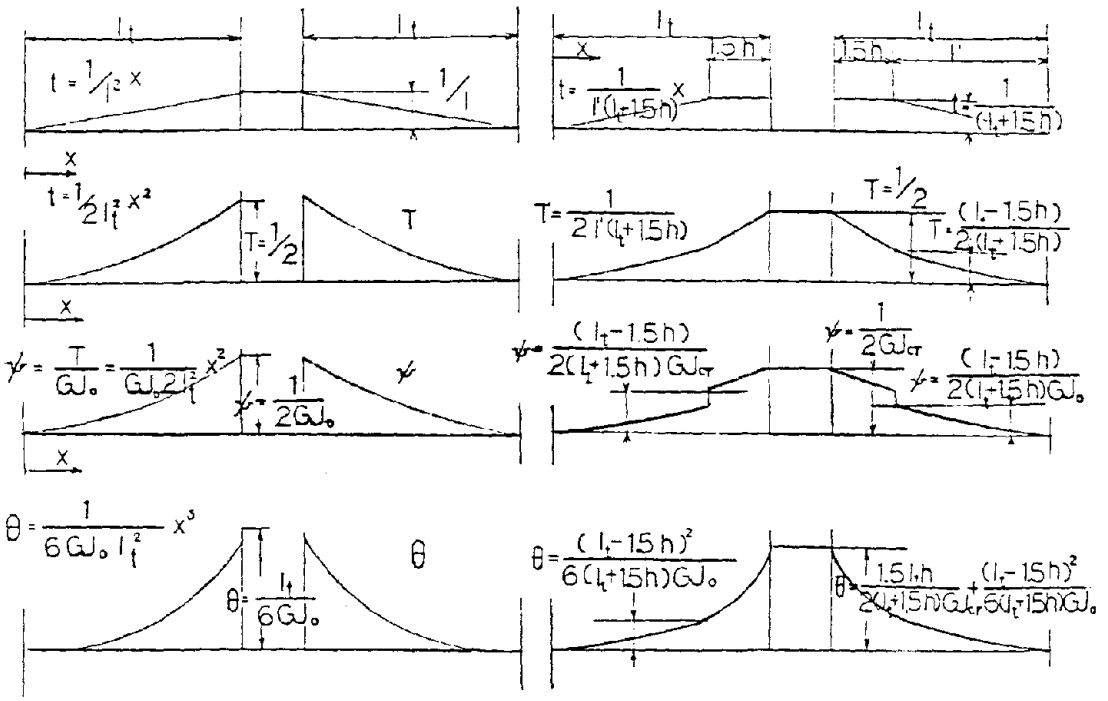

$$\theta = \frac{l_t}{6GJ_o}$$

$$K_{t1} = \frac{6GJ_o}{l} \quad \text{for both sides}$$

$$K_{t1} = \frac{3GJ_o}{l} \quad \text{for one side}$$

$$\theta = \frac{1.5\,l_t\,h}{2(l_t+1.5h)GJ_{cr}} + \frac{(l_t-1.5h)^2}{6(l_t+1.5h)GJ_o}$$

$$K_{t2} = \frac{6(l_t+1.5h)}{\left\{\frac{4.5l_th}{GJ_{cr}} + \frac{(l_t-1.5h)^2}{GJ_o}\right\}} \quad \text{for both sides}$$

$$K_{t2} = \frac{3(l_t+1.5h)}{\left\{\frac{4.5l_th}{GJ_{cr}} + \frac{(l_t-1.5h)^2}{GJ_o}\right\}} \quad \text{for one side}$$

(c) rigidity before cracking (d) after cracking

FIG. 2.16 DISTRIBUTION OF MOMENT IN TORSIONAL ELEMENT

where ℓ_t is the distance from column face to the edge of the slab, and GJ_o is the torsional rigidity of the element in pure torsion calculated as described in the next section. Stiffnesses calculated from Eq. (2.12) are slightly less than the stiffnesses specified in ACI Code 318, Chapter 13, for the torsional member in the equivalent frame method.

The distribution of the unit twisting moment for the post-cracking condition differs from that for the uncracked condition. The distribution takes into account the cut-off in unit twisting moment imposed by yieding of the reinforcing bars. While the shift from the "before cracking" condition to the "after cracking" condition is in fact continuous, the recognition of only two stages is adequate enough for this analysis. The distribution shown in Fig. 2.16 with a step change in unit twist at 1.5h from the column face is used for the post-cracking condition. The stiffness of the torsional spring for that stage is then as follows

$$T = KT_2\theta \tag{2.13}$$

where

$$KT_2 = \frac{6(\ell_t + 1.5h)}{\frac{4.5\ell_t h}{GJ_{cr}} + \frac{(\ell_t - 1.5h)^2}{GJ_o}} \quad \text{or} \quad \left(KT_2 = \frac{3(\ell_t + 1.5h)}{\frac{4.5\ell_t h}{GJ_{cr}} + \frac{(\ell_t - 1.5h)^2}{GJ_o}}\right. \text{for one side only)} \tag{2.14}$$

GJ_{cr} is the torsional rigidity of the element in pure torsion after cracking. Since GJ_{cr} is very small compared to GJ_o, Eq. (2.14) can be simplified as follows:

$$KT_2 = \frac{6(\ell_t + 1.5h)}{4.5\, h\ell_t} GJ_{cr} \text{ or } \left(KT_2 = \frac{3(\ell_t + 1.5h)}{4.5\, h\ell_t} GJ_{cr} \right. \quad (2.15)$$

for one side only)

The stiffness predicted by Eq. 2.15 is much less than the uncracked section stiffness. However, it is close to the result measured in slab-column tests. Symonds (5) neglected the stiffness contribution of the portion of the slab more than 1.5h from column face. That assumption, while simple, results in a torsional stiffness, significantly less than that measured in tests.

Since test data that can define this distribution precisely are lacking, it is difficult to check in detail these assumptions concerning that distribution. However, from the University of Washington test results, as shown in Fig. 2.15, it is apparent that this assumption must be close to what actully occurs.

The rigidities GJ_o and GJ_{cr} are obtained as described in the next section.

2.2.2.3 Monotonic Loading Response

The hexa-linear curve of Fig. 2.17(a) defines the monotonic loading response and the cyclic loading envelope. As was the case for the flexural element, critical torques and twists are again calculated using widely accepted reinforced concrete formulas. The first break in the curve occurs at cracking. The coordinates (T_{cr}, θ_{cr}) for that condition are:

$$T_{cr} = GJ_o\, \psi_{cr} = KT_1\, \theta_{cr} \quad (2.16)$$

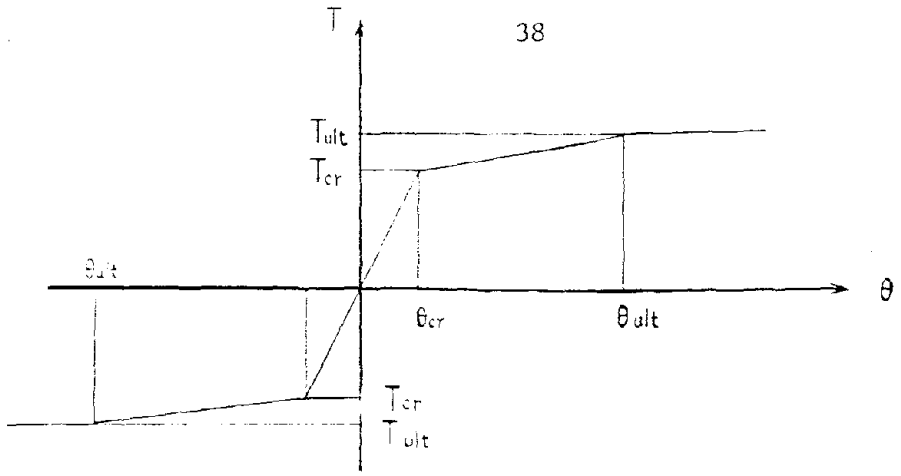

(a) primary curve for torsional stiffness

$$T_{cr} = 6c_1 \sqrt[3]{f'_c}(h^2 + 10) \tag{2.18}$$

$$\theta_{cr} = T_{cr}/KT_1 \tag{2.19}$$

$$KT_1 = 6GJo/\ell t \tag{2.12}$$

$$T_y = 0.8c_t h^2\sqrt{f'_c} + \alpha c_t d^*\left(\frac{A_{h2}f_y}{sh_2} + \frac{A_v f_y}{s_v}\right) \tag{2.20}$$

$$(\alpha = 0.66 + 0.33ct/d^* \leq 1.5) \tag{2.21}$$

$$\frac{T_u}{T_y} + \left(\frac{V_g}{V_o}\right)^2 \leq 1.0 \quad \text{or} \tag{2.23}$$

$$\left(\frac{3T_u\delta}{12c_t^2\, h\sqrt{f'_c}}\right)^2 + \left(\frac{V_g}{V_o}\right)^2 \leq 1.0 \tag{2.24}$$

$\delta = 3(c_t - \frac{2}{3}h)h/c_t^2$ when $c_t \geq 2h$; otherwise $\delta = 1$

where

$$V_o = 4c_t d\sqrt{f'_c} \tag{2.25}$$

without shear reinforcement

$$V_o = 2c_t d\sqrt{f'_c} + 2A_v f_y d/s_v \leq 10c_t d\sqrt{f'_c} \tag{2.26}$$

with shear reinforcement

FIG. 2.17 FORCE-DEFORMATION RELATIONSHIP FOR TORSIONAL ELEMENT

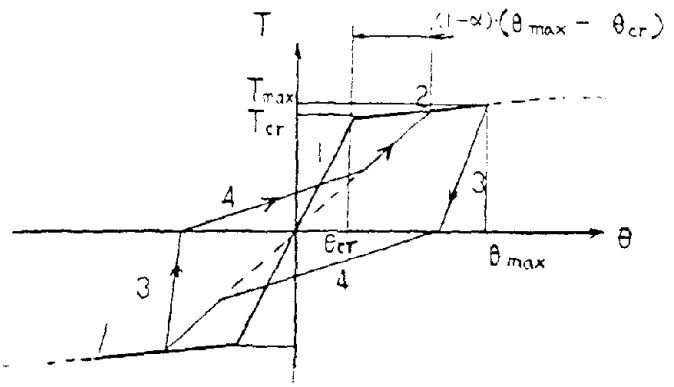

(b) excursion between cracking and maximum capacity

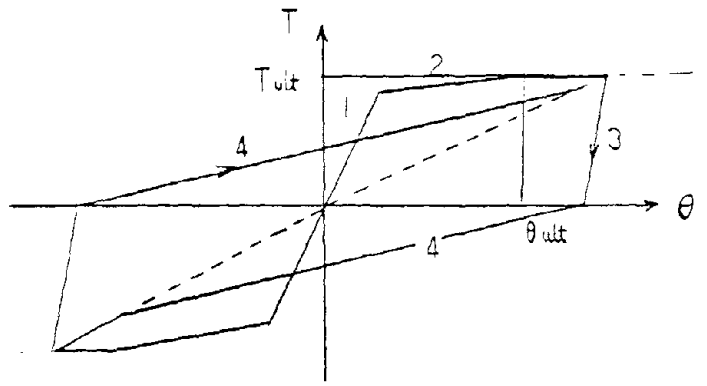

(c) excursion after reaching maximum capacity

FIG. 2.17 CONTINUED

where:

$GJ_o = G_c J_o$; G_c = shear rigidity of concrete ($G_c = \frac{E_c}{2(1+\nu)}$), ψcr = unit rotation which causes cracking; KT_1 is given by Eq. (2.12); and J_o is the torsional constant which for a rectangular section, free to warp, has been derived by Timoshenko (35) as

$$J_o = \frac{1}{3} h^3 c_1 \left(1 - 0.63 \frac{h}{c_1}\right) \tag{2.17}$$

For an interior column connection or an edge column connection transferring moment parallel to the edge, J_o is increased by the warping restraints imposed by the surrounding slab. For this analysis J_o is multiplied by $h/(h - 0.27\ c_1) < 2.0$ to account for those restraints. That factor is similar to that derived by Timoshenko (35) for a beam completely restrained against warping.

Based on experimental evidence, Hsu (36) has proposed that the nominal ultimate torsional capacity of plain concrete is that given by the following expression:

$$T_{cr} = 6c_1 \sqrt[3]{f'_c}\ (h^2 + 10) \tag{2.18}$$

The influence of the direct shear caused by the gravity load on the T_{cr} value is small and generally can be neglected. θ_{cr} is obtained from Eqs. (2.16, 2.17 and 2.18) as follows:

$$\theta_{cr} = T_{cr}/KT_1 \tag{2.19}$$

The second break in the curve occurs at the ultimate strength of the element. The coordinates at that break (T_u, θ_u) are calculated as follows:

$$Ty = 0.8\ c_t h^2 \sqrt{f'_c} + \alpha(c_t - \ell_g)\ d^* \left(\frac{A_{h2} f_y}{s_{h2}} + \frac{A_v f_y}{s_v}\right) \qquad (2.20)$$

$$\alpha = 0.66 + 0.33\ (c_t - \ell_g) / d^* \leq 1.5 \qquad (2.21)$$

where, $c_t = (c_1 + d)$ for interior connnections and edge connections transferring moment parallel to the edge; and $c_t = (c_1 + d/2)$ for all other cases. In the case of an edge column connection transferring moment normal to the edge, and a corner column connection, when s_v or s_{h2} is larger than 0.75d or $\frac{(c_t - \ell_g) + (d-d')}{4}$, Ty should be calculated as follows:

$$T_y = 6h\ (c_t^2 + 10)\ \sqrt[3]{f'_c} \qquad (2.22)$$

Equation 2.22 implies that the ultimate capacity equals the torsional capacity for a plain concrete section that fails as a result of cracking of its larger cross-sectional dimension.

The quantities A_{h2}, A_v, s_{h2}, s_v, d* and ℓg have the values shown in Fig. 2.18. The capacity in combined shear and torsion is given by:

$$\frac{T_u}{T_y} + \left(\frac{V_g}{V_o}\right)^2 \leq 1.0 \qquad (2.23)$$

or

$$\left(\frac{3\ Tu}{12\ c_t^2 h \sqrt{f'_c}}\right)^2 + \left(\frac{Vg}{V_o}\right)^2 \leq 1.0 \qquad (2.24)$$

whichever is the lesser value for T_u

where $V_o = 4c_t d \sqrt{f'_c}$ for a connection without shear reinforcement (2.25)

and

$V_o = 2c_t d \sqrt{f'_c} + 2A_v f_y d/s_v \leq 10c_t d\sqrt{f'_c}$ for a connection with shear reinforcement.

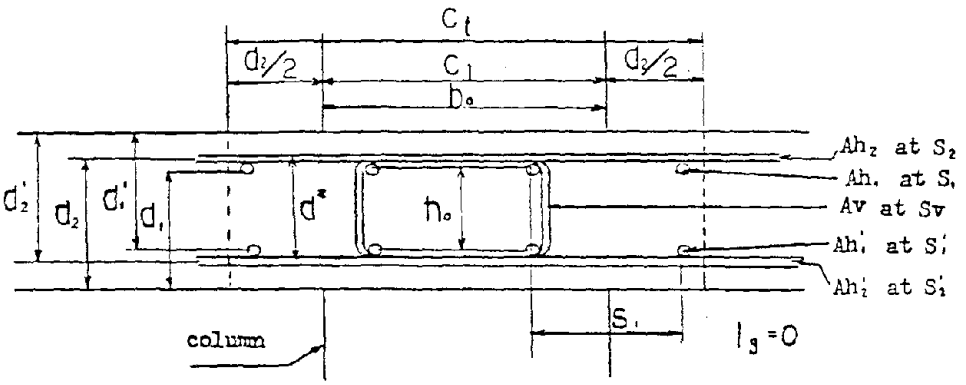

Because of downward shear loading, preexisting on the connection due to gravity load Ah for Eq. 2.28 equals Ah_2 and $A_\ell = 2Ah_1 + 2Ah_1'$

(a) Typical Face of Interior Connection

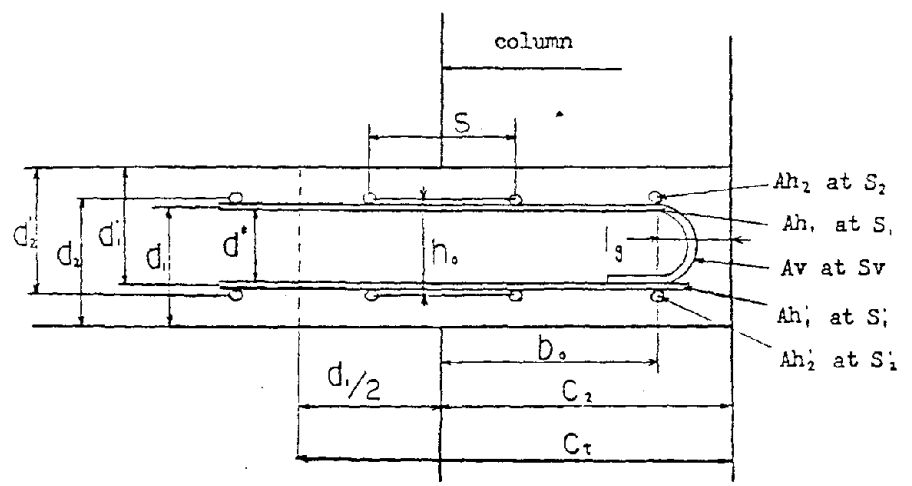

For Eq. 2.28 $Ah = Ah_1$ and $A_\ell = 2Ah_2 + 2Ah_2'$

(b) Side Face of Exterior Connection

FIG. 2.18 TYPICAL FACE AND NOTATIONS

When c_t is more than twice h, T_u in Eq. 2.24 must be multiplied by $3(c_t - 3h)h/c_t^2$ (35) in order to recognize that the torsional moment is resisted primarily by the outer fibers of the section.

As discussed previously, if the shear in the flexural element exceeds the shear capacity of that element, then excess shear is transferred to the torsional element and the value of V_g in Eqs. (2.23) and (2.24) must be increased accordingly. The ultimate deformation θ_u is obtained from the following equation:

$$T_u = GJ_{cr}\,\psi_u = KT_2\,\theta_u \tag{2.27}$$

where

J_{cr} = torsional rigidity of a cracked torsional element in pure torsion and KT_2 is given by Eq. (2.15). Lampert (37) has derived an expression for GJ_{cr} using the space truss model shown in Fig. 2.19(a). When the governing equations for that model are solved, the following expression is obtained for GJ_{cr}.

$$GJ_{cr} = \frac{4E_s\,(b_o h_o)^3}{u^2} \quad \frac{1}{\left(\frac{1}{\rho h} + \frac{1}{\rho s} + 4u\lambda\frac{b_o h_o}{ut}\right)} \tag{2.28}$$

where

$u = 2\,(b_o + h_o)$; $\rho h = \frac{A_h u}{s b_o h_o}$; $\rho \frac{A_\ell}{s\ b_o h_o}$; t is nominal wall thickness, $t = b_o/5$ for solid member; λ is a modification factor; A_h, A_ℓ b_o and h_o are as shown in Fig. 2.18.

Lampert concluded that the influence of λ was not small, as shown in Fig. 2.19(b), but he neglected that term for simplicity. Therefore, for simplicity for this study λ is also taken as zero.

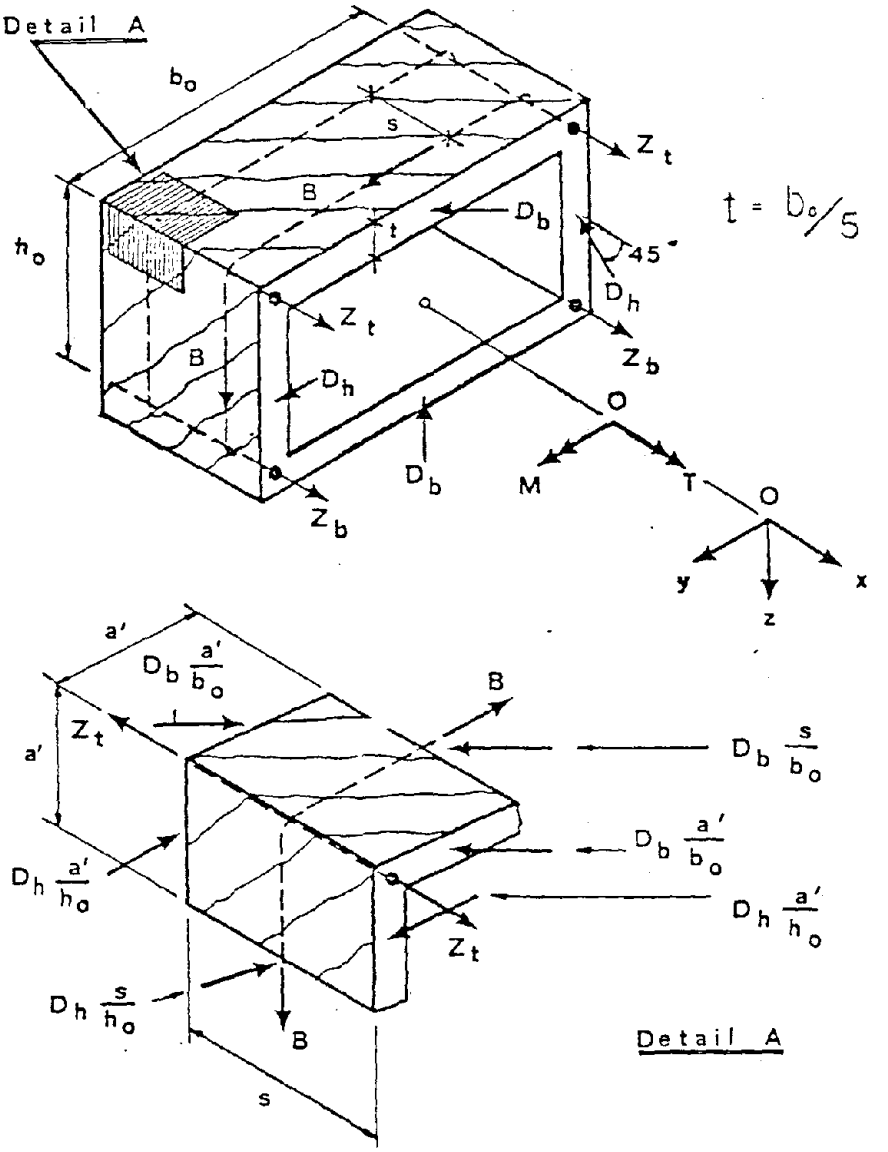

FIG. 2.19(a) RECTANGULAR SPACE TRUSS MODEL WITH 45° DIAGONALS (REFERENCE(37))

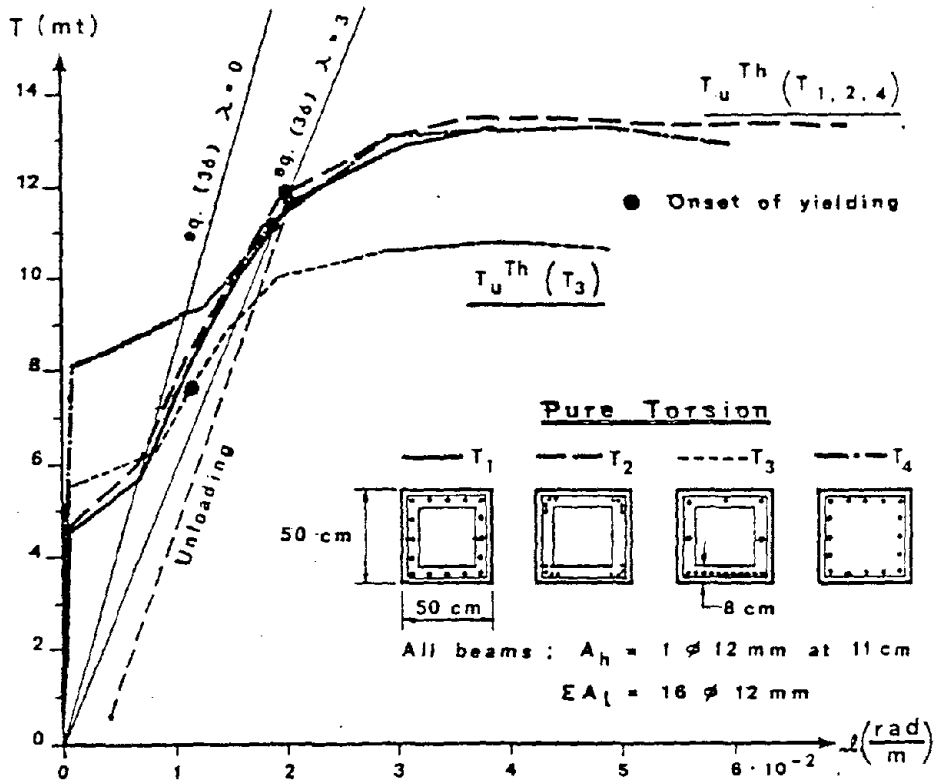

FIG. 2.19(b) TORQUE-TWIST CURVES OF HOLLOW AND SOLID CROSS-SECTIONS WITH DIFFERENT DISTRIBUTIONS OF LONGITUDINAL STEEL (Ref.37)

In accordance with accepted experimental evidence the influence of bending moment and shear on the torsional rigidity is neglected since in general that influence is small. However, for interior column connections or edge column connections transferring moment parallel to the edge, GJ_{cr} is multiplied by $h/(h-0.27c_1) \leq 2.0$ to account for the stiffening effect of the surrounding slab. That is the same multiplication factor as used for the before cracking condition.

The stiffness between cracking and the ultimate condition is given by the following expression:

$$KT_2 = (T_u - T_{cr}) / (\theta_u - \theta_{cr}) \qquad (2.29)$$

2.2.2.4 Cyclic Loading Response

For dynamic analysis, a series of rules are established for the load-deformation relationship for loading reversals. Most of those rules for a given point on the loading history are the same as the rules for the same conditons for the flexural element. In the following, rules are stated only where they differ from those for the flexural element. The rules are illustrated in Fig. 2.17(b) and (c).

Condition 1. Unloading from primary curve after cracking.

Rule - Unloading stiffness is given by Eq. (2.16).

Example - Segment 3 in Fig. 2.17(b).

Condition 2. Reloading after major excursion in opposite direction.

Rule - Reloading stiffness is calculated from Eq. (2.30) until the loading path intersects the line which connects the origin and the coordinate $[\alpha(\theta_{max} - \theta_{cr}),\ \alpha(T_{max} - T_{cr})]$ where

α is defined in the same manner as for the flexural element (Fig. 2.11(b))and equals unity when the previous excursion exceeds θ_u.

Example - Segment 4 in Fig. 2.17(b) and segment 4 in Fig. 2.17(c). The reloading stiffness for condition 2 is calculated as follows:

$$GJ_{re} = \frac{4\,(b_o h_o)^3}{u} \quad \frac{1}{\frac{s}{K_h} + \frac{u}{2}\left(\frac{1}{K} + \frac{1}{K'}\right)} \tag{2.30}$$

where K_h = bondslip stiffness of shear reinforcement; K = bondslip stiffness of top reinforcement, and K' = bondslip stiffness of bottom reinforcement.

The bondslip stiffness is discussed in Section 2.2.4.

2.2.3 Connecting Bar Element

This element interconnects the torsional element at a distance 1.5h from the column face to the end of flexural element as shown in Fig. 2.20(a).

A torsional element 1.5h long rotating freely under an imposed torque develops relative displacements as shown in Fig. 2.20(b). However, for the slab-column connection the torque is imposed by bending and shear transferred from the slab to the torsional element. Deformations are as shown in Fig. 2.20(a). If the torsional element is represented by a rigid bar only, then direct interconnection of the ends of the torsional and flexural elements results in too large a stiffness for the connection. The rotation of end of the flexural element is completely governed by the rotation of torsional element.

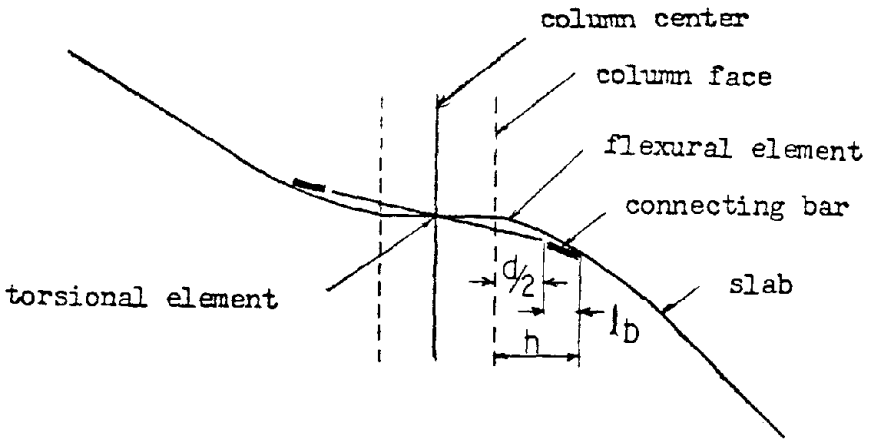

(a) General Deformed Shape

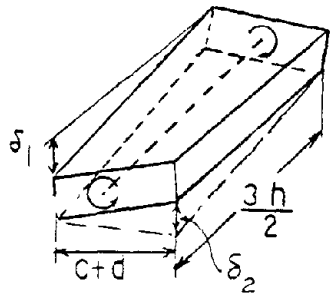

$$\theta = \frac{\delta_1 + \delta_2}{C+d}$$

(b) Deformation of Beam in Torsion

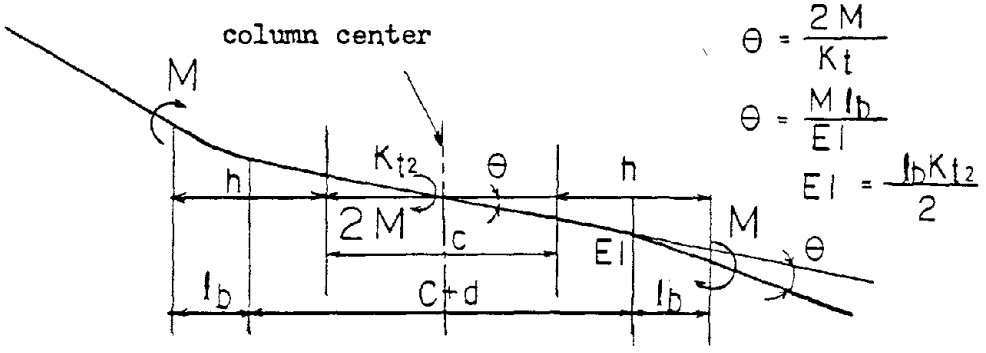

$$\theta = \frac{2M}{K_t}$$

$$\theta = \frac{M l_b}{EI}$$

$$EI = \frac{l_b K_{t2}}{2}$$

(c) Stiffness of Connecting Bar

FIG. 2.20 STIFFNESS OF CONNECTING BAR

To avoid that problem, a connecting bar is introduced into the model. The influence of the rigidity of that bar on the total stiffness is significant. Presently there are no test data available against which the stiffness of this element can be calibrated. Therefore, properties for the connecting bar were determined by trial and error utilizing the overall stiffness measured in the tests and the general deformed shape for the connection region in those tests.

The stiffness is calculated as shown in Fig. 2.20(c) using the following assumptions:

1. The length of the connecting bar is taken as $\ell_b = h - \frac{d}{2}$.
2. For this connecting bar, the change in slope is the same as that which occurs at the center of the torsional element at 1.5h from the column face when the same amount of moment is applied.
3. The torsional stiffness is calculated assuming that the element is cracked.
4. The stiffness of the connecting bar is calculated assuming that the torsional element is cracked, even when that element is uncracked.
5. For cyclic loading the stiffness used for both loading and unloading is the same as that for monotonic loading.

The first and second assumptions are appropriate because the rotation of the connecting bar then becomes independent of its length, and the appropriate length for that bar is not obvious. The fourth assumption is necessary because, even for gravity loadings, the connecting bar has a stiffness markedly less than the uncracked

stiffness due to stress concentration effects introduced by the column corners. The fifth assumption is appropriate because all energy absorption and dissipation are then provided by other elements of the connection. That assumption is consistent with observed results.

2.2.4 Bond Slip Element

2.2.4.1 General Configuration

As shown in Fig. 2.2 and 2.3 this element is a semi-rigid connection between the flexural elements and the front and back faces of the column. A bond slip element is necessary because the University of Washington tests showed wide cracks at the column faces as indicated in Fig. 2.6. Further, analysis of those tests results showed that the influence of bond slip on deformations was very significant (12) (13).

2.2.4.2 Monotonic Loading Response

As shown in Fig. 2.21(a) a bi-linear curve in each quadrant defines the monotonic loading response curve. The break in the curve occurs at yielding of the reinforcing bars. The coordinates of that point (M_{yb}, θ_{yb}) are obtained as follows:

$$M_{yb} = KB_1\theta_y \tag{2.31}$$

$$M_{yb} = M_y c_2/(c_2 + d) \tag{2.32}$$

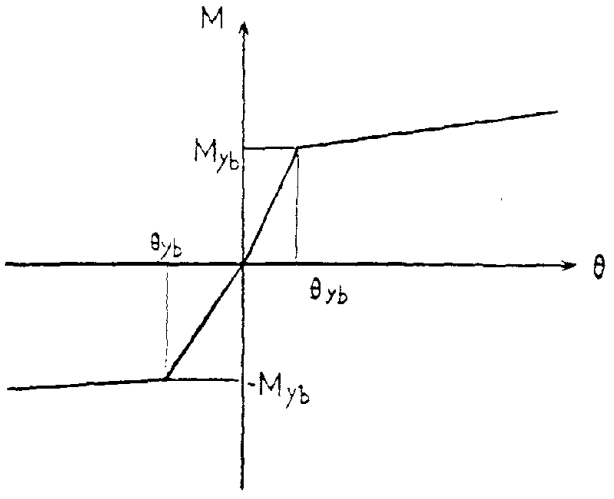

primary curve for bond slip element

$$M_{yb} = 0.95\rho c_2 d^2 f_y (1 - 0.6\rho f_y / f'_c) \quad (2.32)$$

$$\theta_{yb} = M_{yb} / KB_1 \quad (2.31)$$

$$KB_1 = (d - kd/3) n_b Kd^* \quad (2.37)$$

$$KB_2 = 1/30\ KB_1 \quad (2.39)$$

FIG. 2.21 FORCE-DEFORMATION RELATIONSHIP FOR BONDSLIP ELEMENT

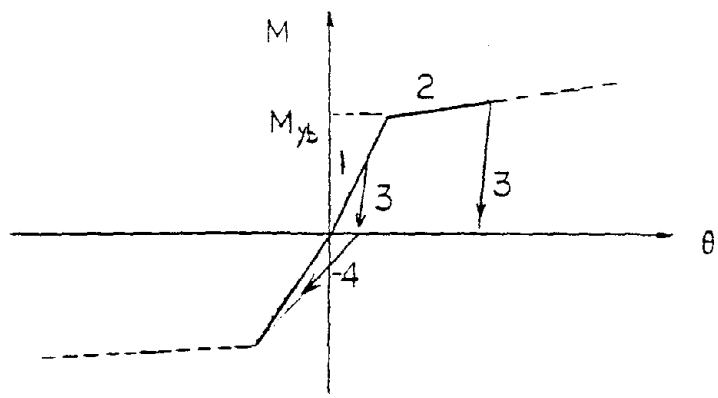

(b) unloading stiffnes

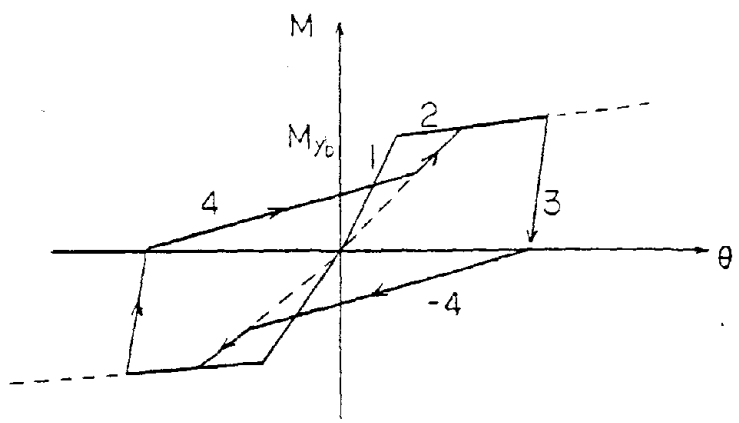

(c) reloading stiffness

FIG. 2.21 CONTINUED

where M_y is the yield moment defined by Eq. (2.4) and KB_1 is obtained from test results and the assumptions described in this section.

The relation between the amount of bond slip and the rotation of the edge of the flexural element when a crack does not extend through the depth of the element, is shown in Fig. 2.22. The slip for the reinforcing bar in compression in the bottom of the section is small compared to that for the top bar and therefore bottom bar slip effects for a non-through depth crack are ignored. As the top bar slips under the applied moment, the rotation increases from the value indicated by the dash-dot line to that represented by the broken line. Strictly speaking, such a rotation causes a decrease in both the force in the tension bar and in the compression strain in the compression region. Those changes decrease the bond sip to the final rotation indicated by the unbroken line. However, that decrease is a second order effect and can be neglected. Thus, the increase in rotation caused by bond slip can be approximated by the following equation.

$$\theta \text{ by bond slip} = \Delta \text{ slip}/d^* \tag{2.33}$$

$$\Delta \text{ slip} = Fy/n_b\ K \tag{2.34}$$

$$F_y = M_{yb}/\left(d - \frac{kd}{3}\right) \tag{2.35}$$

$$\theta_{yb} = \frac{1}{\left(d - \frac{kd}{3}\right) n_b\ K\ d^*}\ M_{yb} \tag{2.36}$$

$$KB_1 = \left(d - \frac{kd}{3}\right) n_b\ K\ d^* \tag{2.37}$$

where d = the effective depth; d* = the distance between the compression and tension bars; F_y = tension force; and n_b = the number of

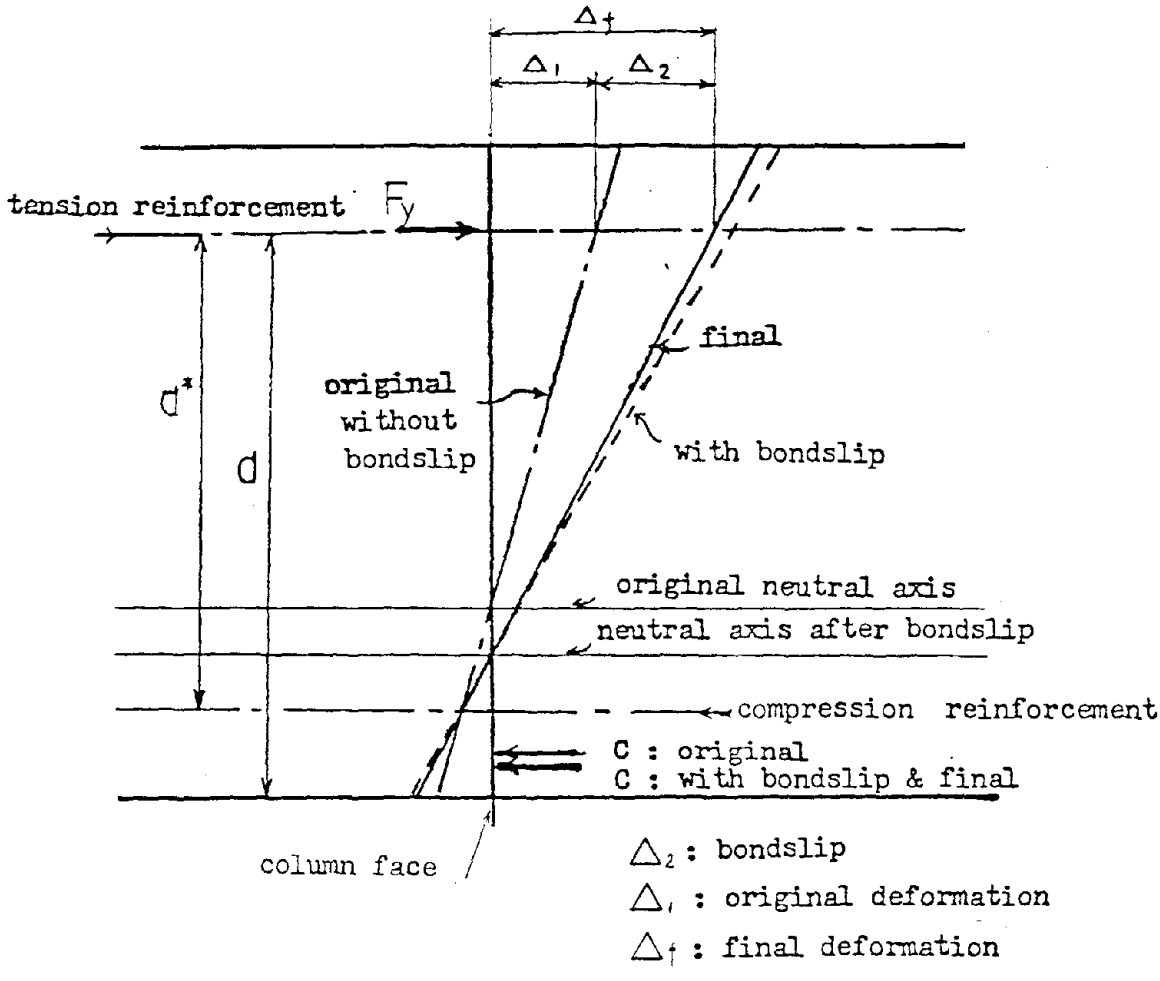

FIG. 2.22 STRESS AND ROTATION RELATIONSHIP WITH BONDSLIP

tension bars within the width c_2 of the flexural element of width c_2. The quantity K is the bond slip stiffness. It is a function of bar diameter and concrete strength. The following expression for that stiffness has been recommended by Hawkins (12) for the range where a bar is not yielding.

$$K = (1{,}250\ d_b^2 + 1{,}900)\ \sqrt{f'_c/3{,}200} \quad \text{(kips per inch)} \tag{2.38}$$

where d_b is the bar diameter in inches.

After yield of the bar, the K value decreases very rapidly. According to Ref. (38), that decrease is in direct proportion to the ratio Esy/Es where Esy is the strain hardening modulus for the reinforcing bars after yield. Stress-strain curves for the bars used in specimens S1, S2, etc of the University of Washington tests are shown in Fig. 2.23. For those curves the ratio Esy/Es is about 1/30. Hence, Eq. 2.39 is used for this investigation.

$$KB_2 = 1/30\ KB_1 \tag{2.39}$$

2.2.4.3 Cyclic Loading Response

Most of the possible alternatives for each point in the loading history are the same as those for the torsional element. The only differences are in the values for the unloading and reloading stiffnesses.

As shown in Fig. 2.21(b) the unloading stiffness for a crack not extending through the depth of the member is taken as twice the initial stiffness KB_1 (38). Thus segment 1 in Fig. 2.21(b) has a stiffness KB_1 and segments 3 have stiffnesses (2 KB1). If unloading occurs from the envelope before yielding then after the zero moment

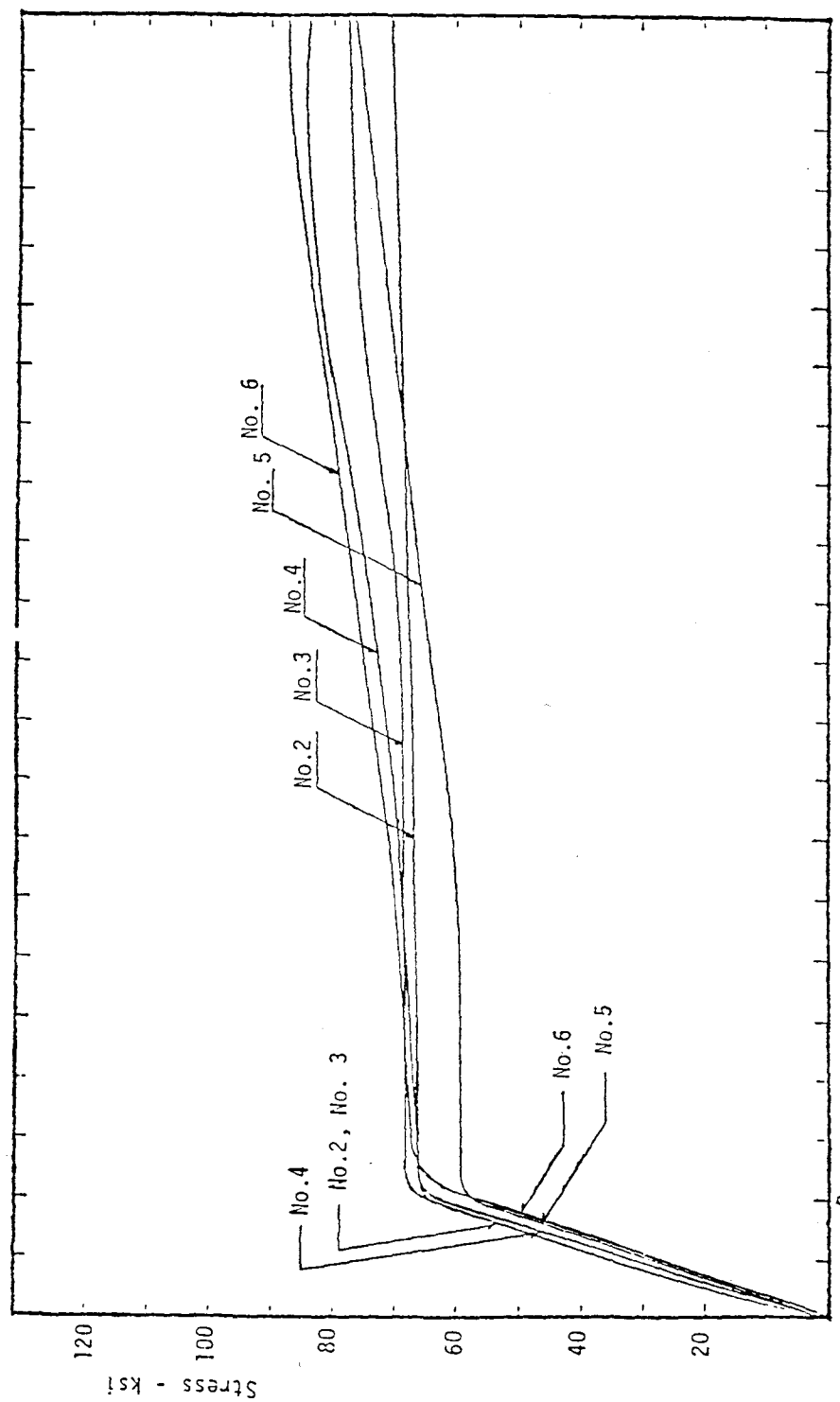

FIG. 2.23 STRESS - STRAIN CURVES FOR REINFORCING BARS S1, S2, S3, S4, SS1 AND SS2

line is reached the response heads towards the yield condition for the opposite loading direction (segment-4).

Because the unloading stiffness is higher than the loading stiffness, and the amount of top reinforcement greater than the amount of bottom reinforcement, it frequently happens that once a crack develops through the full-depth of the section, and one of the reinforcements yields, then the concrete on either side of that crack at the column face at the level of both the top and bottom reinforcements may not be in contact. The response for that situation is indicated by the segments (-4) and (4) in Fig. 2.21(c). The response depends on both the top and bottom reinforcement bond slip stiffness and Eq. (2.40) must be used instead of Eq. (2.35) to determine the bar force

$$F_y = M_{yb}/d^* \tag{2.40}$$

The total stiffness becomes

$$KB\ (\text{reloading}) = \frac{K\,K'}{K + K'}\ n_b\ d^{*\,2} \tag{2.41}$$

where K′ is the bond slip stiffness of the reinforcing bar for the condition of being pushed back after being pulled out. The push back stiffness K′ is twice the pull out stiffness K (38). However, for simplicity a KB (reloading) value is used equal to KB_2 until the crack closes.

2.3 Formulation of Model for Response of Slab-Column Connection

2.3.1 Strength of Connection

The post-cracking stiffness of the torsional element depends on the ultimate strength of that element. That strength depends, in turn, on both the shear and torsion acting on the element at failure. Therefore, before an overall stiffness model can be formulated for the connection its ultimate moment transfer capacity must be determined.

The beam anlaogy (2) presumes that the shears caused by gravity loads are reacted by shear stresses distributed uniformly around the column perimeter, and that the shears caused by lateral loads transfer initially to the column through the stiffer flexural elements. A redistrubiton of the lateral load shears does not occur until the shear acting on those flexural elements exceeds the shear capacity of those elements, thereby markedly decreasing their stiffness, and causing shears in excess of the shear caspacity of the flexural elements to be transferred to the column through the torsional elements.

This overflow condition for shear can be checked only by comparing the final shear force acting on the front flexural element with the shear capacity of that element. If overflow occurs, the ultimate strength of the torsional element must be decreased according to Eq. (2.23) or (2.24). The total moment that can be transferred to the column, and thus the shear that acts on the front face of the column

must be decreased. That decrease, in turn, influences the torsional capacity.

When the gravity load is small all the beam elements framing into the column reach their ultimate capacities before failure occurs. However, when the gravity load is large, the flexural element at the back face of the column cannot reach its limiting capacity before the strengths of both the front flexural element and the torsional elements are exhausted. In that case the moment transfer strength of the connection deteriorates rapidly with increasing rotations. The ductility of the connection is markedly less than for the case where all beam elements framing into the column develop their ultimate strength.

Theoretically the stiffness model developed later in this section can be used to calculate results for the final stage by trial and error. However, it is more direct to calculate the moment transfer strength first and then use that result as input for the stiffness model. Therefore, that is the procedure followed here.

2.3.1.1 Moments Caused by Gravity Loading

The University of Washington test results showed that the moment transfer capacityof a connection is greatly influenced by gravity load conditions existing prior to that transfer. Thus, it is important to determine first the moments caused by gravity loading.

Theoretically, it is possible to determine the effects of gravity loading on a flat plate structure by a step by step finite element analysis or by equivalent frame methods (1)(39) provided the

loading is restricted to the elastic range. However, such analyses are unnecessarily complicated and expensive, and the resulting predictions relatively meaningless when account is taken of the lack of advance knowledge on construction methods, likely strengths for the materials to be used in the construction, and creep and shrinkage effects. A vivid illustration of this fact is the disparity between predicted gravity load moments for the frame discussed in Chapter 4, and the gravity load moments found to exist in that frame at the start of lateral load testing.

Thus, so far as the moments caused by gravity loading are concerned, the ACI Code 318-83 procedure is a reasonable method for predicting fixed end moments. However, that procedure provides no information on the transverse distribution moments in the column strip and such information is needed for predictions of moment transfer effects. Therefore, based on the results of the University of Washington tests, and finite element analyses, empirical distribution are proposed for the moments around different column types. Those distributions are shown in Fig. 2.24.

(a) Interior Column Connection or Edge Column Connection Transferring Moment Parallel to the Edge

The influence of the gravity loading was checked using the test result for specimen S-8. Shown in Fig. 2.25(a) is the relation between the gravity load applied to that specimen and the strain distribution across the width of the specimen for the reinforcing bars in the direction of moment transfer. The loading pattern for that specimen can be regarded as modeling reasonably well the

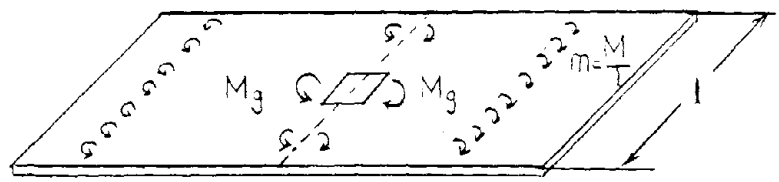

(a.) Interior column connection

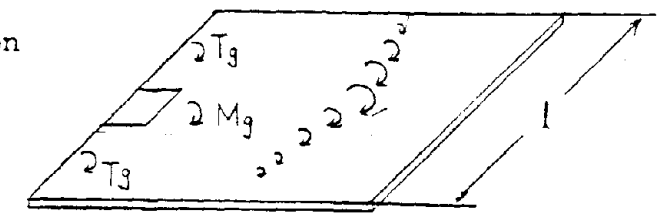

(c.) Edge column connection transferring moment normal to the edge

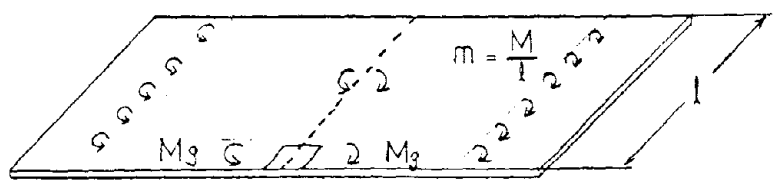

(b.) Edge column connection transferring moment parallel to the edge

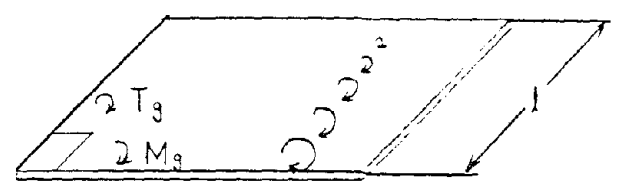

(d.) corner column connection

Fig. 2.24 MOMENT DISTRIBUTION MODEL FOR GRAVITY LOAD CONDITION

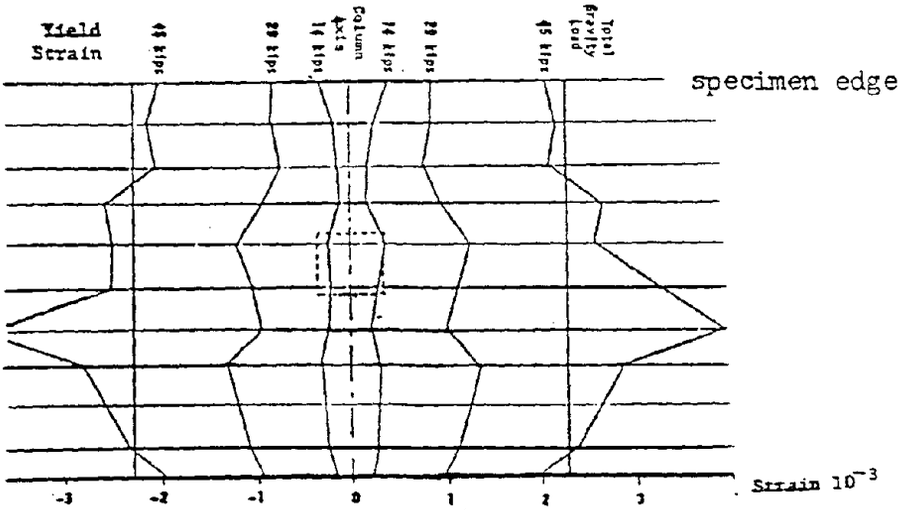

(a) Interior column connection (S-8)

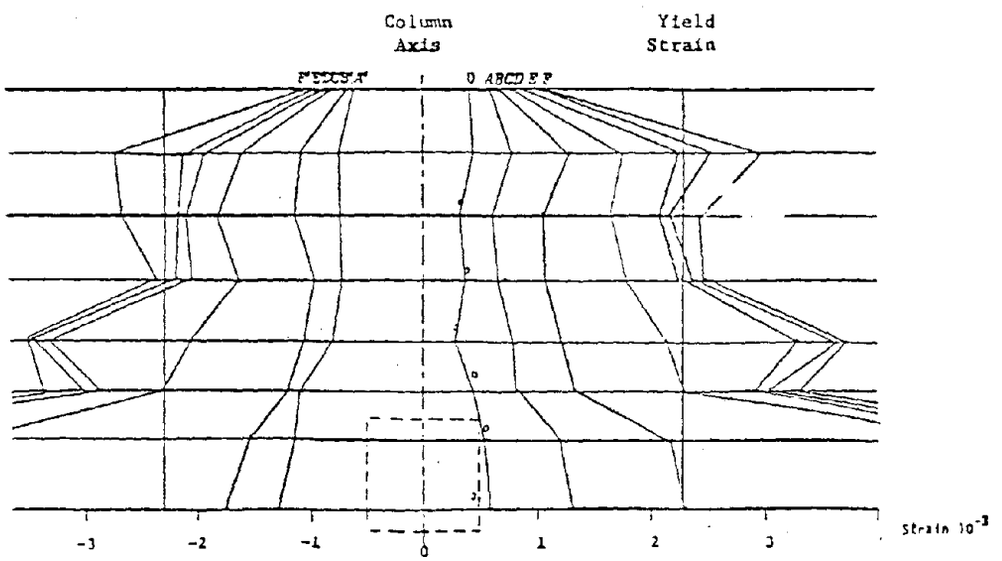

(b) Edge column connection transferring moment normal to the edge (ELS-2)

FIG. 2.25 TYPICAL EXAMPLES FOR STRAIN DISTRIBUTIONS IN REINFORCEMENT ACROSS WIDTH OF SPECIMEN FOR GRAVITY LOAD CONDITION

standard gravity load condition (5). Thus, it is apparent that for gravity loading, strains in the reinforcing bars are almost constant across the width of the slab. For S-8 that width was approximately the width of the column strip for the prototype slab.

Since reinforcing bars strains are caused primarily caused by flexural effects, the moment distribution must be proportional to the strain distribution. Thus, the unit moments due to gravity loading must be approximately constant across the width of the slab. It is reasonable to assume that the gravity load causes a moment, M_g, in the flexural element which can be expressed as:

$$M_g = \frac{c_m}{l_c} M \tag{2.42}$$

where c_m = width of flexural element; l_c = width of the slab or column strip width; and M = total moment caused by the gravity loading. The portion of the moment $(M-M_g)$ not transferred through the flexural element is balanced by moment from the adjoining bay.

The result for edge column ELS-2 is shown in Fig. 2.25(b). From that result it is apparent that the same procedure is appropriate for an edge column when moments are transferred parallel to the edge. If the remaining moment $(M-M_g)$ is not balanced, an unbalanced moment (T_g) is created which must be transferred to the column through the torsional elements.

(b) Edge Column Connections Transferring Moment Normal to the Edge and Corner Connections

In these cases, the stress distribution in the reinforcing bars becomes triangular as shown in Figs. 2.26(a) and 2.26(b) for specimens ES-2 and C-3, respectively. It is proposed that M_g be calculated as follows:

$$M_g = (2 - \frac{c_m}{\ell c}) \frac{c_m}{\ell c} M \qquad (2.44)$$

Again any remaining moment ($T_g = M - M_g$) is transferred to the column through the torsional elements.

2.3.1 Moment Transfer Strength

The following assumptions are used for calculations of the ultimate strength for moment transfer

1. The shear forces caused by the gravity load are evenly distributed around the column.
2. The moment caused by the lateral live load is transferred to the column first through the flexural element and after the flexural element looses it rigidity through attainment of its flexural capacity, that moment is transferred through the torsional elements.
3. A connection can be regarded as having failed when the front or back side of the torsional element reaches its ultimate strength. That strength is taken as half of the total torsional capacity for that element.

The first assumption is the same as that used by Symonds (5) in his analysis. The second assumption is unique to this analysis and is appropriate because the stiffness of the flexural element before

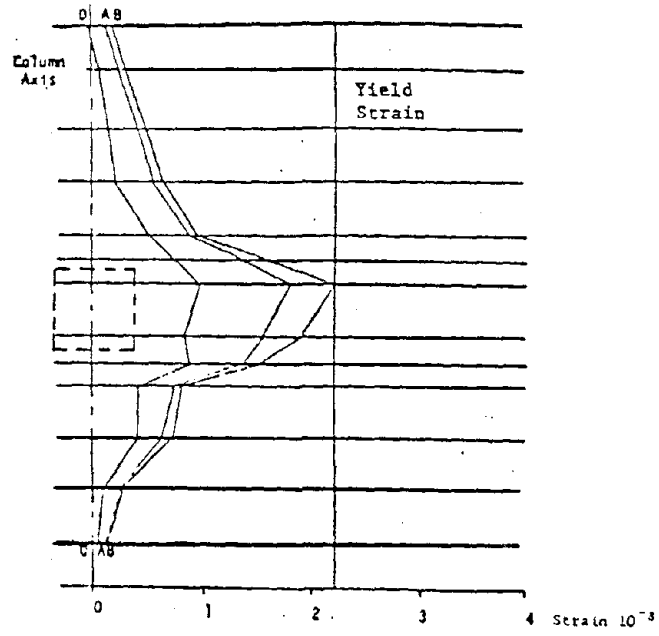

(a) Edge column connection transferring moment normal to the edge (ES-2)

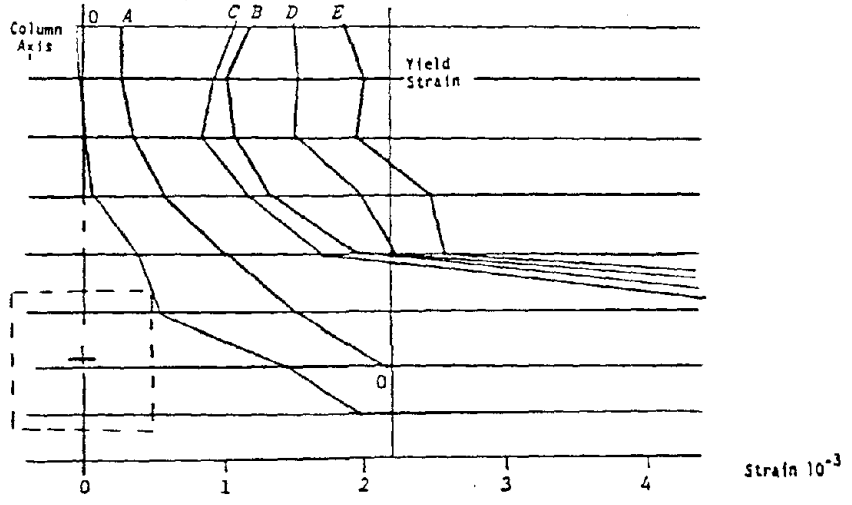

(b) Corner column connection (C-3)

FIG. 2.26 TYPICAL EXAMPLES FOR STRAIN DISTRIBUTION IN REINFORCEMENT FOR GRAVITY LOAD CONDITION

yielding is much larger than the torsional stiffness of the torsional element. Also, Symonds (5) and Kanoh (30) found that before yielding of the flexural element, resistance was provided primarily by the flexural element while after yielding the resistance was provided primarily by the torsional element. In reality, actual conditions cannot be divided so neatly into two stages. However, because the objective in this step is only to check the ultimate capacity, that assumption is reasonable. The third assumption differs from that used by Symonds (5). It makes calculations of the effects of the gravity load on the moment transfer strenght easy and is justified by the University of Washington test results and by the finite element analyses conducted by Yamazaki (13).

(a) Interior Column Connections and Edge Column Connections Transferring Moments Parallel to the Edge

The stiffness and strength of the front face flexural element and the back face flexural element differ and therefore the shear force and the moment acting on the torsional element differ for the front and back sides of that element.

Usually, for the back side of the torsional element, the direction of the shear force caused by the lateral load and that caused by gravity load are opposite and therefore those forces partially cancel one another. By contrast on the front side those two shears add and therefore the front side of a torsional element is usually subject to much more severe loading than its back side. When the front side crushes, deterioration spreads rapidly to backside. The total torsional element fractures and the total connection fails.

This effect has been demonstrated analytically in the finite element study of moment transfer for interior column connections reported in Reference 13. This observation suggests that, as shown in Fig. 2.27, the torsional face should be considered as composed of two halves, a front side and a back side and the torsional capacity of either half limited to half the torsional capacity for the total face. Then, as shown in Fig. 2.27, there are three possible failure modes for an interior column connection transferring moment and having inadequate shear reinforcement. Those modes are categorized here as flexural crushing, torsional crushing and shear punching.

1. For a flexural crushing failure the flexural capacity of the back face element is reached, the flexural capacity of the front face element is reached and failure occurs when the front half of torsional face reaches its ultimate capacity. This condition is Mode 1 of Fig. 2.27 and the maximum ductility is associated with this failure mode.
2. For a torsional crushing failure the the back face element does not reach its flexural capacity, the front face element reaches its flexural capacity and is subject to a shear less than its shear capacity limit V_o, and failure occurs when the front half of the torsional face reaches its ultimate capacity. This condition is Mode 2 of Fig. 2.27. The ductility achieved in this mode is less than that for Mode 1 but greater than that for Mode 3.
3. For a shear punching failure the failure mechanism is similar to that for torsional crushing except that for

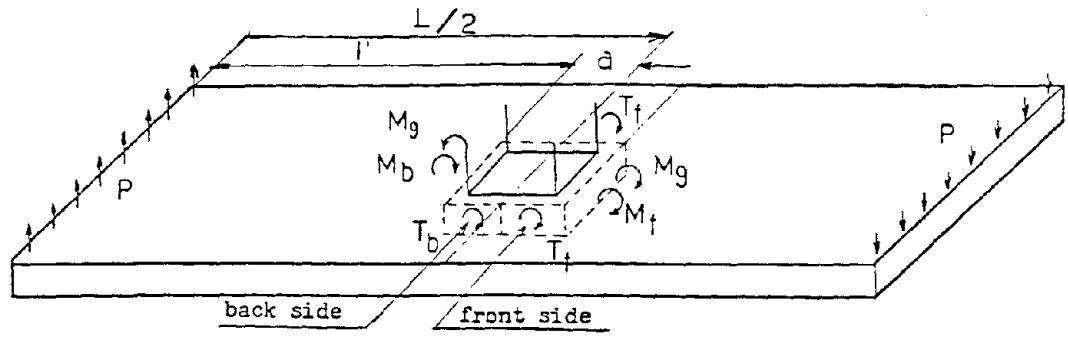

Moments Acting on Connection

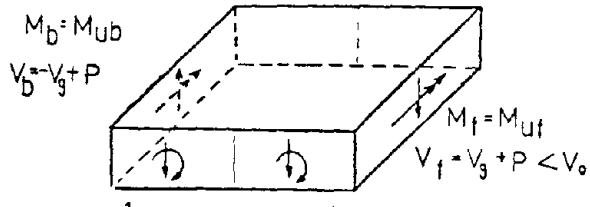

$T_b < \frac{1}{2} T_u$ $T_f = \frac{1}{2} T_u$

$V_{tb} = V_g$ $V_{tf} = V_g$

(a) Mode 1. Flexural Crushing Failure

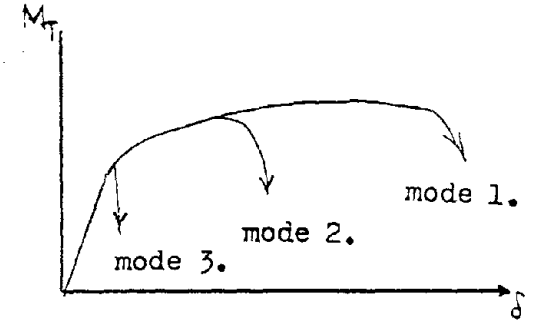

Failure Mode in M – δ Relationship

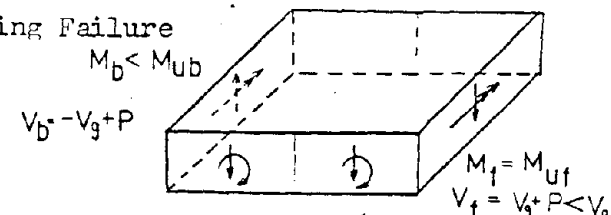

$T_b = 0$ $T_f = \frac{1}{2} T_u$

$V_{tb} = V_g$ $V_{tf} = V_g$

(b) Mode 2. Torsional Crushing Failure

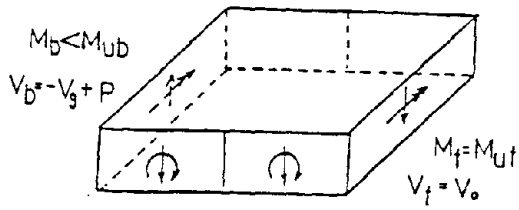

$T_b = 0$ $T_f = \frac{1}{2} T_u$

$V_{tb} = V_g$ $V_{tf} = V_g + P - V_o$

(c) Mode 3. Shear Punching Failure

FIG. 2.27 FAILURE MODELS FOR INTERIOR COLUMN CONNECTIONS

front face element the shear tries to exceed V_o and therefore the shear in excess of V_o must be redistributed to the torsional element. This condition is Mode 3 of Figure 2.27.

For a connection with adequate shear reinforcement only a Mode 1 failure is possible. For all three modes the strength is governed by the strength of the front half of the torsional element (right side of figure). The ultimate moment transfer capacity of the connection is calculated as follows:

$$P\frac{L}{2} = (M_{u\,f} - M_g) + 2T_u/2 + V_f a \tag{2.45}$$

$$M_T = P \cdot L \tag{2.46}$$

$$V_f = P + V_g \text{ or } V_f = V_o \text{ (whichever is smaller)} \tag{2.47}$$

where, V_f is the shear in the flexural element caused by lateral loading, and a is the distance between the center of the column and the center of the flexural element. M_b is given by

$$M_b = -M_g + P(\frac{L}{2} - a) \tag{2.48}$$

If the value of M_b calculated from Eq. (2.48) exceeds M_{ub} a flexural crushing Model is predicted. If the value of M_b calculated from Eq. (2.48) is less than M_{ub} and $P + V_g < V_o$ a torsional crushing, Mode 2, failure is predicted. If the value of M_b calculated from Eq. (2.48) is less than M_{ub} and $P + V_g > V_o$ a shear punching, Mode 3, failure is predicted. The shear applied to the torsional element is $V = P + V_g - V_o$.

The total torsional moment acting on the connection can be calculated as:

$$T_T = T_f \text{ (front side)} + T_b \text{ (back side)} \qquad (2.49)$$

As indicated in Fig. 2.27 account can be taken of T_b (back side) only if the back face element has reached its flexural capacity.

Some special cases arise, as for example, for University of Washington test specimens S-6 and S-7, where the gravity load was so large that the back face flexural element could not develop a positive (upward) deflection before failure occurred. In such cases, the ultimate strength of the torsional element is much smaller than T_u and there is a moment-torsion interaction effect for those elements. In practice, such conditions, where the steel passing through the column is almost yielding under the gravity loads, are very undesirable and should be avoided by concentrating flexural reinforcement in the column head region. Further in cases where the gravity load is small and the capacity of front face flexural element is much larger than that of the back face flexural element, the back side strength for the torsional element can become more critical than the front side strength for that element.

(b) Edge Column Connections Transferring Moments Normal to the Edge and Corner Column Connections

In these cases, since there is no back side flexural element, the limiting conditions for the moment transfer mechanism are relatively simple. As shown in Figs. 2.26(c) and (d), because there is no balancing moment at the edge, torque is applied to the tor-

sional element by the gravity load. The gravity torque can be calculated as follows:

$$T_g = M - M_g \tag{2.50}$$

The ultimate moment transfer capacity, including the moment transferred by the gravity load, can be calculated as follows:

$$M_T = M_{uf} + T_u + V_f a \tag{2.51}$$

$$V_f = V_o \text{ or } V_f = V_g + P \text{ (whichever is smaller)} \tag{2.52}$$

As before, T_u must be calculated taking into account any shear in excess of the shear capacity of the front face flexural element ($V = P - V_o + V_g$).

If the classification system used for failure modes is the same as for interior column connections, then only torsional crushing, Mode 2, and shear punching, Mode 3, failures are possible.

(c) Rotation Limits

In the University of Washington tests, failure always occurred by punching if the slab did not contain shear reinforcement and the connection was rotated without limit. Mode 1 failures were easily distinguishable because strain gages on the bottom steel indicated yielding at the back face prior to punching. However, it was almost impossible to separate through observations Modes 2 and 3 failures even though, on the average, the rotations at maximum load were greater for Mode 2 than Mode 3 failures. For all three modes the test data were insufficient to define specific limiting rotation conditions.

2.3.2 Stiffness of Connection

Once the characteristics of each element are defined, then the stiffness of the connection is calculated by interconnecting those elements according to the geometric conditions existing at the given connection, and developing the appropriate stiffness matrix. In this section the development of an appropriate stiffness model for lateral loading is discussed. The starting point for application of that model is the deformations existing for gravity loading. The lateral load stiffness is dependent on the moments associated with that gravity loading condition but not with the deformations associated with that condition. Thus for comparisons with test data made in Chapter 3 the starting deformations for gravity loading were not calculated but were taken as those determined in the actual test.

2.3.2.1 Interior Column Connection

The general configuration for the deformed connection, the notation for the forces, the deformations and their positive directions are shown in Fig. 2.28. Note that "P", upper case, is used to denote forces applied at the ends of the slab and "p", lower case is used to denote forces applied at the ends of the flexural elements. Equilibrium of forces dictates:

$$\Delta M_T = \Delta M_f + \Delta M_b + \Delta T + (\Delta p_{mf} + \Delta p_{mb}) \left(\frac{c + h}{2}\right) \quad (2.53)$$

$$\Delta M_f = \Delta m_f + \Delta p_{mf} \cdot h / 2 \text{ (or } \Delta M_{fo} = \Delta m_f + \Delta p_{mf} \cdot h) \quad (2.54)$$

$$\Delta M_b = \Delta m_b + \Delta p_{mb} \cdot h / 2 \text{ (or } \Delta M_{bo} = \Delta m_b + \Delta p_{mb} \cdot h) \quad (2.55)$$

$$\Delta T = \Delta t_f + \Delta t_b + (\Delta p_{tf} + \Delta p_{tb}) \cdot a \quad (2.56)$$

$$\Delta P = \Delta P_{mf} + \Delta P_{tf} \quad (2.57)$$

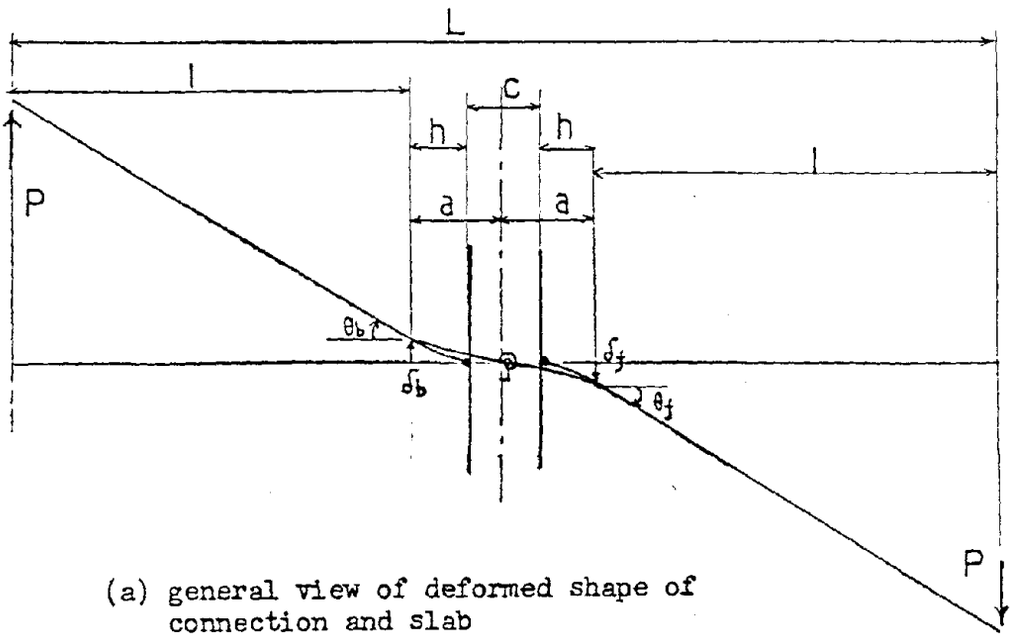

(a) general view of deformed shape of connection and slab

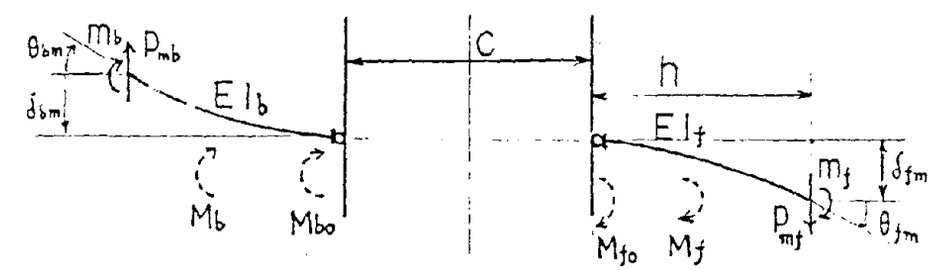

conditions for flexural elements

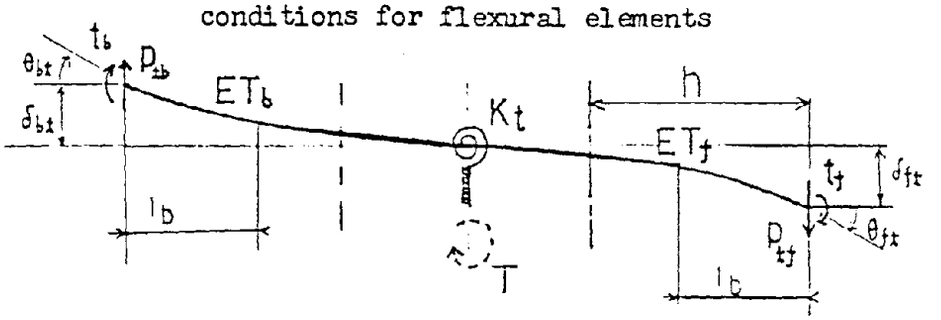

conditions for torsional elements

(b) conditions at connection

FIG. 2.28 GENERAL CONFIGURATION AND NOTATION FOR DEFORMED CONNECTION

$$\Delta P = \Delta P_{mb} + \Delta P_{tb} \tag{2.58}$$

$$\Delta P\ \ell = \Delta m_f + \Delta t_f \tag{2.59}$$

$$\Delta P\ \ell = \Delta m_b + \Delta t_b \tag{2.60}$$

Compatibility of deformations requires that:

$$\Delta\delta_{fm} = \Delta\delta_{ft} = \Delta\delta_f \tag{2.61}$$

$$\Delta\delta_{bm} = \Delta\delta_{bt} = \Delta\delta_b \tag{2.62}$$

$$\Delta\theta_{fm} = \Delta\theta_{ft} = \Delta\theta_f \tag{2.63}$$

$$\Delta\theta_{bm} = \Delta\theta_{bt} = \Delta\theta_b \tag{2.64}$$

The relationship between force increments and deformation increments are as follows:

$$\Delta\delta_{fm} = a_{11}\Delta p_{mf} + a_{12}\Delta m_f + a_{13}\,(\Delta m_f + \Delta p_{mf} h) \tag{2.65}$$

$$\Delta\delta_{ft} = a_{21}\Delta p_{tf} + a_{22}\Delta t_f + a_{23}\,(\Delta t_f + \Delta t_b + \Delta p_{tf}\cdot a + \Delta p_{tb} a) \tag{2.66}$$

$$\Delta\delta_{bm} = a_{31}\Delta p_{mb} + a_{32}\Delta m_b + a_{33}\,(\Delta m_b + \Delta p_{mb}\cdot h) \tag{2.67}$$

$$\Delta\delta_{bt} = a_{41}\Delta p_{tb} + a_{42}\Delta t_b + a_{43}\,(\Delta t_f + \Delta t_b + \Delta p_{tf}\cdot a + \Delta p_{tb}\cdot a) \tag{2.68}$$

$$\Delta\delta_{fm} = a_{51}\Delta p_{mf} + a_{52}\Delta m_f + a_{53}\,(\Delta m_f + \Delta p_{mf}\cdot h) \tag{2.69}$$

$$\Delta\theta_{ft} = a_{61}\Delta p_{tf} + a_{62}\Delta t_f + a_{63}\,(\Delta t_f + \Delta t_b + \Delta p_{tf}\cdot a + \Delta p_{tb}\cdot a) \tag{2.70}$$

$$\Delta\theta_{bm} = a_{71}\Delta p_{mb} + a_{72}\Delta m_b + a_{73}\,(\Delta m_b + \Delta p_{mb}\cdot h) \tag{2.71}$$

$$\Delta\theta_{bt} = a_{81}\Delta p_{tb} + a_{82}\Delta t_b + a_{83}\,(\Delta t_f + \Delta t_b + \Delta p_{tf}\cdot a + \Delta p_{tb}\, a) \tag{2.72}$$

where a_{11} to a_{83} are coefficients calculated as follows:

$$a_{11} = \frac{h^3}{3EI_f} \qquad a_{12} = \frac{h^2}{2EI_f} \qquad a_{13} = \frac{h}{K_b} \tag{2.73}$$

$$a_{21} = \frac{\ell b^3}{3ET_f} \qquad a_{22} = \frac{\ell b^2}{2ET_f} \qquad a_{23} = \frac{h + c/2}{K_T} \tag{2.74}$$

$$a_{31} = \frac{h^3}{3EI_b} \qquad a_{32} = \frac{h^2}{2EI_b} \qquad a_{33} = \frac{h}{K'_b} \tag{2.75}$$

$$a_{41} = \frac{\ell_b^3}{3ET_b} \qquad a_{42} = \frac{\ell_b^2}{2ET_b} \qquad a_{43} = \frac{h + c/2}{K_T} \tag{2.76}$$

$$a_{51} = \frac{h^2}{2EI_f} \qquad a_{52} = \frac{h}{EI_f} \qquad a_{53} = \frac{1}{K_b} \tag{2.77}$$

$$a_{61} = \frac{\ell_b^2}{2ET_f} \qquad a_{62} = \frac{\ell_b}{ET_f} \qquad a_{63} = \frac{1}{K_T} \tag{2.78}$$

$$a_{71} = \frac{h^2}{2EI_b} \qquad a_{72} = \frac{h}{EI_b} \qquad a_{73} = \frac{1}{K_b'} \tag{2.79}$$

$$a_{81} = \frac{\ell_b^2}{2ET_b} \qquad a_{82} = \frac{\ell_b}{ET_b} \qquad a_{83} = \frac{1}{K_T} \tag{2.80}$$

For the solution of these equations all forces and deformations can be represented in the form:

$$\Delta \text{ Force} = r_f \, \Delta P \tag{2.81}$$

$$\Delta \text{ Deformation} = r_d \Delta P \tag{2.82}$$

where r_f and r_d are coefficients composed only of the stiffness nad length of each element. Details are shown in Appendix B

If one more equation is supplied, forces and deformations are defined uniquely. A program for dynamic analysis that utilizes a step by step procedure, such as Drain-2D, solves those equations by assuming some constant force increment ΔP. A solution is also possible by recognizing that all the foregoing equations are linear in ΔP, and therefore, if the points where the force-deformation relationships change slope are claculated, the response between those points can be interpolated by straight lines. Thus, if one of the forces is assumed known, then from that, ΔP and all the other forces can be calculated.

For each of the elements, forces can be checked as follows:

1. Moments M_f and M_b in the flexural elements are checked at M_{cr}, M_y, and M_u.
2. Moments M_{fo} and M_{bo} in the bond slip element are checked at M_{yb}.
3. Torsions T in the torsion elements are checked at T_{cr} and T_u.

When one of those forces reaches the critical value for a change in slope, the corresponding stiffness is changed for the next step in the analysis. The same procedure is continued until the ultimate load of the connection is achieved. The forces acting on the connections and the deformations caused by those forces can be obtained by summing up the results for each increment.

The program listed in Appendix B was develped to perform that calculation. While the procedure may appear cumbersome, the resulting equations are well conditioned and their solution proceeds readily.

2.3.2.2 Edge Column to Slab Connection Transferring Moment Parallel to Edge

The equations for this case are the same as those for an interior connection. The stiffness of the torsional element and the connecting bars (KT, ET) must be halved.

2.3.2.3. Edge Column to Slab Connection Transferring Moment Normal to Edge

The terms for the back face flexural element dissappear and Eq. (2.53) becomes:

$$\Delta M_T = \Delta M_f + \Delta T + \Delta p_{mf} \frac{c + h}{2} \tag{2.83}$$

Eq. (2.56) becomes:

$$\Delta T = \Delta t_f + \Delta p_{tf} \cdot a \tag{2.84}$$

and Eqs. (2.66) and (2.70) become:

$$\Delta\delta_{ft} = a_{21}\Delta p_{tf} + a_{22}\Delta t_f + a_{23}(\Delta t_f + \Delta p_{tf}\, a) \tag{2.85}$$

$$\Delta\theta_{ft} = a_{61}\Delta p_{tf} + a_{62}\Delta t_f + a_{63}(\Delta t_f + \Delta p_{tf}\, a) \tag{2.86}$$

Also, KT is decreased by the amount $(h - 0.26\, c_1)/h$ 1/2, (it is usually halved), due to the loss of the stiffening effect of the surrounding slab.

2.3.2.4 Corner Column to Slab Connection

The equations for this connection are the same as those for edge column-slab connections transferring moment normal to the edge. However, the stiffness of the torsional element for the connecting bars (KT, ET) must be halved. Thus, KT becomes about one-fourth that for an interior column connection.

CHAPTER 3

CYCLIC LOADING BEHAVIOR OF SLAB-COLUMN CONNECTIONS

3.1 General

In Chapter 2 an analytical model was developed for predictions of the strength, stiffness, and hysteretic characteristics of column-slab connections transferring moments. That model was calibrated through comparisons with the experimental results for nine interior column-slab subassemblages S1 through S4 and SS1 through SS5 tested at the University of Washington and reported in References (3) and (4).

This chapter examines the agreement between predictions made using the analytical model of Chapter 2 and the experimental results for all the column-slab subassemblages tested at the University of Washington. Those experimental results are summarized in Appendix A and include tests on eight interior, thirteen exterior, and five corner column-slab assemblages in addition to the nine interior column-slab subassemblages used initially for calibration of the analytical model. In Section 3.2, the strengths of the flexural and torsional elements of each of the connections are determined, and thus the ultimate moment transfer capacity of each connection. In Section 3.3 the partial rigidities of each element are calculated, and those rigidities are used to determine load-deflection envelopes and hysteretic responses for each of the connections. Finally in Section 3.4 the influence of different parameters on the load-deflection response is examined using the analytical model of Chapter 2.

3.2 Strength of Connections

The moment transfer capacities of the connections were calculated using the methods described in Section 2.3. Results are shown in Table 3.1. Table 3.1(a) contains predictions for interior column connections without shear reinforcement and Table 3.1(b) predictions for the same connections with shear reinforcement. Each row in these Tables has the following significance:

1st row: M_g = the initial flexural moment caused by the gravity loading,

2nd row: M_{uf} = the predicted capacity for the front face flexural element,

3rd row: $M_f(\text{rest})$ = the residual flexural capacity for the front face flexural element ($M_f(\text{rest}) = M_{uf} - M_g$),

4th row: P_m = lateral force for crushing of front face flexural element ($P_m = M_f(\text{rest})/\ell$),

5th row: T_f = the ultimate capacity of front half of torsional element ($T_f = 1/2T_u$),

6th row: P_t = lateral force which causes crushing of front half of torsional element ($P_t = 2T_f/L$),

7th row: P = predicted lateral force capacity ($P = P_t + P_m$),

8th row: M_b = the moment consumed by the back-face flexural element ($M_b = P\ell \leq M_{ub} + M_g$),

9th row: T_b = the torsion consumed by the back half of the torsional element in the final stage ($T_b = (P - \frac{M_{ub}}{\ell}) \frac{L}{2} \leq \frac{1}{2} T_u$)

TABLE 3.1(a) STRENGTH OF CONNECTIONS

Interior column connection without shear reinforcement

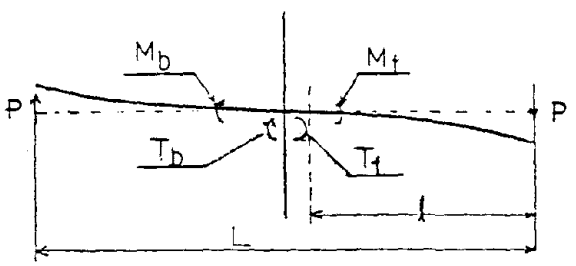

		S-1	S-2	S-3	S-4	S-6	S-7	S-8
1	M_g (†)	78	85	83	89	148	148	130
2	M_{uf} (†)	296	215	144	294	390	218	144
3	M_f(rest) (†)	218	130	61	205	242	70	14
4	P_m(for M_f) (††)	3.43	2.05	0.96	3.23	3.81	1.10	0.22
5	$T_f(=\frac{1}{2}Tu)$ (†)	366	235	166	337	79	89	125
6	P_t(for T_f) (††)	5.08	3.26	2.31	4.68	1.10	1.24	1.96
7	$P(=P_m+P_t)$ (††)	8.51	5.31	3.27	7.91	4.91	2.34	2.18
8	M_b(used) (†)	142	124	104	149	163	0	8
9	T_b(used) (†)	363	145	23	300	0	0	0
10	$M_T=(P\ L)$ (†)	1,225	765	471	1,139	707	337	314
11	M(test) (†)	1,280	778	475	1,110	644	376	289
12	$\frac{M(test)}{M_T}$ *	1.04	1.02	1.01	0.97	0.91	1.11	0.92

*Avg=1.00

(†) Kips·inches
(††) Kips

S1 through S4 were used to calibrate the analytical model.

TABLE 3.1(b) STRENGTH OF CONNECTIONS

Interior column connection with shear reinforcement

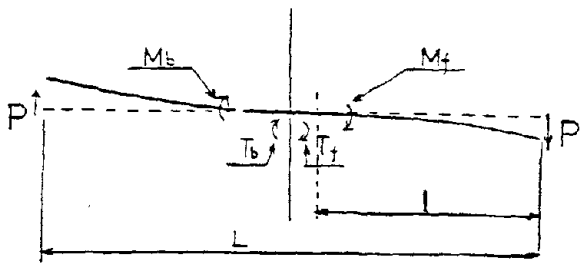

		SS-1	SS-2	SS-3	SS-4	SS-5	SS-6 +	SS-7 +	SS-8	SS-11	SS-12
1	Mg (+)	77	79	78	78	77	148	148	97	60	113
2	Muf (+)	278	217	407	400	222	212	399	525	360	653
3	Mf (rest) (+)	201	138	329	322	145	64	251	428	300	540
4	Pm for Mf (++)	3.17	2.17	5.18	5.07	2.28	1.00	3.95	6.58	5.42	8.51
5	Tf=½Tu (+)	345	327	303*	322*	417	308	328	372	523	177
6	Pt for Tf (++)	4.84	5.15	4.21	4.47	5.79	4.28	4.55	5.17	7.27	2.46
7	P=Pm+Pt (++)	8.01	7.32	9.39	9.54	8.07	5.28	8.50	12.14	12.27	10.68
8	Mb (used) (+)	146	125	220	219	126	123	218	284	201	370
9	Tb (used) (+)	324	296	339*	350*	351	73	197	427*	570*	240*
10	M_T(P·L) (+)	1,153	1,054	1,352	1,374	1,162	760	1,224	1,748	1,777	1,538
11	M (test) (+)	1,440	1,120	1,570	1,339	1,353	605	942	1,995	1,981	1,732
12	$\frac{M\ (test)}{M_T}$ **	1.25	1.06	1.16	0.98	1.16	0.80	0.77	1.14	1.11	1.13

** Avg= 1.12 excluding SS-6;SS-7

* governed by back side condition

\+ governed by punching around end of stirrups

(+) Kips-inches

(++) Kips

SS1 through SS5 were used to calibrate the analytical model.

TABLE 3.1(c) STRENGTH OF CONNECTIONS

Edge column connections transferring moment parallel to the edge

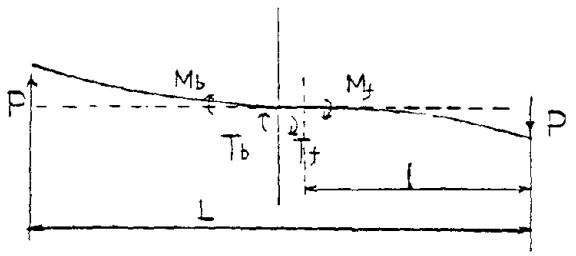

		EL-1	EL-2	ELS-1	ELS-2	ELS-3
1	M_g (†)	45	57	51	48	29
2	M_{uf} (†)	211	457	341	362	296
3	M_f(rest) (†)	166	380	290	314	267
4	P_m for T_f (††)	2.62	6.22	4.57	4.45	4.52
5	$T_f=\frac{1}{2}T_u$ (†)	181	166*	118*	155*	257*
6	P_t for T_f (††)	2.51	2.51	1.63	2.15	3.57
7	$P=P_m+P_t$ (††)	5.13	8.53	6.20	7.10	8.09
8	M_b(used) (†)	153	217	179	181	123
9	T_b(used) (†)	144	292*	216*	282*	397*
10	$M_T=(P\cdot L)$ (†)	739	1,228	893	1,022	1,165
11	M(test) (†)	779	1,159	995	1,151	1,169
12	$\frac{M\ (test)}{M_T}$ **	1.05	0.94	1.11	1.11	1.00

(†) Kips•inches

(††) Kips

* governed by back side condition

** Avg = 1.04

TABLE 3.1(d) STRENGTH OF CONNECTIONS

Edge column connections transferring moment normal to the edge

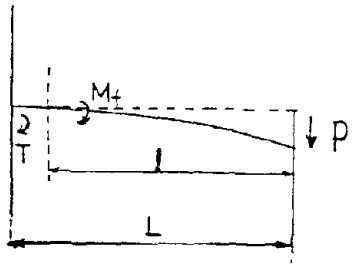

		E-1	E-2	E-3	ES-1	ES-2	ES-3	ES-4	ES-5
1	M_g (+)	120	169	110	143	143	104	102	234
2	M_{uf} (+)	244	508	360	479	482	484	366	731
3	$M_{f(rest)}$ (+)	124	339	250	336	339	380	264	497
4	P_m for $M_{f(rest)}$ (#)	1.96	5.49	4.19	5.47	5.52	6.19	4.42	7.56
5	T_g (+)	214	224	253	255	255	185	261	233
6	$T_f = T_u$ (+)	244	483	606	305	528	320	885	223
7	$T_{f(rest)}$ (+)	30	260	353	50	273	135	624	-10
8	P_t for $T_{f(rest)}$ (#)	0.47	3.61	4.90	0.69	3.79	1.88	8.67	-0.14
9	$P_{(total)}$ (#) $=(P_m+P_t)$	2.43	9.10	9.08	6.16	9.31	8.07	13.09	7.42
10	$M = P\,L$ (+)	175	655	654	444	670	580	942	534
11	$P_{(test)}$ (#)	2.66	10.61	7.54	5.87	8.94	9.57	14.64	7.21
12	$\frac{P_{(test)}}{P_{(total)}}$ *	1.09	1.16	0.83	0.95	0.96	1.18	1.12	0.97
13	$\frac{M_{(test)}}{M_{(total)}}$ **	1.03	1.10	0.89	0.97	0.98	1.13	1.09	0.99

* Avg = 1.03

** $M_{(test)} = M_g + P_{(test)}\,L + T_g$

$M_{(total)} = M_g + P_{(total)}\,L + T_g$

(+) Kips·inches

(#) Kips

TABLE 3.1(e) STRENGTH OF CONNECTIONS

Corner column connections

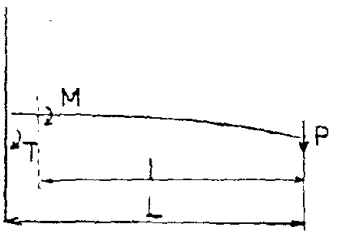

		C-1	C-2	C-3	CS-1	CS-2
1	M_g (+)	77	77	87	82	61
2	M_f (+)	214	205	452	427	301
3	M_f (rest) (+)	137	128	365	345	240
4	P_m for M_f (rest) (#)	2.16	2.02	5.97	5.47	3.89
5	T_g (+)	56	56	43	61	71
6	$T_f = T_u$ (+)	155	126	237	253	597
7	T_f (rest) (+)	99	70	194	192	526
8	P_t for T_f (rest) (#)	1.56	0.97	2.69	2.66	7.51
9	P (total) = Pm+Pt (#)	3.88	2.99	8.66	8.13	11.20
10	M=P L (+)	279	220	623	585	806
11	P (test) (#)	3.29	3.23	8.95	6.33	10.08
12	$\frac{P(test)}{P(total)}$ *	0.85	1.08	1.03	0.78	0.90
13	$\frac{M(test)}{M(total)}$ **	0.90	1.05	1.03	0.91	0.91

* Avg = 0.93

(+) Kips·inches

(#) Kips

** M (test) = Mg + P (test) L + T_g

M (total) = Mg + P (total) L + T_g

10th row: M_T = the predicted total moment transfer capacity which is

$$M_T = PL$$

The 12th row lists ratios of the predicted moment transfer capacity, row 10, to the test results shown in row 11. Predictions are very good for the S series, without shear reinforcement, and comparatively good for the SS series with shear reinforcement.

For S-1, S-2, S-3 and S-4, the capacities of both the front face and back face flexural elements and the front half of the torsional elements are fully consumed and only the back half of the torsional element does not reach its capacity. For the categorization system shown in Fig. 2.27, these failures are flexural crushing failures even though the observed failure modes for all four specimens were punching shear failures (4). Before failure, yielding and large strains were observed for the reinforcement in the flexural elements in every case.

For S-6, S-7 and S-8, the moments caused by the gravity load were large. Consequently, positive moment yield conditions were never reached for the back face flexural elements, and for S7 and S8, the amount of moment transfer achieved was insufficient even to rotate those elements to their original horizontal position. All three failures are torsional crushing failures according to the system of Fig. 2.27. Although there was no redistribution of shear from the flexural to the torsional element, the shear in the torsional element due to gravity loading had a large influence on the capacity of that element. The observed failures were all reported as

punching shear failures (5), but the failure modes for these three specimens were more of the shear type than the failure modes of specimens S-1 through S-4.

For SS-1, SS-2, SS-5, SS-6, and SS-7 with shear reinforcement, the capacities of the front half of the torsional element, the front face flexural element, and the back face flexural element were all exhausted. Only the back half of the torsional element did not reach its capacity. For SS-3 and SS-4 the capacities of both the back half of the torsional element and the back face flexural element were fully consumed. This occurred because the difference between the capacity for the front face flexural element and the back face flexural element was large compared to the moment caused by the gravity load. That condition is checked by the following equation:

$$M_{uf} - M_g > M_{ub} + M_g \qquad (3.1)$$

If the left side of Eq. (3.1) is bigger than the right side, the failure is governed by the back face capacity, and if the right side is bigger than the left side, the failure is governed by the front face capacity. In such cases large upward deflections were observed in the tests. It was difficult to judge which side was critical, the front face or the back face.

Specimens SS-6 and SS-7, did not reach their predicted capacities. This was because punching failures occurred around the ends of the stirrups on all four sides of the column and limited the capacity of the slab-column connection region. The conditions governing that development are fully discussed in Reference (5).

Such failures can be avoided by extending the stirrups further out into the slab.

Except for SS-6 and SS-7, all SS specimens exhibited flexural crushing failures. That categorization agrees with the observed failures (3). There was extensive yielding of the reinforcement in the flexural elements prior to failure and, even where the final failure was by punching, after the maximum capacity was reached the connection could continue to transfer, with increasing rotations, moments close to those transferred at the maximum capacity.

For edge column connections transferring moments parallel to the edge, predicted strengths are summarized in Table 3.1(c) and compared with the test results. The EL′ and ELS specimens were without and with shear reinforcement, respectively. The agreement between predicted and measured results is good. In most cases the moments caused by the gravity loading were small compared to the flexural strengths so that the strength of the connections was governed by conditions for the back face element in accordance with Eq. (3.1).

Results are shown in Table 3.1(d) for edge column connections transferring moment normal to the edge. In that case the specimen is not symmetric with respect to the column and therefore, even for the gravity load condition, some moment transfer occurs. That moment influences the lateral load resisting capacity of both the flexural and torsional elements.

The residual capacities $M_f(\text{rest})$ and $T_f(\text{rest})$ are obtained as follows:

$$M_f(\text{rest}) = M_{uf} - M_g \text{ (by gravity)} \tag{3.2}$$

$$T_f(\text{rest}) = T_u - T_g \text{ (by gravity)} \qquad (3.3$$

Those capacities are listed in the 3rd and 7th rows, respectively, o Table 3.1(d).

The agreement between measured and predicted results does not appear to be as good as that for the connections examined previously. However, that is because the comparison in row 12 is between measured and predicted lateral load resisting capacities. If, as shown in row 13, the comparison is made for the total moment transferred by both gravity and lateral loads, the difference between measured and predicted capacities is less than 10%.

Results for corner column connections are shown in Table 3.1(e). The force system acting on those connections is basically the same as that for edge connections transferring moment normal to the edge. Again, the agreement in row 12 is not as good as that in row 13 where the comparison is based on the total moment transferred for both gravity and lateral loadings.

3.3 Stiffness of Connections

Rotational stiffnesses for the slab-column connections were calculated using the step-by-step procedures described in Section 2.3. The stiffness of each element was calculated according to the procedures described in Section 2.2 for ultimate capacities calulated as shown in Table 3.1.

In this section the stiffnesses predicted for the test specimens are compared with the test results as characterized by the relation between the slab's edge deformation and the applied lateral load.

The slab's edge deformation rather than the rotations measured at the connection, or some other quantity, was used for this comparison because that deformation was the most stable and the most reliable measured deformation.

(1) Interior Column

The force-deformation relationships for flexure, torsion and bondslip are idealized as shown in Fig. 3.1. The critical points for each change in stiffness and the stiffnesses for each specimen at each stage of each relationship are shown in Tables 3.2(a) and (b).

With those values and the step-by-step program shown in Appendix B, envelopes for the relationships between the lateral load and the slab edge deflection for each specimen were predicted and compared to the test results as shown in Fig. 3.2. Most of the predicted relationships are essentially trilinear with the first critical point occurring with the yielding of both the front and back face bondslip elements and the second with the yielding of the torsional element.

For the specimens without shear reinforcement and subject to a small gravity load only (S-1, S-2, S-3 and S-4), the predictions were in comparatively good agreement with the test results. Typical examples are shown in Figs. 3.2(a), (b), (c) and (d). The starting point for the calculated lateral load response must be consistent with the measured conditions for gravity loading. For S-1 through S-4, the back and front face flexural elements were calculated to be cracked but not yielding for the gravity load condition. However, in the case of S-6, S-7 and S-8, those elements were calculated as yielding or nearly yielding under gravity load conditions. The

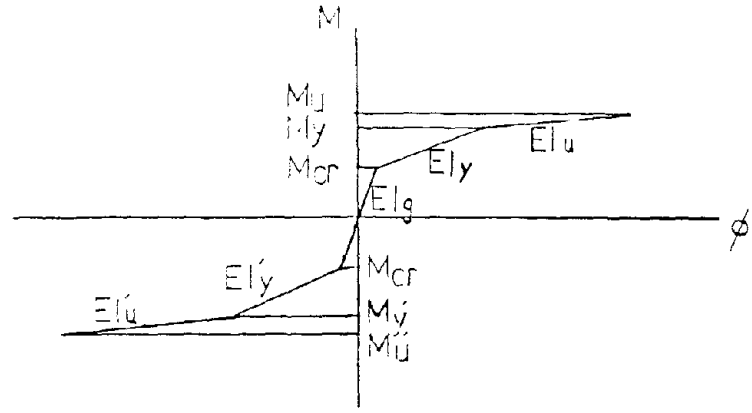

(a) stiffness of flexural element

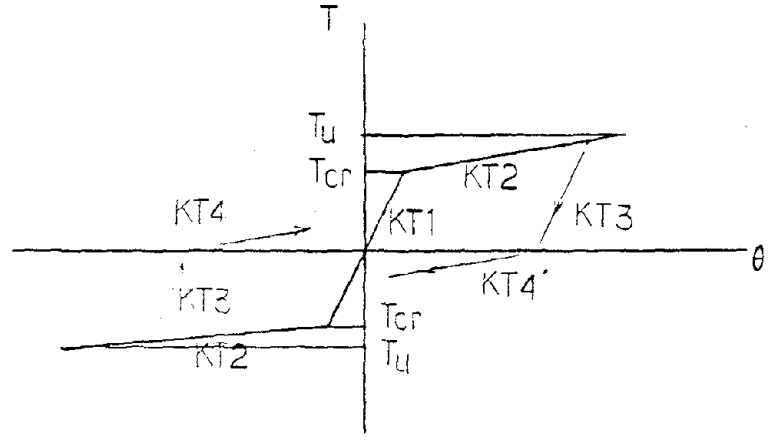

(b) stiffness of torsional element

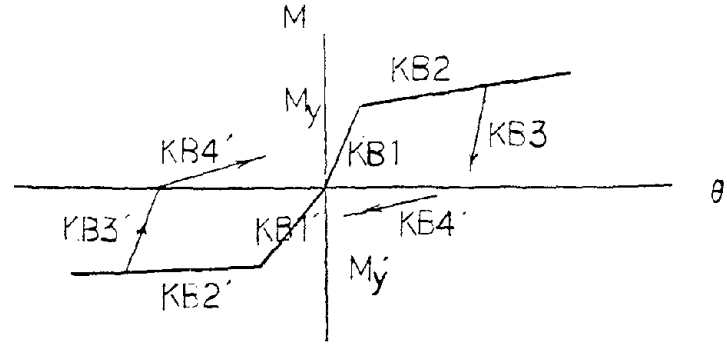

(c) stiffness of bondslip element

FIG. 3.1 STIFFNESS RELATIONSHIPS

TABLE 3.2(a) LIMITING MOMENTS AND PARTIAL RIGIDITIES

Interior Column connection specimens without stirrups

Specimens S1 through S4 were used to calibrate the analytical model.

a) FOR FLEXURE

	critical point (kip -inch)					rigidity ($x10^3$ kip -inch^2)				
	Mcr	My	My'	Mu	Mu'	EI-g	EI-y	EI-y'	EI-u	EI-u'
S-1	38	281	142	296	150	875	358	183	5.46	1.17
S-2	32	204	118	215	124	718	265	153	4.25	1.10
S-3	31	137	104	144	109	696	183	131	1.64	0.82
S-4	37	279	142	294	149	843	355	185	6.01	1.11
S-6	31	370	205	390	216	714	422	274	31.1	4.32
S-7	34	207	119	218	125	763	270	153	3.64	0.96
S-8	31	137	101	144	107	700	183	125	1.62	0.98

b) FOR TORSION

	critical point (kip -inch)		rigidity ($x10^3$ kip -inch^2)				
	Tcr	Tu	KT-1	KT-2	KT-3	KT-4	ET
S-1	102	718	347	49.6	347	2,17	174
S-2	86	378	285	38.6	285	2.36	135
S-3	87	189	277	23.1	277	2.57	81
S-4	100	637	335	49.3	335	2.10	173
S-6	25	79	283	49.0	283	2.17	172
S-7	55	89	303	20.4	303	2.36	71
S-8	64	125	278	10.2	278	1.40	36

c) FOR BONDSLIP

	critical point (kip -inch)		rigidity ($x10^3$ kip -inch^2)							
	My	My'	KB-1	KB-1'	KB-2	KB-2'	KB-3	KB-3'	KB-4	KB-4'
S-1	209	106	114	108	3.80	3.60	228	216	3.80	3.60
S-2	150	87	93.7	91.7	3.12	3.06	187	183	3.12	3.06
S-3	100	76	92.5	78.1	3.08	2.60	185	156	3.08	2.60
S-4	208	106	116	109	3.87	3.63	232	218	3.87	3.63
S-6	275	153	93.2	88.7	3.11	2.96	186	177	3.11	2.96
S-7	152	88	101	99.2	3.37	3.31	202	198	3.37	3.31
S-8	100	73	93.6	78.0	3.12	2.60	187	156	3.12	2.60

TABLE 3.2(b) LIMITING MOMENTS AND PARTIAL RIGIDITIES

Interior connection specimens with stirrups SS1 through SS5 were used to calibrate the analytical model.

a) FOR FLEXURE

	critical point (kip -inch)					rigidity ($x10^3$ kip -inch^2)				
	Mcr	My	My'	Mu	Mu'	EI-g	EI-y	EI-y'	EI-u	EI-u'
SS-1	34	273	140	287	148	779	344	184	6.97	1.51
SS-2	33	206	119	217	125	752	269	153	3.78	0.99
SS-3	33	380	208	400	219	754	445	279	23.4	3.76
SS-4	34	386	209	406	220	779	456	281	20.6	3.47
SS-5	37	211	120	222	126	841	277	151	2.87	0.78
SS-6	32	205	118	216	125	729	267	152	4.08	1.24
SS-7	34	386	209	407	220	769	449	281	25.3	3.58
SS-8	42	525	270	553	284	967	687	400	32.8	4.90
SS-11	24	360	191	379	201	538	479	299	16.8	2.90
SS-12	54	653	352	688	370	1,240	853	524	37.5	5.99

b) FOR TORSION

	critical point (kip -inch)		rigidity ($x10^3$ kip -inch^2)				
	Tcr	Tu	KT-1	KT-2	KT-3	KT-4	ET
SS-1	89	669	309	50.4	309	2.17	176
SS-2	93	623	299	41.0	299	2.36	146
SS-3	94	642	299	58.5	299	2.17	205
SS-4	96	672	309	31.8	309	2.17	111
SS-5	104	768	334	42.3	334	2.36	148
SS-6	31	381	290	44.8	290	2.36	157
SS-7	43	525	305	62.0	305	2.17	217
SS-8	134	842	453	89.0	453	3.56	173
SS-11	175	1,086	580	92.0	580	3.68	180
SS-12	69	396	137	40.0	137	1.60	78

c) FOR BONDSLIP

	critical point (kip -inch)		rigidity ($x10^3$ kip -inch^2)							
	My	My'	KB-1	KB-1'	KB-2	KB-2'	KB-3	KB-3'	KB-4	KB-4'
SS-1	203	104	95.0	90.1	3.17	3.00	190	180	1.90	1.80
SS-2	152	88	100.3	98.1	3.33	3.27	200	196	2.01	1.96
SS-3	283	153	99.5	94.7	3.32	3.16	199	189	1.99	1.89
SS-4	287	155	103	98.0	3.43	3.27	206	196	2.06	1.96
SS-5	155	88	113	110.7	3.77	3.67	226	222	2.27	2.21
SS-6	151	87	89.2	87.4	2.97	2.91	178	175	1.78	1.75
SS-7	287	155	97.7	93.0	3.26	3.10	195	186	1.86	1.86
SS-8	395	203	170.0	155.0	5.67	5.17	340	310	3.40	3.10
SS-11	217	115	251.0	229.0	8.36	7.63	502	458	5.02	4.58
SS-12	514	277	119.0	108.0	3.96	3.60	238	216	2.38	2.16

Reproduced from best available copy.

TABLE 3.2(c) LIMITING MOMENTS AND PARTIAL RIGIDITIES

Edge Column connections transferring moment parallel to the edge

a) FOR FLEXURE

	critical point (kip -inch)					rigidity ($x10^3$ kip -inch^2)				
	Mcr	My	My'	Mu	Mu'	EI-g	EI-y	EI-y'	EI-u	EI-u'
EL-1	43	200	145	211	153	1,064	276	214	2.74	1.14
EL-2	58	415	206	437	217	1,546	626	326	13.80	2.50
ELS-1	42	324	176	341	179	1,118	514	222	15.40	2.93
ELS-2	44	344	172	362	181	1,178	519	264	15.40	2.60
ELS-3	33	281	145	296	123	890	454	188	7.86	1.12

b) FOR TORSION

	critical point (kip -inch)		rigidity ($x10^3$ kip -inch^2)				
	Tcr	Tu	KT-1	KT-2	KT-3	KT-4	ET
EL-1	62.7	325	203	24.1	203	2.03	99
EL-2	86.2	458	344	67.4	344	3.44	317
ELS-1	63.1	235	205	32.7	205	2.05	154
ELS-2	65.3	310	216	34.8	216	2.16	164
ELS-3	115	654	461	79.3	461	4.61	373

c) FOR BONDSLIP

	critical point (kip -inch)		rigidity ($x10^3$ kip -inch^2)							
	My	My'	KB-1	KB-1'	KB-2	KB-2'	KB-3	KB-3'	KB-4	KB-4'
EL-1	141	71	168	167	5.61	5.56	336	334	5.61	5.56
EL-2	323	163	227	213	7.55	7.10	454	426	7.55	7.10
ELS-1	266	145	145	137	4.84	4.57	290	274	4.84	4.57
ELS-2	283	142	152	143	5.06	4.77	304	286	5.06	4.77
ELS-3	239	95	210	198	6.99	6.59	420	398	6.99	6.59

TABLE 3.2(d) LIMITING MOMENTS AND PARTIAL RIGIDITIES

Edge connection tests transferring moment normal to the edge

a) FOR FLEXURE

	critical point (kip -inch)					rigidity ($\times 10^3$ kip -inch^2)				
	Mcr	My	My'	Mu	Mu'	EI-g	EI-y	EI-y'	EI-u	EI-u'
E-1	36	232	154	244	162	895	335	228	4.68	1.78
E-2	64	483	261	508	275	1,705	791	418	12.4	2.96
E-3	28	342	180	360	189	746	522	312	18.9	3.08
ES-1	47	455	263	479	277	1,249	732	415	16.5	4.16
ES-2	48	458	263	482	277	1,267	738	414	15.8	4.02
ES-3	48	460	263	484	277	1,278	743	415	15.4	3.94
ES-4	29	348	195	366	205	778	536	316	16.4	3.43
ES-5	74	694	363	731	382	1,956	1,040	596	32.6	5.76

b) FOR TORSION

	critical point (kip -inch)		rigidity ($\times 10^3$ kip -inch^2)				
	Tcr	Tu	KT-1	KT-2	KT-3	KT-4	ET
E-1	112	244	171	14.1	171	1.71	58
E-2	184	485	379	35.2	379	3.79	165
E-3	205	606	224	67.6	224	2.24	318
ES-1	136	312	229	25.2	229	2.29	118
ES-2	137	528	232	32.0	232	2.32	150
ES-3	138	320	234	25.3	234	2.34	119
ES-4	211	885	234	74.3	234	2.34	349
ES-5	88	332	201	19.7	201	2.01	93

c) FOR BOUNDSLIP

	critical point (kip -inch)		rigidity ($\times 10^3$ kip -inch^2)							
	My	My'	KB-1	KB-1'	KB-2	KB-2'	KB-3	KB-3'	KB-4	KB-4'
E-1	166	110	117	114	3.90	3.80	234	228	3.90	3.80
E-2	375	202	247	233	8.23	7.77	494	466	8.23	7.77
E-3	217	114	142	135	4.73	4.50	284	270	4.73	4.50
ES-1	328	190	158	150	5.27	5.00	316	300	5.27	5.00
ES-2	330	190	161	152	5.37	5.07	322	304	5.37	5.07
ES-3	332	190	163	154	5.43	5.13	326	308	5.43	5.13
ES-4	220	124	149	141	4.97	4.70	298	282	4.97	4.70
ES-5	561	293	307	291	10.23	9.70	614	582	10.23	9.70

Reproduced from best available copy.

TABLE 3.2(e) LIMITING MOMENTS AND PARTIAL RIGIDITIES
Corner connections

a) FOR FLEXURE

	critical point (kip -inch)					rigidity ($x10^3$ kip -inch^2)				
	Mcr	My	My'	Mu	Mu'	EI-g	EI-y	EI-y'	EI-u	EI-u'
C-1	48	212	136	224	143	593	148	90	1.23	0.44
C-2	37	204	133	214	140	458	143	95	1.89	0.74
C-3	63	430	213	452	225	835	332	168	5.80	1.20
CS-1	45	336	174	354	183	596	255	132	5.60	1.07
CS-2	31	286	151	301	159	416	216	119	5.50	1.08

b) FOR TORSION

	critical point (kip -inch)		rigidity ($x10^3$ kip -inch^2)				
	Tcr	Tu	KT-1	KT-2	KT-3	KT-4	ET
C-1	67.4	1[illegible]	113	7.18	113	1.13	29.4
C-2	56.7	129	87.5	7.18	87.5	0.88	29.4
C-3	90.7	237	186	21.1	186	1.86	99.2
CS-1	65.9	253	109	14.7	109	1.09	69.1
CS-2	110	597	125	40.9	125	1.25	192.2

c) FOR BONDSLIP

	critical point (kip -inch)		rigidity ($x10^3$ kip -inch^2)							
	My	My'	KB-1	KB-1'	KB-2	KB-2'	KB-3	KB-3'	KB-4	KB-4'
C-1	177	113	157	167	5.23	5.57	314	334	1.57	1.67
C-2	170	111	120	128	4.00	4.26	240	256	1.20	1.28
C-3	376	186	243	230	8.10	7.07	486	460	2.43	2.30
CS-1	282	146	154	118	5.13	3.90	308	236	1.54	1.18
CS-2	222	117	163	127	5.40	4.20	326	254	1.63	1.27

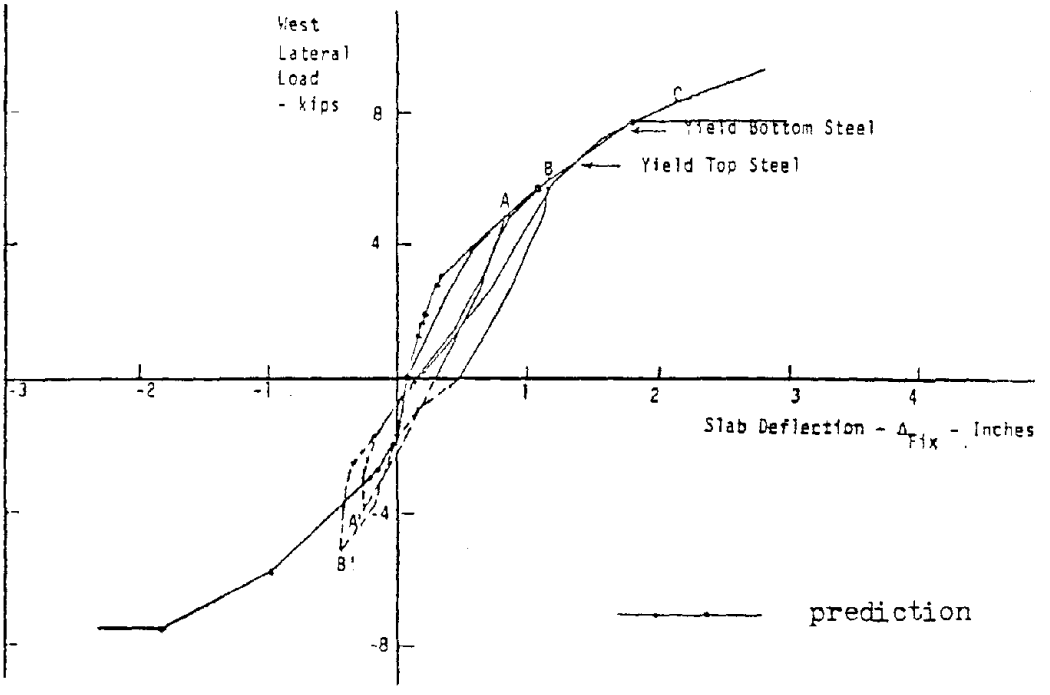

(a) S - 1 (Used for calibration)

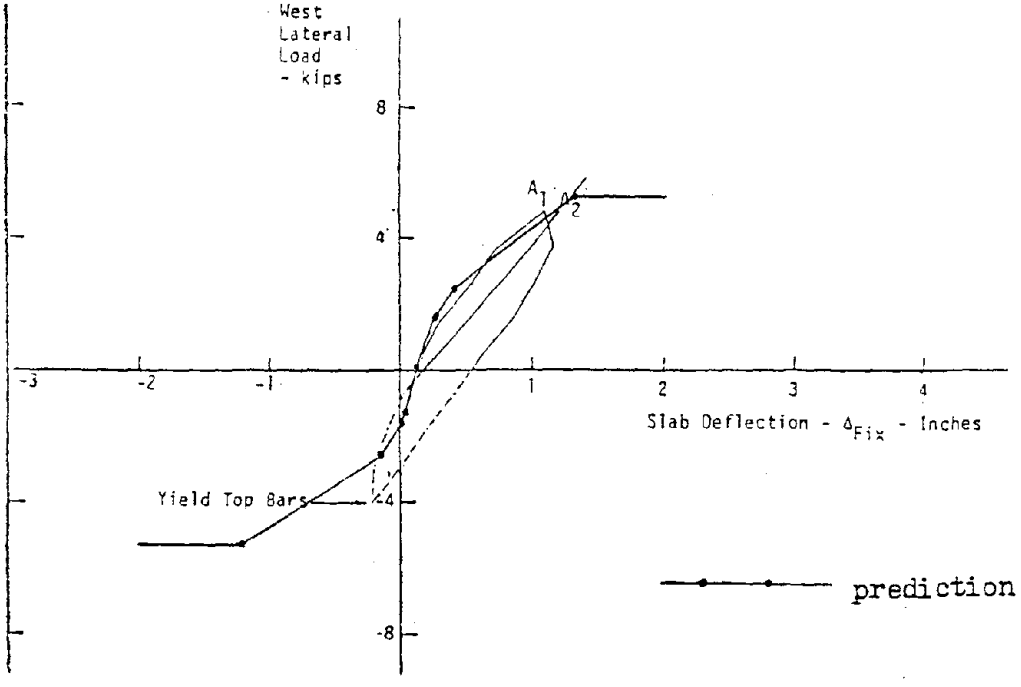

(b) S - 2 (Used for calibration)

FIG. 3.2 LATERAL LOAD-SLAB DEFLECTION RELATIONSHIP
(interior column connections)

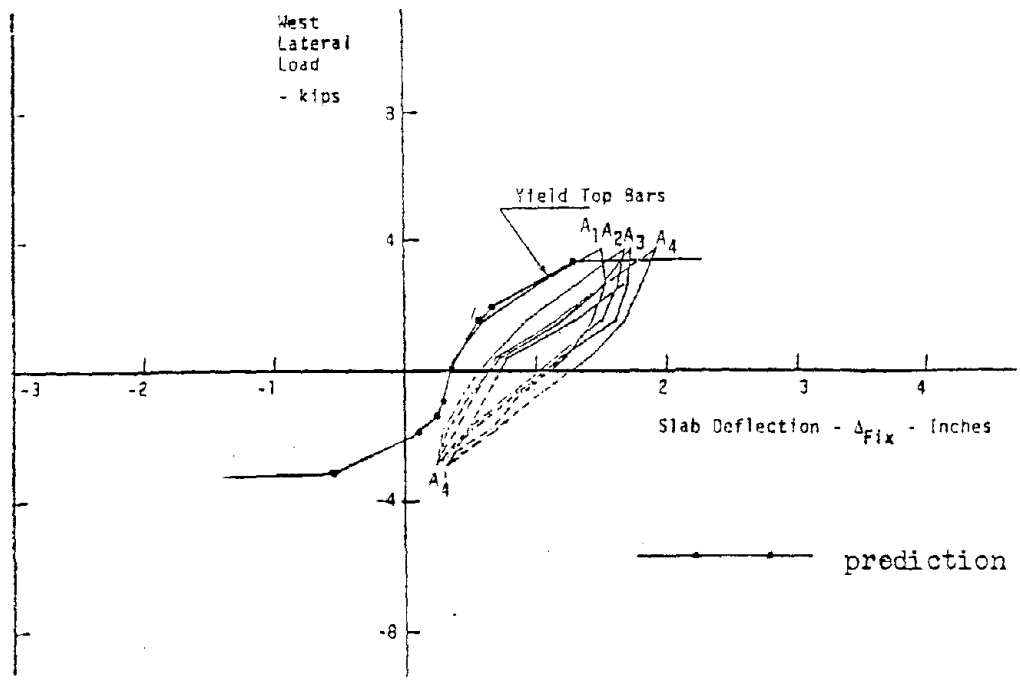

(c) S - 3 (Used for calibration)

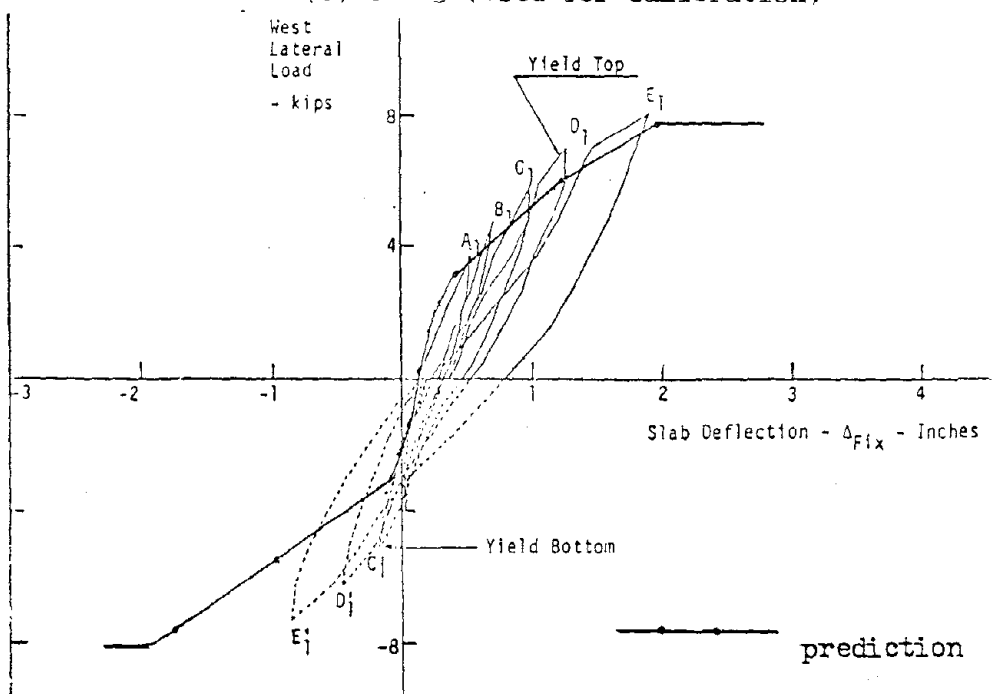

(d) S - 4 (Used for calibration)

FIG. 3.2 LATERAL LOAD-SLAB DEFLECTION RELATIONSHIP

(interior column connections)

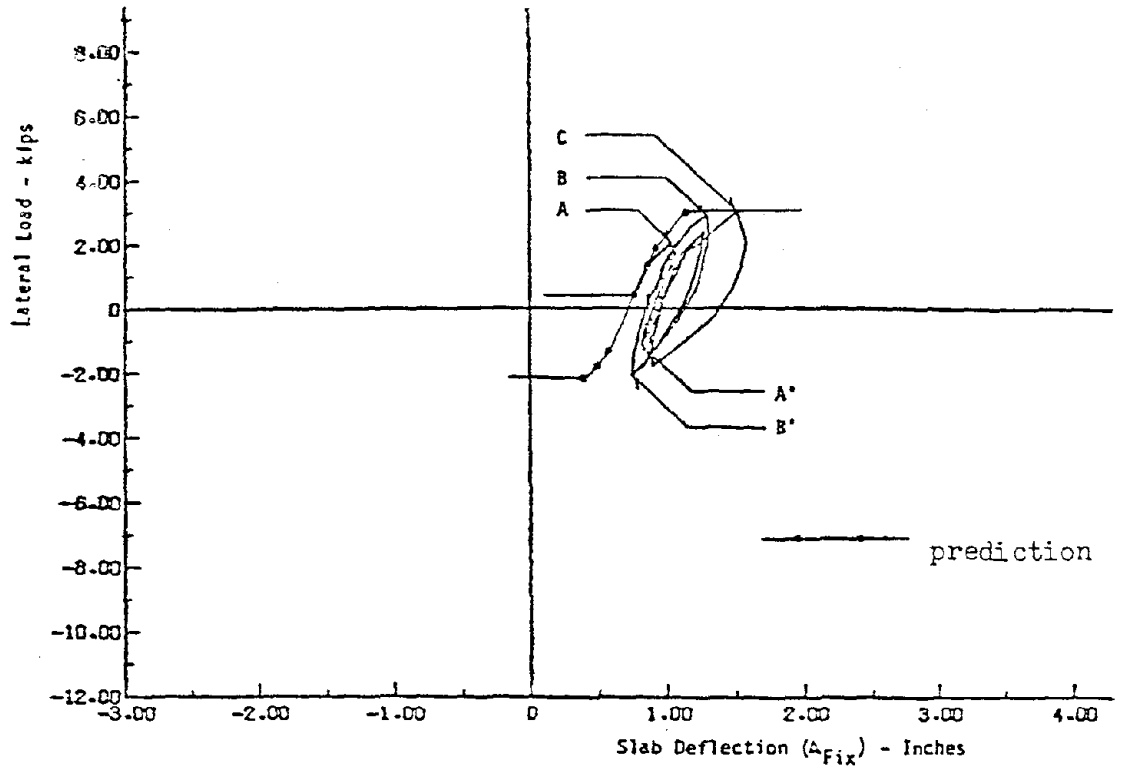

(e) S - 7

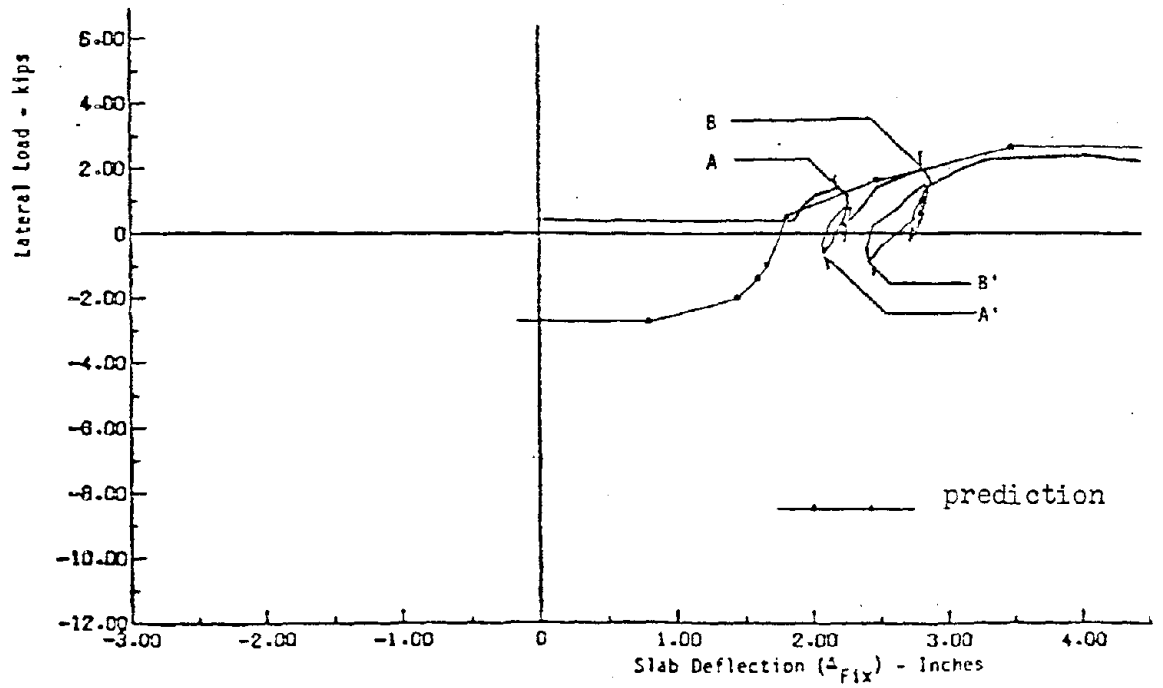

(f) S - 8

FIG. 3.2 LATERAL LOAD-SLAB DEFLECTION RELATIONSHIP
(interior column connections)

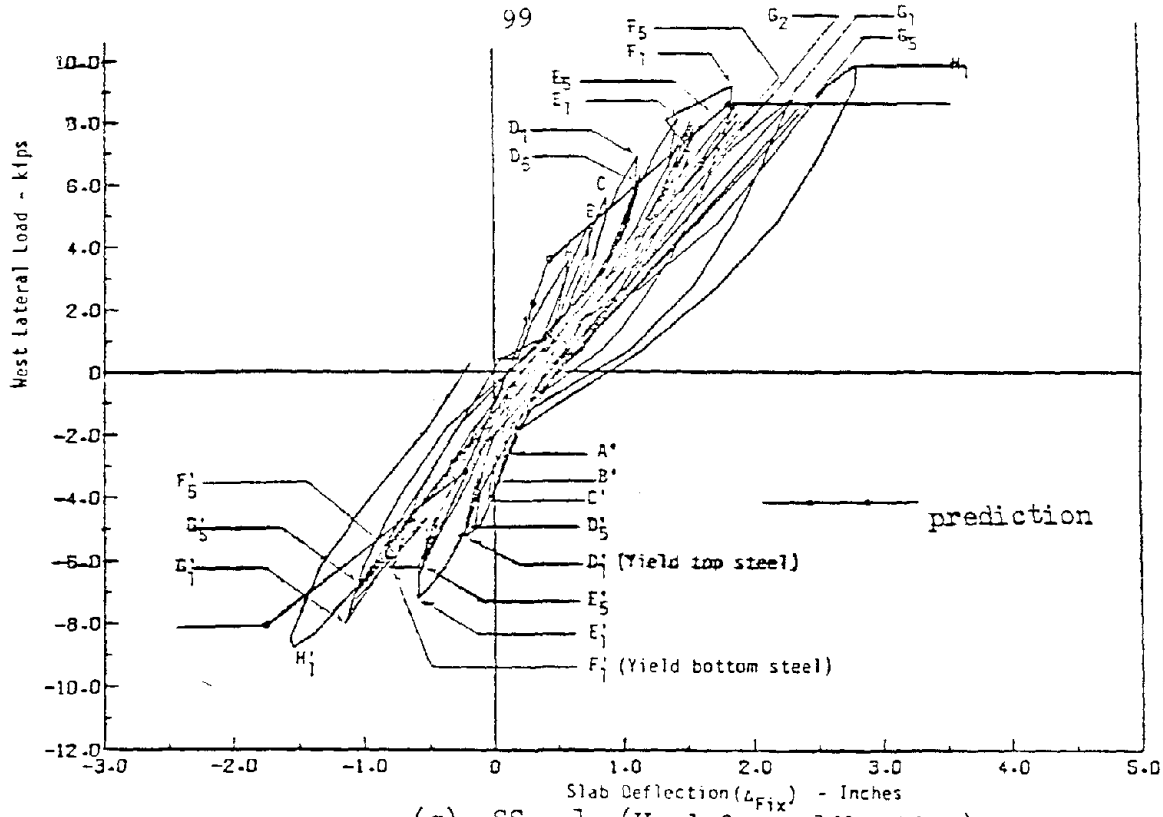

(g) SS - 1 (Used for calibration)

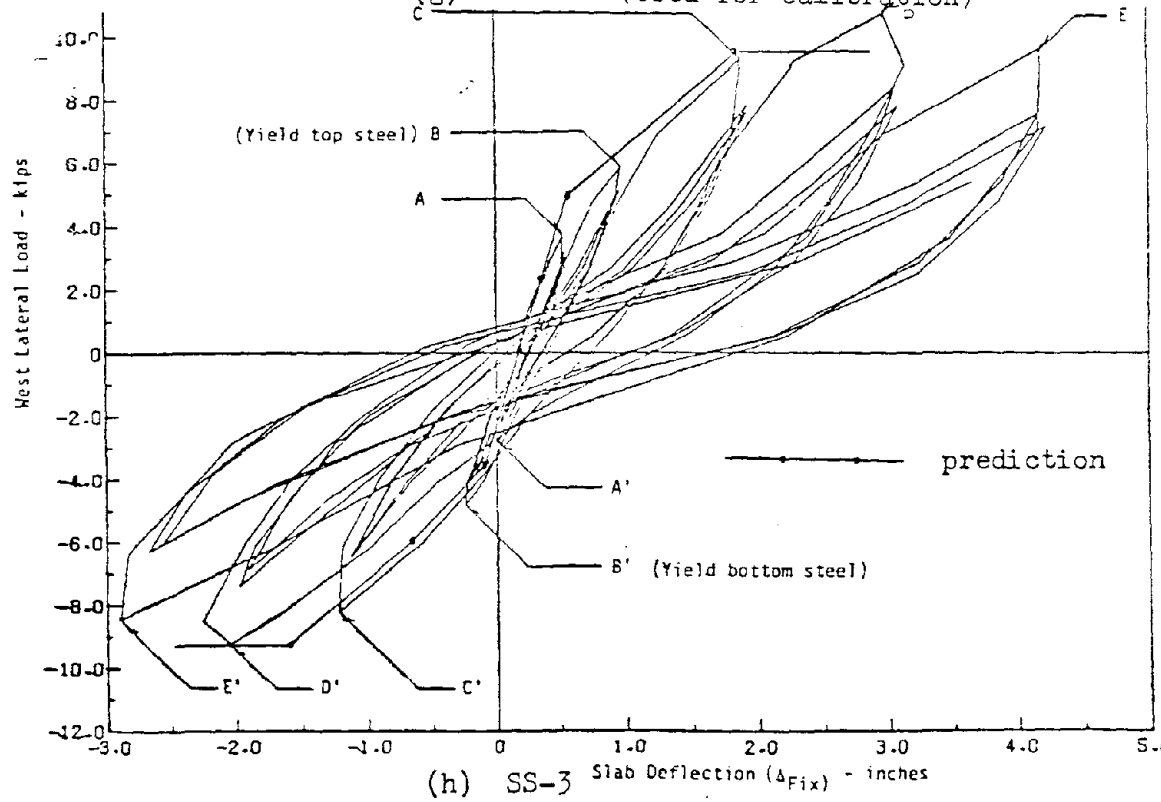

(h) SS-3 (Used for calibration)

FIG. 3.2 LATERAL LOAD-SLAB DEFLECTION RELATIONSHIP (interior column connections)

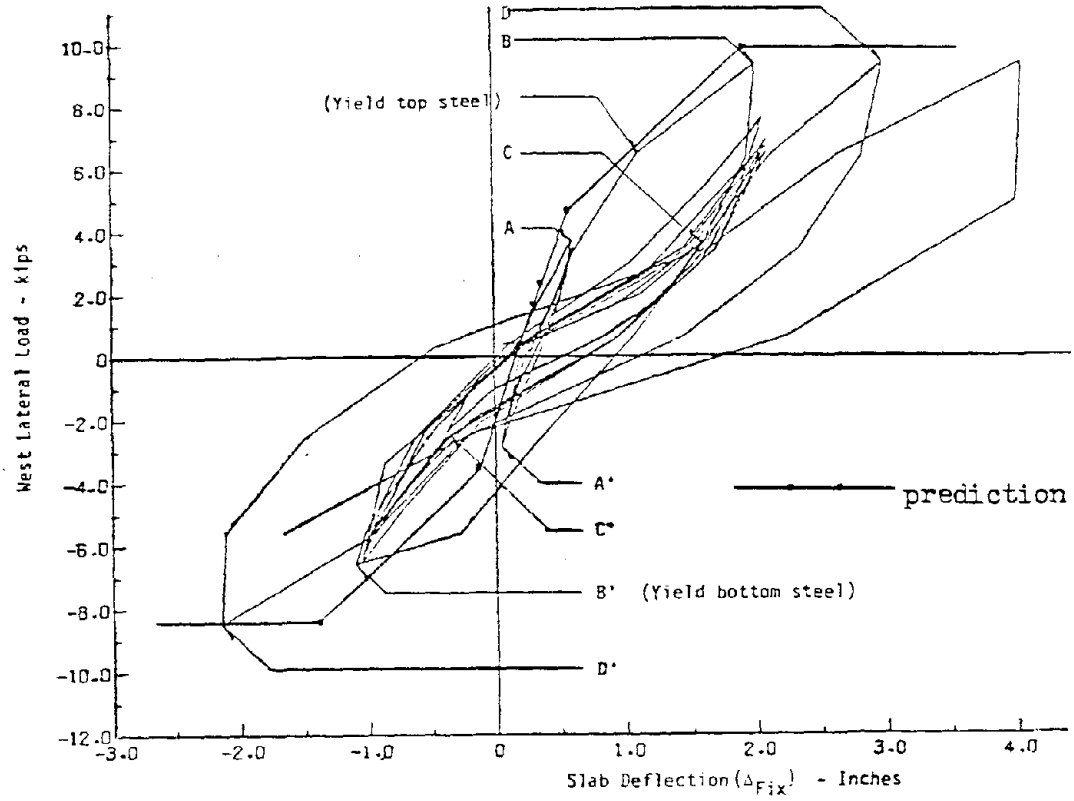

(i) SS - 4 (Used for calibration)

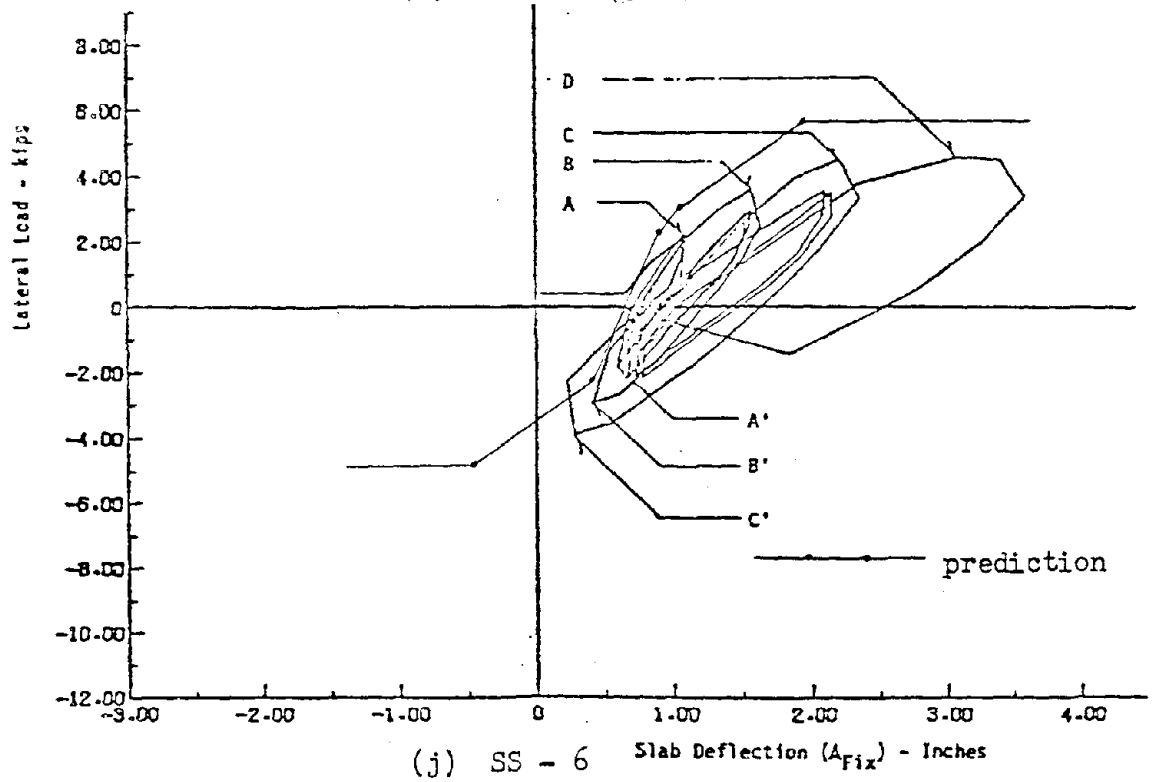

(j) SS - 6

FIG. 3.2 LATERAL LOAD–SLAB DEFLECTION RELATIONSHIP (interior column connections)

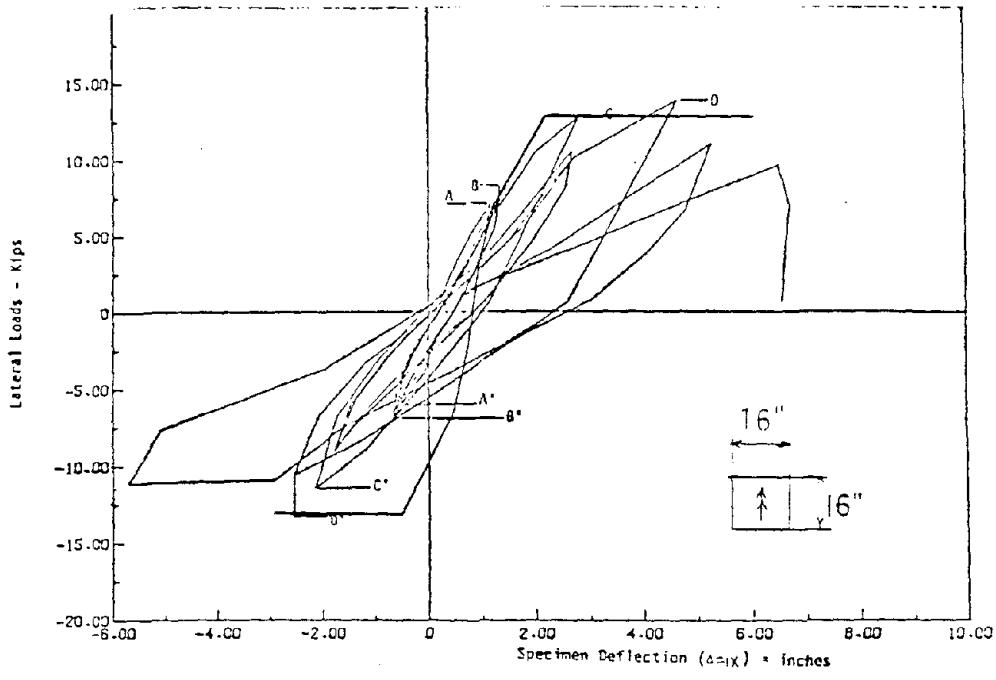

(k) SS-8

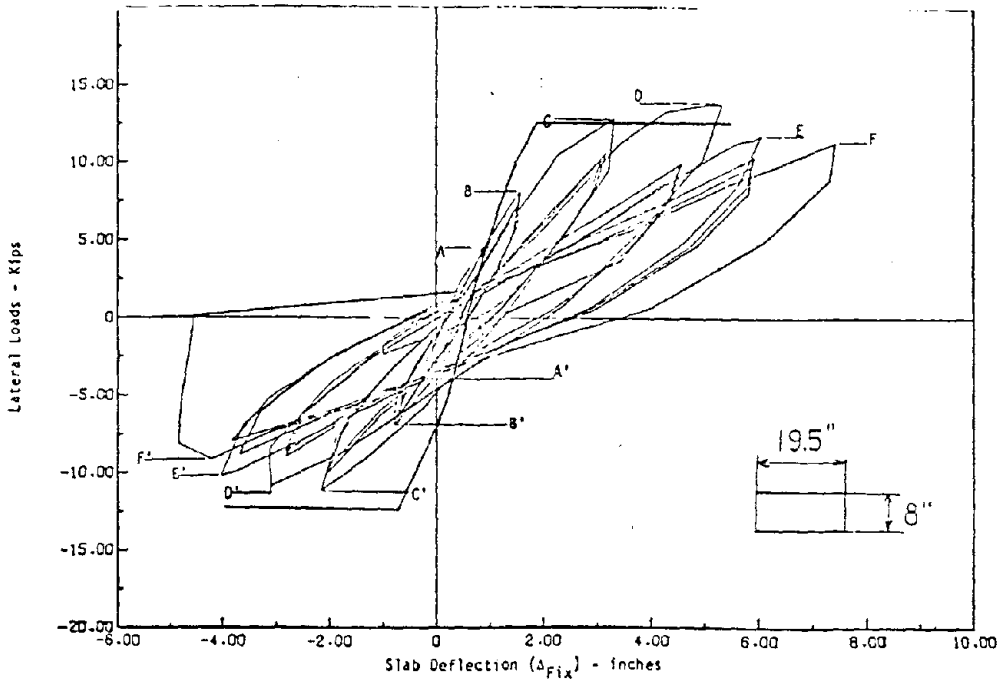

(l) SS-11

FIG. 3.2 LATERAL LOAD-SLAB DEFLECTION RELATIONSHIP (interior column connections)

analysis utilized a cracked section stiffness for the flexural element that was assumed constant until yielding. However, that is a simplistic assumption. The total stiffness is non-linear over the range between the cracked and yielding condition and there is a gradual loss in stiffness as conditions approach those for yielding. That result is clearly apparent from the relationship shown in Fig. 3.2(f) for S-8. Further, from Fig. 2.24(a), it is apparent that for that specimen the maximum strain for a lateral load of 29 kips was more than four times larger than the strain for a lateral load of 14 kips and two-thirds less than the strain for a lateral load of 45 kips. This gradual change in stiffness with increasing post-cracking loads is also probably the main reason why the large stiffness change between conditions before and after yielding of the reinforcing bars at the column face predicted by the analysis is not reflected in the test results.

For the specimens with shear reinforcement and with low intensity gravity loadings, SS-1, SS-2, SS-3, and SS-4, the predicted stiffnesses are again in good agreement with the test results. Examples are shown in Figs. 3.2(g), (h) and (i) for SS-1, SS-3 and SS-4, respectively. However, for the specimens with high gravity loadings, SS-6 and SS-7, typified by the result for SS-6 shown in Fig. 3.2(j), the predicted stiffness and strength are much larger than the test results. For stiffness, that discrepancy is attributed to the gradual decrease in stiffness caused by cracking as well as the wide shear crack that occurred around the end of the stirrups and eventually caused failure at a reduced capacity.

For predictions of the behavior of interior connections under reversed cyclic loading, it is possible, but cumbersome, to utilize the step-by-step method of Section 2.3 and Appendix B. However it is also possible, and much easier to use the Drain-2D program shown in Appendix C. Therefore that was the procedure used in this study. The stiffness matrix of Section 2.3 was built in to the modified Drain 2D program of Appendix C.

When the cyclic loading rules for each element were taken as described in Section 2.2 the modified Drain 2D was utilized, and the loading history for specimen SS-3 was applied to a computer model of that connection, the predicted behavior was as shown in Fig. 3.3. The time scale used for the loading history for Drain 2D was, as shown in Fig. 3.3(a), elongated enough to eliminate dynamic effects. The elongation necessary for the time scale was determined by trial and error, since the specimen was loaded by forces P applied at the ends of the slab while the Drain 2D model dealt with the forces generated at the ends of the slab by the excitation of a mass situated on the column line. When the lateral load-slab edge deflection relationship of Fig. 3.3(b) is compared to the test results shown in Fig. 3.2(h), it can be seen that the two are in good agreement. Although as shown in Fig. 3.1, the unloading stiffness for each element changed only at the M or T = 0 line, the sum of the effects for the different elements was such that, as apparent in Fig. 3.3(b), the total unloading stiffness changed before the P = 0 line was reached. Consequently, the hystereses loops became spindle-shaped after the flexural element yielded.

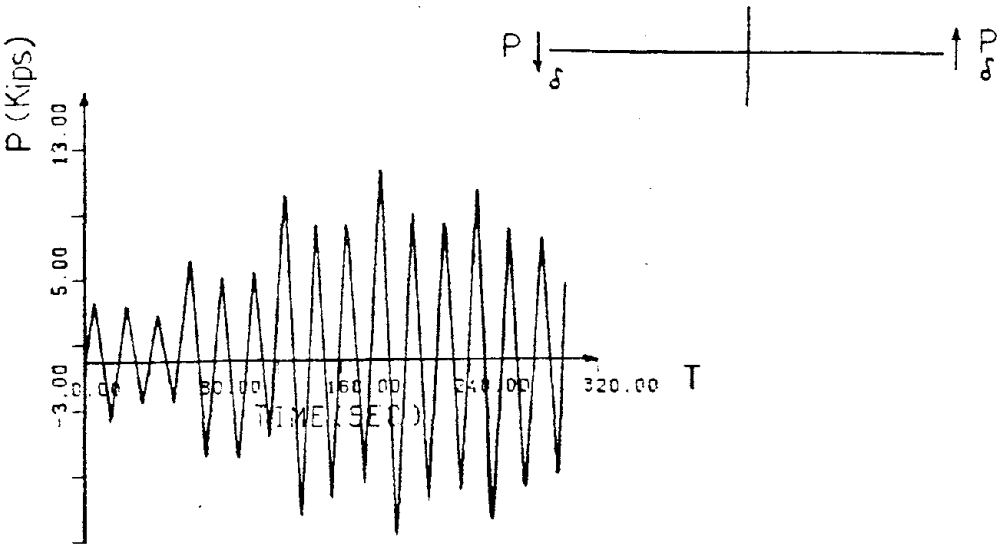

(a) loading history

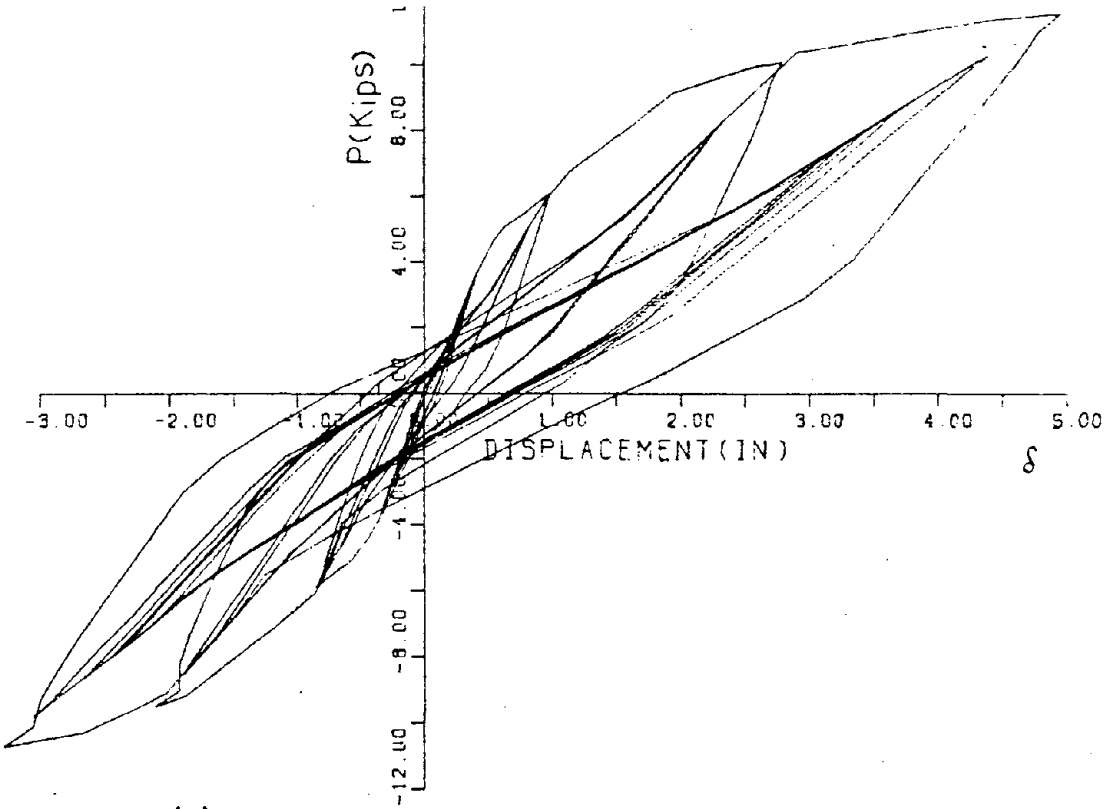

(b) lateral load - displacement relationship

FIG. 3.3 CYCLIC BEHAVIOR PREDICTION FOR SS - 3

From a comparison of Figs. 3.2(h) and 3.3, it can be seen that the cyclic loading rules defined in Section 2.2 can only predicted the measured response up to the maximum load achieved in a test. If, for increasing maximum displacements, the capacity degenerates then the small amplitude rules of Fig. 2.9(e) result in the hysteretic loops for that degenerated capacity lying within those for the prior maximum load. While that result deviates from the actual behavior, it is desirable for design purposes since it is conservative.

(2) Edge Connections Transferring Moment Parallel to the Edge

The critical points for change in stiffness and the stiffnesses at each loading stage are shown for each specimen in Table 3.2(c). The predicted and measured load-deflection envelopes are shown in Figs. 3.4(a) and (b). The predicted cyclic behavior for ELS-2 is also shown in Fig. 3.4(c). In all cases, differences for strength, stiffness, and hysteretic behavior between predicted and measured results are not large. It can be concluded that the step-by-step method is also applicable for predictions of the behavior of edge connections transferring moments parallel to the edge.

(3) Edge Connections Transferring Moment Normal to the Edge

Computed critical points and stiffnesses for each specimen for each loading stage are shown in Table 3.2(d) and predicted and measured envelopes for typical specimens E-1 and ES-2 are compared in Figs. 3.5(a) and (b). The predicted cyclic behavior for ES-2 is shown in Fig. 3.5(c). Measured and computed results for strength, stiffness, and hysteretic behavior are in good agreement.

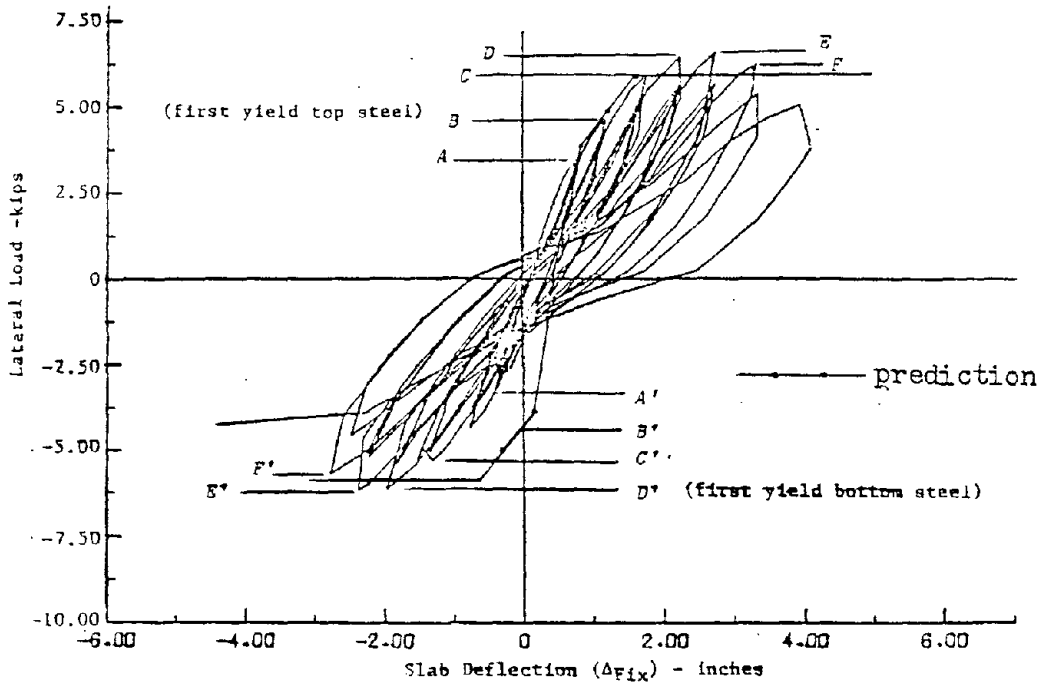

(a) ELS - 1

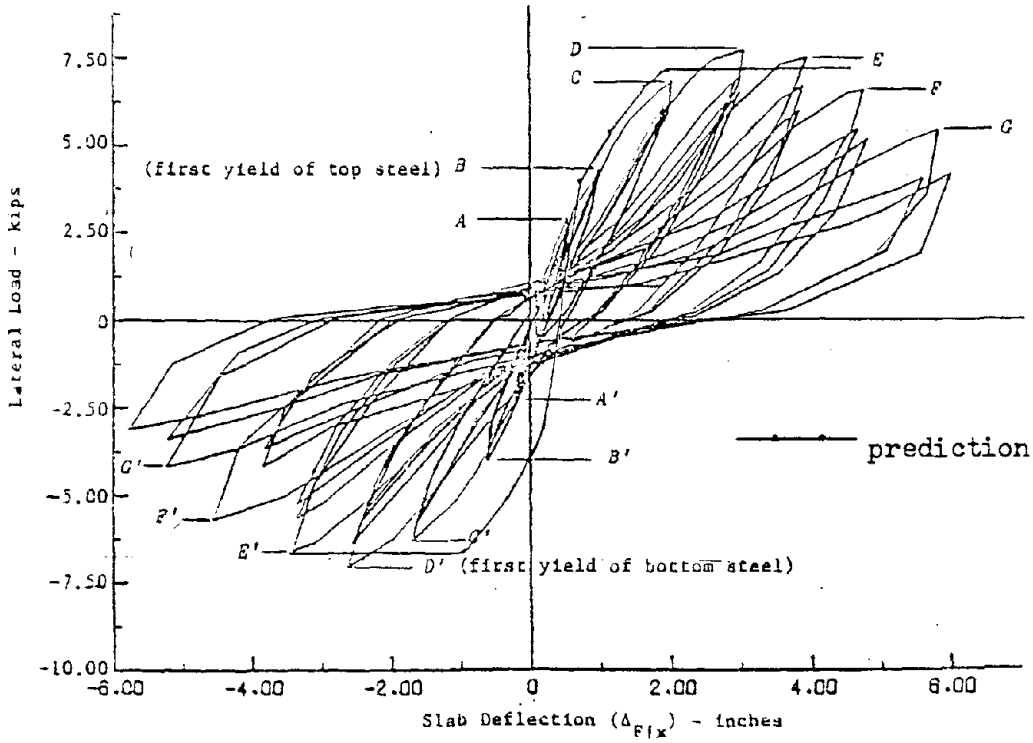

(b) ELS - 2

FIG. 3.4 LATERAL LOAD–SLAB DEFLECTION RELATIONSHIP (edge column connection transferring moment parallel to the edge)

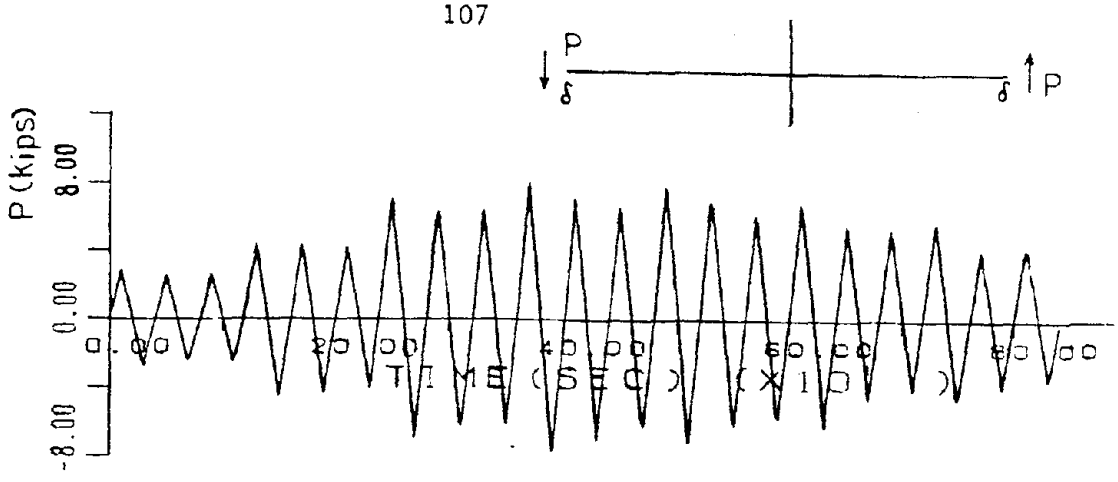

loading history

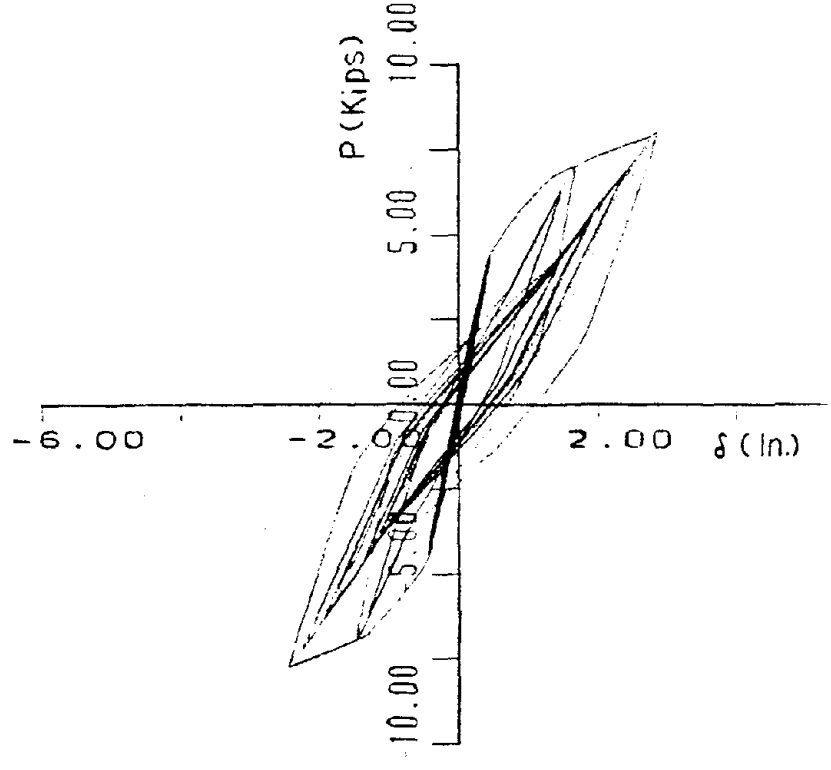

(c) cyclic behavior prediction for ELS - 2

FIG. 3.4 LATERAL LOAD-SLAB DEFLECTION RELATIONSHIP
(edge column connection transferring moment parallel to the edge)

Reproduced from
best available copy.

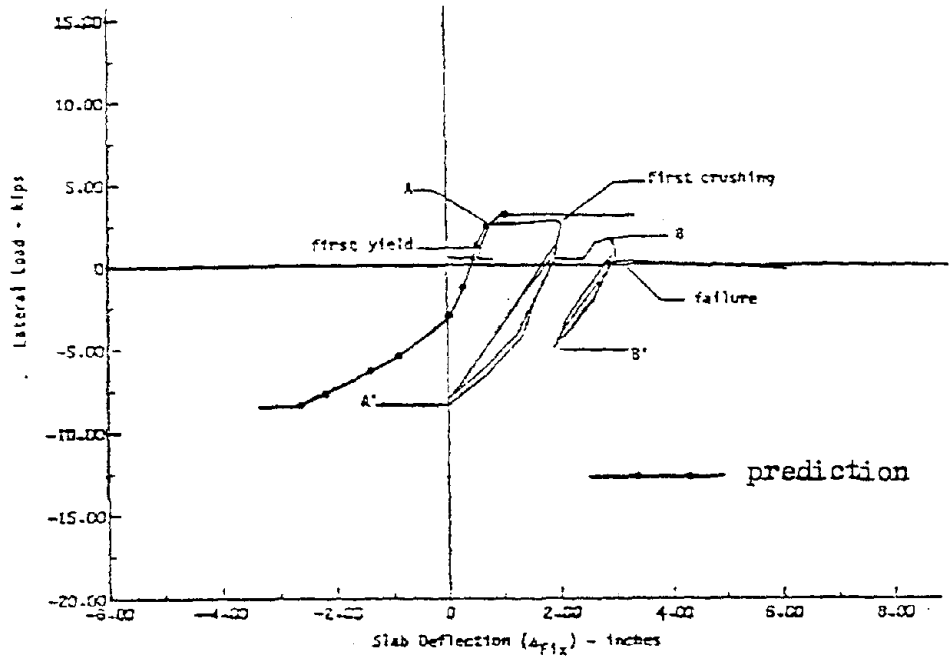

(a) E - 1

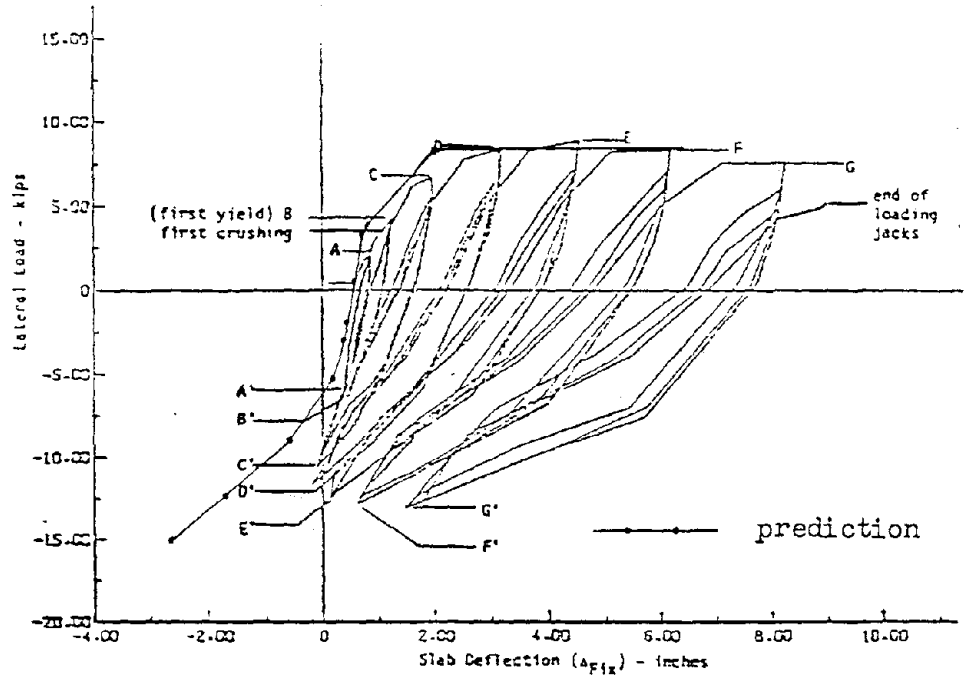

(b) ES - 2

FIG. 3.5 LATERAL LOAD – SLAB DEFLECTION RELATIONSHIP (edge column connection transferring moment normal to the edge)

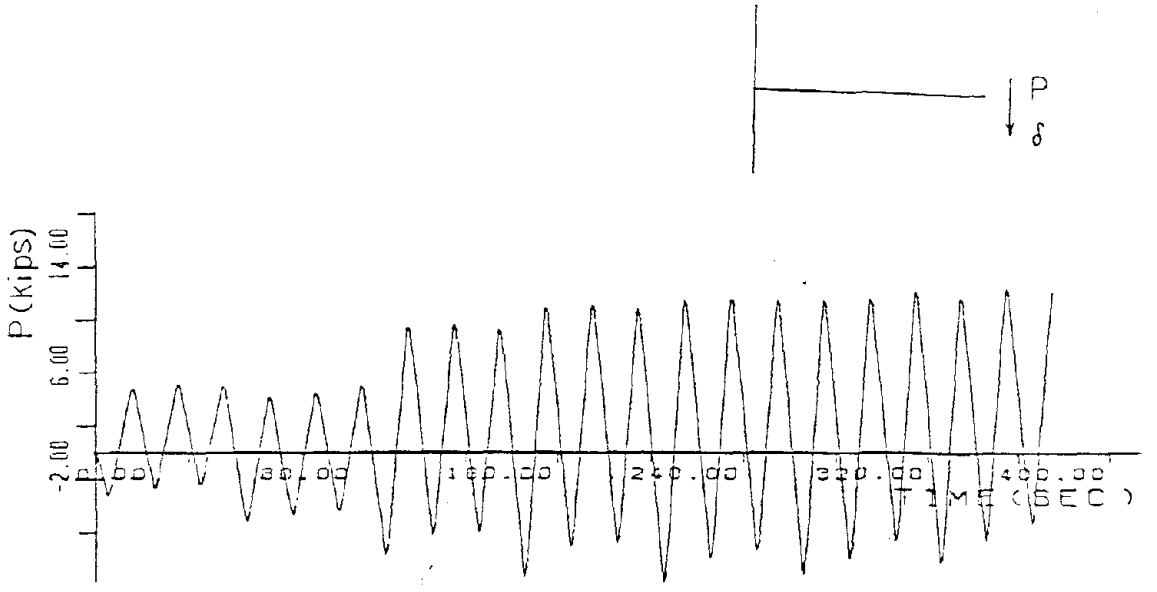

loading history

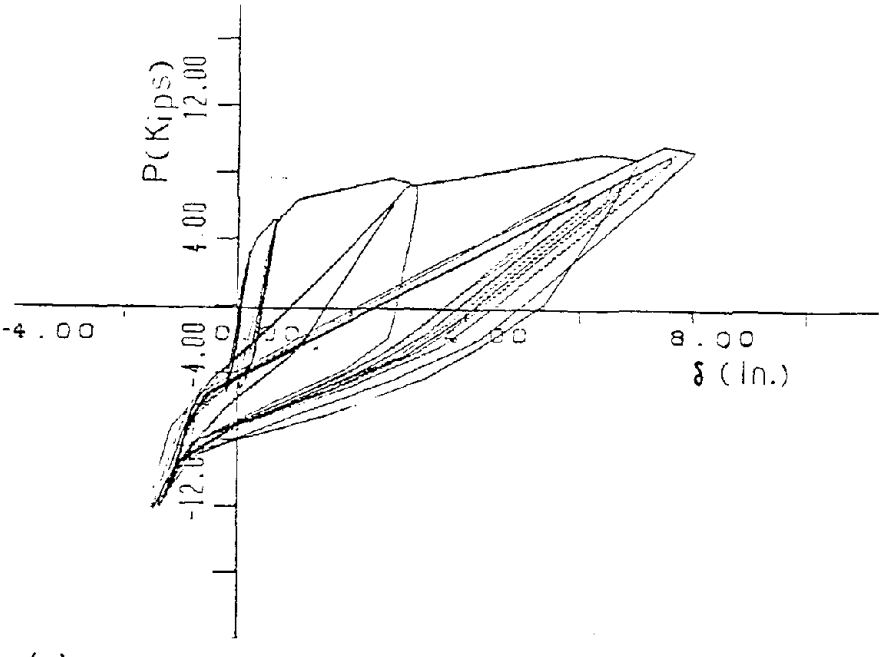

(c) cyclic behavior prediction for ES - 2

FIG. 3.5 LATERAL LOAD - SLAB DEFLECTION RELATIONSHIP
(edge column connection transferring moment normal to the edge)

(4) Corner Connections

Computed critical points and stiffnesses for each specimen for each loading stage are shown in Table 3.2(e). Predicted and measured envelopes for typical specimens C-1 and CS-1 are compared in Figs. 3.6(a) and (b) and the predicted cyclic behavior for CS-2 is shown in Fig. 3.6(c). Predicted and measured curves are in comparitively good agreement. There is, of course, a discrepancy between measured and predicted strengths for C-1 that follows from the computations shown in Table 3.1 (e):

3.4 Parameters Influencing Connection Behavior

The failure modes predicted for the connections have been categorized as punching shear, torsional crushing, and flexural crushing. Each mode is influenced by both gravity and lateral loading conditions and by physical and mechanical properties for the connection such as the amount and distribution of the reinforcing bars, the concrete strength, the shape of the column, etc. The effects of each of those parameters is examined in turn in this section using the analytical model of Chapter 2.

3.4.1 Loading Conditions

(1) Gravity Load Conditions

This influence is obvious from a comparison of the results for test specimens with identical reinforcement and geometry and differing gravity loadings, such as S-2 and S-7, S-4 and S-8, SS-4 and SS-7, SS-2 and SS-6 and ES-1 and ES-3. From such comparisons, it is

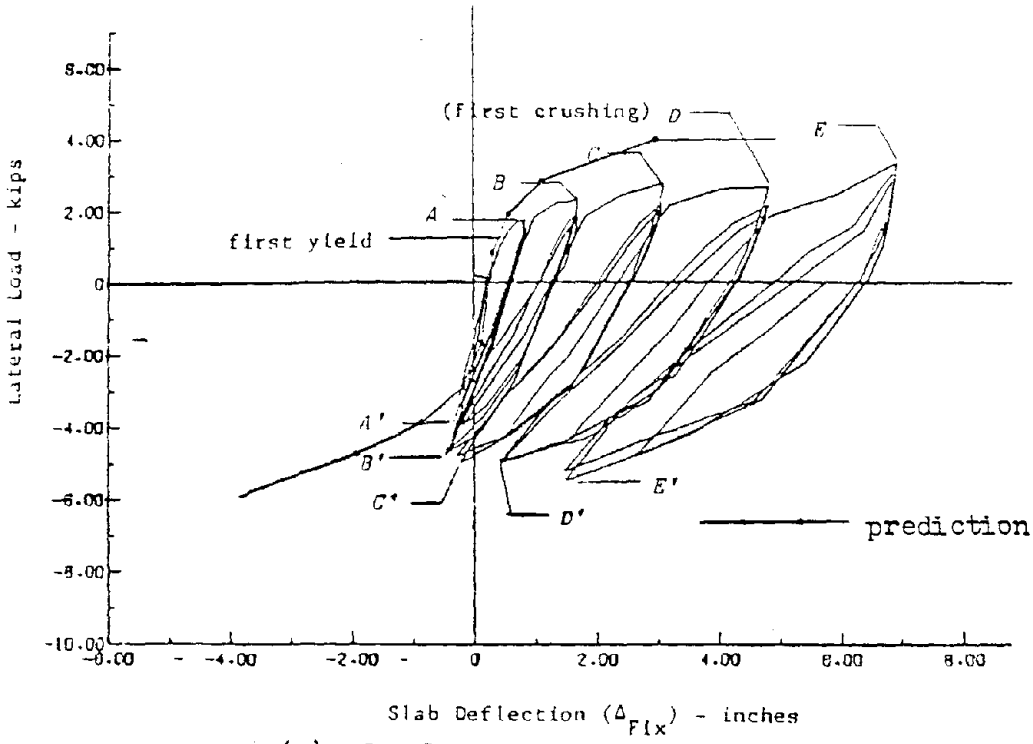

(a) C - 1

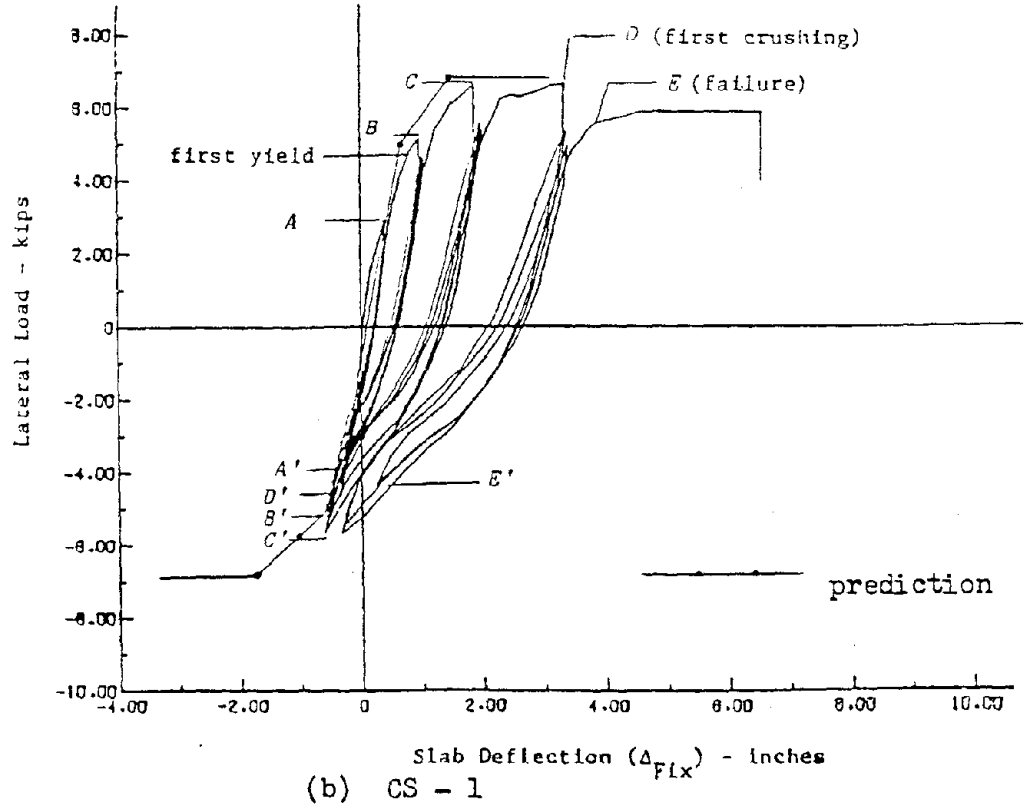

(b) CS - 1

FIG. 3.6 LATERAL LOAD - SLAB DEFLECTION RELATIONSHIP (corner column connection)

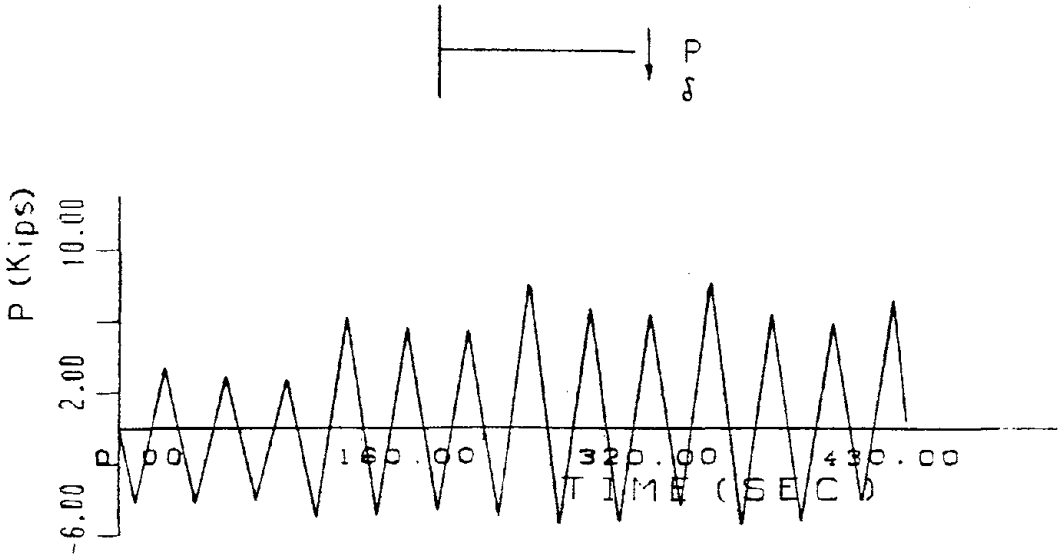

loading history

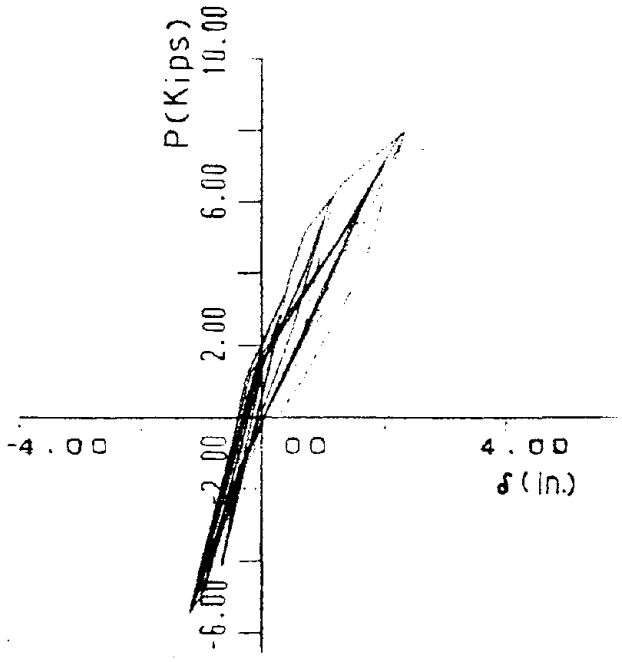

(c) cyclic behavior prediction for CS - 1

FIG. 3.6 LATERAL LOAD-SLAB DEFLECTION RELATIONSHIP (corner column connection)

clear that both strength and stiffness are greatly influenced by gravity loading.

Symonds, et al, (5) tried to take this influence into account in their beam analogy through the torsion-shear interaction relationship (Eq. 2.23 and 2.24). However, when the gravity load is large, it is not possible to correctly estimate the decrease in capacity caused by that load by decreasing only T_u. With the beam analogy proposed here, the responses of both the torsional and flexural elements are influenced by gravity load conditions. (Eq. 2.45). The result is a better prediction of gravity load effects than with the model of Ref. (5).

Shown in Fig. 3.7 are measured and predicted load-deflection responses that clearly demonstrate that the procedure developed here predicts gravity load effects. Fig. 3.7(a) compares responses for S-2 and S-7. The gravity load on S-2 was half that on S-7. Fig. 3.7(b) compares the responses predicted for a specimen without any gravity load, SS-4 with a gravity load of 29 kips, and SS-7 with a load of 61 kips.

The influence of the gravity loading is larger for the specimens without shear reinforcement than for those with shear reinforcement. Two effects are predicted: (1) an increased initial deflection with increasing gravity loads, and (2) an increased stiffness at loads approaching the failure load for increasing gravity loads. The strength and stiffness observed for SS-7 were smaller than the predicted because of the impending shear failure that occurred outside the ends of the stirrups. Except for that case, it is

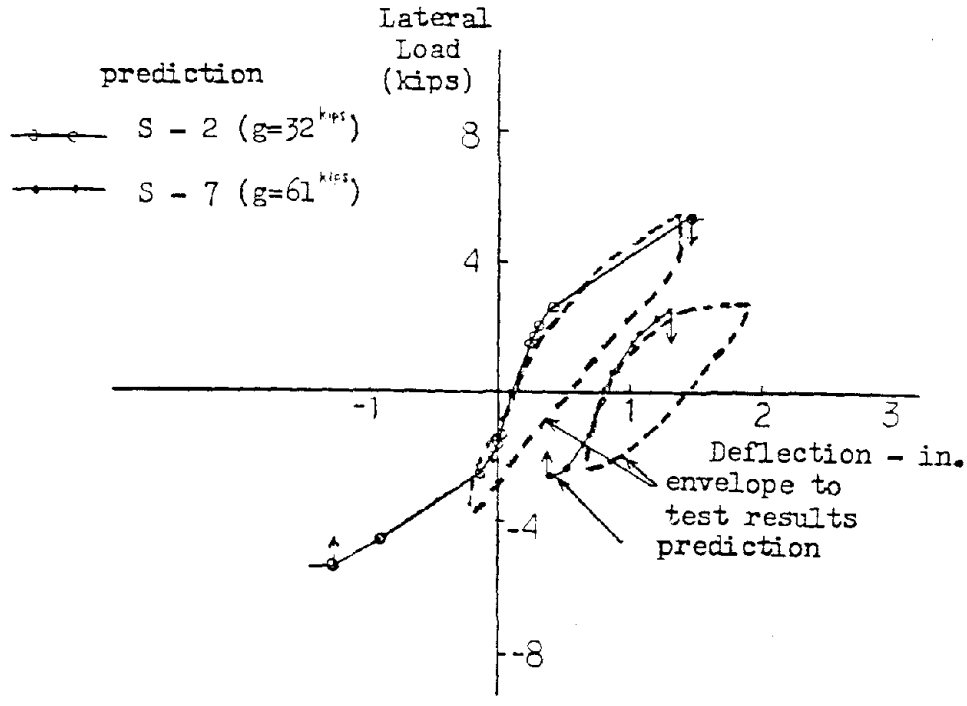

(a) Specimens without shear reinforcement

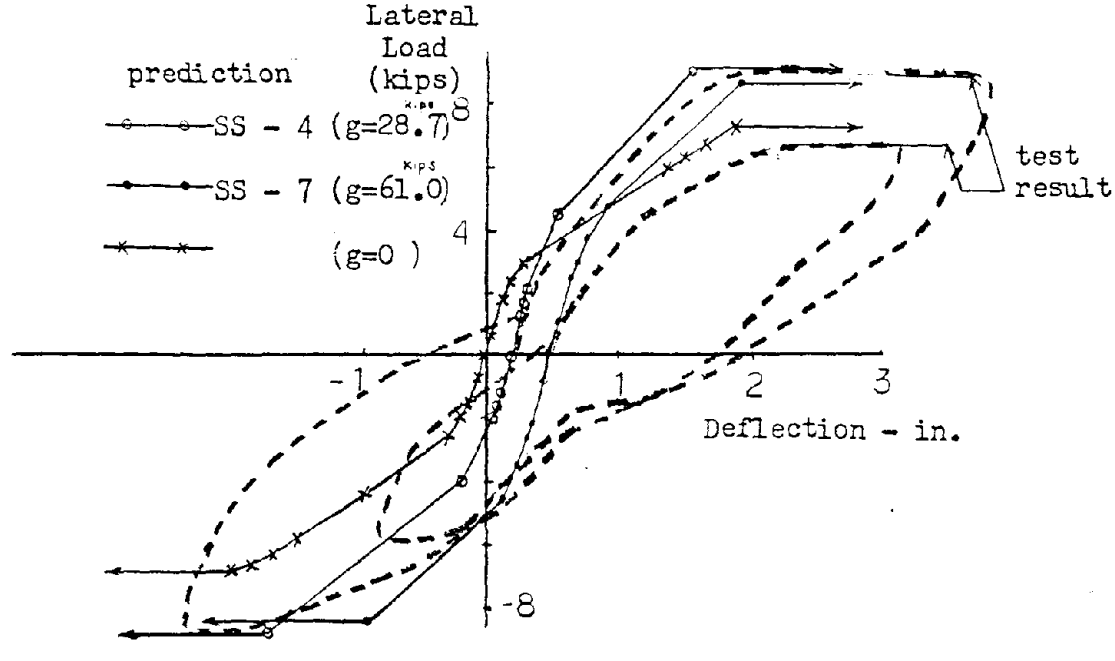

(b) Specimens with shear reinforcement

FIG. 3.7 INFLUENCE OF GRAVITY LOAD

apparent that the procedure developed here represents well the influence of gravity loading.

Shown in Fig. 3.8 is the effect predicted for the gravity load on the ultimate capacity for moment transfer. That capacity increases to a limited extent with increasing gravity load because usually the top reinforcing ratio for the slab is larger than the bottom reinforcing ratio. However, as apparent from Fig. 3.8(b), once the maximum capacity condition is exceeded, the capacity decreases rapidly with increasing gravity load. The maximum capacity condition occurs when the gravity load moment equals the difference in the positive and negative moment capacities for the flexural elements.

(2) Lateral Loading History

The influence of the lateral loading history can be examined by comparing the measured and predicted responses for SS-3 and SS-4. The distribution and amounts of flexural and shear reinforcement for SS-4 were identical to those for SS-3. The concrete strength for SS-4 was only ten percent greater than that for SS-3 so that the main difference for the two specimens was their loading history.

As shown in Figs. 3.2(h) and (i) for the B sequence, SS-4 was cycled eleven times between fixed deflection limits while SS-3 was cycled only three times in that sequence. An attempt was then made to cycle SS-4 between increasing fixed load levels rather than the fixed deflection levels, used for SS-3. SS-4 failed during the second half of the second cycle of the subsequent loading sequence, whereas SS-3 was able to sustain many more cycles of loading before

$$M_{max} \propto M_f + M_b + T$$

$$= 2 \times (M_{uf} - M_g + \tfrac{1}{2} T_u) \quad \text{or} \quad = 2 \times (M_{ub} + M_g + \tfrac{1}{2} T_u)$$

whichever is smaller

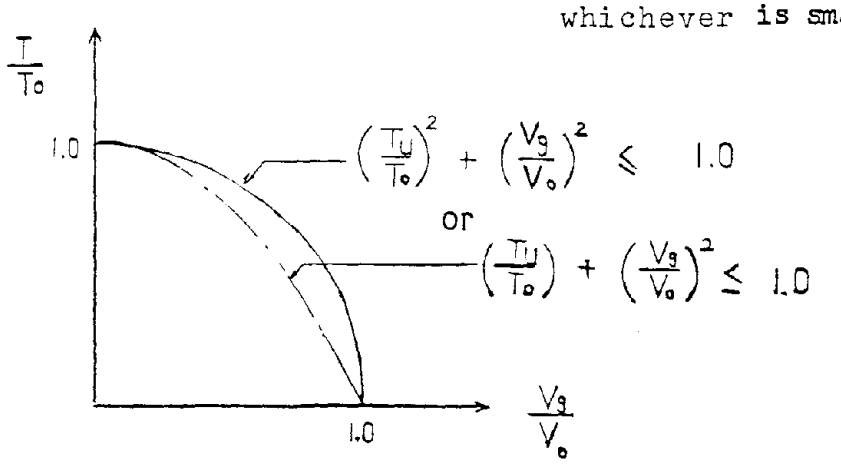

(a) for torsional capacity

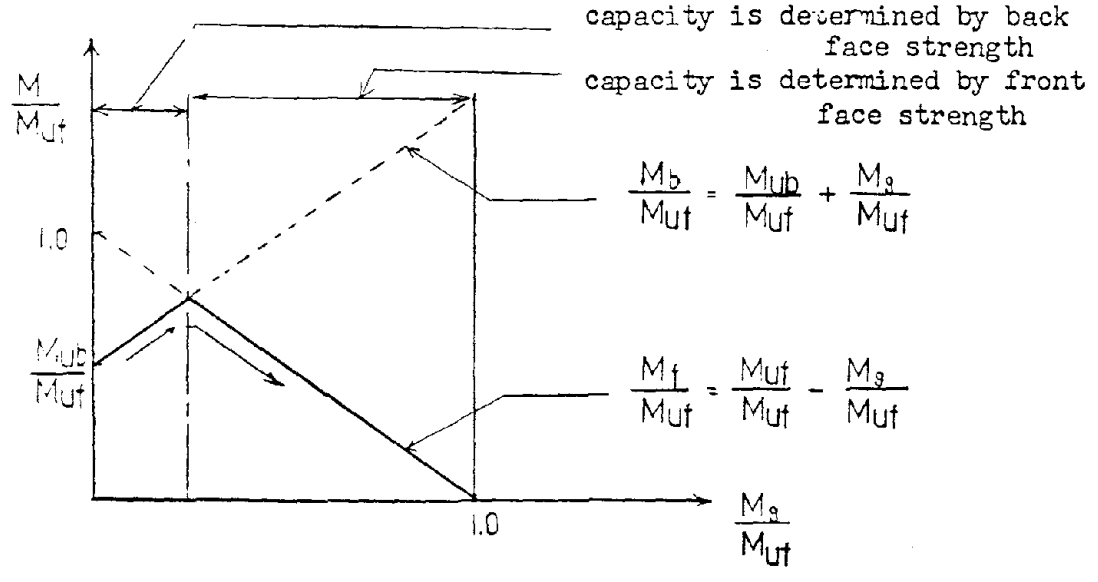

(b) for flexural moment capacity

FIG. 3.8 INFLUENCE OF GRAVITY LOAD ON MOMENT TRANSFER CAPACITY

loading had to be discontinued due to the development of excessive deflections.

From a comparison of the load-deflection curves for SS-4 with those for SS-3, it is apparent that the response of the two specimens was very similar. The shape of hysteresis loops and the shape of the envelope to those loops were very similar.

The ultimate load for SS-4 was about 18 percent less than that for SS-3. That result clearly demonstrates that the lateral loading history affects the ultimate capacity and that cycling between fixed load limits is more damaging than cycling between fixed deflection limits. This can be checked also by comparing tensile strains for the top reinforcement for the two specimens. Those results are plotted in Fig. 3.9. For SS-3, the yielding region is considerably wider than for SS-4 where yielding is virtually confined to the critical section of width $(c_2 + d)$ centered on the column. From this it can be concluded that cycling between fixed deflection limits redistributes the moment better than cycling between fixed load limits and that monotonically increased loading to a large deflection before reversed cycling is begun is much more damaging than building up to the same deflection with multiple reversed cycles between increasing deflection limits.

This phenomenon of differing amounts of moment redistribution with differing loading patterns is not predictable with the beam analogy presented here. It would be necessary to take into account the change in the stress-strain characteristics for the steel and the

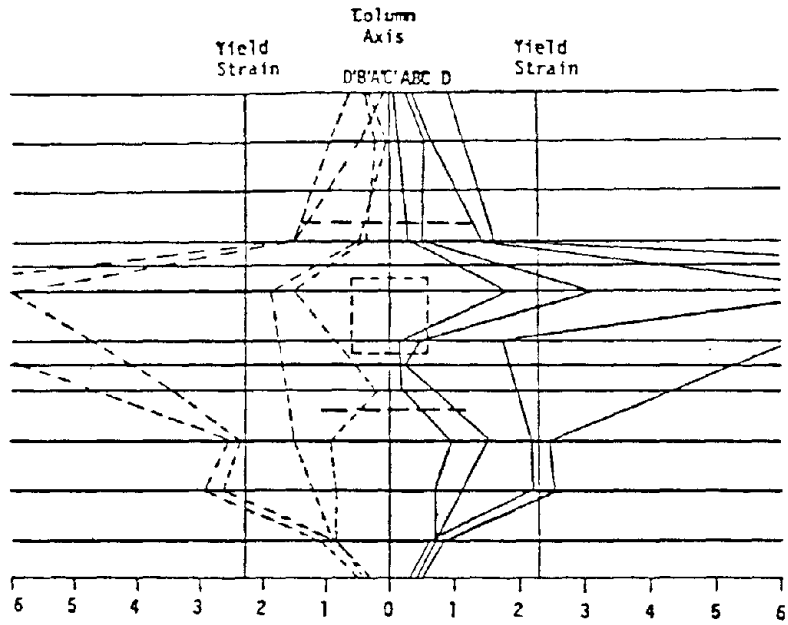

(a) SS – 3

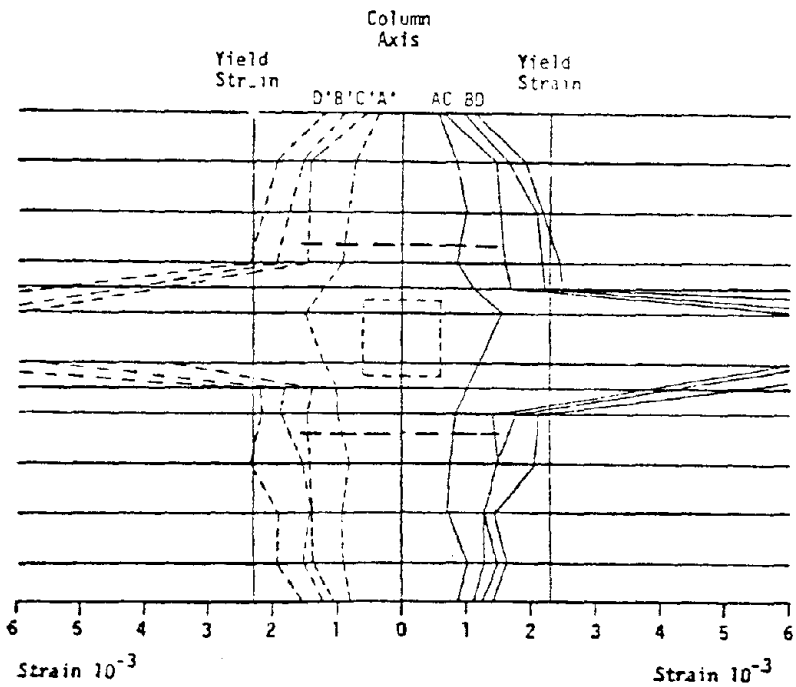

(b) SS – 4

FIG. 3.9 INFLUENCE OF LOADING HISTORY ON STRAIN IN TOP REINFORCING BARS

concrete caused by reversed cycling for perfect representation of the behavior.

3.4.2 Physical and Mechanical Conditions

(1) Concrete Strength

This influence can be examined by comparing results for pairs of test specimens similar in most respects except concrete strength, such as S-1 and S-4, SS-2 and SS-5, and C-1 and C-2. From Fig. 3.10 it can be seen that the influence of the concrete strength is not negligible. The higher the concrete strength, the stronger is the connection. However, the change in stiffness with concrete strength is virtually negligible.

In the beam analogy, concrete strength increases the capacity of both the flexural and torsional elements (M_{cr}, M_y, M_u, T_{cr} and T_u) and particularly reduces the impact of any shear cut-off on the strength of the flexural element. Further, if the capacity of the torsional element is dictated by Eq. (2.22) or (2.24) rather than Eq. (2.21), that influence becomes dominant.

Some examples are shown in Figs. 3.10(c) and (d). In Fig. 3.10(c), the moment transfer capacity of an interior column connection, represented by $2T_u + 1.5M_u$ for simplicity, is shown. That capacity is calculated from Eqs. (2.7), (2.21) and (2.24). For a reinforcement ratio of one percent f'_c has a large influence on the capacity because T_u is dictated by Eq. (2.24). However, as apparent for the result for a reinforcement ratio of 0.3% that influence becomes almost negligible when T_u is dictated by Eq. (2.21).

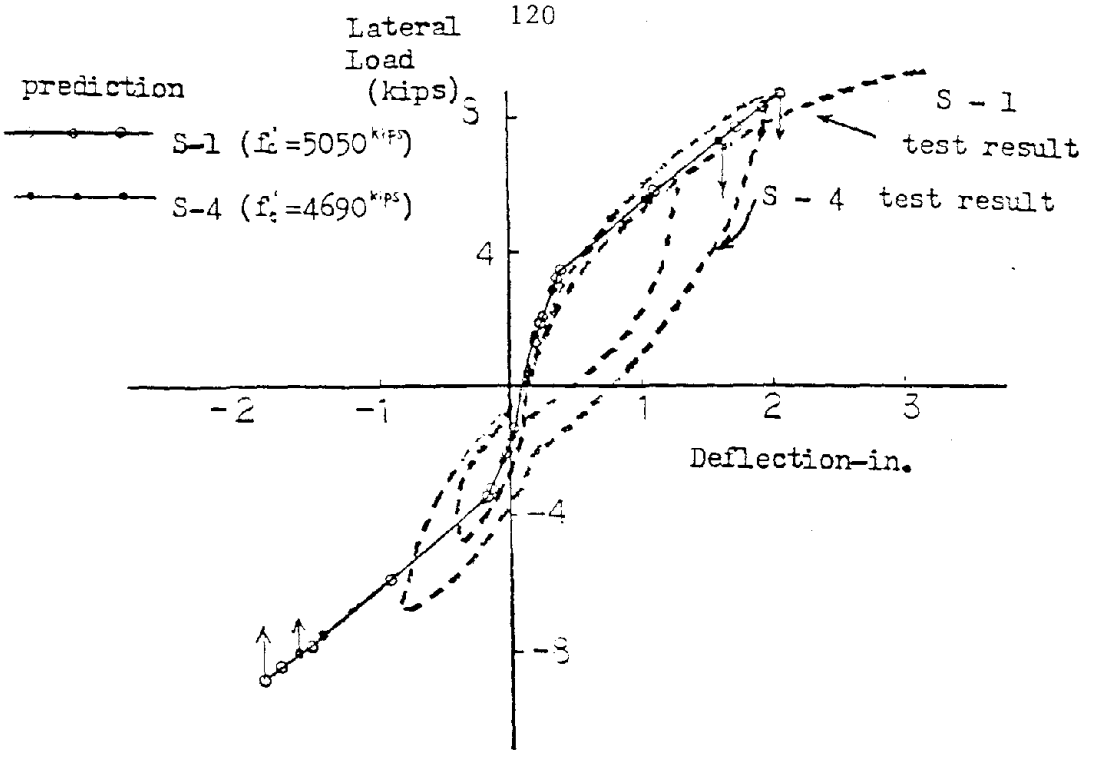

(a) without shear reinforcement

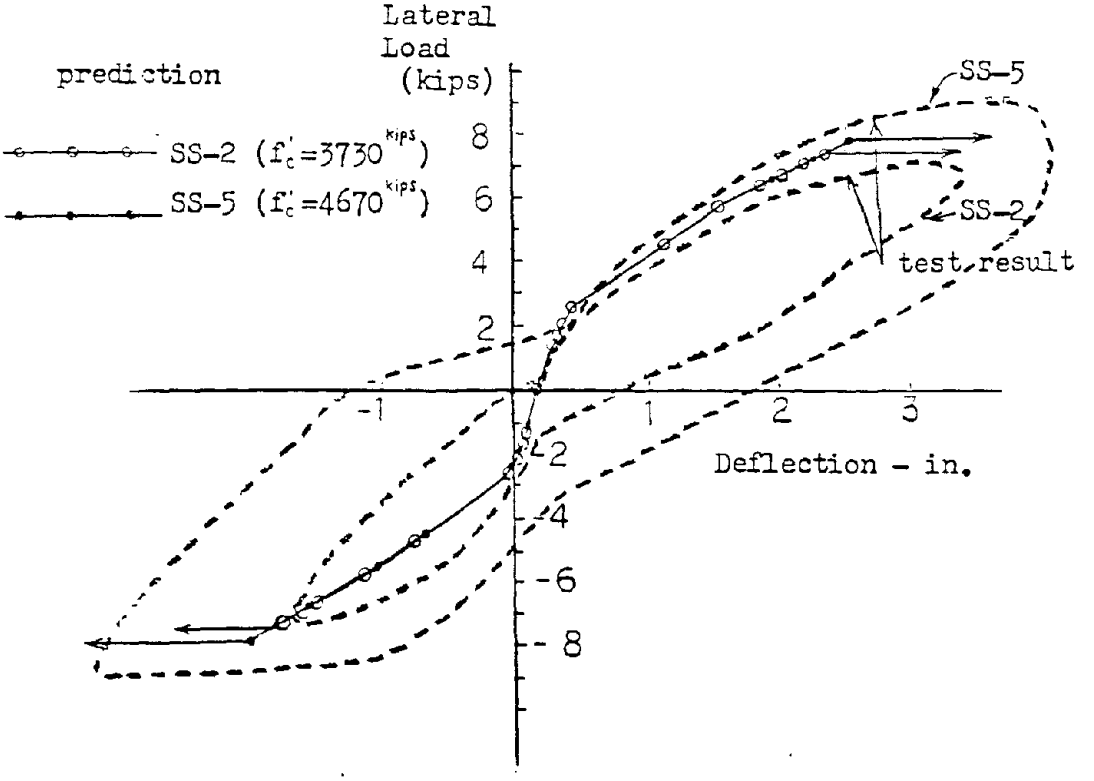

(b) with shear reinforcement

FIG. 3.10 INFLUENCE OF CONCRETE STRENGTH

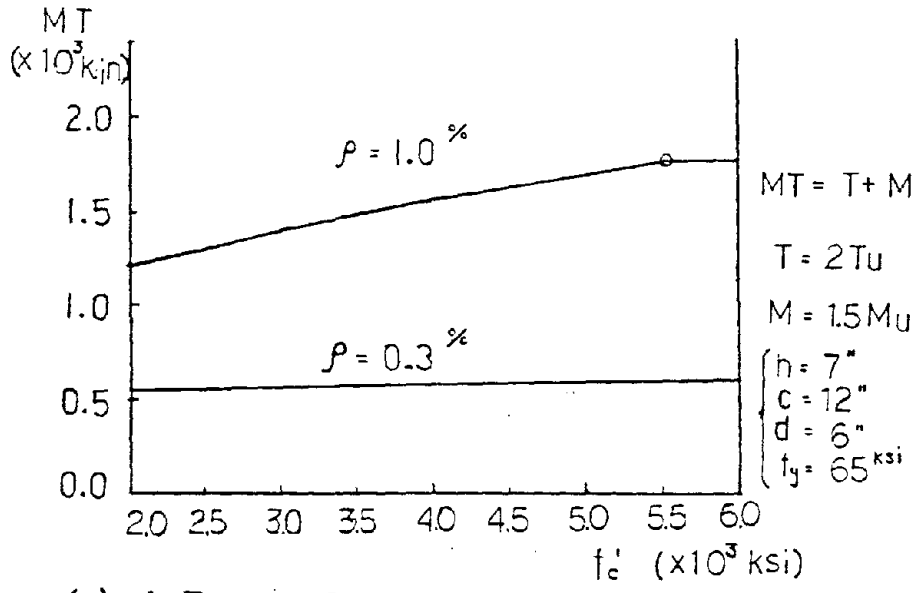

(c) influence of concrete strength on moment transfer capacity

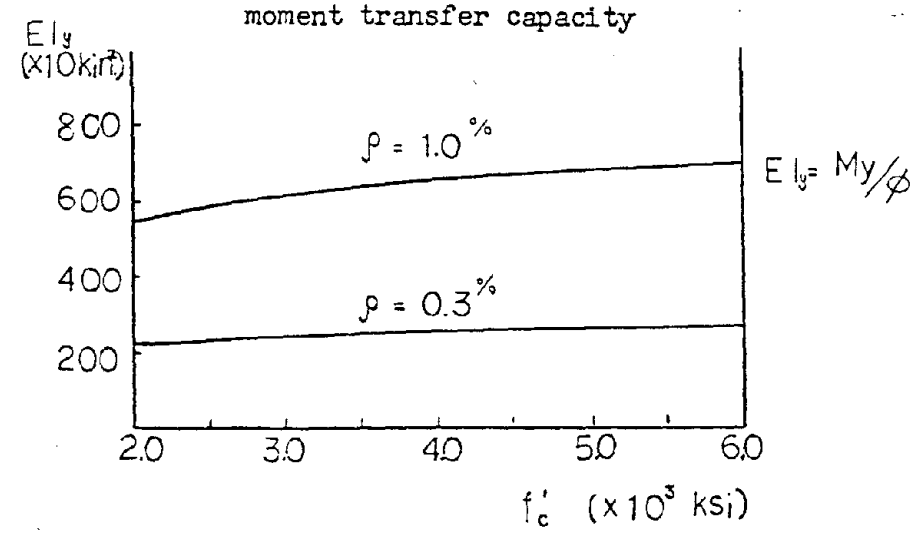

(d) influence of concrete strength on the stiffness of connection

FIG. 3.10 INFLUENCE OF CONCRETE STRENGTH

The influence of f'_c on the stiffness of connection is small compared to its influence on the strength of the connection. The stiffness after the yielding of the flexural element is governed by the stiffness of the torsional element which is represented by GJ_{cr}, Eq. (2.28). GJ_{cr} is clearly not influenced by f'_c. The stiffness before yielding of the flexural element is governed mainly by the stiffness of the flexural element. Shown in Fig. 3.10(d) is an example for the stiffness of the flexural element calculated from Eqs. (2.4) and (2.5). From Fig. 3.10(d) it is clear that the influence of f'_c on EI is not large and is almost negligible for the range of $3,500 < f'_c < 5,000$ psi.

The good agreement between predicted and measured results in terms of relative magnitudes of stiffness, strength and ductility shows that the effects of concrete strength are properly evaluated by the beam analogy.

(2) Flexural Reinforcement

The influence of the reinforcing ratio can be examined by comparing results for test specimens S-1, S-2 and S-3, or SS-2 and SS-3. As apparent from Figs. 3.11(a) and (b), the influence of the reinforcing ratio is very large and is properly evaluated by the beam analogy. Usually, if the reinforcing bars are distributed so that they provide a high ratio in one direction, then they are also distributed so that they provide a high ratio in the perpendicular direction. According to the beam analogy, as shown in Figs. 3.11 (c) and (d), the distribution of the reinforcement affects both the flexural and torsional capacities, and the stiffness. An increase in

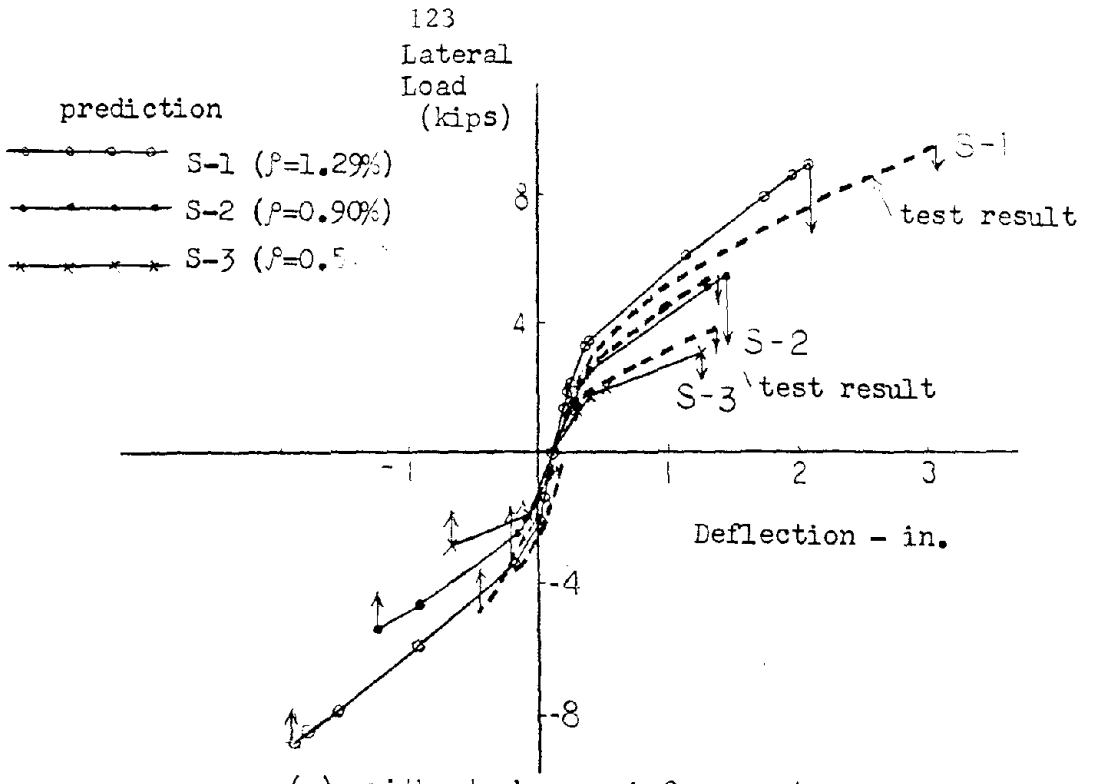

(a) without shear reinforcement

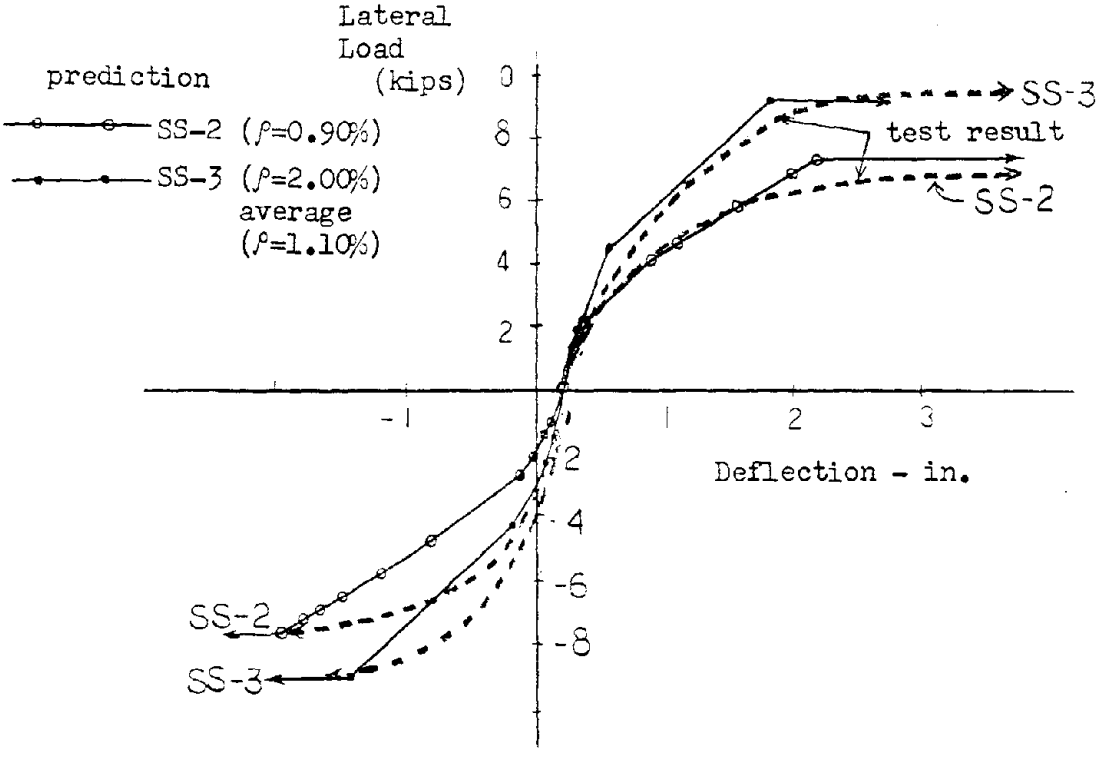

(b) with shear reinforcement

FIG. 3.11 INFLUENCE OF REINFORCEMENT RATIO

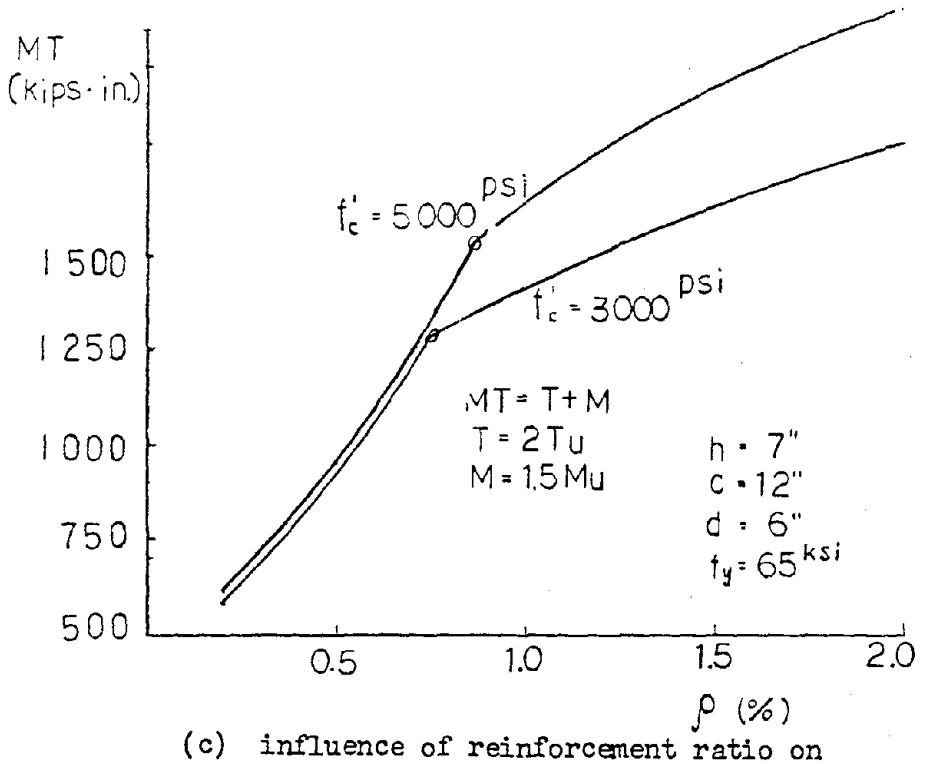

(c) influence of reinforcement ratio on moment transfer capacity

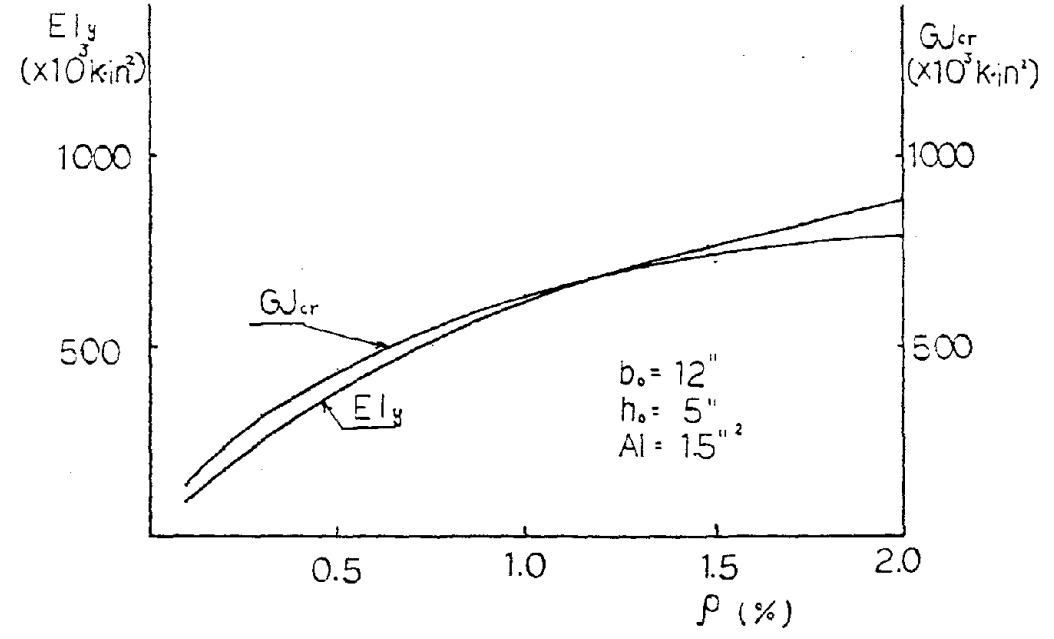

(d) influence of reinforcement ratio on stiffness of connection

FIG. 3.11 INFLUENCE OF REINFORCEMENT RATIO

the reinforcing ratio is effective in increasing the capacity of torsional element so long as the capacity is dictated by Eqs. (2.21) and (2.23). However, once Eq. (2.24) controls, the concrete strength becomes dominant and an increase in the reinforcement ratio does not increase the torsional capacity.

The changover point between Eq. (2.24) and Eqs. (2.21) and (2.23) is shown in Fig. 3.11(c) as a circle. Until a reinforcement ratio of 0.8% both the flexural and torsional capacities are increased by increasing ρ and when ρ becomes bigger than 0.8% only the flexural capacity is increased.

Since the capacity and stiffness of the connection are determined by the torsional, flexural, and bondslip elements which are situated around the column, concentration of reinforcing bars in the connection region is an effective way of increasing strength and stiffness. Test results also show this effect clearly as can be seen from Fig. 3.11. According to the beam analogy, the concentration of bars is effective only in the region of the flexural elements and torsional elements. However, it must be recognized that in the torsion direction, that width is $(c_m + 3h)$ in order that Eq. (2.21) be applicable. Further, it must be recognized that: 1. changing the bar spacing immediately beyond the width $(c_m + 3h)$ could lead to a premature failure or loss in stiffness due to conditions in the region outside $(c_m + 3h)$; and 2. the reinforcement ratio at which Eq. (2.24) rather than (2.23) controls is relatively low compared to the ratio at which a section becomes over-reinforced for flexure. Hence, the advantage to be gained by concentrating reinforcemnt in

the column head region, while considerable,is not as great as might be assumed based soley on flexural behavior concepts.

(3) Stirrups

The influence of the presence of stirrups can be checked by comparison of the results for SS-2 and S-2 shown in Fig. 3.12. Stirrups increase the capcity of the connection but have little effect on the stiffness. In the beam analogy, the influence of stirrups is taken into account by variations in the strength and stiffness of the torsional element according to Eqs. (2.21) and (2.28) for torsion effects, and Eqs. (2.23) through (2.26) for shear effects.

The largest influence of the stirrups is on the ductility of the connection and the shape of the hysteresis loops after the maximum capacity is reached. Those effects can be summarized as follows:

1. With enough stirrups, the connection can maintain its maximum capacity even for reversed cyclic loadings to deformations several times larger than the deformation at which the maximum capacity is first achieved.
2. Without stirrups, the connection abruptly looses stiffness for reversed cyclic loadings to deformations equal to or greater than that at which the maximum capacity is achieved.

Comparison of the results for SS-2 and SS-5 shows the influence of the extent of the region reinforced by stirrups. As is clear from Fig. 3.13, that extent influences the ultimate capacity. However, the analogy proposed here does not provide information on that

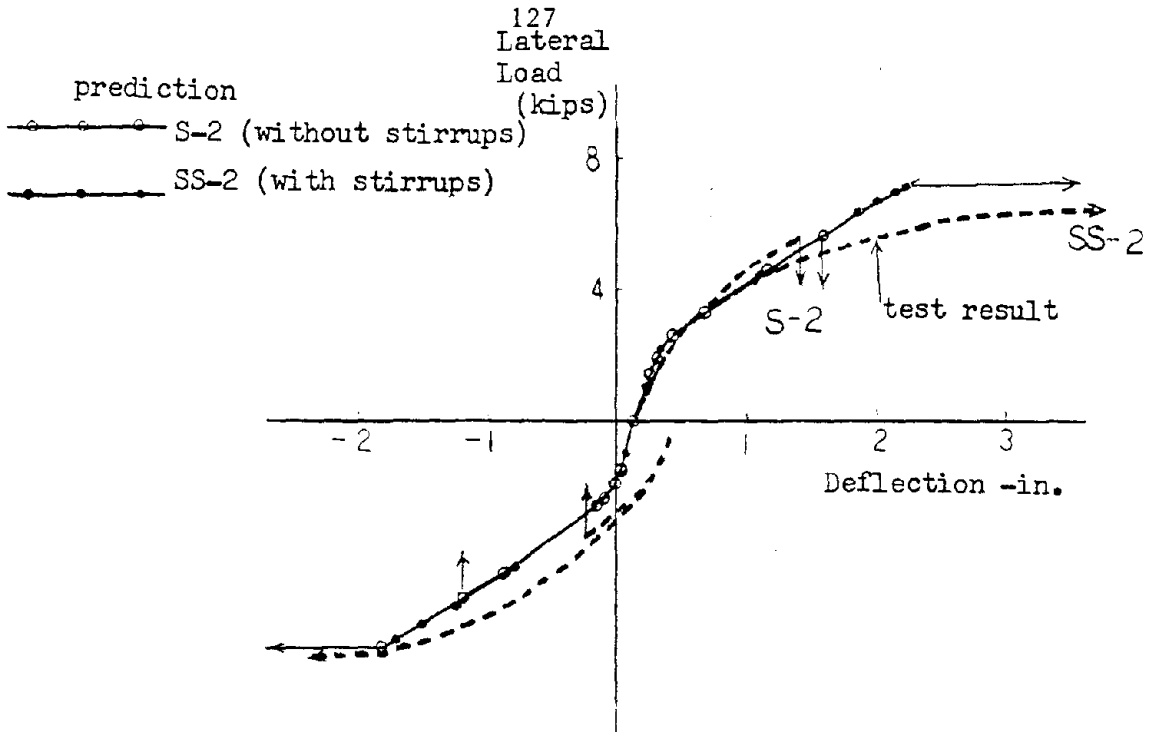

FIG. 3.12 INFLUENCE OF STIRRUPS

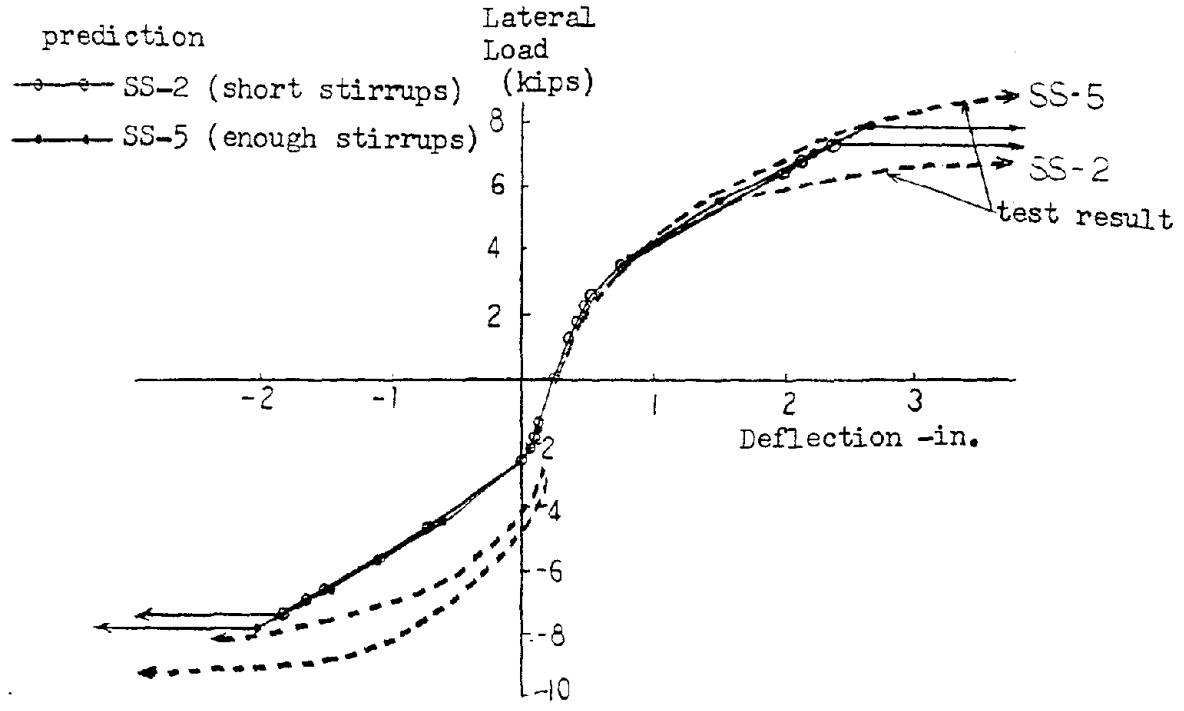

FIG. 3.13 INFLUENCE OF EXTENT OF REGION REINFORCED BY STIRRUPS

effect. Obviously, the stirrups must extend far enough to prevent failure on a perimeter outside the reinforced region and the rules governing that extension can only be established experimentally. For SS-2 and SS-5 the differences between measured and predicted results are larger than those which can be explained by the influence of concrete strength as predicted by the beam anlogy. That is, of course, reasonable since SS-2 failed in punching on a perimeter lying outside the ends of the stirrups whereas SS-5 failed due to excessive deflections and not loss in capacity.

CHAPTER 4

CYCLIC BEHAVIOR OF A FRAME

4.1 General

In Chapter 3 the predictions of the beam analogy developed in this dissertation were checked against the results of a wide ranging series of tests made on different types of column-slab connections.

In this chapter, as a third step, the predictions of that beam analogy are checked against the results of a frame test. Theoretically, if the behavior of the slabs, column, and connections are properly evaluated by a given analytical model, then that model should also be able to predict well the results of any frame test. From a practical standpoint, however, if the analytical model becomes too complex, then accurate predictions become more difficult. Each model of a given element has a certain amount of error and an error in one element can be critical for evaluation of the complete behavior of the frame. Alternatively, errors in elements may interact with each other and cause an amplified error for the total frame. However, when the system becomes very complex, as is the case for a total building, the prediction again becomes easier and probably more accurate because the errors for individual frames are self-canceling. In that sense, the prediction of the behavior of a one-bay frame may be the most severe test of the model, just as the testing of such a frame is the most severe test of testing techniques.

As described in Appendix A, two frame specimens were tested at the University of Washington. The test procedures and results were reported in detail in Refs. (10) and (11) together with in-depth discussions of predictions of the measured ultimate strengths and stiffnesses for the specimens. The prediction procedures used in those References were the ACI Code method and the beam analogy as described by Symonds (5). The accuracy and significance of those procedures were fully discussed in Refs. (10) and (11) and will not be repeated here. In this chapter the response of the frame with one interior and one exterior column is compared with the predictions of the beam analogy described in Chapter 2. The results are shown in Figs. 4.1, 4.2, and 4.3 in terms of the relation between the lateral load and column tip deflection.

4.2 Test Frame

A plan view of the typical prototype flat plate structure from which the test frame was idealized is shown in Appendix A (Fig. A.3e). That flat plat had 18 ft. spans in the longitudinal direction, 14 ft. spans in the transverse direction and 1 ft. square columns. A 7 in. thick slab was required according to ACI Code 318-77 provisions for gravity load stiffness considerations. With 0.25% column strip negative moment reinforcement at the exterior column and 0.42% column strip negative moment reinforcement at the interior column, that prototype structure could support a service gravity live load of approximately 60 psf. The columns were deliberately chosen to have a side dimension less than that likely in

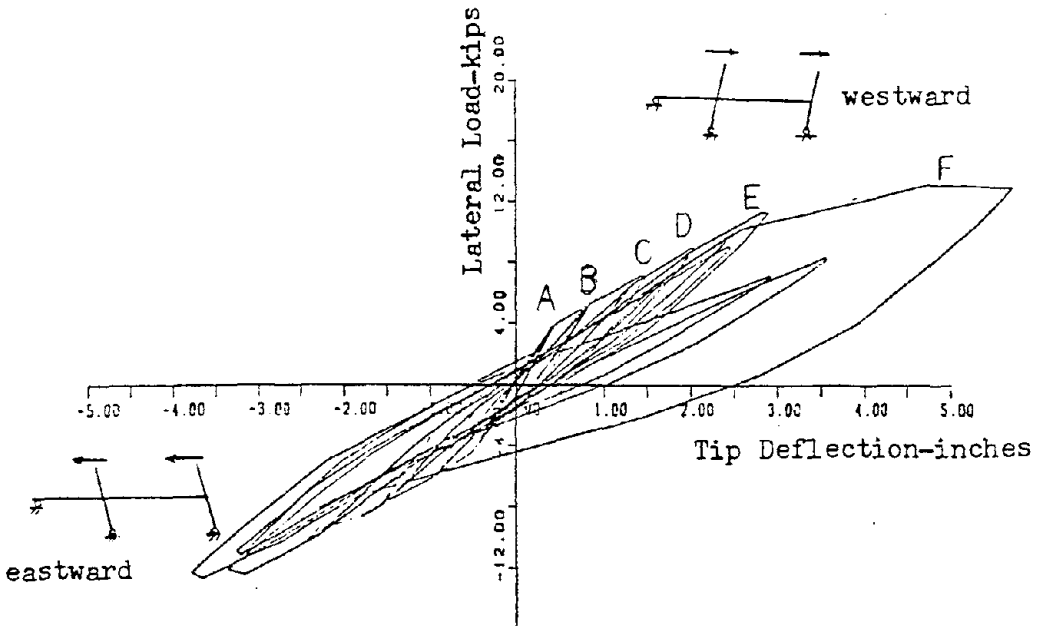

a) prediction

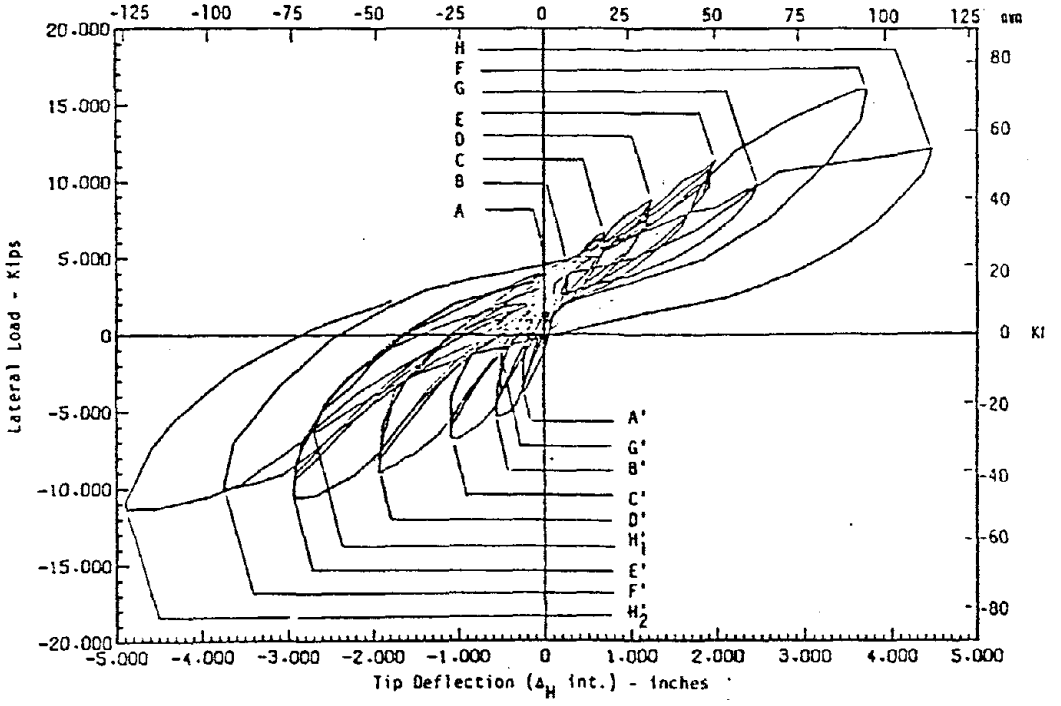

b) observed

FIG. 4.1 LATERAL LOAD - HORIZONTAL DEFLECTION - INTERIOR COLUMN

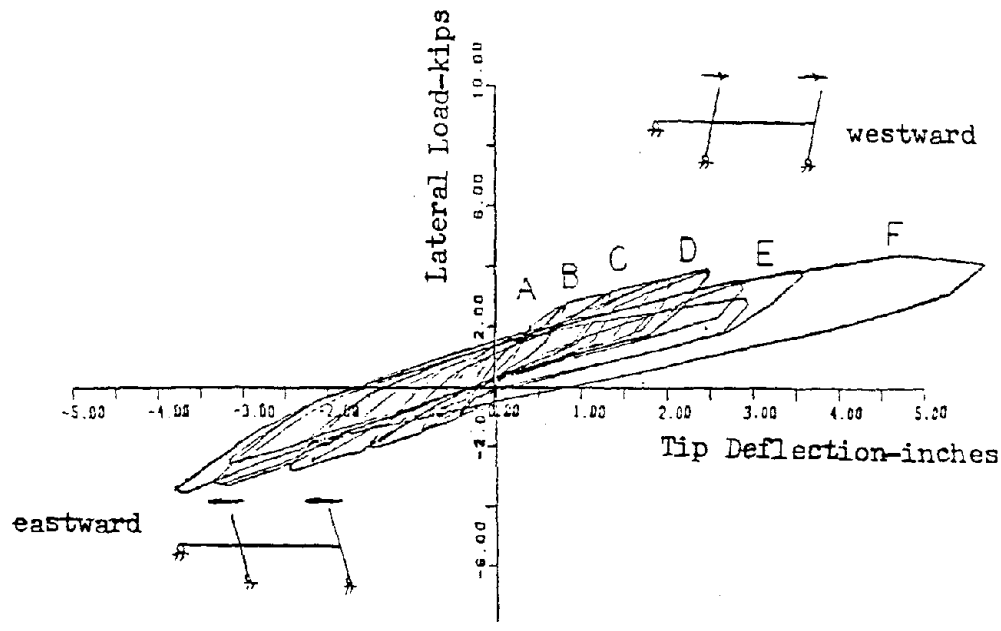

a) prediction

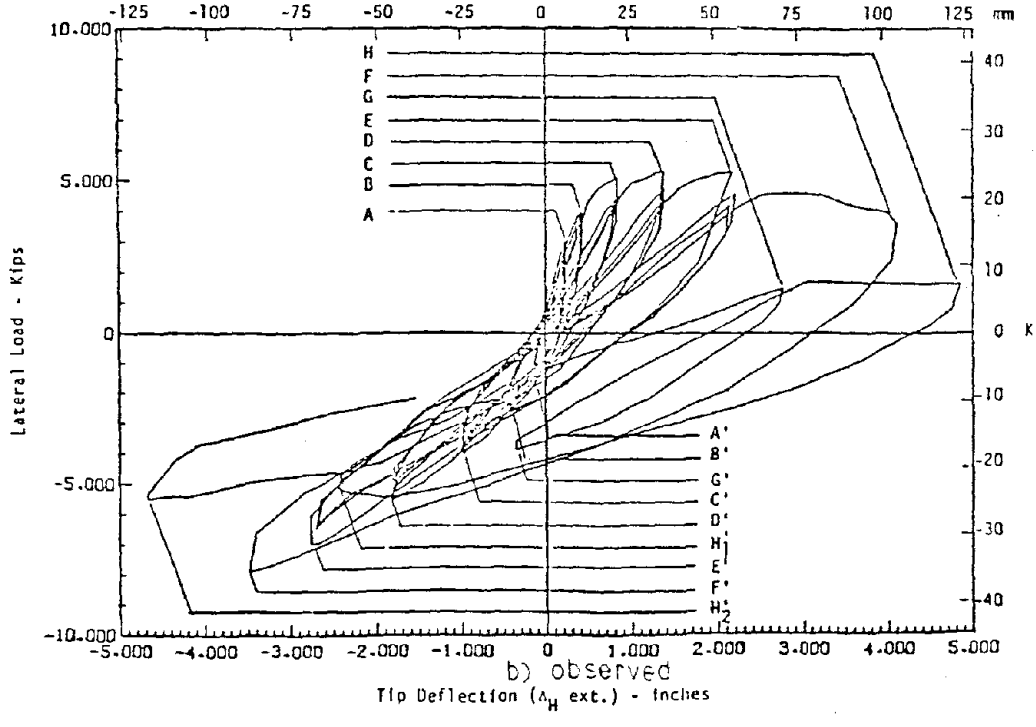

b) observed

FIG. 4.2 LATERAL LOAD - HORIZONTAL DEFLECTION - EXTERIOR COLUMN

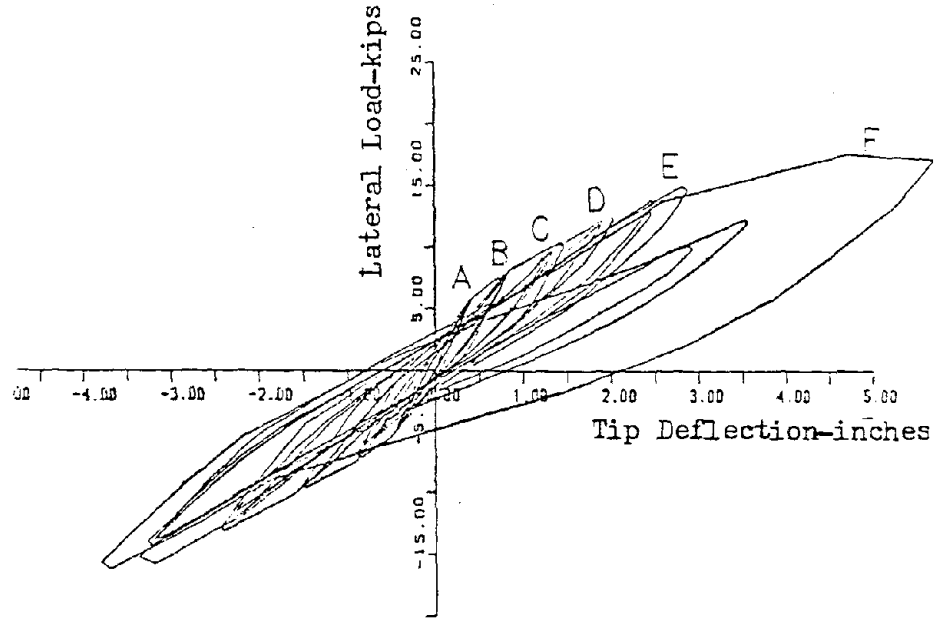

a) prediction

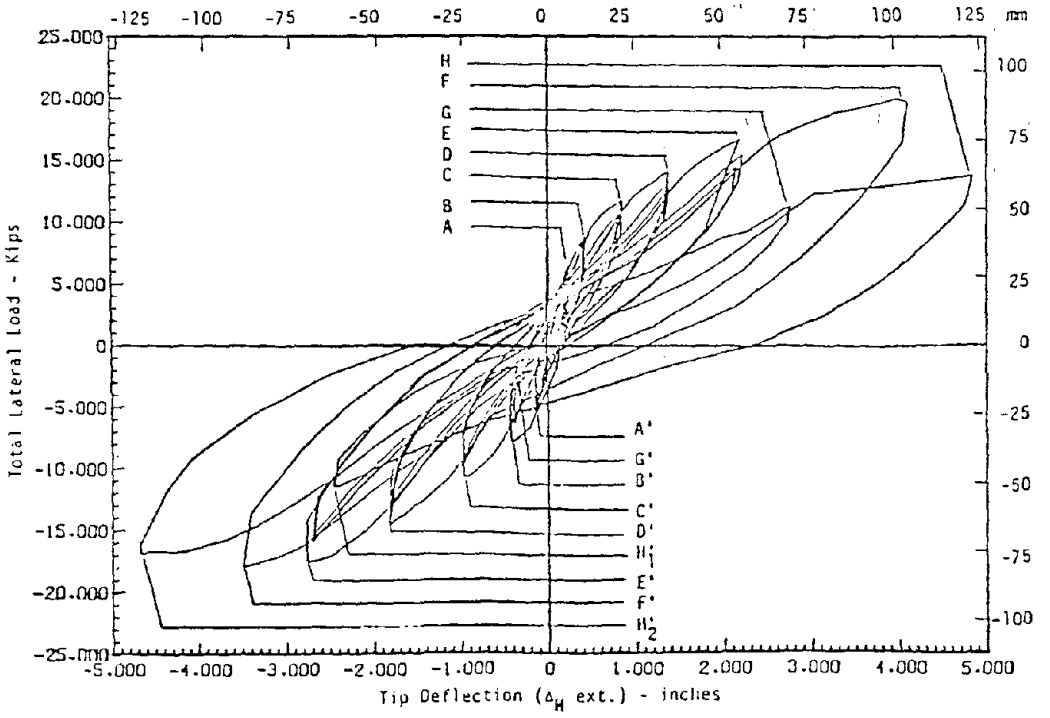

b) observed

FIG. 4.3 TOTAL LATERAL LOAD - EXTERIOR COLUMN HORIZONTAL DEFLECTION

practice in order that shear effects would be significant. Alternatively, the prototype structure can be viewed as a three-quarter scale version of that likely to be economic in practice.

This test specimen was intended to represent the hatched area of Fig. A.3e. The extension of the slab either side of the column for the transverse direction was chosen as a quarter of the span length in that direction and therefore equal to the column strip width for the longitudinal direction. In the longitudinal direction (i.e., the direction in which the lateral load was applied), the slab extended from the discontinuous edge across the exterior span and out to the midpoint of the first interior span. The columns for the frame extended above and below the slab a distance equal to half their likely height in the prototype structure.

The overall dimensions of the test frame are shown in Appendix A (Fig A.3f). The slab was 7 ft. wide and 28 ft. long, with two 1-ft. square columns framing a 18-ft. exterior panel. The 9-ft. long portion of the slab extending past the interior column was simply supported at its center. That support idealized the point of contraflexure for the slab for lateral loading. The bases of the columns were pinned at their connection to the laboratory floor.

Loads were added to represent the dead weight effects for the missing middle strip portions of a typical panel. Those loads were a mixture of concrete blocks and steel plates which were supported in such a manner that analyses indicated that the effects of a uniformly distributed dead load would be closely similated for the exterior bay of the test frame. The locations at which the loads were applied and

the magnitude of those loads are shown in Fig. 4.4. However, erection limitations dictated that the top of the columns could not be restrained during application of those dead weights and that undoubtedly influenced the distribution of moments that resulted. Further the method of construction prevented the development of self weight moment transfer effects thus introducing a further discrepancy between the initially predicted moments and the moments that apparently existed at the beginning of seismic testing.

The loads that caused effects representing seismic forces were applied at the top of the columns which, as shown in Appendix A (Fig. A.3f), were located 4 ft. above the upper surface of the slab. There was a tie rod connecting the two column tops so that the distance between those tops should have remained essentially constant during testing.

The slab was reinforced both top and bottom with two-way reinforcing mats. Integral beam stirrup reinforcement was provided at the interior column connection and hairpin stirrups extending perpendicular to the discontinuous edge were provided at the exterior column connection. Details of the reinforcement are shown in Figs. 4.5 (a) through (d) and Appendix A (Table A.1e).

Load cells were inserted beneath the exterior column and the slab support, and used to determine the reactions R_a and R_c, Fig. 4.6, caused by loading.

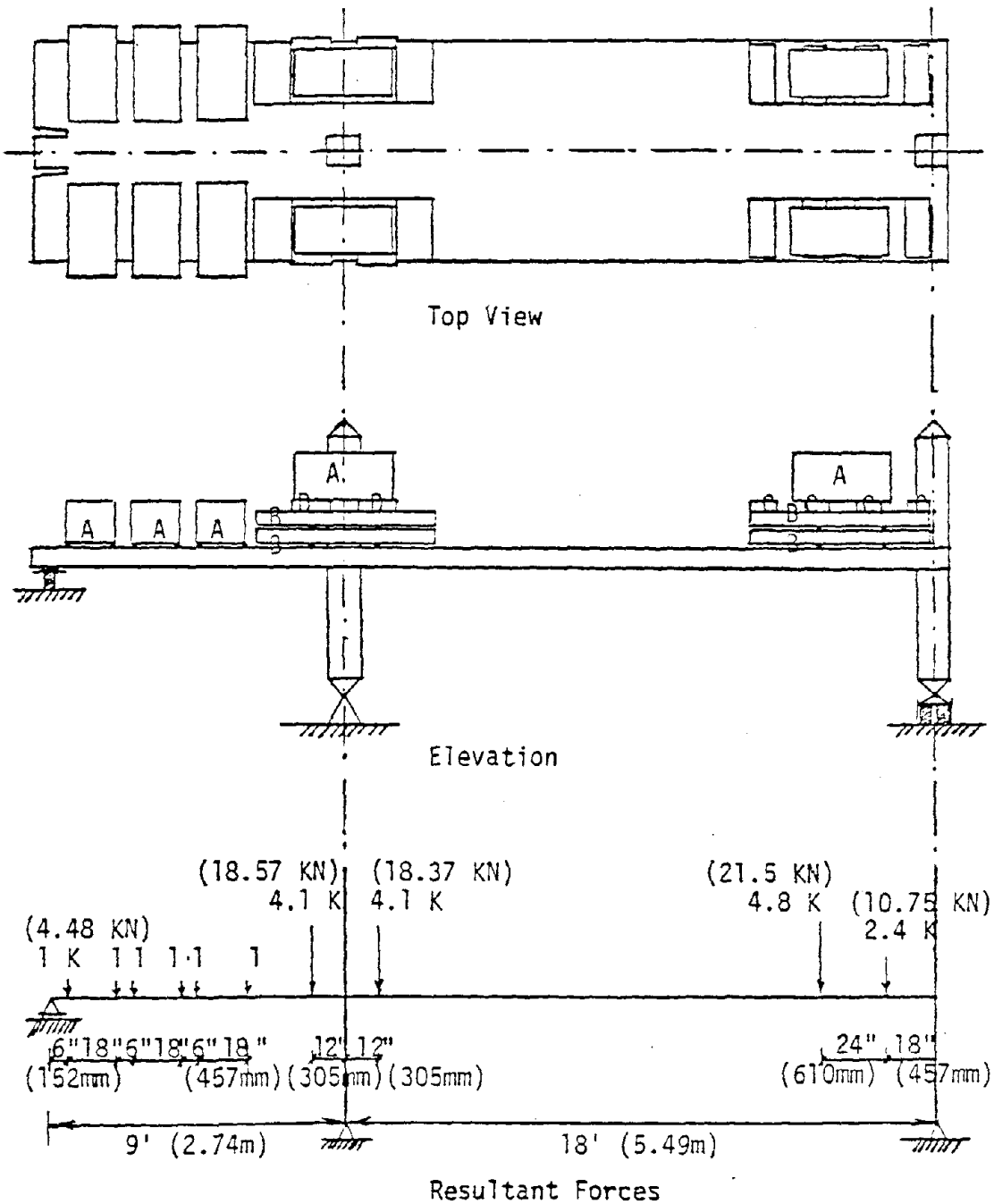

FIG. 4.4 DISTRIBUTION OF WEIGHT MODELING DEAD WEIGHT
(For Exterior Column Frame)

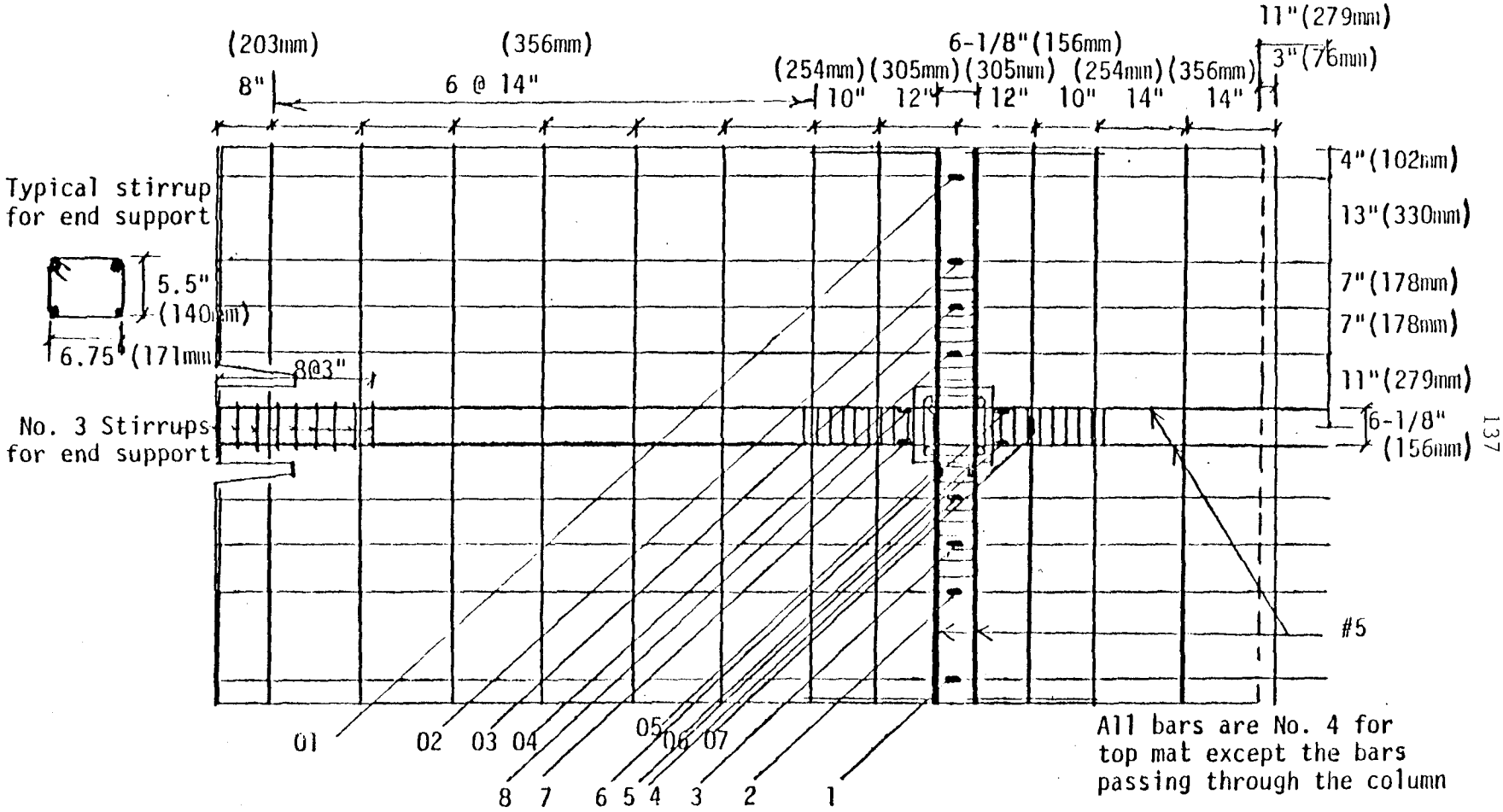

(a) Top Mat of East Half Portion

FIG. 4.5 REINFORCING MAT AND GAGES FOR EXTERIOR FRAME

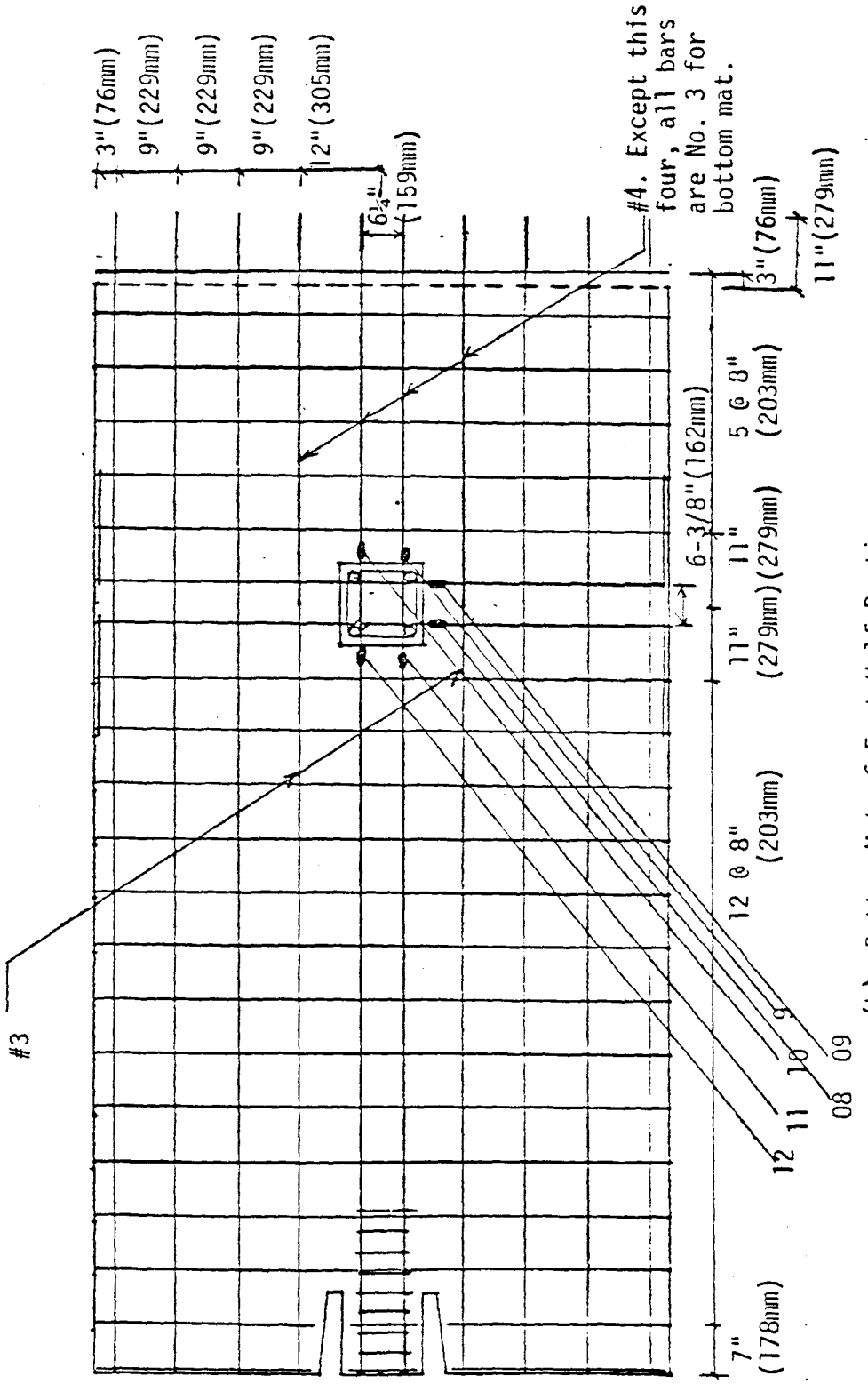

(b) Bottom Mat of East Half Portion

FIG. 4.5 Continued

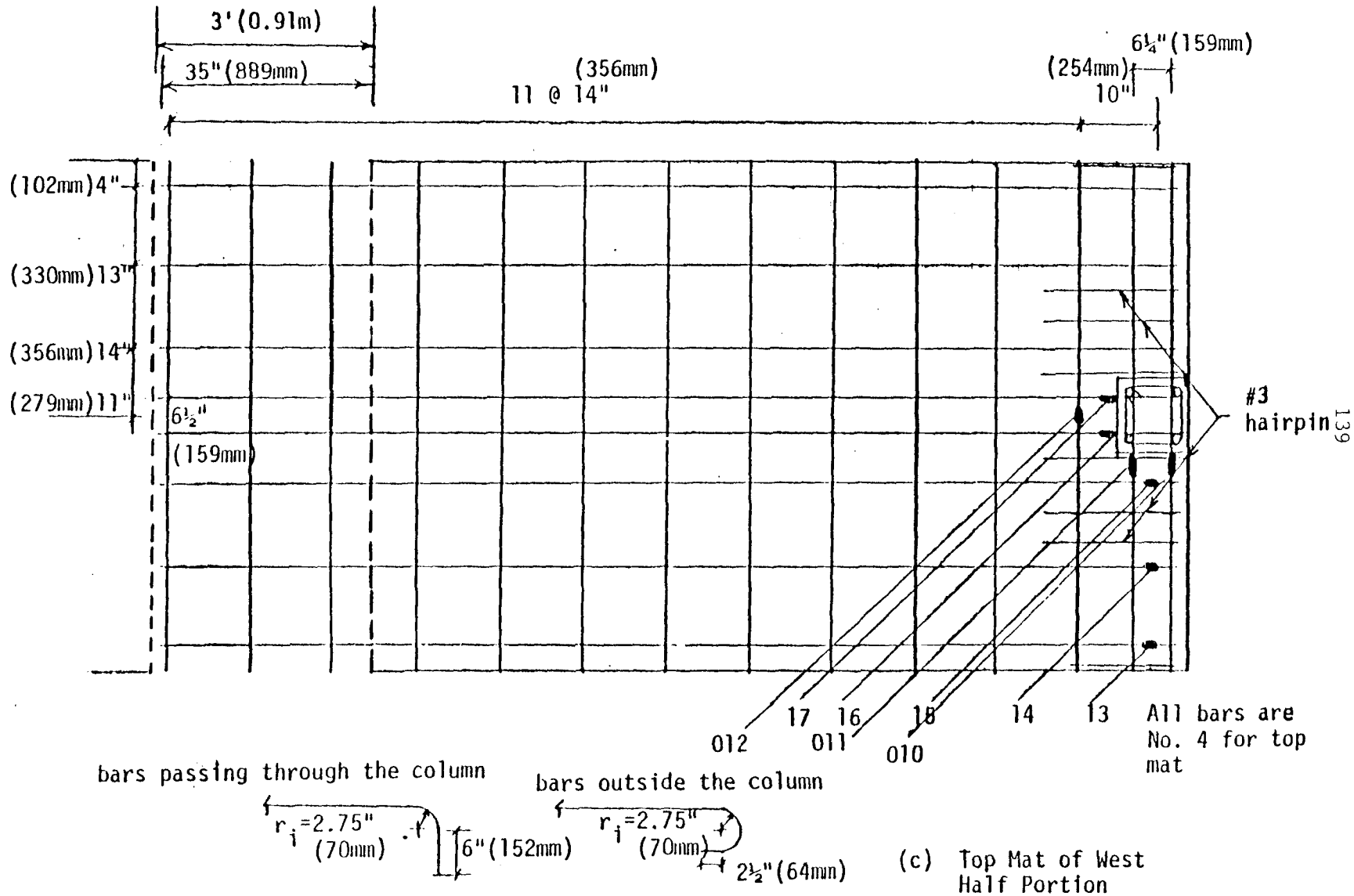

(c) Top Mat of West Half Portion

FIG. 4.5 CONTINUED

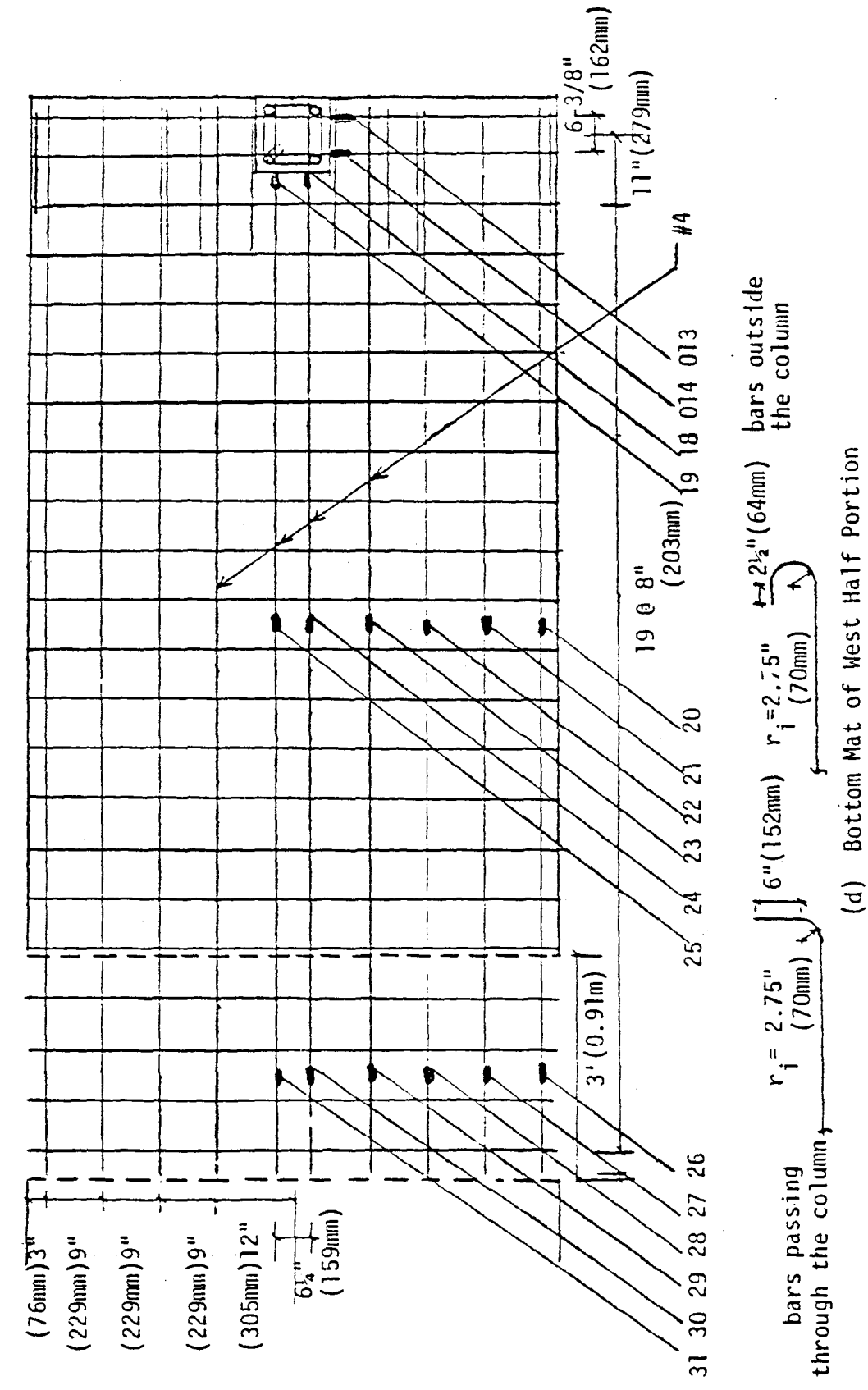

(d) Bottom Mat of West Half Portion

FIG. 4.5 CONTINUED

4.3 Strength of Connections

4.3.1 Moments Caused by Gravity Loading

The vertical reactions R_a and R_c, for the exterior column and the slab support, after addition of the dead load were 11.3 kips and 6.00 kips, respectively as shown in Fig. 4.6. From those values and the known distribution of the weights modeling the dead weight, the resultant internal forces were calculated. Those forces are shown in Fig. 4.6.

The initial moments for each element of each connection for gravity loading were determined from those internal forces using the procedures described in Section 2.3. Results are shown in Fig. 4.7. Slab moments at each connection were unbalanced and therefore torsional moments existed for the gravity load condition.

4.3.2 Ultimate Strength of Frame

Since the frame was indeterminate, even if one connection lost its rigidity and became a hinge, the system could still maintain its lateral load resisting capacity. Therefore, provided neither connection failed in shear, the lateral load resisting capacity of the frame should have equalled the summation of the moment transfer strengths for both connections. If, however, one connection failed in shear, that connection would not be able to maintain its maximum capacity and the total resisting capacity of the frame would be determined by stiffness considerations for the conditions at which the connection failed.

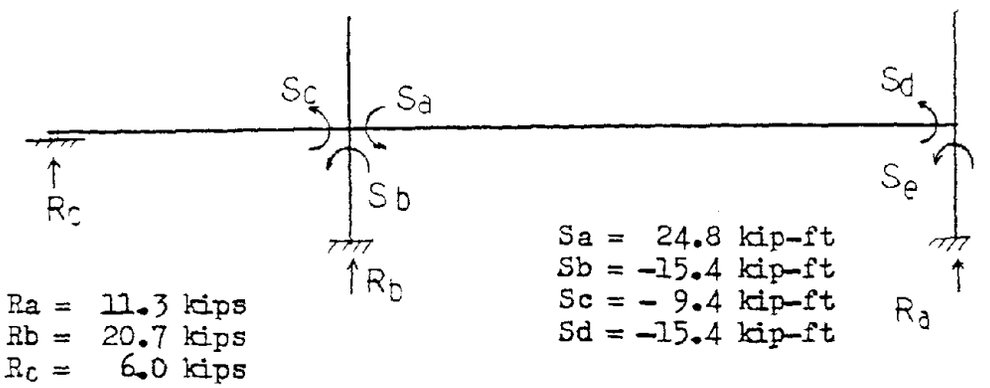

FIG. 4.6 INTERNAL FORCES CAUSED BY GRAVITY LOADING

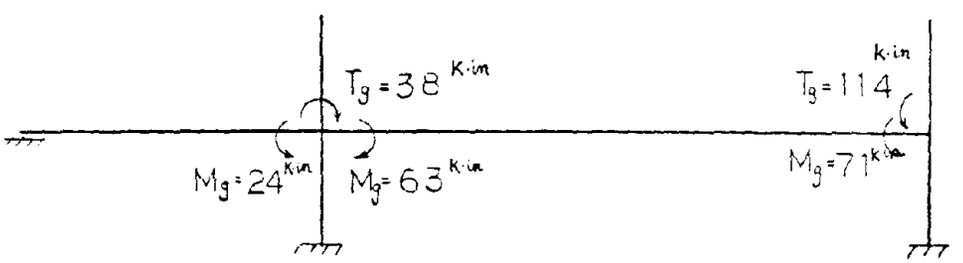

FIG. 4.7 INITIAL MOMENTS CAUSED BY GRAVITY LOADING

The ultimate strengths of the connections were predicted using the beam analogy described in Section 2.3. Results are summarized in Table 4.1. Both connections were well reinforced by stirrups and there was no overflow of shear from the flexural elements to the torsional elements. The strength of neither connection was predicted as controlled by shear. The values in the 9th row of Table 4.1 are the fictious lateral loads applied to the slab midway between columns, and the values in the 10th row are the corresponding lateral load for the column tops (and bottoms). The calculated forces for the column tops are compared to the forces measured in the test in the 11th and 12th rows. Differences between measured and predicted forces are negligible except for the west edge, column for westward loading. The difference between measured and predicted results for that connection for westward loading is striking and may well be a result of the hairpin edge reinforcement also being effective in providing torsional resistance. If the ratio for the measured to predicted moment transfer strength for that connection is based on values that include the moment transferred by gravity laoding, then the difference between measured and computed capacities is less. Further, if ratios are expressed in terms of the total resisting capacity of the frame, measured and predicted values are within 10% of each other for both loading directions.

The failure modes observed for the test frame for both eastward and westward loading are shown in Fig. 4.8. For the analytical model it was found that the capacity of the torsional element for the edge column connection was controlled by plain concrete strength consider-

TABLE 4.1 ULTIMATE CAPACITY OF LABORATORY TEST FRAME

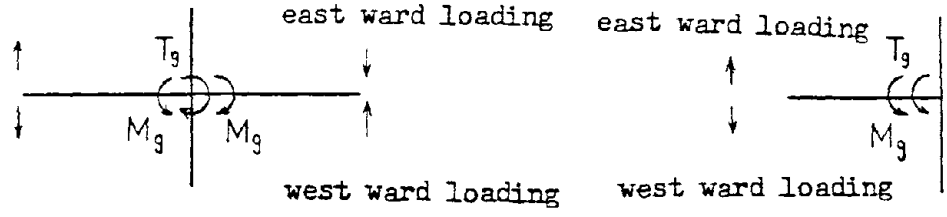

		EAST COLUMN		WEST COLUMN	
		east ward	west ward	east ward	west ward
1	M_g (t)	63	24	71	71
2	M_{ut} (t)	270	270	179	179
3	M_f (rest) (t)	207	246	250	108
4	P_M (rest) (tt)	2.18	2.59	2.63	1.13
5	T_g ($\frac{1}{2}T_g$ original) (t)	73	-73	-114	114
6	T_f ($\frac{1}{2}T_u$) (t)	410	410	398	393
7	T_f (rest) (t)	337	483	512	284
8	P_t (rest) (tt)	3.12	4.47	4.74	2.63
9	P_{total} ($P_M + P_T$) (tt)	5.30	7.06	7.37	3.76
10	P_c (at column) (tt)	11.11	14.80	7.72	3.95
11	P_c (test) (tt)	11.4	15.3	7.8	5.0
12	$P_{c(test)}$ / $P_{c(pred.)}$	1.03	1.03	1.01	1.26

(t) : kips·inch
(tt) : kips

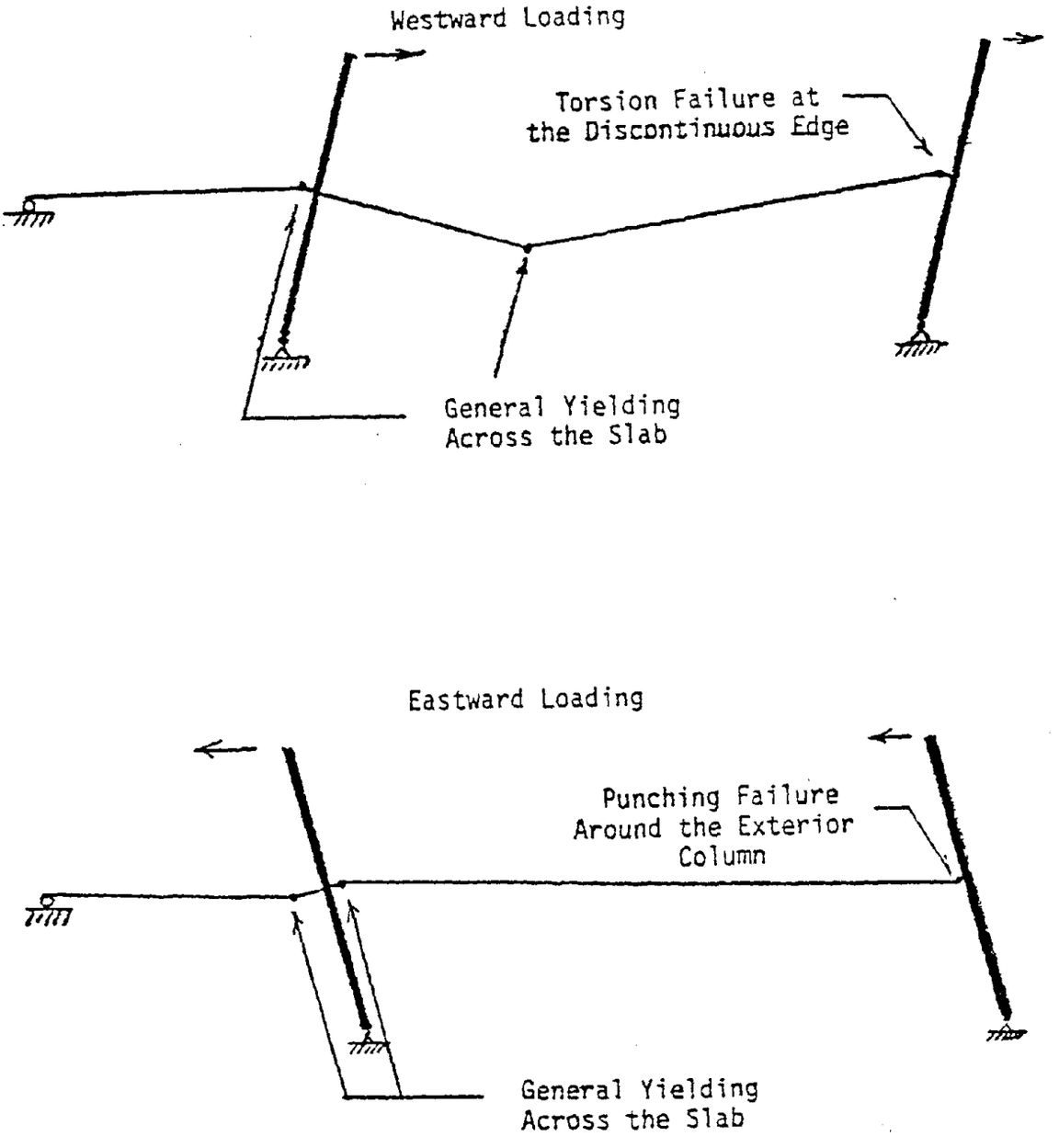

FIG. 4.8 SCHEMATIC DIAGRAM OF FAILURE MODES IN TEST

ations, Eq. 2.22 rather than by yielding considerations, Eq. 2.21. Thus, it was to be expected that the failure mode would be brittle and take the form of a punching failure. In the test it was observed that the terminal failure condition for the exterior column connection formed first and that the deterioration in capacity that occurred with reversed cycling precipitated the shear failure for eastward loading. In the case of the interior column connection, the strengths of both the flexural and torsional elements were controlled by yielding considerations and the failure mode was therefore predicted as a gradual, flexural type, failure. Thus, the predictions coincide with the observed behavior of the specimen.

4.4 Cyclic Response of Frame

4.4.1 Stiffness Model for Frame

The specimen was tested to failure under reversed cyclic loading. For cyclic loading predictions, use of the Drain-2D program is more appropriate and easier than use of the step-by-step procedure. Therefore, for the analytical model discussed here the Drain-2D program was used together with the rules of Section 2.2.

Stiffness values for each connection were obtained by synthesizing stiffness values for each element of each connection. Partial stiffness values and the critical points for change in stiffness for each element were calculated using the procedure described in Section 2.3. Results are summarized in Table 4.2.

TABLE 4.2 PARTIAL STIFFNESS AND LIMITING MOMENT VALUES FOR LABORATORY TEST FRAME

a) FOR FLEXURE

	Critical Points (k.-in.)					Rigidity ($\times 10^3$ k.-in.^{2})				
	M_{cr}	My	M$\acute{y}$	M_u	M$\acute{u}$	EI-g	EI-y	EI-$\acute{y}$	EI-u	EI-$\acute{u}$
EAST COLMN	42	257	165	270	171	1135	439	305	274	0.61
WEST COLMN	43	170	170	179	179	1132	281	281	1.30	1.30

b) FOR TORSION

	Critical Points (k.-in.)		Rigidity ($\times 10^3$ k.in.^{2})				
	T_{cr}	T_u	KT 1	KT 2	KT 3	KT 4	ET
EAST COLMN	126	820	478	62.9	478	4.78	220
WEST COLMN	126	398	236	15.3	236	2.36	54

C) FOR BONDSLIP

	Critical Points(k.-in.)		Crigidity ($\times 10^3$ k.-in.^{2})							
	M_y	$M_y{}'$	KB-1	KB-1$\acute{}$	KB-2	KB-2$\acute{}$	KB-3	KB-3$\acute{}$	KB-4	KB-4$\acute{}$
EAST COLMN	171	110	88	87	2.9	2.9	176	174	88	8.7
WEST COLMN	113	113	89	89	3.0	3.0	198	198	89	8.9

EIS (stiffness of slab) = 7862×10^3
EIC (stiffness of column) = 6965×10^3

The appropriate idealization for the frame for Drain 2D analysis is that shown in Fig. 4.9. For simplicity, the slab between the two columns was represented by a simple beam with a stiffness equal to the uncracked section stiffness of the slab for its full width. Thus, the possibility of a flexural hinge forming across the width of the slab was ignored in the analysis. However, that condition could have been checked by inserting hinges in the slab at selected locations within the length in which on check on yielding was desired. The designations for the stiffnesses of the various elements shown in Fig. 4.9 correspond to the designations used for the quantities listed in Table 4.2. The moments caused by the gravity loading were applied directly to the elements as initial forces. The cyclic lateral load was applied to the frame model by masses attached to the tops of the columns. Accelerations for those masses were given long term, high damping values so that the inertia force effects were essentially without dynamic vibration effects and the loading was very similar to the cyclic loading applied to the test specimens.

4.4.2 Results and Discussion

The time history displacements for the column tops were obtained using the loading history shown in Fig. 4.10. The column tops for the laboratory frame were connected together by a tie bar and as shown in Fig. 4.9 that tie bar was simulated in the analytical model by a rigid bar. However, the simultaneous constraints on displacement and loading conditions for the column tops were difficult to simulate with the Drain-2D program, as is apparent from the differ-

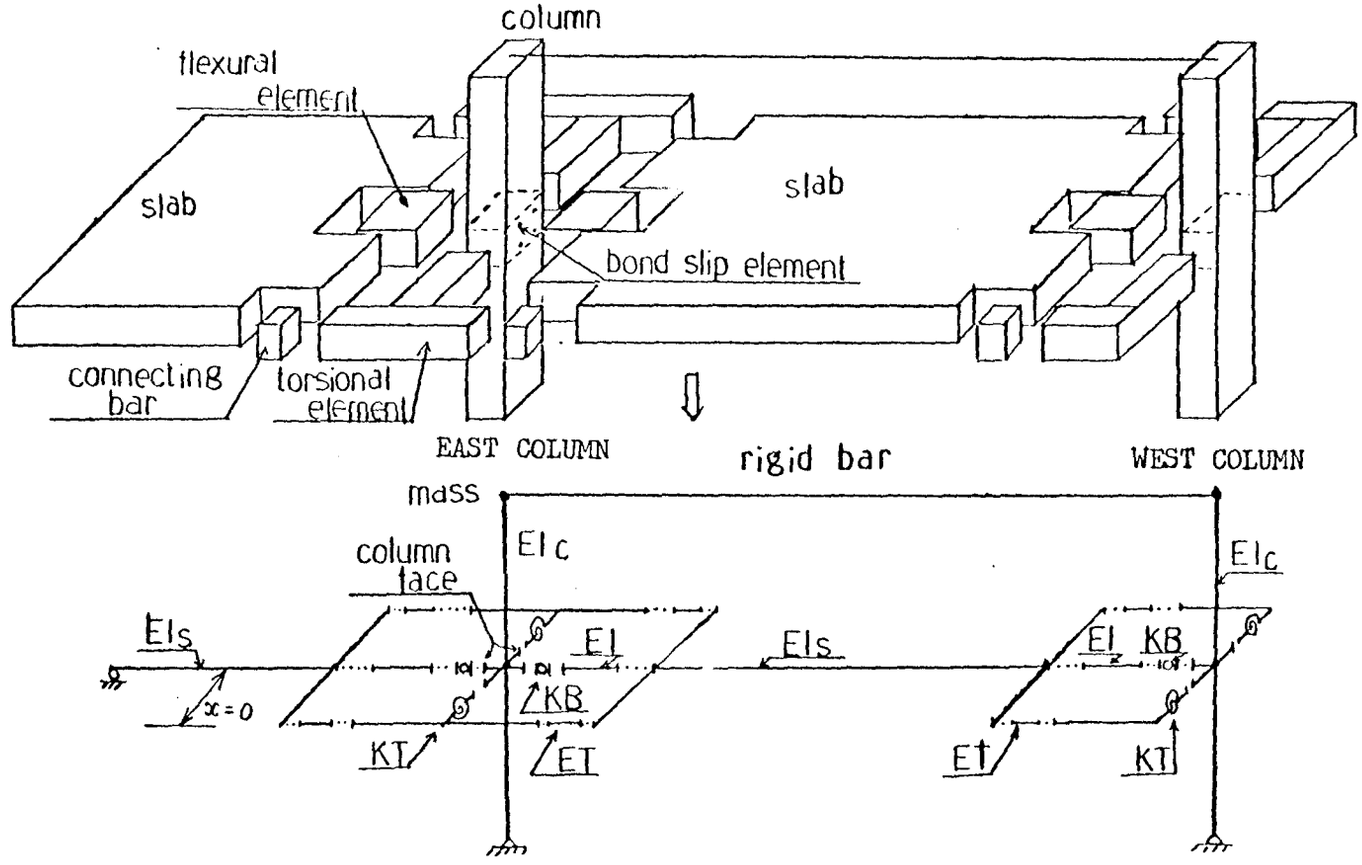

FIG. 4.9 IDEALIZATION OF THE FRAME FOR ANALYSIS

Reproduced from
best available copy.

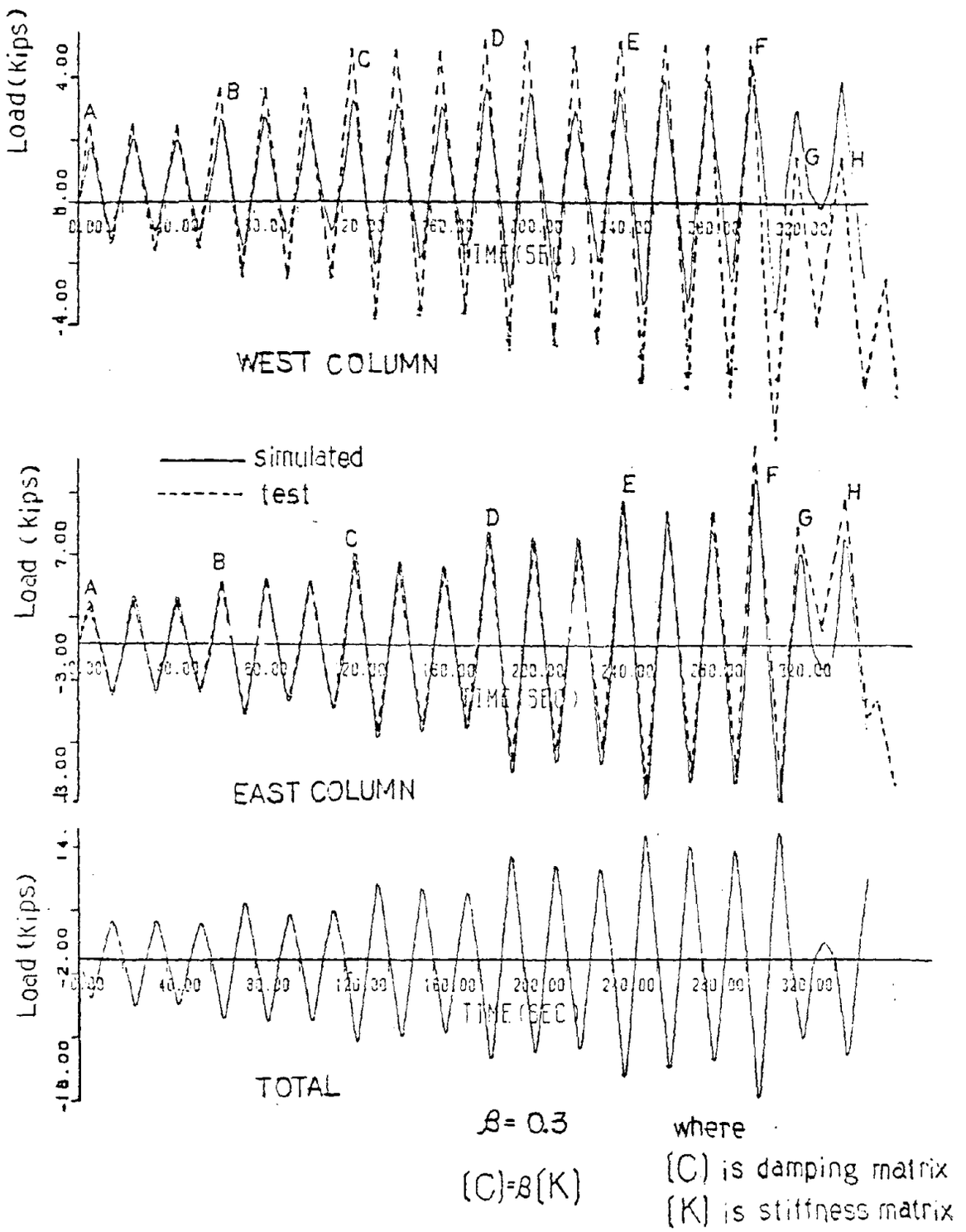

FIG. 4.10 LATERAL LOAD HISTORY (SIMULATED)

ences in simulated and test load-time histories shown in Fig. 4.10. Consequently discrepancies between measured and predicted results were to be expected especially for the west column.

Measured and predicted relationships between the lateral load applied at each column top and the corresponding displacement are shown in Figs. 4.1 and 4.2 for the interior and exterior columns, respectively. Since both column tops were forced to move as one by the tie-rod, the total lateral load-column tip displacement relationship of Fig. 4.3 was obtained by summing the loads acting on the interior and exterior column tops. From a comparision of the measured and predicted responses, it is apparent that:

1. The cyclic loading response predicted for the exterior column was considerably more flexible than the observed result. Thus, not only are predictions for the ultimate capacity of that connection too low, as discussed previously in Section 4.3.2, but also predictions for the yield moment for the flexural element and the cracking moment for the torsional element must also be too low. In Reference (10) Hsiang also found that current procedures underestimated the capacity at the west column and concluded that behavior to be due to the neglect of strain-hardening effects for the reinforcing bars. From Figs. 4.1 and 4.2 it is apparent that while neglect of strain hardening may be one reason for the discrepancy between measured and computed results, that effect does not fully explain the observed behavior since that discrepancy began

to develop well in advance of loads at which there would be significant strain-hardening effects.

2. Due partially to the influence of the discrepancy between measured and predicted results for the exterior coumn connection the hysteretic behavior predicted for the interior column connection also deviates from the observed results. However, the overall accuracy of the prediction is much better than in the case of the exterior column connection.

3. Since the strength and stiffness of the interior column connection were much greater than that of the exterior column connection, the predicted relation between the total lateral load and the column tip deflection is similar to the relation for the interior column connection. For any given cycle an average stiffness, strength and energy dissipation are predicted slightly smaller than the test results. However, that finding is reasonable because the analytical model does not consider the degradation in stiffness caused by repeating loading between given deflection limits.

Overall, it can be concluded that the stiffness, strength, and energy dissipation predicted for the test frame are in reasonable agreement with the test results inspite of some obvious discrepancies between the analytical modeling procedure used and the test constraints.

CHAPTER 5

DYNAMIC RESPONSE OF A BUILDING

5.1 General

In this chapter, the beam analogy method developed in this dissertation is used to analyze the dynamic behavior of a real flat plate building for which earthquake records are available. The building selected for this analysis was the Holiday Inn, Orion Avenue, Los Angeles which underwent considerable displacement and suffered considerable damage in the 1971 San Fernando earthquake. Previous investigations have shown that the response of reinforced concrete frame structures in strong earthquakes can be predicted using available dynamic analysis techniques provided a model of the structure is used that recognizes the continually varying stiffness and energy absorbing characteristics of the structure.

For the analysis described here it was assumed that the stiffness changes in the flat plate concrete frame of the Holiday Inn under earthquake forces could be adequately described using the beam analogy method developed in Chapter 2. For dynamic analyses, however, some additional assumptions must also be made about damping. The energy-absorbing characteristics of the structure are determined by its damping characteristics which have two components. One component is the viscous damping of the structure which depends not only on the characteristics of the members of the frame but also the nature of any non-structural attachments to that frame. The other component is the hysteretic response of the structure (i.e., the area

within the hysteresis loop), resulting from yielding of the flexural memebers. For flat plate frames, it is to be expected that yielding of the flexural memebers will occur initially at the slab-column connections and that damping caused by the hysteretic behavior of those connections can be properly evaluated by the analytical model for the cyclic behavior developed here and checked against test results for subassemblages and frames in Chapters 3 and 4, respectively.

The dynamic anlaysis was performed using a Drain-2D program (34). That program permits the viscous damping matrix at any time to be based on the mass matrix, the current tangent stiffness matrix and the original elastic stiffness. Although it is largely a matter of engineering judgment, many analyists prefer the use of a damping matrix dependent on the original elastic stiffness. Since there is no general agreement as to which procedure is best, the elastic stiffness approached is used here and the influence of the damping ratio on the response of the total building checked.

The geometry and reinforcement for the Holiday Inn, the damage it suffered, and the earthquake records obtained for the structure are described in Section 5.2. The model used for the analysis is described in Section 5.3. The predicted response is compared to that observed in Fig. 5.1 and the results of that analysis are discussed in Section 5.4.

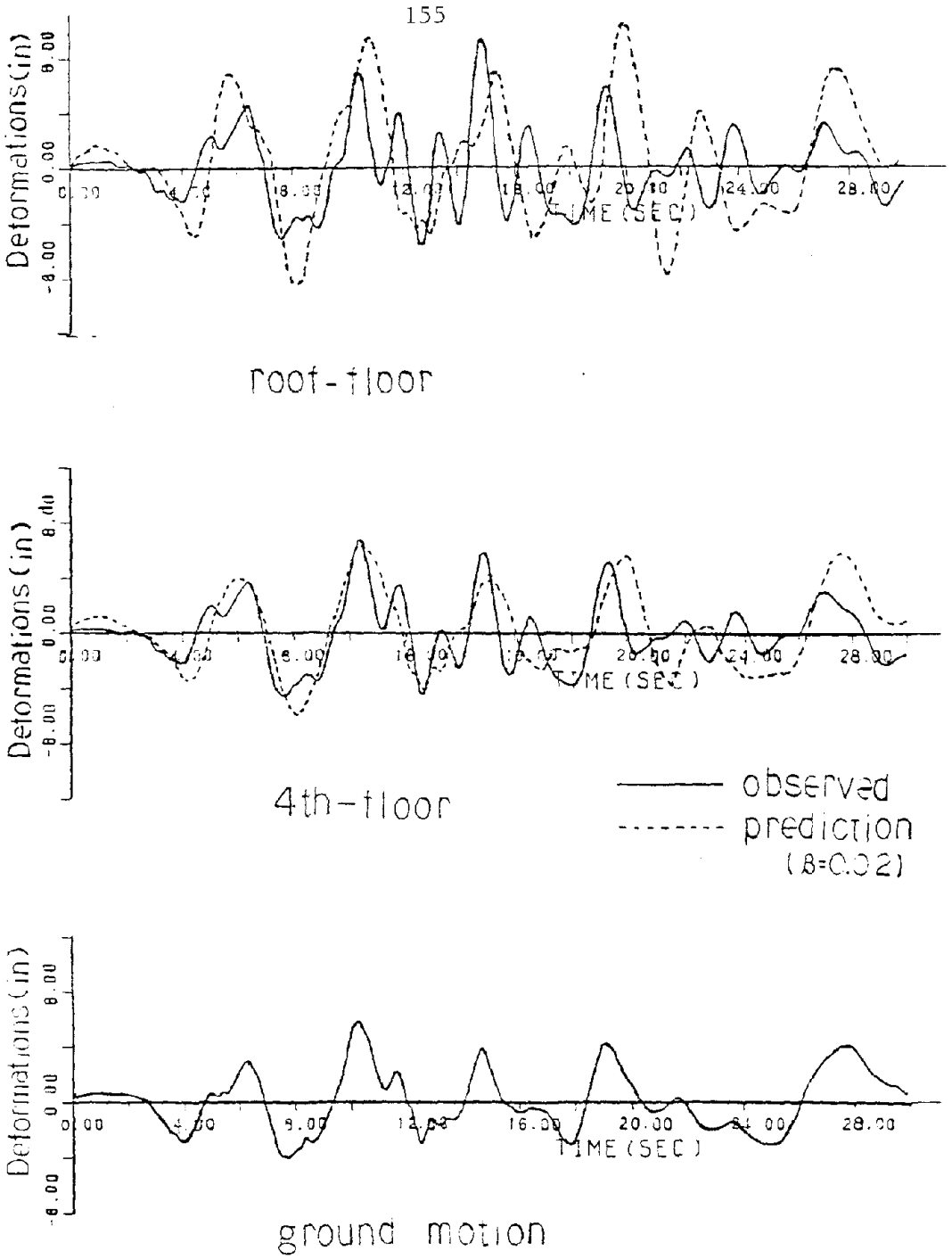

FIG. 5.1 DEFORMATIONS FOR HOLIDAY INN
(OBSERVED AND PREDICTED)

5.2 Holiday Inn, Orion Street

The geometry, reinforcement, and architectural components for this building, and its behavior during the 1971 San Fernando earthquake are reported in detail in Reference (40). In this section, only those features of the structure relevant to its subsequent analysis are highlighted.

5.2.1 Description of Building

The Holiday Inn is a seven-story reinforced concrete structure with plan dimensions of approximately 62 by 160 feet. It is located immediately east of the San Diego Freeway at Toscoe Boulevard, and was about 13 miles south of the earthquake's epicenter.

The geometry and reinforcement for the structure are apparent from Figs. 5.2 through 5.5. The first floor is a slab on grade placed on over 2 feet of compacted fill. Except for two small areas at the ground floor, covered by one-story canopies, the plan configurations for each floor, including the roof, are the same. The canopy covered areas are indicated by hatching in Fig. 5.2. The typical framing consists of columns spaced at 20-foot centers in the transverse direction and 19-foot centers in the longitudinal direction. Spandrel beams surround the perimeter of the structure. The floor system is a reinforced concrete flat plate, 10 inches thick at the second floor, 8 1/2 inches thick at the third to seventh floors, and 8 inches thick at the roof (Fig. 5.5). A penthouse with mechanical equipment covers approximately 10 percent of the roof area.

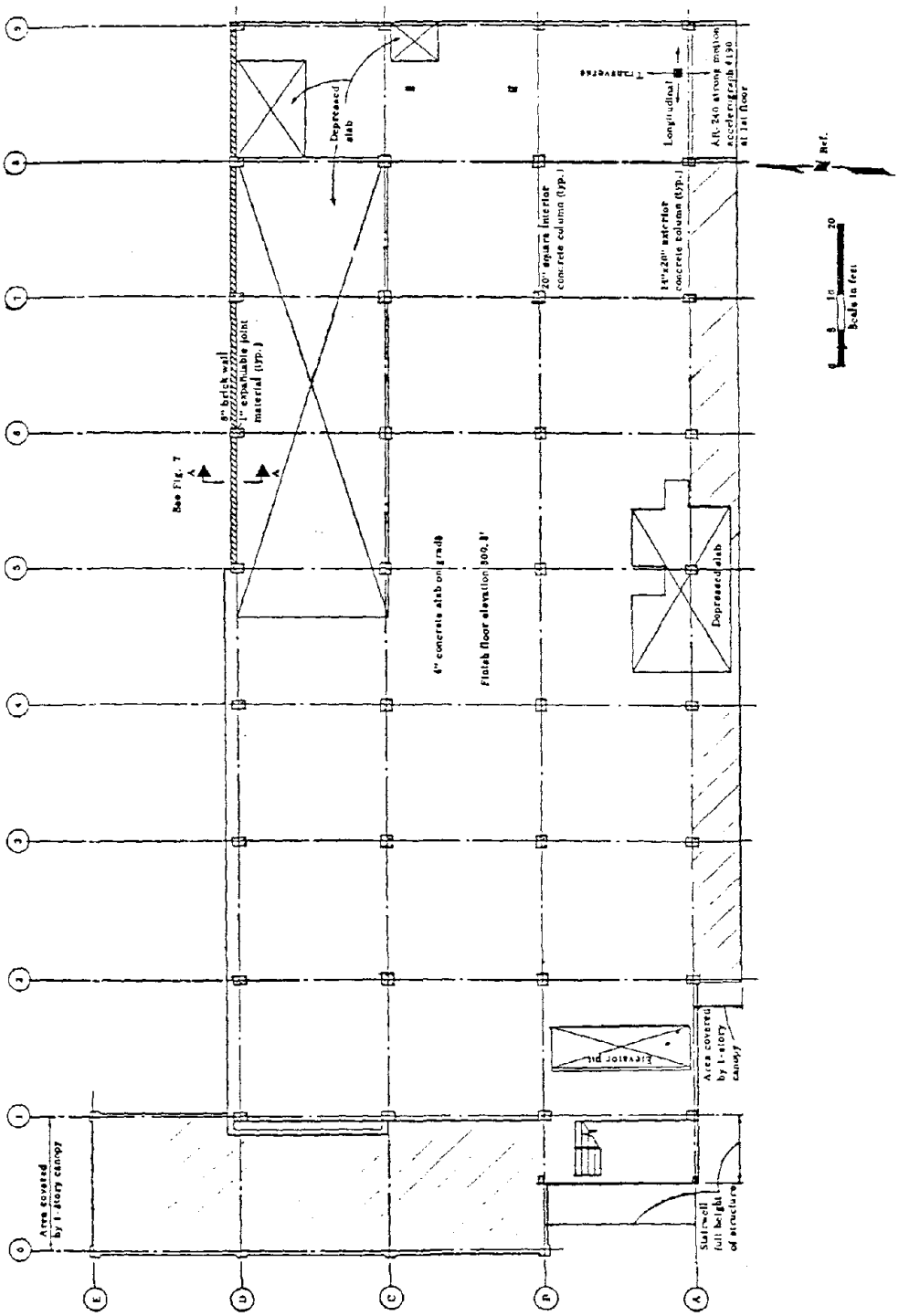

FIG. 5.2 HOLIDAY INN, ORION AVENUE. FIRST-FLOOR PLAN.

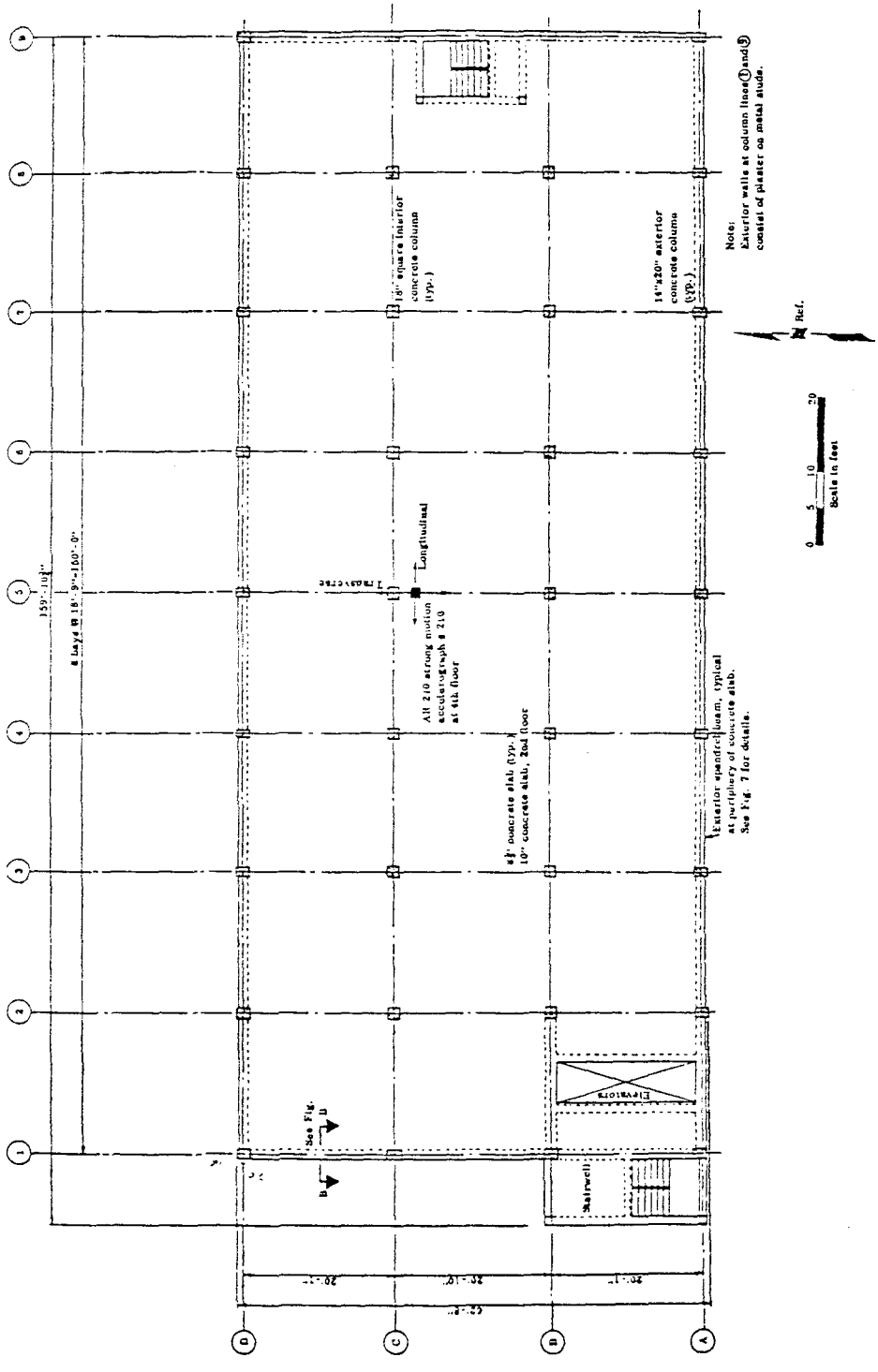

FIG. 5.3 HOLIDAY INN, ORION AVENUE. TYPICAL FLOOR FRAMING PLAN.

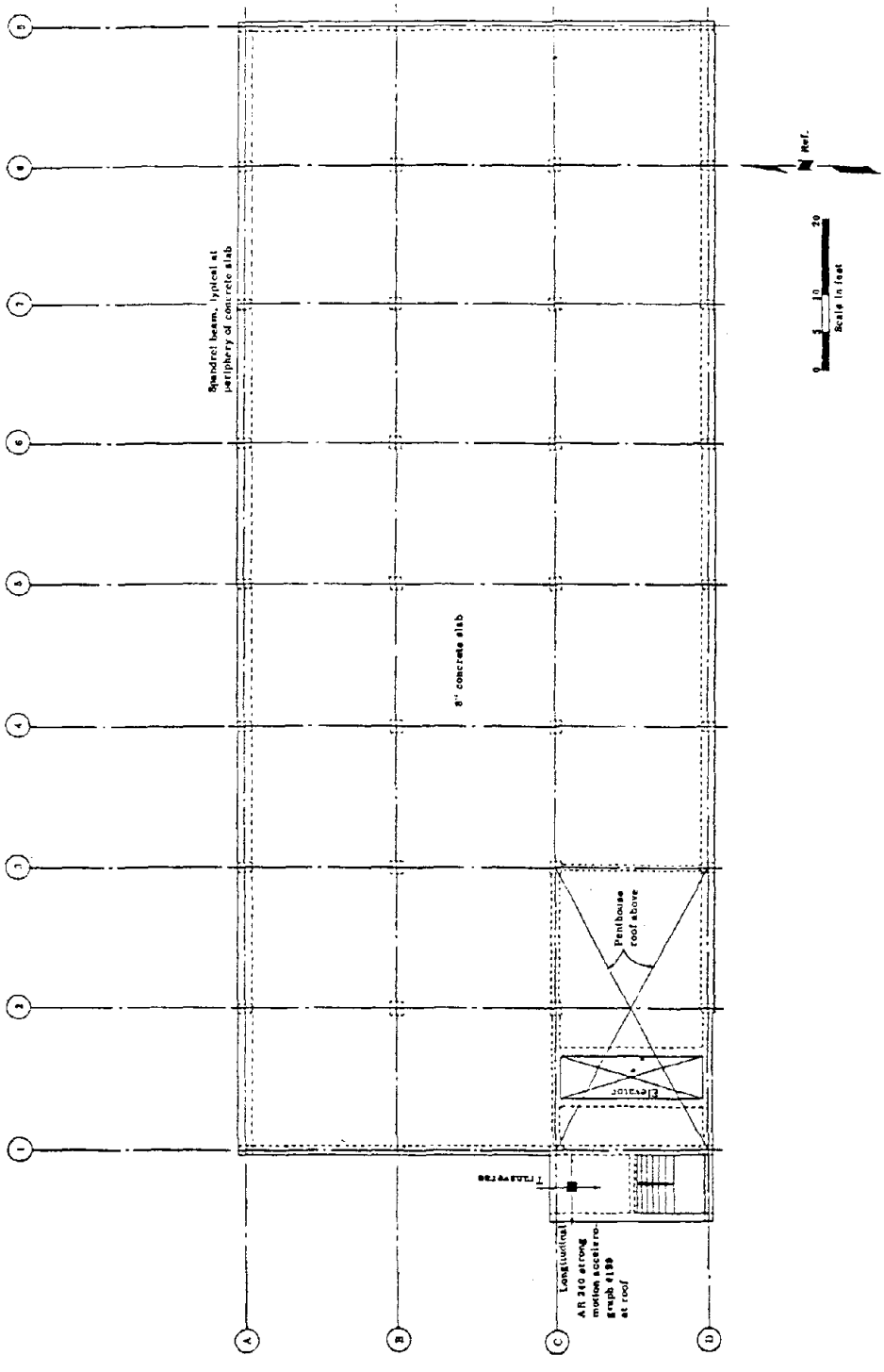

FIG. 5.4 HOLIDAY INN, ORION AVENUE. ROOF FRAMING PLAN.

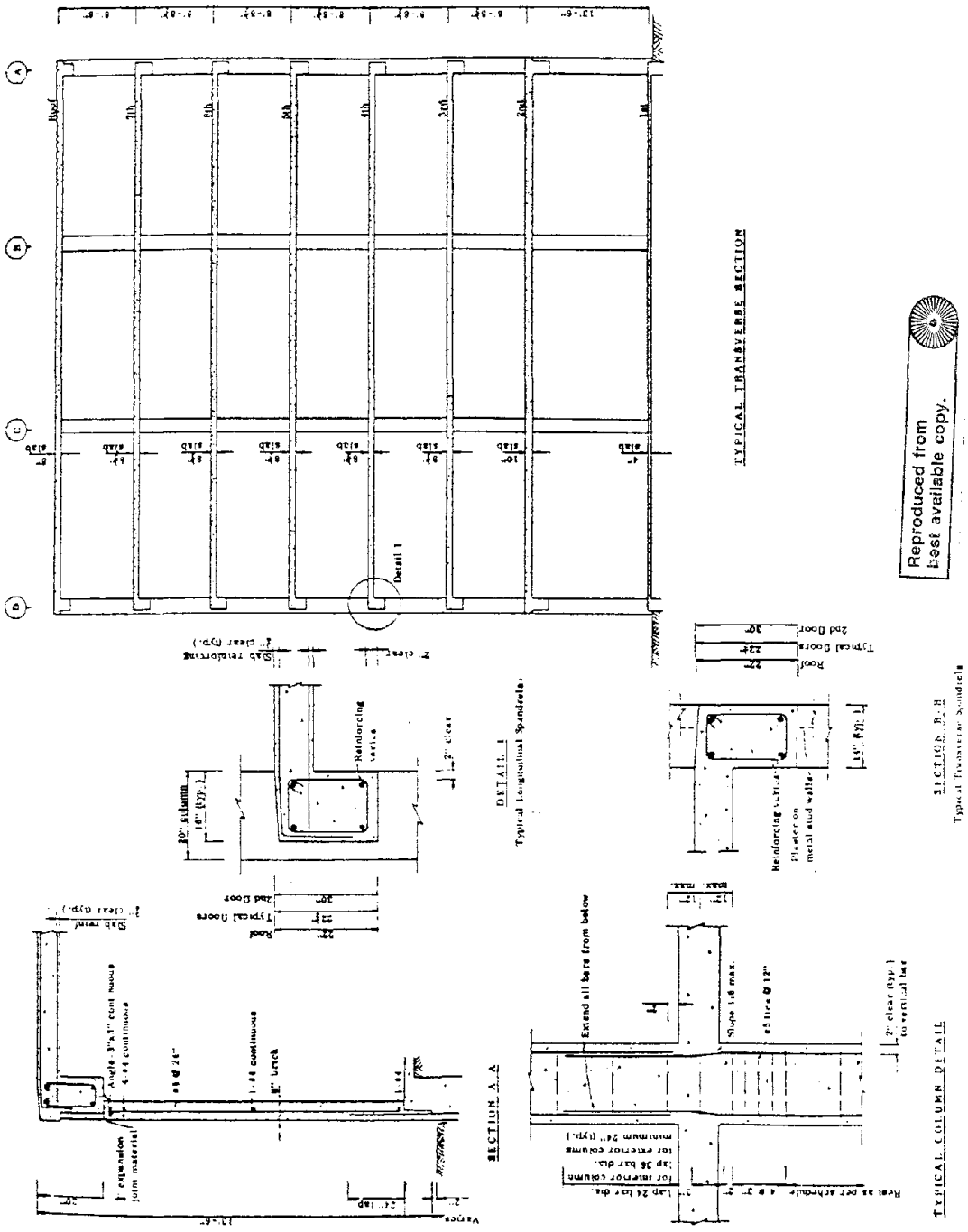

FIG. 5.5 HOLIDAY INN, ORLON AVENUE. SECTIONS AND DETAILS.

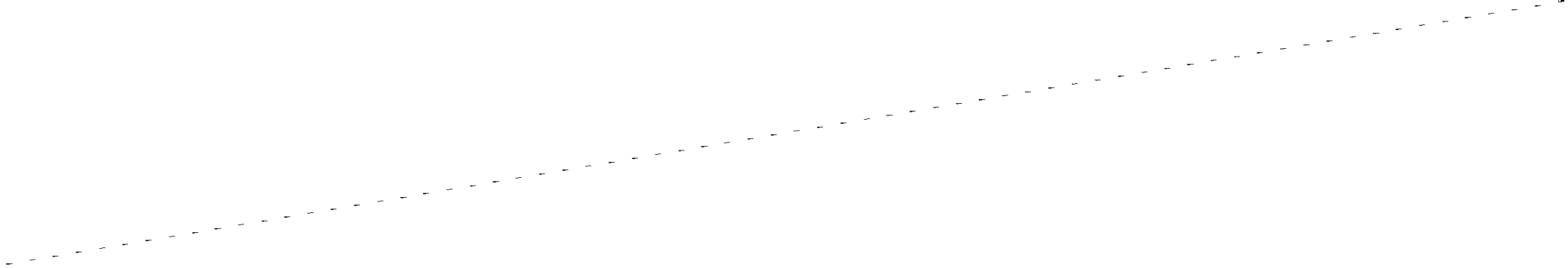

The structure was constructed of normal weight reinforced concrete. Table 5.1 lists the properties for the structural materials specified in the construction documents.

Interior partititons were, in general, gypsum wallboard on metal studs. Cement plaster, 1 inch thick, was used for the exterior facing at each end of the buiding and at the stair and elevator bays on the long side of the building. Double 16-gauge metal studs supported the cement plaster. Some additional cement plaster walls were located on the south side of the building at the first floor. The north side of the building, along column line D, had four bays of brick masonry walls located between the ground and the second floor at the east end of the structure (Fig. 5.2). Nominal 1-inch wide expansion joints separated the walls from the underside of the second-floor spandrel beams. Although none of those wall elements were designed to be part of the lateral force-resisting system, they undoubtedly contributed in varying degrees to the total stiffness of the structure, especially at low loads.

Lateral forces for each direction of the building are resisted both by the interior column flat plate frames and by the exterior column-spandrel beam ductile moment resistant frames. The spandrel beams resulted in exterior fames with a gross section elastic stiffness roughly twice that of the interior flat plate frames.

With the exception of some light framing members supporting the stairway and elevator openings, the structure is essentially symmetrical. The participation of the non-structural, brick filler walls, and some exterior cement plaster, could cause some asymmetry

TABLE 5.1 PROPERTIES OF CONSTRUCTION MATERIAL FOR HOLIDAY INN

Concrete (regular weight, 150 pcf[1] unit weight)			
Location in structure		Minimum specified compressive strength (f'_c)	Modulus of elasticity (E)
		psi[2]	psi[2]
Columns, 1st to 2d floors.....		5,000	4.2×10^6
Columns, 2d to 3d floors.....		4,000	3.7×10^6
Beams and slabs, 2d floor.....		4,000	3.7×10^6
All other concrete, 3d floor to roof.....		3,000	3.3×10^6
Reinforcing steel			
Location in structure	Grade	Minimum specified yield strength (f_y)	Modulus of elasticity (E)
		ksi[3]	psi[2]
Beams and slabs...	Intermediate-grade deformed billet bars (ASTM A-15 and A-305).	40	29×10^6
Column bars.....	Deformed billet bars (ASTM A-432)	60	29×10^6

[1] Pounds per cubic foot.
[2] Pounds per square inch.
[3] Kips per square inch.

for lateral motion in the longitudinal direction. For simplicity that asymmetry was ignored.

5.2.2 Earthquake Damage

After the earthquake, structural repair was necessary for the second-floor beam-column connection on the north side (east end) of the structure. Some structural distress also occurred in several column joints adjacent to the spandrel beam soffits.

Nonstructural damage was extensive. Almost every guest room suffered some damage. About 80 percent of the costs for repair were spent on drywall partitions, bathroom tile, and plumbing fixtures. The damage was most severe on the second and third floors and least severe on the sixth and seventh floors.

5.2.3 Recorded Earthquake Response

The motion caused by the San Fernando earthquake was recorded by Earth Sciences AR-240 strong motion accelerographs located at the roof, fourth floor, and first floor (ground) levels. At each location (Figs. 5.2, 5.3, and 5.4), motion was recorded for the three principal axes of the building, namely parallel to the long direction of the building (longitudinal), parallel to the short direction of the building (transverse), and vertically. Approximately 40 seconds of motion was recorded for each component of motion at each location.

The acceleration-time records shown in Fig. 5.6 were plotted by computer from the digitized strong motion results. From a visual examination of the longitudinal and transverse direction records for

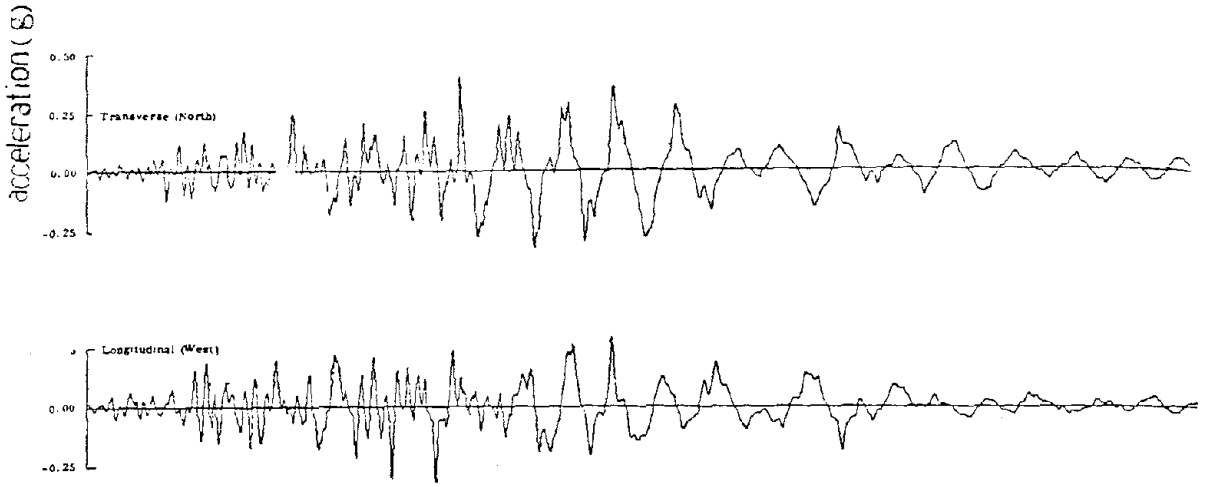

—*Holiday Inn, Orion Avenue. Recorded acceleration at the roof level.*

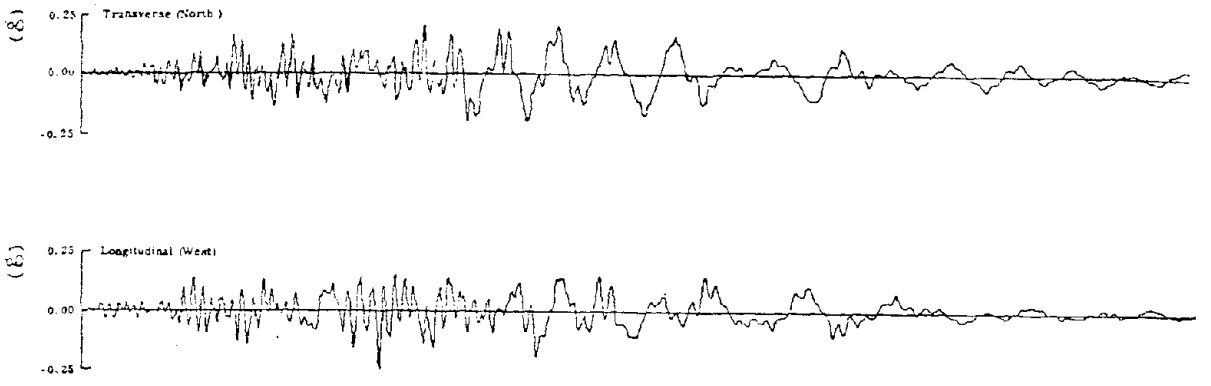

—*Holiday Inn, Orion Avenue. Recorded acceleration at the fourth-floor level.*

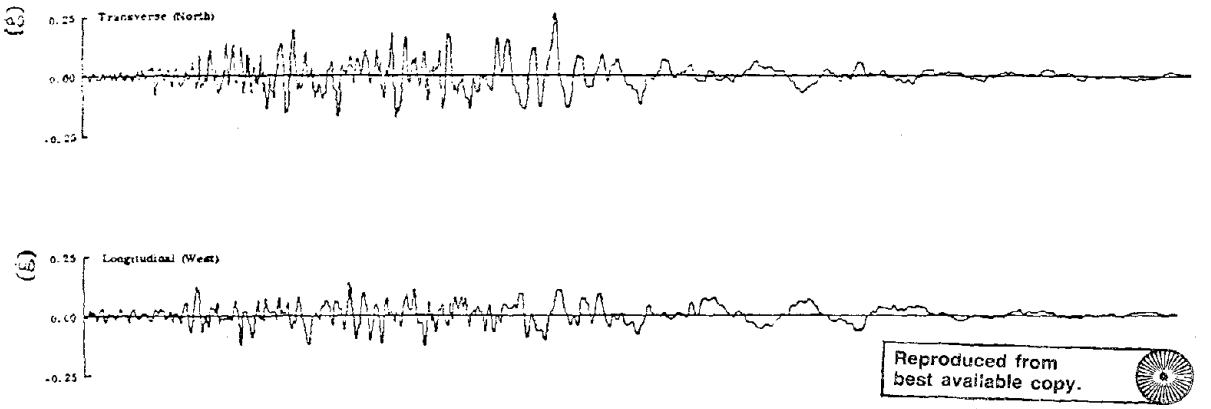

Reproduced from
best available copy.

—*Holiday Inn, Orion Avenue. Recorded acceleration at the ground level.*

FIG. 5.6 HOLIDAY INN, ORION AVENUE. RECORDED ACCELERATION

the fourth floor and roof levels, the following observations can be made: For the first 6 seconds of motion, the fundamental period in each direction was roughly 0.7 seconds. However by 9 seconds, the fundamental period had lengthened to be about 1.5 seconds, and stayed at about that value for the remainder of the period of shaking. This change in period suggests that the elastic limits of some elements in the structure were exceeded between 6 and 9 seconds after the start of shaking and that thereafter, the structure responded periodically in an inelastic manner.

5.3. Computer Modeling of Holiday Inn

5.3.1 Sectioning of Building

In accordance with the procedure described in Section 2.1, the original three dimensional space structure was divided into a series of two dimensional frames. Since the building was essentially symmetrical the frame was divided in the transverse direction along panel center lines symmetrical about the 5th row columns. Even if the spandrel beam results in an exterior frame with a stiffness double that of an interior flat plate frame, it is still clear that the properties of the interior frame dominate over those of the exterior frame. If the stiffness of the interior frame is unity, then that of the exterior frame is two, and that of the total structure is eleven. Hence 64% of the stiffness of the building for the N-S direction will be determined by the flat plate frame properties. By contrast, only one third of the stiffness of the building

is governed by flat plate properties for the E-W direction. The gross dimensions of the interior frame used for analysis purposes are shown in Fig. 5.7.

5.3.2 The Moment Caused by Gravity Load

The variation in moment along the frame caused by gravity laoding can be obtained from one of either two methods described in ACI Code 318. Both methods are generally accurate when lateral load effects do not dominate over gravity load effects. One procedure is the direct design method and the other is the equivalent frame method. The former is simpler but applicable only for vertical gravity load. The latter, while apparently more general than the direct design method, does not, in reality, offer more accuracy for gravity load effects. Since in this case the lateral loading response is being determined with the beam analogy, gravity loading effects are determined using the direct design method.

The idealized frame of Fig. 5.7 can be divided into three sub-frames. As shown in Fig. 5.8, one sub-frame is a roof floor frame (frame A), another is the 3rd to 7th floor frame (frame B) and the third is the 2nd-floor frame (frame C). For the structural dimensions shown in Fig. 5.7, a concrete weighing 150 pcf and a service load of 20 psf, initial moments for application of the beam analogy become as shown in Fig. 5.8.

The moments of Fig. 5.8 were divided into middle strip and column strip moments in a manner consistent with ACI Code methods. The moments attributed to the column strip and middle strip must be

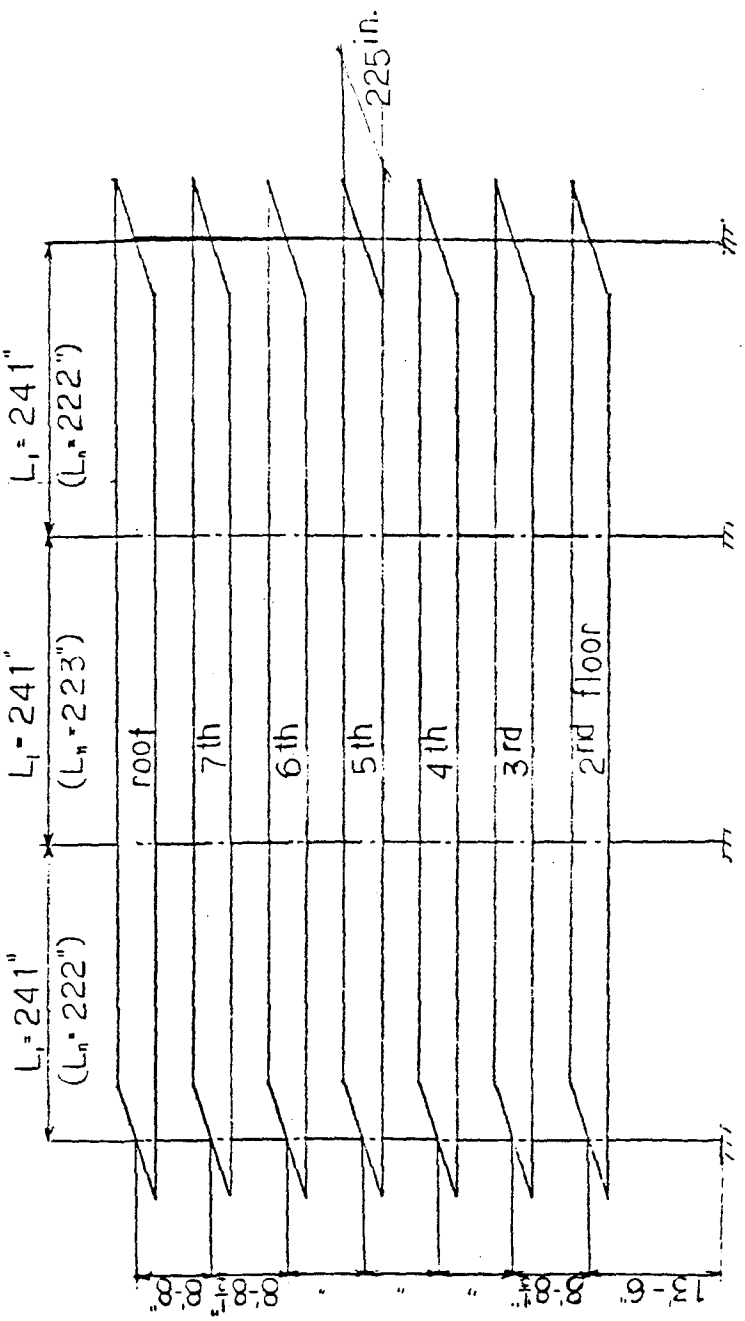

FIG. 5.7 EXTRACTED FRAME MODEL

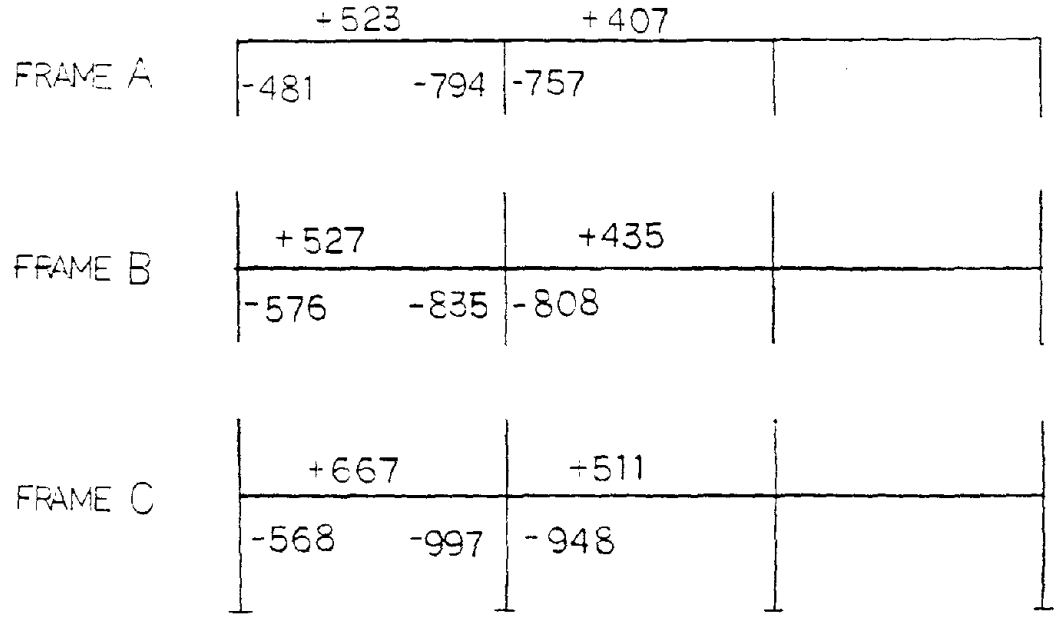

FIG. 5.8 MOMENTS CAUSED BY GRAVITY LOAD (k.in.)

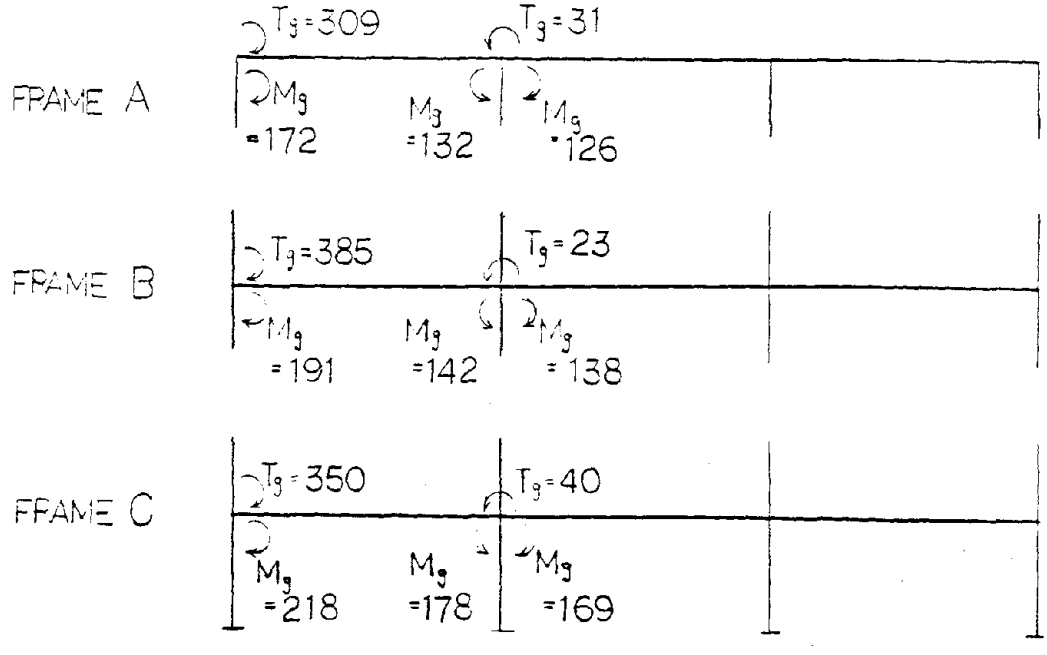

FIG. 5.9 BEAM ANALOGY MOMENTS DUE TO GRAVITY LOAD (k.in.)

distributed between the flexural and torsional elements of the beam analogy. That distribution is made using the procedure described in Section 2.3.1. The result is shown in Fig. 5.9. Those moments are applied directly to the frame as initial moments for the beam anlogy model.

5.3.3 Lateral Load Model

5.3.3.1 General

A lateral load model was developed for the frame using the method described in Chapter 2. However, it was not realistic to analyze the behavior of the Holiday Inn in detail, using the step by step procedure of Chapter 2 since many properties of the as-built structure are unknown. Therefore a simplified analytical model, consistent with the concepts of the more comprehensive model of Chapter 2, was developed for time history analyses using the Drain-2D program. That model is shown in Figs. 5.10 and 5.11. The stiffness of the columns and the slabs were calculated using accepted ACI Code procedures and assuming uncracked sections. The idealized model used for the frame for lateral load analysis is shown in Fig. 5.12. The numbering of the nodes is also shown in Fig. 5.12. Masses were distributed to the nodes 5 through 46 according to the volume of the slab tributary to each node.

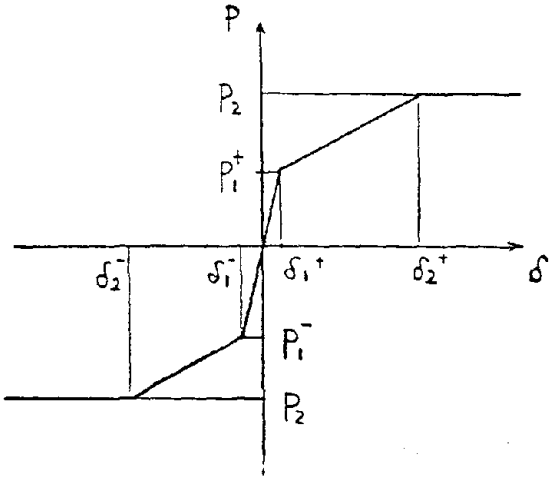

(a) primary curve

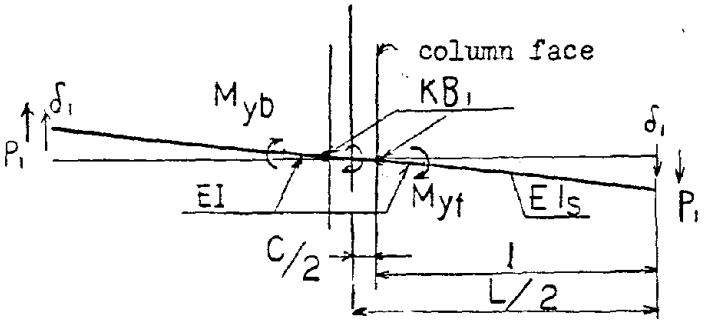

$$P_1^+ = (M_{yf} - M_g + \frac{1}{2}T_{cr}) / (\frac{L - C_r - h}{2})$$

$$P_1^- = (M_{yb} + M_g + \frac{1}{2}T_{cr}) / (\frac{L - C_r - h}{2})$$

$$\delta_1^+ = P_1^+ / K_1$$

$$\delta_1^- = P_1^- / K_1$$

$$\frac{1}{K_1} = \frac{(1+h)^2}{KB_1} + \frac{h\,l^2}{EI} + \frac{l}{3EI_S}$$

$$EI = (EI_f + EI_b)/2$$

$$KB = KB_1 + KB_1'/2$$

(b) stiffness model of first stage

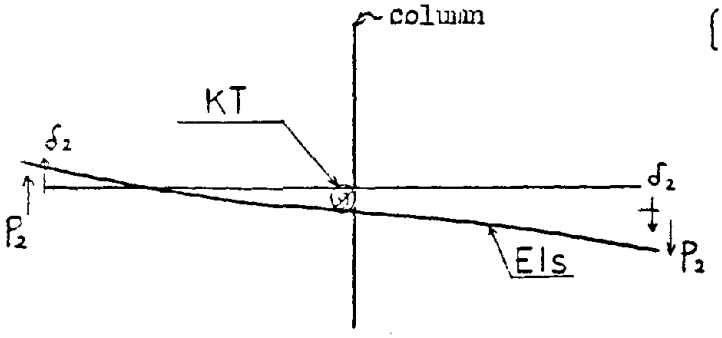

$$P_2 = (M_{uf} - M_g + \frac{1}{2}T_u) / (\frac{L - C_r - h}{2})$$

or

$$P_2 = (M_{ub} + M_g + \frac{1}{2}T_u) / (\frac{L - C_r - h}{2})$$

$$\delta_2^+ = \delta_1^+ + (P_2 - P_1^+)/K_2$$

$$\delta_2^- = \delta_1^- + (P_2 - P_1^-)/K_2$$

$$\frac{1}{K} = \frac{4\,l^2}{KT} + \frac{l^3}{3EI_S}$$

(c) stiffnes model of second stage

FIG. 5.10 SIMPLIFIED BEAM ANALOGY

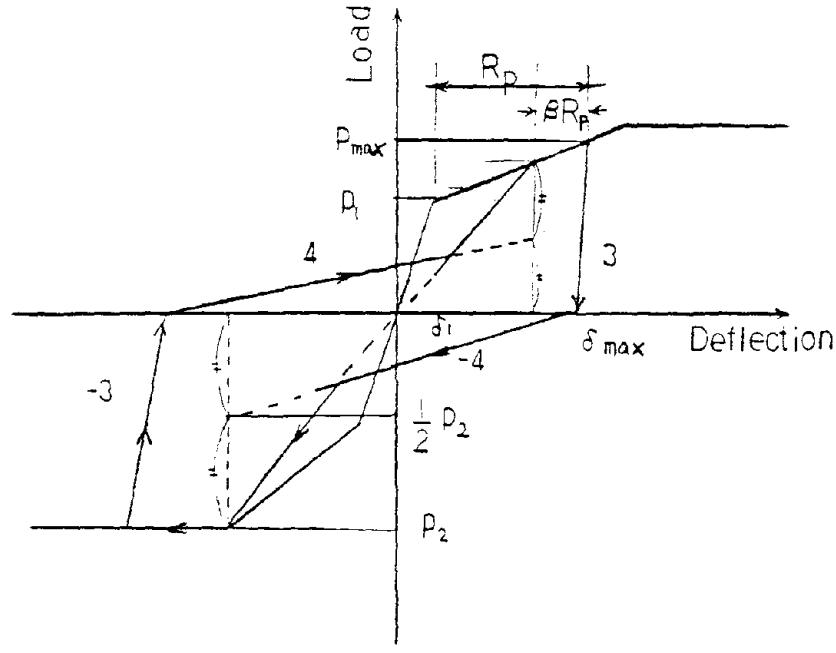

FIG. 5.11 EXCURSION AFTER FIRST BREAK UNTIL SECOND BREAK FOR SIMPLIFIED MODEL CYCLIC LOADING RESPONSE

Reproduced from
best available copy.

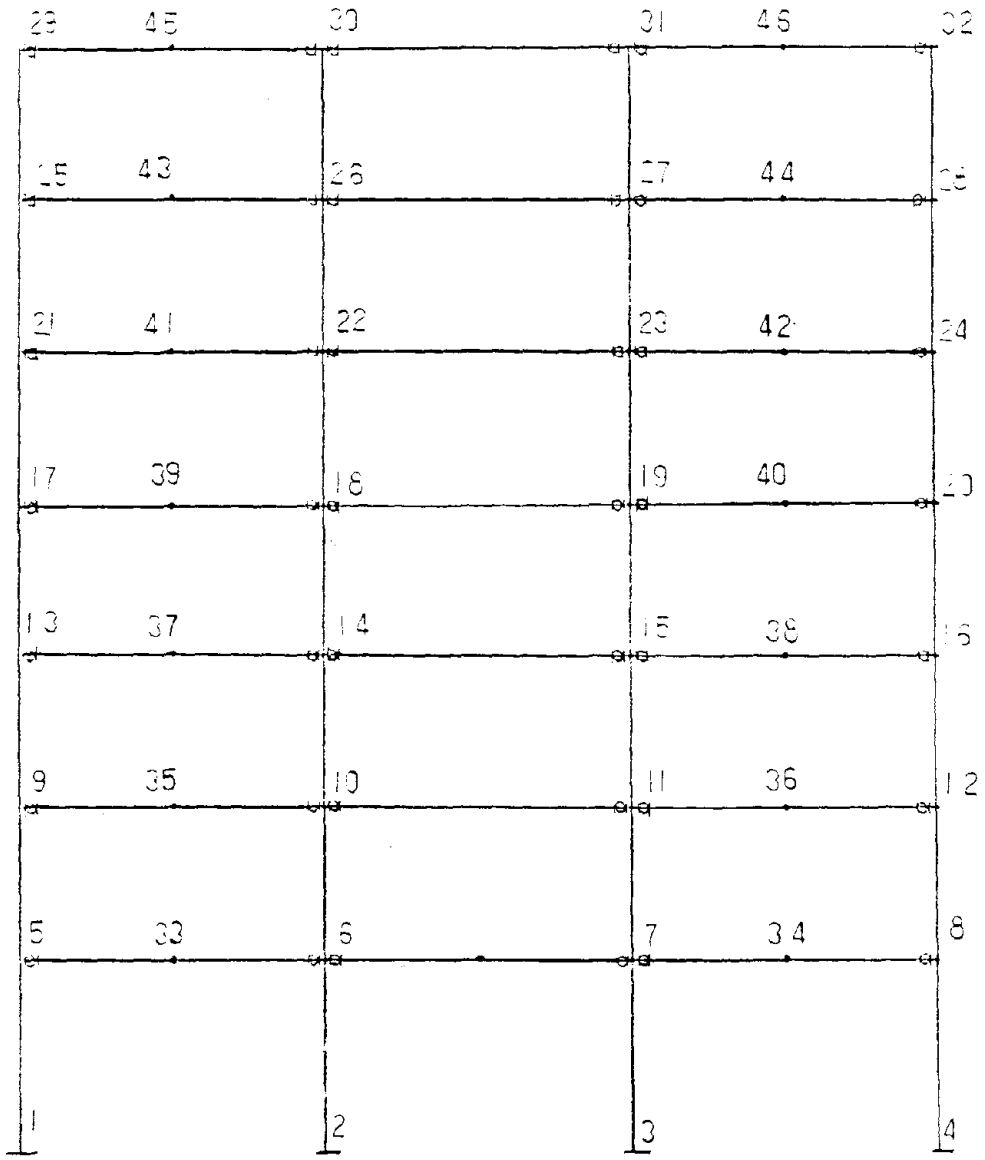

FIG. 5.12 IDEALIZED FRAME MODEL

5.3.3.2 Simplified Column-Slab Connection Model

If a beam analogy is defined as a method for analyzing column-slab connections by representing them with a set of beams, then there can be various kinds of beam analogy.

The analytical model developed in Chapter 2 is directly usable for ordinary structural analysis and for practical design. Further it incorporates all the elements normally required for orderly structural analysis, namely:

1. Use of the governing constitutive equations for the materials used in the structure.
2. Satisfaction of compatibility of deformations, and
3. Satisfaction of equilibrium of forces.

As demonstrated in prior chapters a solution results that is in comparatively good agreement with available test results for both strength and stiffness and is not too complex.

However, for the analysis of large buildings, involving many connections, it is appropriate to make the analysis as simple as possible. That can be done by neglecting some of the constraints imposed on the step-by-step model and developing a simplified model that predicts essentially the same response as the step-by-step-model. From a practical viewpoint prime criteria for judging whether a model is appropriate or not are as follows:

1. How well does it predict the measured strength and stiffness of column-slab connections?; and
2. How easy is it to use?

So far as the second criterion is concerned, the model proposed in Sections 2.3 contains some undesirable features. There are at least two ways that analogy can be simplified. One possibility is to represent the connection only by flexural elements and to compensate for the torsional elements by increasing the width of the flexural elements. That is the procedure implied in the ACI Code and in the concept of an effective slab width. However, that procedure is only possible when the reinforcing system is the same both in the direction of the span and transverse to it. Further, to develop such a model it would be necessary to make extensive trial and error investigations. For example, for an exterior bay the presence or absence of an edge beam has a large influence on the lateral load stiffness of that bay but little influence on the stiffness of the adjacent interior bay.

A second possibility is to represent the connection by bond slip, flexural and torsional elements only. That second possibility is adopted here because it can be transformed into a general procedure that is not difficult to apply.

In the following, a simple model is developed for the case of an interior column-slab connection. For other connections, similar methods can easily be developed by altering the governing equations according to the governing geometric constraints.

The cyclic response is idealized by first defining a primary curve for initial loading and then a set of rules for loading reversals.

(a) Primary curve

As shown in Fig. 5.10 (a) the step by step method of Section 2.3 predicts what is essentially a tri-linear curve. The first break in the curve corresponds to yielding of the flexural elements and cracking of the torsional elements. The second break corresponds to crushing of the flexural and torsional elements. If those two break points are properly evaluated, the result is a simplified model that predicts a solution close to the real behavior of the connection.

The coordinates of the first break in the curve $(P_1^+ + \delta_1^+)$, (P_1^-, δ_1^-) can be obtained as follows:

$$P_1^+ \cdot \frac{L}{2} = (M_{yf} - M_g) + \frac{1}{2} T_{cr} + \frac{c_1 + h}{2} P_1^+ \qquad (5.1)$$

$$P_1^- \cdot \frac{L}{2} = (M_{yb} + M_g) + \frac{1}{2} T_{cr} + \frac{c_1 + h}{2} P_1^- \qquad (5.2)$$

where M_{yf} and M_{yb} are calculated using Eq. (2.4) and T_{cr} is calculated using Eq. (2.18). In the case of a large gravity loading, it is better to use Eq. (2.19). Then,

$$P_1^+ = (M_{yb} - M_g + \frac{1}{2} T_{cr}) \; / \; (\frac{L - c_1 - h}{2}) \qquad (5.3)$$

$$P_1^- = (M_{yb} + M_g + \frac{1}{2} T_{cr}) \; / \; (\frac{L - c_1 - h}{2}) \qquad (5.4)$$

The moment transferred to the column (M_1) at the first break becomes:

$$M_1 \pm = LP_1 \pm \qquad (5.5)$$

The stiffness prior to the first break can be obtained easily from the determinate frame shown in Fig. 5.10(b). The torsional elements are removed from the frame model in accordance with the assumption that the characteristics of the system for that stage of the behavior

are determined primarily by the response of the flexural elements. That assumption is in agreement with the results of previous research (12).

$$\delta_1^{+} = \left(\frac{(\ell+h)^2}{KB_1} + \frac{h\ell^2}{EI} + \frac{\ell^3}{3EI_s}\right) P_1^{+} \tag{5.6}$$

$$\delta_1^{-} = \left(\frac{(\ell+h)^2}{KB_1} + \frac{h\ell^2}{EI} + \frac{\ell^3}{3EI_s}\right) P_1^{-} \tag{5.7}$$

where $\ell = \frac{L}{2} - \frac{c}{2} - h$; KB_1 is the bond slip stiffness calculated by Eq. (2.37); EI_s is the stiffness of the slab part; and EI is the average stiffness of the front and back face flexural elements calculated approximately as follows:

$$EI = \left(\frac{M_{yf} + M_{yb}}{2}\right) \frac{E_s\,(d - kd)}{f_y} \tag{5.8}$$

The coordinates of the second break in the curve (P_2, δ_2^{+}), (P_2, δ_2^{-}) can be obtained as the smaller of Eqs. (5.9) or (5.10)

$$P_2 \frac{L}{2} = (M_{uf} - M_g) + \frac{1}{2} T_u + P_2 \left(\frac{c_1 + h}{2}\right) \tag{5.9}$$

$$P_2 \frac{L}{2} = (M_{ub} + M_g) + \frac{1}{2} T_u + P_2 \left(\frac{c_1 + h}{2}\right) \tag{5.10}$$

where, M_{uf} (or M_{ub}) is calculated using Eq. (2.7) and T_u is calculated using Eq. (2.23) or Eq. (2.24).

$$P_2 = \left((M_{uf} - M_g) \text{ (or } M_{ub} + M_g) + \frac{1}{2} T_u\right) \Big/ \left(\frac{L - c_1 - h}{2}\right) \tag{5.11}$$

The moment transferred to the column (M_2) becomes

$$M_2 = LP_2 \tag{5.12}$$

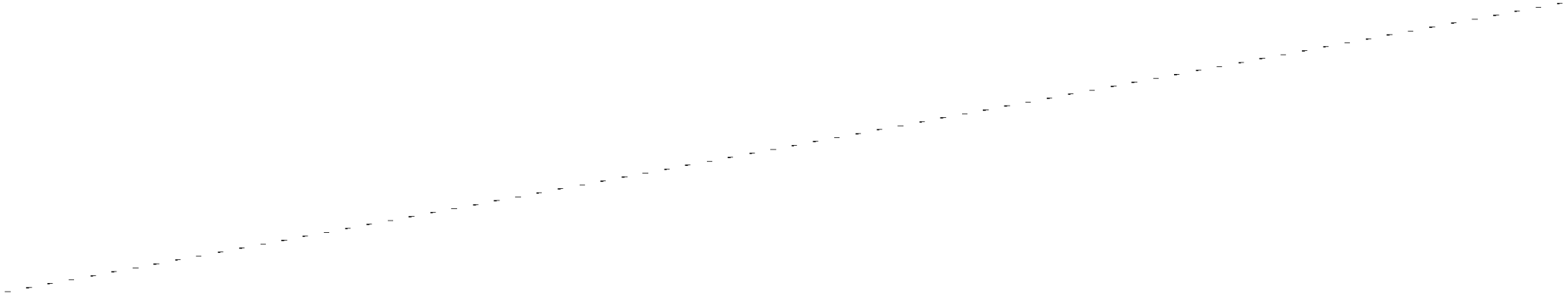

The stiffness between the first break and the second break can be obtained from a model which has no flexural elements as shown in Fig. 5.10(c). This simplification comes from the assumption that the characteristics of the system in this stage are determined by the response of the torsional elements. Thus,

$$\delta_2^+ = \delta_1^+ + \left(\frac{4\,(\ell + c_{1/2})^2}{KT_2} + \frac{\ell^3}{3EI_s}\right)(P_2 - P_1^+) \tag{5.13}$$

$$\delta_2^- = \delta_1^- + \left(\frac{4\,(\ell + c_{1/2})^2}{KT_2} + \frac{\ell^3}{3EI_s}\right)(P_2 - P_1^-) \tag{5.14}$$

where KT_2 is the torsional stiffness calculated using Eqs. (2.15) and (2.28)

The primary curve obtained using this simplified method is compared to that obtained using the original method, described in Section 2.3, for SS-1 and SS-2 in Fig. 5.13. It is apparent that the simplified model predicts the test results reasonably well and that differences between the results predicted by this simplified model and the more complex model of Section 2.3 are minimal.

(b) Response Under Loading Reversals

For dynamic analysis, rules must be established for the load-deformation curve for loading reversals.

Most of the possible alternatives for each point in the loading history are the same as those described in Chapter 2 for the torsional element except for the following rules:

Condition 1. Unloading from the primary curve following the first break:

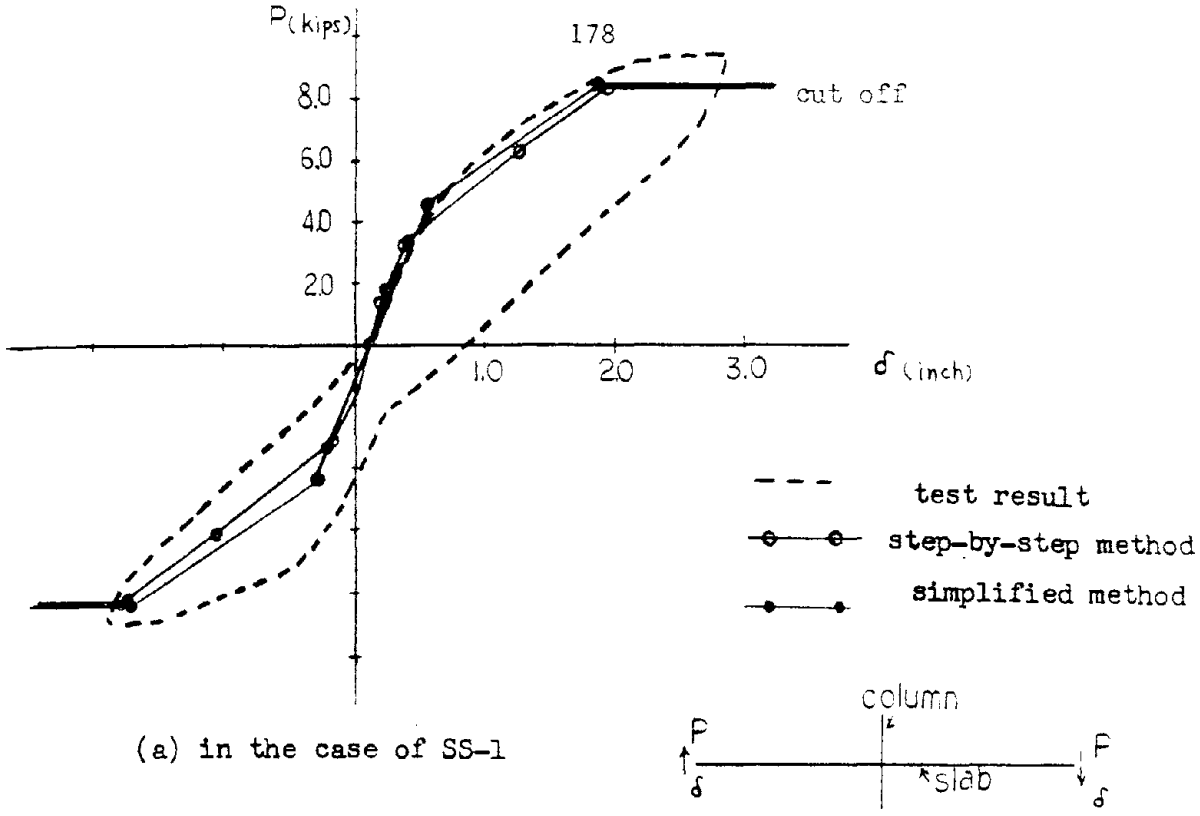

(a) in the case of SS-1

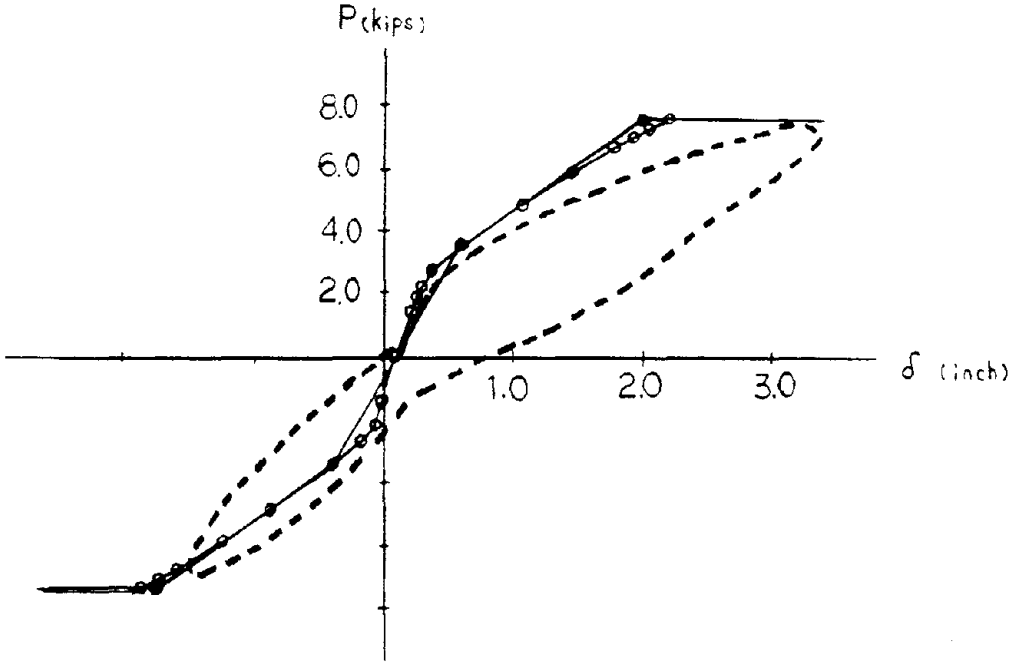

(b) in the case of SS-2

FIG. 5.13 COMPARISON BETWEEN ORIGINAL STEP BY STEP AND SIMPLIFIED METHOD FOR ASSESSING SLAB-COLUMN CONNECTION RESPONSE

Rule - The unloading stiffness is double the stiffness for the "before break" condition.

Example - Segment 3 in Fig. 5.11

Condition 2. Reloading after a large excursion in the reverse direction.

Rule - The reloading stiffness is directed towards the point $\frac{P_{max} - \beta(P_{max} - P_1)}{2}$, $(\delta max - \beta(\delta max - \delta_1))$ until it hits the line which connects the zero point and the coordinate $(P_{max} - \beta(P_{max} - P_1), \delta_{max} - \beta(\delta_{max} - \delta_1)$. β is defined as shown in Fig. 2.10(c). β is taken as 0.2 except when the previous excursion exceeds P_2, in which case it is taken as 1.0.

Example - Segment 4 in Fig. 5.11.

5.4 Dynamic Response of Holiday Inn

5.4.1 Behavior of Holiday Inn As-Built

(1) Model for Slab-Column Connections

The reinforcing ratios for the Holiday Inn slabs are different at each floor. Ratios are higher in the lower floors than in the upper floors. Values are summarized in Table 5.2. The minimum reinforcement ratio permitted under the UBC with which the structure was designed was 0.2% of the gross concrete area. In some areas the ratios approach that minimum. In other areas the ratios are considerably greater than the minimum. Since the lateral load stiffness and strength of a slab-column connection have been shown to

TABLE 5.2 REINFORCEMENT RATIOS FOR HOLIDAY INN

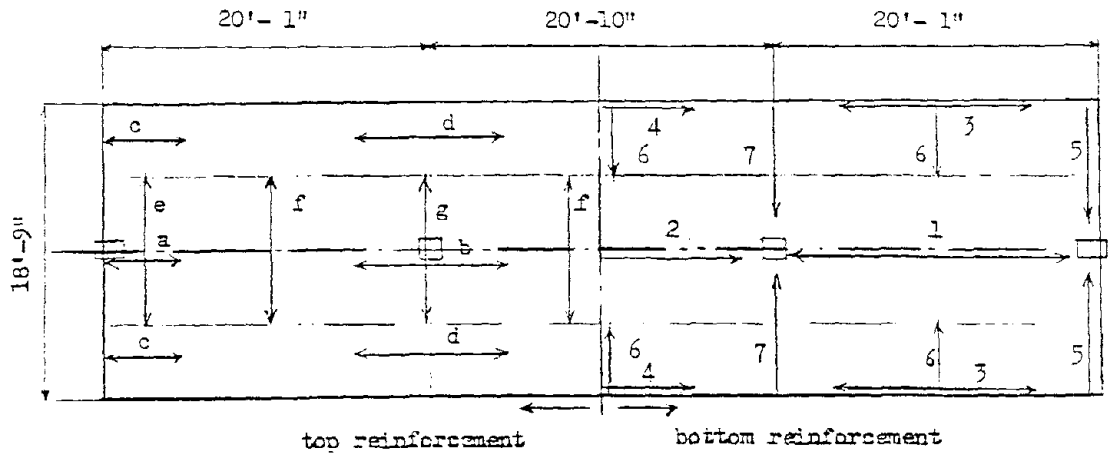

note		length	2nd	3rd	4th	5th	6th	7th	roof
top reinforcement	a	6'-8"	15#6 0.67	16#6 0.85	15#6 0.80	13#6 0.69	13#6 0.69	11#6 0.59	10#5 0.40
	b	10'-6"	16#7 0.97	23#6 1.22	22#6 1.17	21#6 1.12	21#6 1.12	17#6 0.91	19#6 1.09
	c	6'-8"	8#5	7#5	7#5	7#5	7#5	7#5	7#5
	d	10'-6"	8#6	7#5	7#5	7#5	7#5	7#5	7#5
	e	9'-6"	6#6 0.37	5#6 0.37	5#6 0.37	5#6 0.37	5#6 0.37	5#6 0.37	6#5 0.33
	f	9'-6"	8#6	8#5	8#5	8#5	8#5	8#5	6#5
	g	9'-6"	16#7 0.85	18#6 0.84	17#6 0.79	16#6 0.74	16#6 0.74	16#6 0.74	17#6 0.85
bottom reinforcement	1	22'-6"	8#6 0.36	8#6 0.43	8#6 0.43	8#6 0.43	8#6 0.43	8#6 0.43	10#5 0.40
	2	22'-4"	7#6 0.31	7#6 0.37	7#6 0.37	7#6 0.37	7#6 0.37	7#6 0.37	10#6 0.57
	3	21'-6"	8#5	7#5	7#5	7#5	7#5	7#5	8#5
	4	22'-4"	8#5	7#5	7#5	7#5	7#5	7#5	8#5
	5	20'-3"	4#5 0.17	4#5 0.21	4#5 0.21	4#5 0.21	4#5 0.21	4#5 0.21	4#5 0.22
	6	20'-5"	8#5	8#5	8#5	8#5	8#5	8#5	8#5
	7	20'-3"	10#5 0.27	8#6 0.37	8#6 0.37	8#6 0.37	8#6 0.37	8#6 0.37	9#5 0.32

$\rho_{min} = 0.20\%$

be sensitive to the reinforcing ratio in the column head region for prediction purposes connection models had to be made for each floor. The resultant limiting moment values and partial stiffness values for each connection are listed in Table 5.3. Naturally, the capacities and stiffnesses of the connections are higher in the lower floors than in the upper floors.

The torsional capacities and stiffnesses for the spandrel beams were calculated in the manner described in Section 2.2. The possible contribution of any slab extension to that capacity and stiffness was neglected. Further, any influence of non-structural elements such as brick walls, cement plaster, etc. on the limiting moment capacities and stiffnesses was also neglected.

(2) The Behavior of Holiday Inn

For the connection models shown in Table 5.3, and the measured acceleration record at ground level as the input wave, the time history response of the Holiday Inn was calculated using the Drain-2D program.

The predicted deformations are compared in Fig. 5.1 with the deformation records for the fourth and roof floors (Ref. 40). From those results, it can be concluded that:

1. The time history for the predicted deformations is similar to the observed response. The agreement is better for the fourth floor than for the roof.
2. The amplitude for the predicted response is similar for both negative and positive displacements for the fourth

TABLE 5.3 LIMITING MOMENTS AND PARTIAL STIFFNESSES OF CONNECTIONS

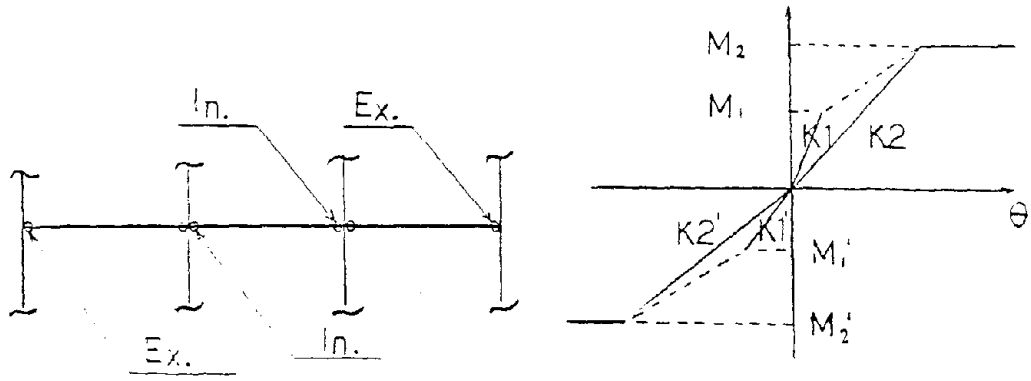

		M_1 (K·in)	M_1' (K·in)	M_2 (K·in)	M_2' (K·in)	K1 (×10³ K·in)	K1' (×10³ K·in)	K2 (×10³ K·in)	K2' (×10³ K·in)	M_s *1 (K·in)	M_s' *1 (K·in)
roof	Ex.	870	1830	1540	2500	70	70	60	60	1500	1500
	In.	620	550	900	900	140	80	50	50	1380	1870
7th	Ex.	930	2000	1700	2840	100	90	66	66	2060	1670
	In.	640	570	950	950	150	90	60	60	2750	1670
6th	Ex.	1040	2000	2000	3200	110	90	75	75	2290	1670
	In.	790	570	1100	1100	160	90	65	65	2660	1670
5th	Ex.	1040	2000	2000	3200	110	90	75	75	2290	1670
	In.	790	570	1100	1100	160	90	65	65	2660	1670
4th	Ex.	1040	2000	2000	3200	110	90	75	75	2520	1670
	In.	790	570	1100	1100	160	90	65	65	3340	1530
3rd	Ex.	1100	2000	2100	3300	140	90	80	80	2660	1670
	In.	850	570	1200	1200	170	90	65	65	3480	1530
2nd	Ex.	1800	2600	2700	3900	220	140	100	100	3190	2150
	In.	1150	740	1700	1700	280	140	90	90	4490	1940

*2
EIS = 31.7x10 (for roof)
38.0x10 (3rd-7th floor)
69.4x10 (2nd floor)

*1 The limiting moments for the development of a hinge across the full width of the slab

*2 The stiffness of the beam representing the slab of full width

floor level. For the roof the predicted ampitude was generally greater than the measured, especially for the negative direction. For that direction measured values were similar for the fourth and roof levels suggesting that there were some restraining mechanism between floors for that direction that was not considered in the analytical model. For the positive direction at the roof level, the measured and predicted absolute maximum displacements are equal.

3. The high frequency vibrations that appeared in the real response wre not present in the predicted response.
4. Until 8 seconds into the earthquake, the observed motion at the 4th and roof floor levels were similar to the ground motion. After the large peak displacement and change in acceleration at about 9 seconds, the fourth and roof floors show vibration characteristics different to those of the ground motion. These characteristics are also present in the predicted results.

The difference between the measured and predicted amplitudes is very large from start to 4.0 seconds. That is probably a result of neglecting the stiffening effects provided by the nonstructural elements such as brick walls and gypsum board partitions. After 4.0 seconds, when large displacements occurred and the non-structural elements probably cracked, the predicted amplitudes are still in general larger than the real. Probably that over prediction is due to neglect of other resisting systems such as shear wall action

provided by elevator shafts and stairwalls and neglect of shear flow from the flexible interior frames to the stiffer exterior frames. Restraints on displacements caused by this latter action would be small at the lower floors and larger for the upper floors. If such resisting systems were included, the total stiffness of the buiding would be larger and the aplitude of the motions smaller.

It is natural that the higher floors exhibit larger sways than the lower floors. However, nonstructural damage is related more to the relative displacement between floors than to the magnitude of the displacement at a given floor. The predicted relative deformations between floors are shown in Fig. 5.14. In that figure, there is not much difference in the relative deformations between floors until the 5th floor. However, for all levels below the 5th floor relative deformations exceed 1 inch and that value is reported enough to cause some damage to nonstructural elements (Ref. 40). Relative deformations are predicted as being smaller between the 6th, 7th and roof floors, than between the 5th and lower floors. Thus, these results predict more damage for the bottom and middle floors than for the upper floors. That prediction coincides with the reported damage which was most severe on the second and third floors and least severe at the sixth and seventh floors.

Shown in Figs. 5.15 and 5.16 are predicted force-deformation relationships and corresponding time histories for the moments acting on typical connections on the second, fourth, and roof floors. After the second and third large excursions at about 6 and 9 seconds many of the interior connections exceeded their M_1' and M_1 values

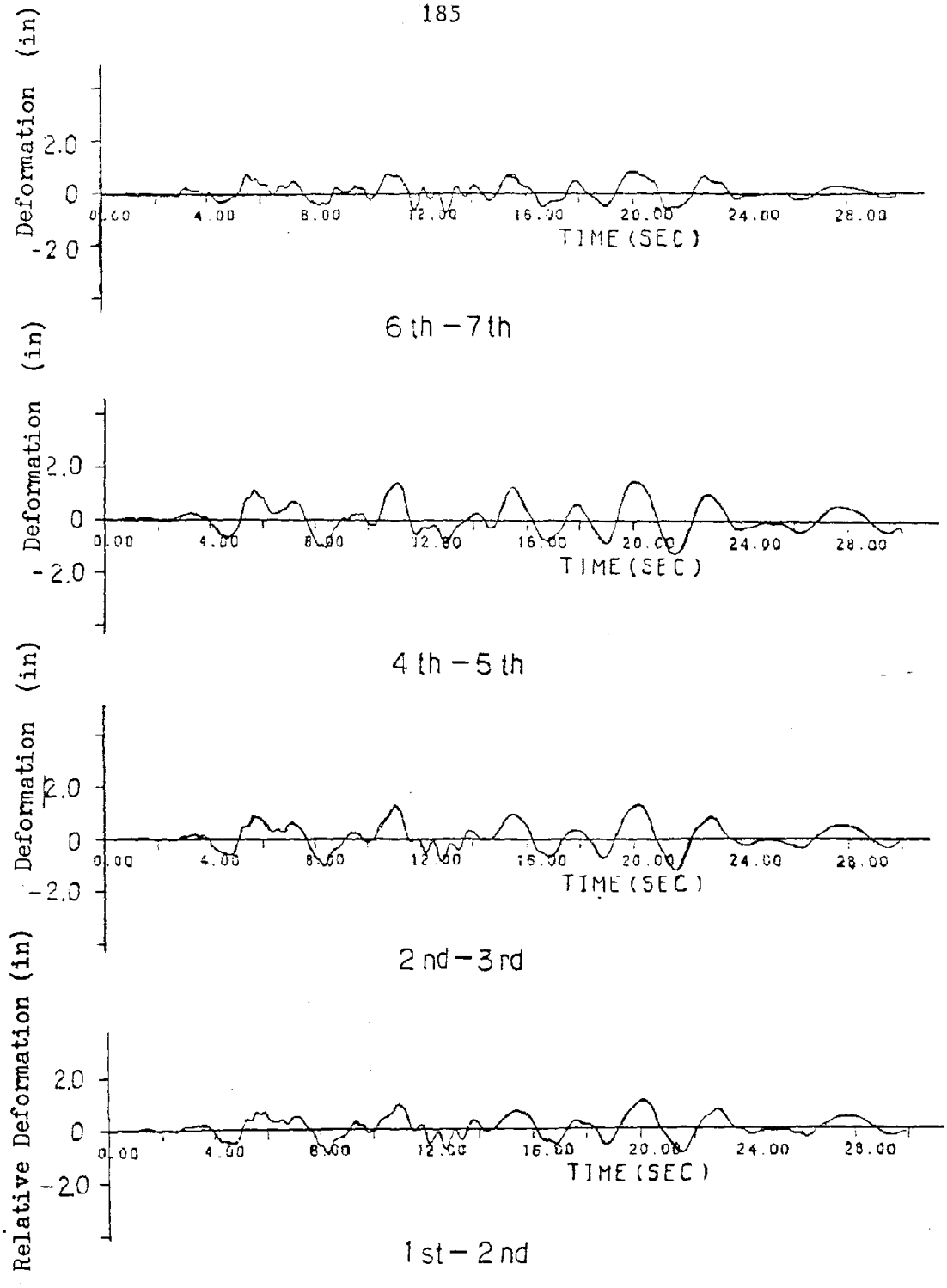

FIG. 5.14 PREDICTED RELATIVE DEFORMATIONS BETWEEN FLOORS FOR HOLIDAY INN

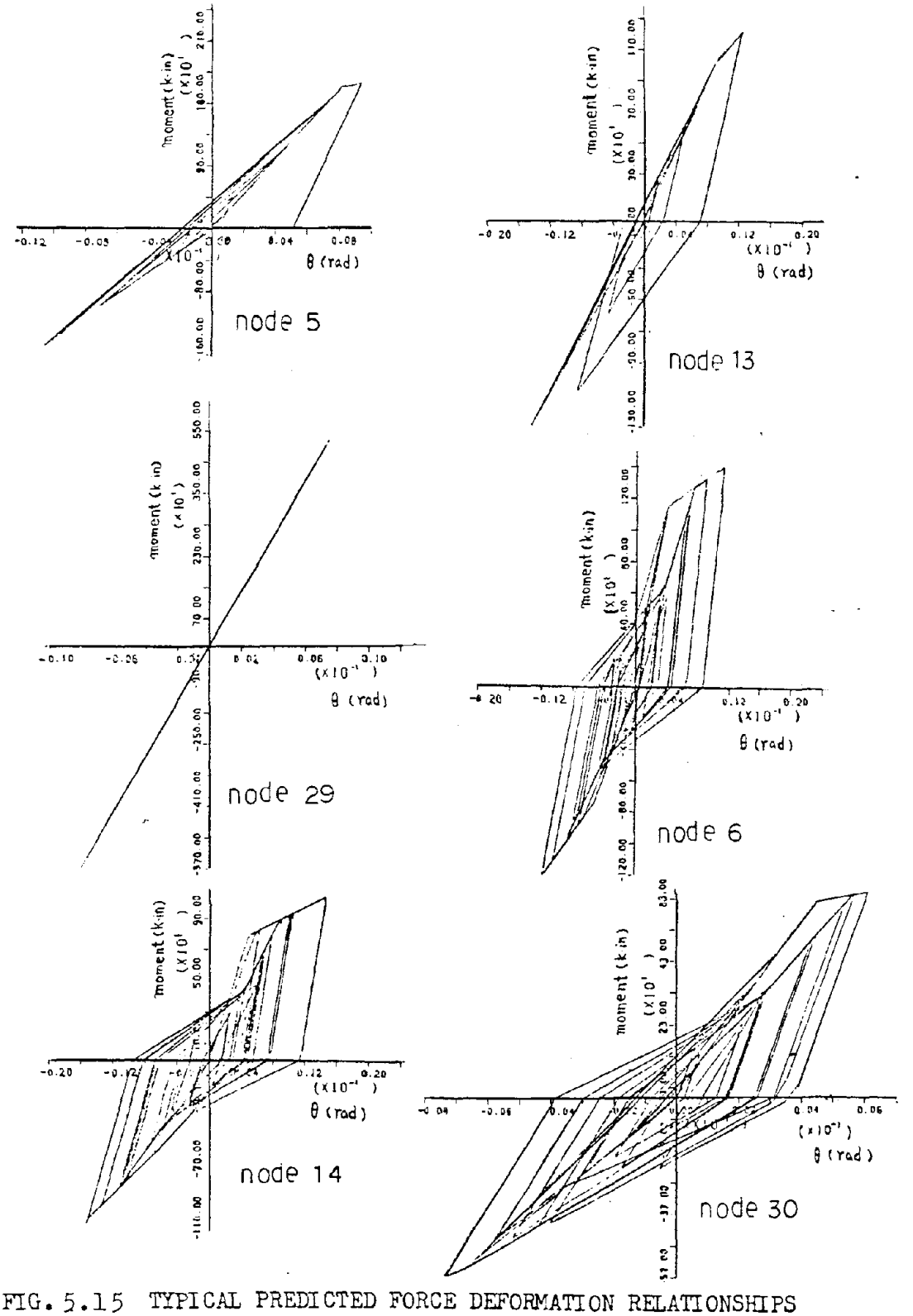

FIG. 5.15 TYPICAL PREDICTED FORCE DEFORMATION RELATIONSHIPS FOR SLAB-COLUMN CONNECTIONS OF HOLIDAY INN

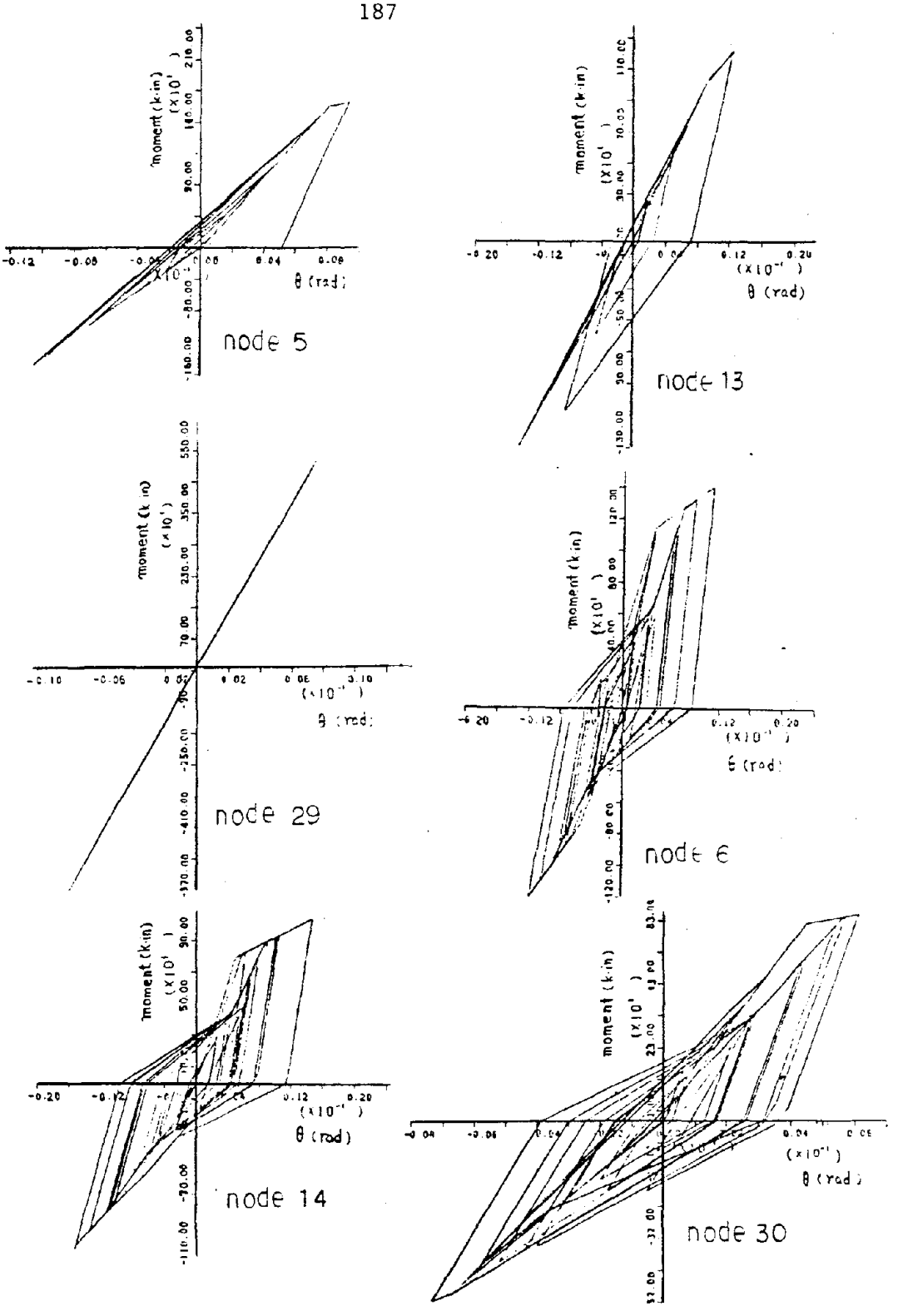

FIG. 5.15 TYPICAL PREDICTED FORCE DEFORMATION RELATIONSHIPS FOR SLAB-COLUMN CONNECTIONS OF HOLIDAY INN

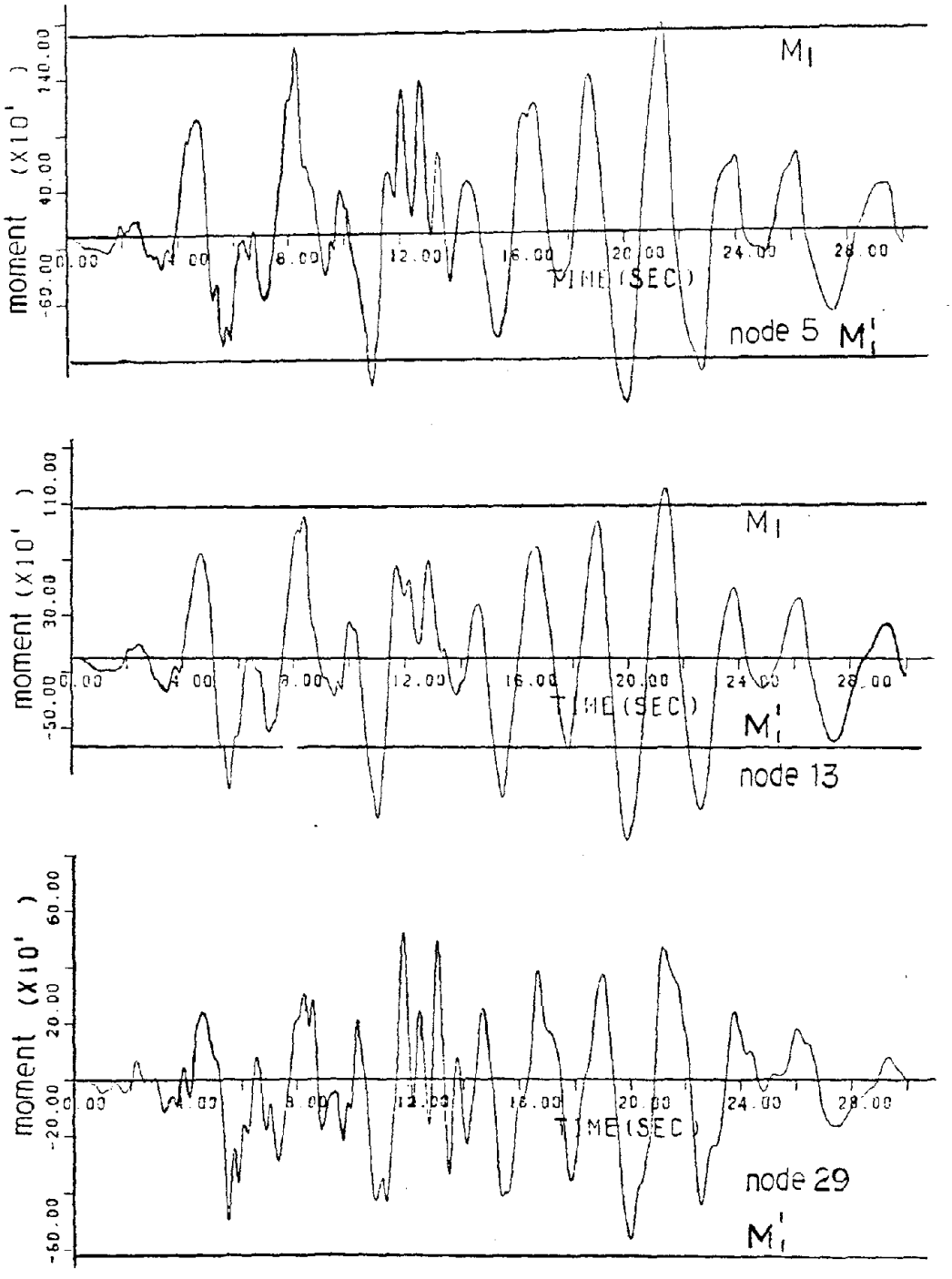

Fig. 516a TYPICAL PREDICTED MOMENTS FOR SLAB-COLUMN CONNECTIONS OF HOLIDAY INN, NODES 5, 13 and 29-EXTERIOR COLUMN TO SLAB BEAM CONNECTIONS

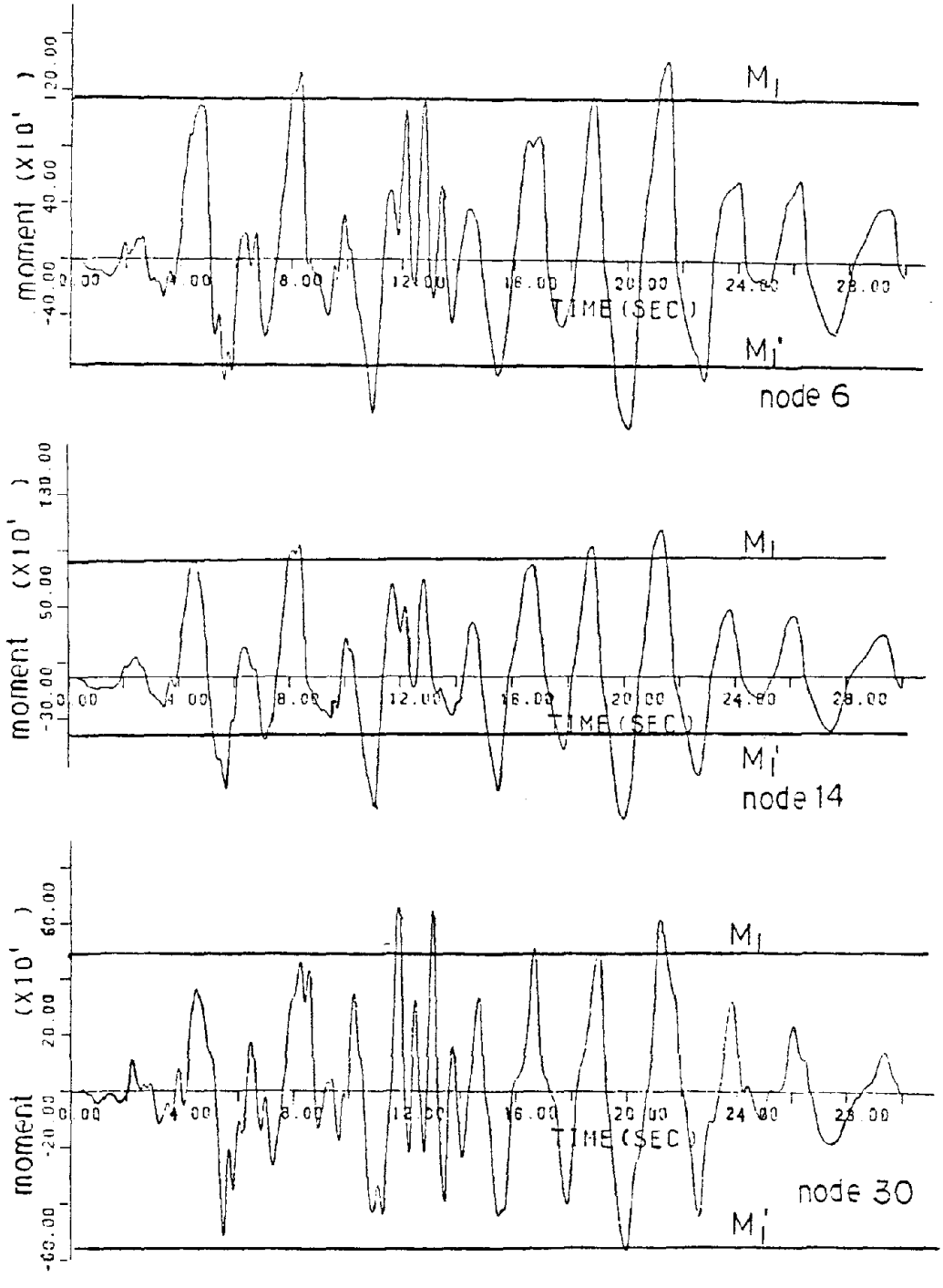

FIG. 5.16b TYPICAL PREDICTED MOMENTS FOR SLAB-COLUMN CONNECTIONS OF HOLIDAY INN, NODES 6, 14 AND 30 (INTERIOR COLUMN TO SLAB CONNECTIONS)

respectively and the stiffnesses change to those associated with the post-yielding response of those connections.

Undoubtedly that yielding is the reason for the lengthening of the fundamental period of the building during the first 6 to 9 seconds of the motion. (Section 5.2.3, Fig. 5.6).

None of the connections in the structure are predicted as developing moments exceeding their M_2 values. Thus, all should have been able to maintain their capacity thorugh the 40 seconds of earthquake shaking. That prediction is consistent with the damage report described in Section 5.2.

In the USGS report (40) on this building a parameteric analysis was made using an SMIS program with consistant stiffnesses and constant natural frequencies and damping ratios. Thus different elastic dynamic models were used to represent pre-and post-yield conditions. The models used gross concrete sectional properties and moduli of elasticity for the concrete of 5.1×10^6 psi for pre-yield and 1.0×10^6 psi for post-yield conditions, respectively. By contrast the procedure described here is an inelastic dynamic analysis procedure that can directly and easily account of the influence on frame behavior of stiffness changes caused by yielding of the slab column connections.

5.4.2 Parameteric Analyses

(1) Influence of the Behavior of Slab-Column Connections

In Section 3.2 it was shown that the properties of the slab have a large influence on the behavior of slab-column connections.

In this section the significance of that influence is checked by examining the effects of such variations on the predicted behavior of the Holiday Inn. In practice that influence would also vary with variations in the ratio of the resistance of the flat plate frames to that of the ductile moment resistant perimeter frames. However, for this comparison the flat plate frame is assumed to be the only lateral load resisting system and so variations in the reinforcing ratio influence only the stiffness of the connections for the flat plate frame.

Shown in Fig. 5.17 are the deformations predicted as a result of changing the M_1 and M_2 values from those listed in Table 5.3 (Case A) to values that are a half, (Case B), and one quarter of those values (Case C). For those changes the slope of the 0-M and M_1-M_2 relationships were kept at their original values. In that figure, it is apparent that the deformations for Case C are the largest and those for Case A, the smallest. The vibration phase for Case C tends to be delayed compared to that for Case A. This result is obvious when it is recognized that the slab-column connections yield earlier for C than case A and therefore the frame becomes more flexible and its natural frequency lower earlier in the shaking than for Case A. However, differences in the total behavior predicted for the frame are not as large as might be expected from the changes in the slab-column connection strengths. This is because the frame is highly indeterminate and yielding of the connections does not occur simultaneously throughout the frame, but one by one at different locations and different times.

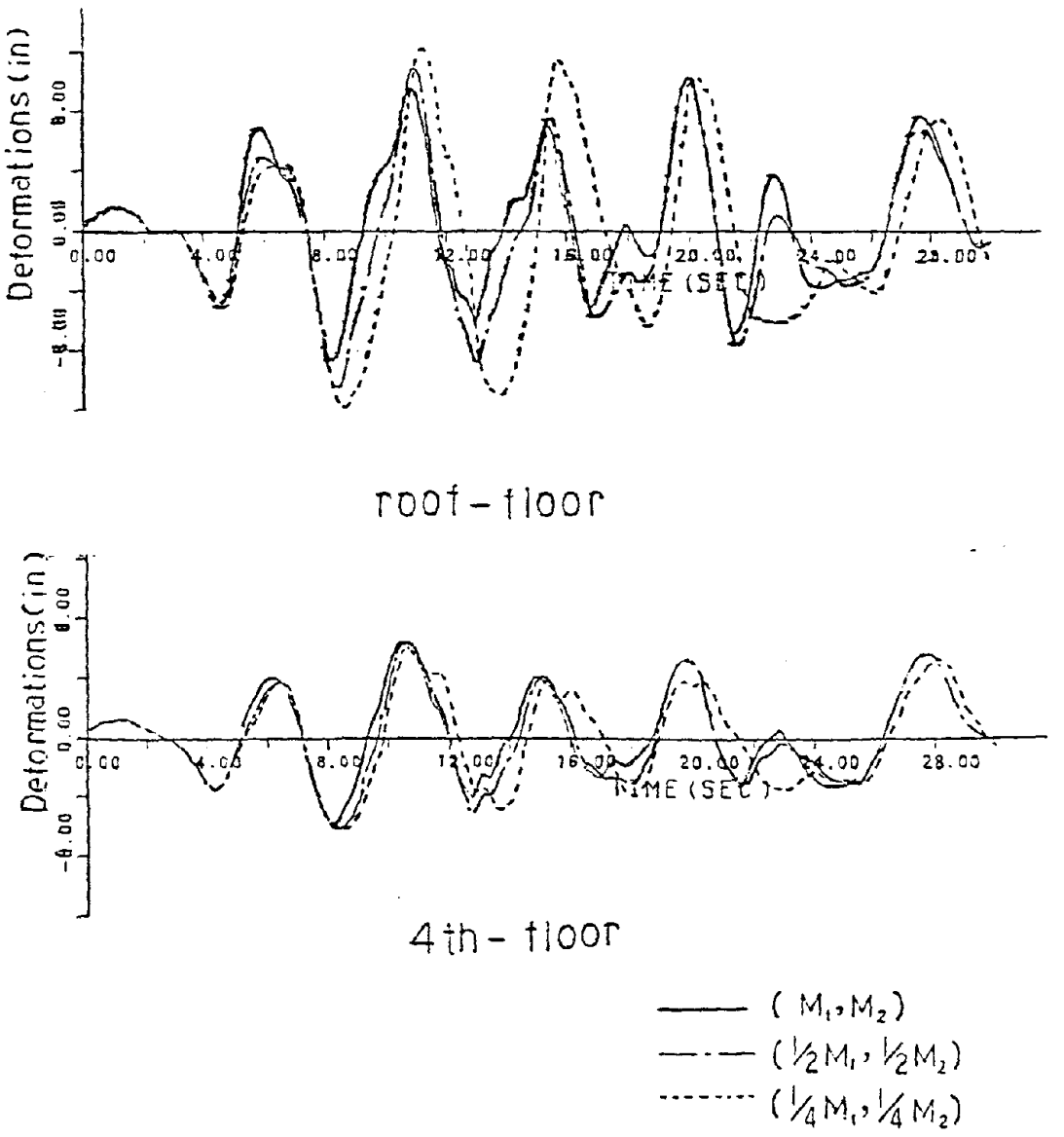

FIG. 5.17 DEFORMATIONS WITH DIFFERENT MOMENT TRANSFER CHARACTERISTICS OF SLAB COLUMN CONNECTIONS

(2) Influence of Damping

The influence of damping was examined by changing the damping ratio in the value for β_o from 2% to 10%. β_o is the coefficient connecting the damping matrix (C) and the stiffness matrix (K) as shown below.

$$(C) = \beta_o (K) \tag{5.15}$$

The changes in the predicted response for the 4th and roof floors are shown in Fig. 5.18. It is clear that the influence of variations in the frequency term is neglibible but that of variations in the ampitude term are significant. That result is consistent with generally accepted principles for the effect of variations in the damping ratio.

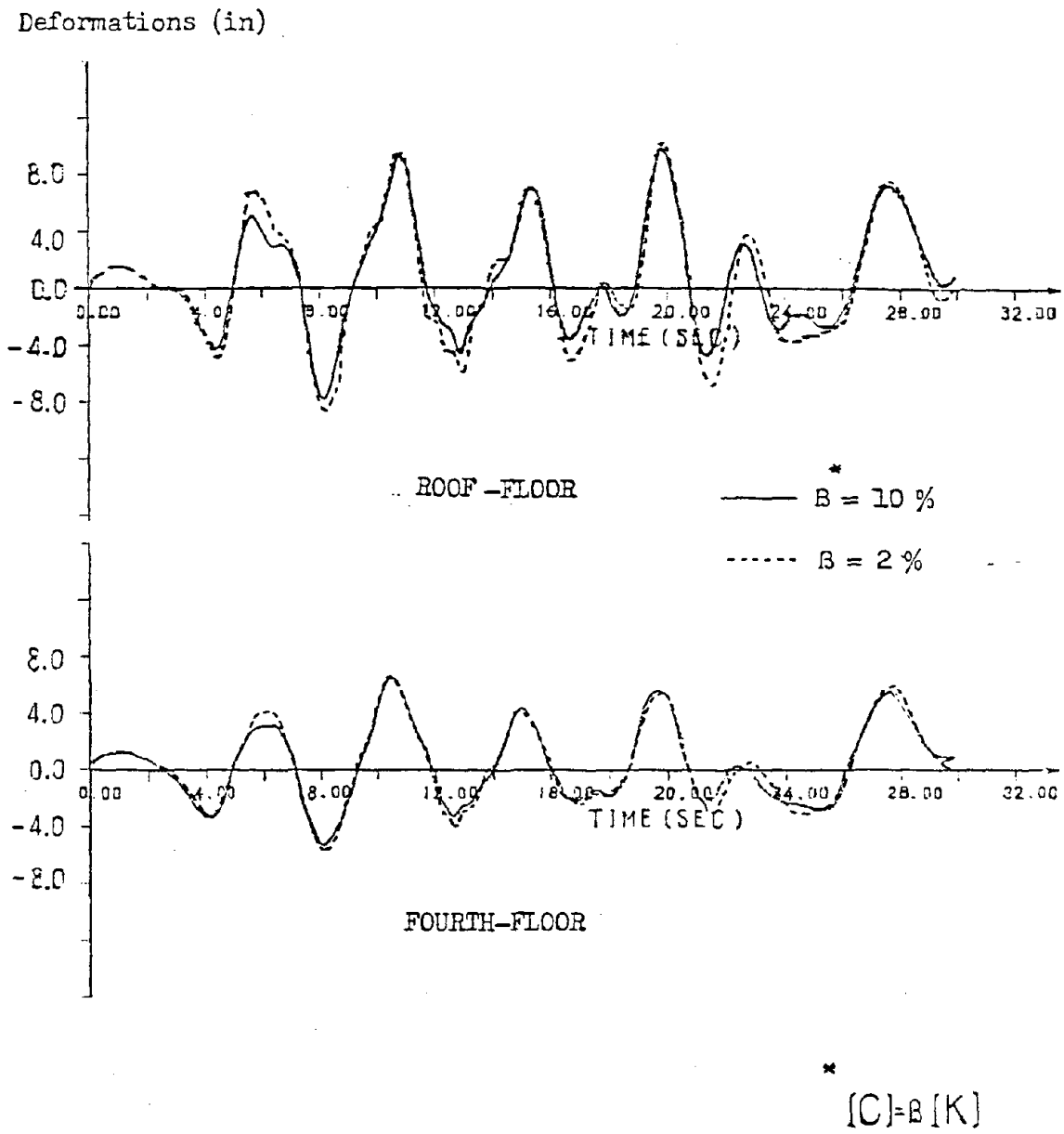

FIG. 5.18 THE INFLUENCE OF DAMPING RATIO ON THE DEFORMATIONS

CHAPTER 6

CONCLUSIONS

From the work reported in this dissertation it is concluded that:

1. The seismic response characteristics of slab-column connections can be accurately predicted by a two-dimensional beam analogy model that contains flexural, torsional, and bond slip elements with stiffness and strength characteristics conforming to those determined from accepted reinforced concrete theory and dimensions defined by local deformations for the slab in the column region. The model reported here contains such elements and can predict the moment-rotation relationships measured in tests to failure on a wide variety of column-slab connections subjected to both monotonic and reversed cyclic loadings.

2. If an analytical model is to accurately predict the seismic response characteristics of slab-column connections, it must recognize that:

    a. The resistance and stiffness of a connection are provided by both flexural and torsional effects. Flexural effects at the front and back faces of the column provide the bulk of the resistance and stiffness initially. However, after those areas yield significant additional resistance but at a reduced stiffness, is provided by torsional effects at the side faces of the column.

b. A connection fails when limiting capacity conditions are developed in the slab next to three adjacent faces of the column. For an interior column connection or an edge column connection transferring moment parallel to the edge, three modes of failure are possible: flexural crushing, torsional crushing and shear punching. In each case the torsional strength at the side face is limited by the strength of the front half of that face. For an exterior column connection transferring moment normal to the edge or a corner column connection, the flexural and torsional crushing modes are similar and the torsional strength at the side face is limited by the strength for the full width of that face.

3. The rotational stiffness and moment transfer capacity of the slab-to-column connections can be increased by concentrating the reinforcing bars for the slab in the column region. However, once the slab reinforcement ratio in that region exceeds about 0.8 percent, further concentration is ineffective in increasing the stiffness.

4. The moments induced at slab-to-column connections by gravity loads have a large influence on the stiffness and the capacity of such connections to absorb lateral loads.

5. The lateral load resistance of flat plate framing is governed primarily by the moment transfer, strength and stiffness characteristics of the slab-to-column connections. The properties of the slab outside the connections have little effect on the lateral load

resistance of flat plate framing. With the connections of a frame modeled using the procedure developed here and gross section properties for the slab and columns for regions remote from the connection regions, lateral load-column top displacement relationships were predicted that were in reasonable agreement with those measured in reversed cyclic loading tests to failure on a full-scale frame that simulated the exterior bay of a flat plate structure.

6. The time history response of a flat plate frame during a severe earthquake, and its seismic resistance, can be predicted with adequate accuracy for design, through use of a Drain-2D program that incorporates beam-analogy models for the connections of the type developed here. With the connections of the structure modeled in that manner, gross section properties used for the slab center-to-center of panels and for the columns, and with time history analysis made using such a Drain-2D program, reasonable agreement was obtained between the predicted and the measured response for the Holiday Inn, Orion Avenue, in the 1971 San Fernando Earthquake.

REFERENCES

1. International Conference of Building Officials. Uniform Building Code, Vol. 1. Whittier, CA. 1983.

2. ASCE-ACI Committee 426. The Shear Strength of Reinforced Concrete Members-Slab. J. of the Struct. Div., ASCE, Vol. 100, No. ST8, August, 1974. pp. 1543-1591.

3. Hanna, S.N., D. Mitchell, and N.M. Hawkins. "Slab-Column Connections Containing Shear Reinforcement and Transferring High Intensity Reversed Moments," Progress Report on NSF Project GI-38717, SM 75-1, Dept. of Civil Engr., University of Washington, Seattle, WA, August, 1975.

4. Hawkins, N.M., D. Mitchell, and M.S. Sheu. "Cyclic Behavior of Six Reinforced Concrete Slab-Column Specimens Transferring Moment and Shear," Progress Report 1973-74 on NSF Project GI-38717, Section II. Dept. of Civil Engr., University of Washington, Seattle, WA, 1974.

5. Symonds, D.W., D. Mitchell, and N.M. Hawkins. "Slab-Column Connections Subjected to High Intensity Shears and Transferring Reversed Moments," Progress Report on NSF Project GI-38717, Dept. of Civil Engr., University of Washington, Seattle, WA, October, 1976.

6. Simpson, E.G., D.W. Symonds, and N.M. Hawkins. "The Effect of Column Properties on the Behavior of Slab-Column Connections Transferring Reversed Moment." Report SM 76-4, Dept. of Civil Engr., University of Washington, Seattle, WA., October, 1976.

7. Chaichanavong, T. "Slab-Edge Column Connections Transferring High Intensity Reversing Moments Parallel to the Edge of the Slab." MSCE Thesis, Dept. of Civil Engr. University of Washington, Seattle, WA, 1979.

8. Hawkins, N.M., C.F. Wong, and C.H. Yang. "Slab-Edge Column Connections Transferring High Intensity Reversing Moments Normal to the Edge of the Slab." Progress Report on NSF Project ENV 72-03585, SM 78-1, Dept. of Civil Engr., University of Washington, Seattle, WA, May, 1978.

9. Yu, S.W. "Reinforced Concrete Slab-Corner Column Connections Transferring High Intensity Cyclic Moments." MSCE Thesis, University of Washington, Seattle, WA, 1979.

10. Hsiang, W.B. "Reversed Cyclic Lateral Loading Resistance of a Flat Plate Exterior Frame." MSCE Thesis, Dept. of Civil Engr., University of Washington, Seattle, WA, January, 1981.

11. Chang, H.J. "Reversed Cyclic Lateral Loading Resistance of a Flat Plate Interior Frame." MSCE Thesis, Dept. of Civil Engr., University of Washington, Seattle, WA, January, 1981.

12. Hawkins, N.M. "Lateral Load Design Considerations for Flat Plate Structures." Study No. 14, Non-linear Design of Concrete Structures, Solid Mechanics Division, University of Waterloo, Waterloo, Canada, 1980.

13. Yamazaki, J. and N.M. Hawkins. "Shear and Moment Transfer Between Reinforced Concrete Flat Plates and Columns," Report SM 75-2, Dept. of Civil Engr. University of Washington, September, 1975.

14. Distasio, J. and M.R. Van Buren. "Transfer of Bending Moment Between Flat Plate Floor and Column." J., ACI, Vol 53, No. 3, September, 1960.

15. Moe, J. "Shearing Strength of Reinforced Concrete Slabs and Footings Under Concentrated Loads." Development Department Bulletin D47, Skokie, IL, Portland Cement Association. April, 1961.

16. Hanson, N.W. and J.M. Hanson "Shear and Moment Transfer between Concrete Slabs and Columns." J. of the Portland Cement Assoc. Research and Devel. Labs, Vol. 10, No. 1. January, 1968.

17. Mast, P.E. "Stresses in Flat Plates Near Column," Journal of American Concrete Institute, Vol. 67, No. 10, October, 1970, pp. 761-768.

18. Long, S.E. "Punching Failure of Reinforced Concrete Slabs," Thesis presented to the Queen's University at Belfast, Northern Ireland, in 1967, in partial fulfillment of the requirements for the degree of Doctor of Philosophy.

19. Hawkins, N.M., D. Mitchell, and M.S. Sheu. "Reversed Cyclic Loading Behavior of Reinforced Concrete Slab-Column Connections." Proceedings, U.S. National Conference on Earthquake Engineering. Ann Arbor, MI. June, 1975. pp. 306-315.

20. Hawkins, N.M., S.N. Hanna, and D. Mitchell. "The Effects of Shear Reinforcement on Reversed Cyclic Loading Behavior of Flat Plate Structures." Canada J. of Civil Engr., December, 1975.

21. Hawkins, N.M., D. Mitchell, and D. Symonds. "Hysteretic Behavior of Slab-Column Connections." Proceedings, Sixth World Conference on Earthquake Engineering, New Delhi, January, 1977.

22. Hawkins, N.M. "Seismic Response Constraints for Slab Systems." Proceedings, Workshop on Earthquake Resistant Reinforced Concrete Building Construction. University of California, Berkeley, July, 1977.

23. Hawkins, N.M. "The Influence of the Slab on the Lateral Load Response of Concrete Buildings," The Profession of a Civil Engineer, Sydney University Press, 1979.

24. Hawkins, N.M. "Shear and Moment Transfer Between Concrete Flat Plates and Columns." Progress Report on NSF Grant No. GK-16375, Dept. of Civil Engr., University of Washington, Seattle, WA., December, 1971.

25. Hawkins, N.M. "Shear Strength of Slabs with Shear Reinforcement," SP-42, Shear in Concrete, American Concrete Institute, Detroit, Michigan. 1974.

26. Hawkins, N.M. "Shear Strength of Slabs with Moments Transferred to Columns." SP-42, Shear in Concrete, American Concrete Institute, Detroit, Michigan, 1977.

27. Park, R. and W.L. Gamble, "Reinforced Concrete Slabs, Sec. 10.3.5. Alternative Beam Analogy Approach for Interior Connections," John Wiley & Sons, New York., 1980.

28. Hawkins, N.M., Hinojosa, R. and Fallsen, H. "Influence of Column Rectangularity on the Shear Strength of Flat Plate Connections." SP-30, Cracking, Deflection and Ultimate Load of Concrete Slab Systems, American Concrete Institute, Detroit, Michigan, 1971.

29. ASCE-ACI Committee 426. Suggested Revisions to Buiding Code Provisions for Shear. ACI Journal, Vol. 74, October, 1977.

30. Kanoh, Y. and S. Yoshizaki. "Strength of Slab-Column Connections Transferring Shear and Moment." ACI Journal, Title No. 76-22, March, 1979.

31. Tsuboi, Y. and M. Kawaguchi. "On Earthquake Resistant Design of Flat Slabs and Concrete Shell Structures." Proceedings of the Second World Conference on Earthquake Engineeirng, Vol. III. 1960, pp. 1693-1703.

32. Park, R. and T. Paulay, "Reinforced Concrete Structures," John Wiley & Sons, pp. 55.

33. Takeda, T., M.A. Sozen, and N.N. Neilson. "Reinforced Concrete Response to Simulated Earthquake," Struc. Div. Journal, ASCE, Vol. 96, No. ST 12, December, 1970.

34. Amin, E. Kawaan and Graham H. Powell. "General Purpose Computer Program for Dyanmic Analysis of Inelastic Plane Structures," Earthquake Engineering Research Center, College of Engineering, University of California, Berkeley, CA, April, 1973.

35. Timoshenko and Goodier. "Theory of Elasticity." Third Edition, McGraw Hill, Torsion of a Bar in Which One Cross-Section Remains Plane, pp. 338-341.

36. Hsu, T.T.C. "Torsion of Structural Concrete-Behavior of Reinforced Concrete Rectangular Members," ACI Publication SP-18. 1968.

37. Lampert, P. "Post-Cracking Stiffness of Reinforced Concrete Beams in Torsion and Bending." SP-35, Analysis of Structural System for Torsion, American Concrete Institute, Detroit, MI. 1973. pp. 385-433.

38. Hawkins, N.M. and Lin, I.J., "Bond Characteristics of Reinforcing Bars for Seismic Loadings," Third Canadian Conference on Earthquake Engineering, Proceedings, Vol. 2, P. 1225-1254.

39. Elias, Z.M. and C. Georgiadis, "STiffness Coefficients and Fixed End Moments for Structural Analysis of Flat Plate Frames." Structures and Mechanics Report SM 78-2, August 1978, Dept. of Civil Engineering, University of Washington, Seattle, WA.

40. USGS Report. "San Fernando Earthquake of 1971." John A. Blune & Associates. Engineers. San Francisco, CA.

41. Hudson, D.E. "Strong Motion Earthquake Accelerograms Index Vol." Earthquake Engineering Research Laboratory Report No. EERL 76-02, California Institute of Technology, 1976.

42. Yamazaki, J. and Hawkins, N.M., "Finite Element Predictions of the Behavior of Slab-Column Connections Transferring Moment," SP-63, Reinforced Concrete Structures Subjected to Wind and Earthquake Forces, American Concrete Institute, Detroit, MI, 1980.

43. Hawkins, N.M., Boa, A. and Yamazaki, J., "Moment Transfer from Concrete Slabs to Columns," paper prepared for submission to ACI as final report on Reinforced Concrete Research Council Project No. 32, Feb. 1985.

44. Hawkins, N.M. and Mitchell, D., "Progressive Collapse in Flat Plate Structures," ACI Journal, Vol. 76, No. 7, July 1979, pp. 775-808.

APPENDIX - A

PREVIOUS RESEARCH

A.1. Previous Experimental Research

A.2. Previous Analytical Research

A.1 Previous Experimental Research

The implications of the experimental data available in 1974 are discussed in Reference (2) and (3) and will not be discussed here. Subsequent to those studies, a series of tests on various column-flat slab subassemblages, as shown in Fig. A.1, have been planned and conducted at the University of Washington.

Tests have been made on:

- Interior column-slab subassemblages (S and SS series), Fig. A.1(f);
- Exterior column-slab subassemblages transferring moments parallel to slab edge (EL and ELS series), Fig. A.1(e);
- Exterior column-slab subassemblages transferring moments normal to the slab edge (E and ES series), Fig. A.1(e);
- Corner column-slab subassemblages (C and CS series), Fig. A.1(d);
- A one-bay frame with one interior and one exterior column, Fig. A.1(c);
- A one-bay frame with two interior columns, Fig. A.1(b).

The results of those tests are reported in References 3 to 6, 7, 8, 9, 10 and 11. Since the Beam Analogy utilized in this dissertation is based on the results of those tests, it is appropriate to review those results here.

A.1.1 Interior Column-Slab Subassemblages

The properties of 20 specimens, described in References 3, 4, 5 and 6 are summarized in Table A.1(a).

Test specimens were intended to represent, to approximately full-scale, the portion of a flat plate structure extending from an interior

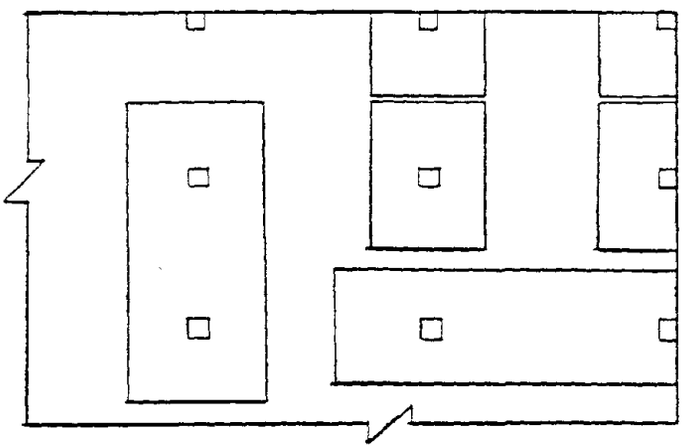

(a) Specimen Locations

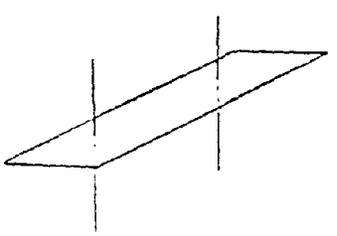

(b) One Bay Frame with Interior Columns

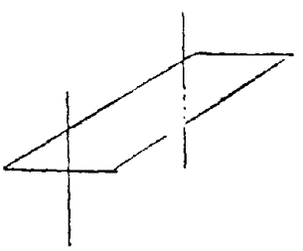

(c) One Bay Frame with Edge and Interior Columns

(d) Corner Columns

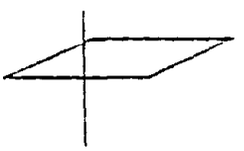

(e) Edge Columns

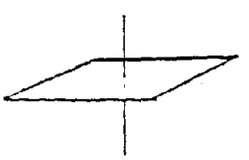

(f) Interior Columns

FIG. A.1 SPECIMENS TESTED AT UNIVERSITY OF WASHINGTON

TABLE A.1(a) PROPERTIES OF TEST SPECIMENS

Interior Connections

Specimen No.	Conc. Strength slab (psi)	Conc. Strength column (psi)	Size slab (in.)	Size column ($c_1 * c_2$) (in.)	Reinforcing Bars top bars #	top bars ρ (%)	top bars fy (Ksi)	bottom bars #	bottom bars ρ (%)	bottom bars fy (Ksi)	shear bars #	shear bars ρ (%)	shear bars fy (Ksi)	Gravity load (kips)
S 1	5050	4600	6	12*12	6	1.29	66.6	4	0.59	66.0	–	–	–	28.8
S 2	3400	3240	6	12*12	5	0.90	67.1	4	0.49	66.0	–	–	–	32.0
S 3	3200	3160	6	12*12	4	0.57	66.0	3	0.40	68.0	–	–	–	31.2
S 4	4690	4760	6	12*12	6	1.29	66.6	4	0.59	66.0	–	–	–	33.7
S 6	3360	3310	6	12*12	6 4	2.00 1.10	66.6 66.0	4 3	0.91 0.56	66.0 68.0	–	–	–	61.0
S 7	3840	3780	6	12*12	5	0.90	67.1	4	0.49	66.0	–	–	–	61.0
S 8	4470	3230	6	12*12	4	0.57	66.0	3	0.40	68.0	–	–	–	53.0
SS 1	4000	3280	6	12*12	6	1.29	66.0	4	0.59	66.0	3	1.5	68.0	28.2
SS 2	3730	3700	6	12*12	5	0.90	67.1	4	0.49	66.0	2	1.5	65.8	29.0
SS 3	3750	3850	6	12*12	6 4	2.00 1.10	66.0	4 3	0.91 0.56	66.0	3	1.5	68.0	28.5
SS 4	4000	4530	6	12*12	6 4	2.00 1.10	66.0	4 3	0.91 0.56	66.0	3	1.5	68.0	28.7
SS 5	4670	2630	6	12*12	5	0.90	67.1	4	0.49	66.0	2	1.5	65.8	28.3
SS 6	3510	3050	6	12*12	5	0.90	67.1	4	0.49	66.0	2	1.5	65.8	61.0
SS 7	3900	3620	6	12*12	6 4	2.00 1.10	66.6 66.0	4 3	0.91 0.56	66.0 68.0	3	1.5	68.0	61.0
SS 8	3470	3600	6	16*16	6 4	1.24	66.0	4 3	0.91	66.0 68.0	3	1.5	68.0	29.8
SS 9	3770	3600	6	16*16	6 4	1.24	66.0	4 3	0.91	66.0 68.0	3	1.5	68.0	61.8
SS 10	3360	4620	6	19.5*8	6 4	1.12	66.0	4 3	0.64	66.0 68.0	3	1.5	68.0	61.8
SS 11	4290	3970	6	19.5*8	6 4	1.12	66.0 65.5	4 3	0.64	65.5 68.0	3	1.5	68.0	29.8
SS 12	3840	4200	6	8*19.5	6 4	1.12	66.0 65.5	4 3	0.64	65.5 68.0	3	1.5	68.0	29.8
SS 13	3960	3770	6	8*19.5	6 4	1.20	61.7 65.3	4 3	0.64	65.3 61.9	3	1.5	61.9	61.8

TABLE A.1(b) PROPERTIES OF TEST SPECIMENS

Exterior connections transferring moment parallel to the edge

Specimen No.	Conc. Strength		Size		Reinforcing Bars									Gravity Load (kips)
					top bars			bottom bars			shear bars			
	slab (psi.)	column (psi.)	slab (in.)	column (in.*in.)	#	ρ (%)	$fy_{(ksi.)}$	#	ρ (%)	$fy_{(ksi.)}$	#	space (in.)	$fy_{(ksi.)}$	
EL 1	4,621	4,000	6.5	12*12	5	0.81	67.1	4	0.40	64.0	-	-	-	16.95
EL 2	3,520	4,000	7.0	16*16	6 4	1.07 0.81	65.0 64.0	4 3	0.49 0.45	64.0 60.5	-	-	-	18.58
ELS 1	3,272	4,000	7.0	12*12	6 4	2.00 0.91	61.7 64.0	4 3	0.98 0.49	64.0 60.5	3	7.5(1)	60.5	19.23
ELS 2	3,688	4,000	7.0	12*12	6 4	2.00 0.91	61.7 64.0	4 3	0.98 0.49	64.0 60.5	3	2.0(2)	60.5	18.17
ELS 3	4,657	4,000	7.0	19.5*8	6 4	1.62 0.84	65.0 64.0	4 3	0.57 0.40	64.0 60.5	3	5.5(1)	60.5	19.12

(1) hairpin stirrups (2) closed stirrups

TABLE A.1(c) PROPERTIES OF TEST SPECIMENS

Edge connection transferring moment normal to the edge

Specimen No.	Conc. Strength		Size		Reinforcing Bars									Gravity Load (kips)
					top bars			bottom bars			shear bars			
	slab (psi.)	column (psi.)	slab (in.)	column (in.*in.)	#	ρ (%)	$fy_{(ksi.)}$	#	ρ (%)	$fy_{(ksi.)}$	#	space (in.)	$fy_{(ksi.)}$	
E 1	3,270	3,060	6.50	12 * 12	5	0.81	67.1	4	0.52	65.3				14.38
E 2	4,280	3,370	7	16 * 16	6 4	1.31 0.87	61.7 65.3	4 3	0.60 0.41	65.3 61.9				18.70
E 3	3,278	3,334	7	19.5*8	6 4	1.56 0.84	64.9 64.3	4 3	0.71 0.40	64.3 60.5				18.50
ES 1	4,080	3,090	7	12 * 12	6 4	1.58 0.91	61.7 69.3	4 3	0.72 0.45	69.3 61.9	3	7.5	61.9	18.70
ES 2	4,200	3,360	7	12 * 12	6 4	1.58 0.91	61.7 69.3	4 3	0.72 0.45	69.3 61.9	3	2	61.9	18.70
ES 3	4,270	3,475	7	12 * 12	6 4	1.58 0.91	61.7 69.3	4 3	0.72 0.45	69.3 61.9	3	7.5	61.9	12.70
ES 4	3,566	3,679	7	19.5*8	6 4	1.56 0.84	64.9 69.3	4 3	0.71 0.40	69.3 60.5	3	2.0	60.5	18.50
ES 5	3,790	3,813	7	8*19.5	6 4	1.62 0.84	64.9 64.3	4 3	0.74 0.40	64.3 60.5	3	7.5	60.5	18.20

TABLE A.1(d) PROPERTIES OF TEST SPECIMENS

Corner connection

Specimen No.	Conc. Strength		Size		Reinforcing Bars									Gravity Load (kips)
	slab (psi.)	column (psi.)	slab (in.)	column (in.*in.)	top bars			bottom bars			shear bars			
					#	ρ(%)	f_y (ksi)	#	ρ(%)	f_y (ksi)	#	space (")	f_y (ksi)	
C 1	5,750	2,875	6.5	12 * 12	5	0.83	67.1	4	0.53	64.3	-	-	-	7.48
C 2	3,430	3,750	6.5	12 * 12	5	0.83	67.1	4	0.53	64.3	-	-	-	7.48
C 3	4,100	5,070	7.0	16 * 16	6 4	1.25 0.89	64.9 64.3	4 3	0.56 0.45	64.3 60.5	-	-	-	7.81
CS 1	3,725	4,100	7.0	12 * 12	6 4	1.25 0.93	66.0 67.5	4 3	0.56 0.45	67.5 60.5	3	7.5	60.5	7.65
CS 2	4,060	4,280	7.0	19.5*8	6 4	1.50 0.85	66.0 67.5	4 3	0.68 0.41	67.5 60.5	3	6.5	60.5	7.65

TABLE A.1(e) PROPERTIES OF TEST SPECIMENS

A one-bay frame with one interior and one exterior column

Over-all dimension of the specimen ft.(m), in.(mm)	28 ft.(8.53m) long, 7 ft.(2.13m) wide, 7 in.(178mm) thick slab; two 1 ft.(305mm) square column extended 3.5 ft. (1.07m) above and below the slab.		
	West Portion	Closure Strips	East Portion
	with an exterior column at the discontinuous edge; ρ_c=2.05%		with an overhanging slab and an interior column
Length, ft.(m)	11.5(3.51)	3(0.91)	13.5(4.11)
Concrete Strength; Top Column Psi (MPa)	3364(23.20) 5066(34.94)	3370(23.24)	3289(22.68) 4786(33.01)
Top Bars: Number; Size; Spacing, in.(mm); Percent; Yield Strength Ksi(MPa).	4#4 for central region and 4#4 at 14 in.(356mm) centers for outside region. pave.=0.32% pave.col.region=0.38% #4-68.25 ksi (470.6 MPa)	same as west portion	2#5 and 2#4 for central region and 6#4 for outside region pave.=0.44% pave.col.region=0.57% #5-67.1 ksi (462.7 MPa)
Bottom Bars: Number; Size; Spacing, in.(mm); Percent; Yield Strength Ksi(MPa).	4#4 for central region, 6#3 at 9 in.(229mm) centers for outside region	same as west portion	2#4 and 2#3 for central region, 6#3 at 9 in. (229mm) centers for outside region

TABLE A.1(f) PROPERTIES OF TEST SPECIMENS

A one-bay frame with two interior columns

Slab Size	25 ft.(7.62 m) long, 6 ft.(1.83 m) wide
Column Size: $c_1 \times c_2$	13" × 6" (330 × 152 mm)
Slab Thickness	4.5" (114 mm)
Concrete Strength	4340 psi (29.92 MPa) for east part 4200 psi (28.96 MPa) for west part 4640 psi (31.99 MPa) for connection
Top Bars: Number; Size; Spacing; Percent; Yield Strength	6 No.4 at 3" (76 mm) for central 15.5" (476 mm); 10 No.4 at 5.25" (133 mm) for outside region; ρ_{avg} = 1.23%; No.4-67.5 ksi (465.4 MPa)
Bottom Bars: Number; Size; Spacing; Percent; Yield Strength	2 No.3 at 3.5" (89 mm) through the column; 10 No.3 at 6.25" (159 mm) for outside region; ρ_{avg} = 0.51%; No.3-60.5 ksi (417.1 MPa)
Load History	3 cycles each @ 0.23" to -0.23" (6 to -6 mm) 0.67" to -0.89" (17 to -23 mm) 1.25" to -1.20" (32 to -30 mm) 1.75" to -1.80" (44 to -46 mm) 2.57" to -2.61" (65 to -66 mm) 1 cycle @ 4.20" to -4.25" (107 to -108 mm) Half cycles each @ 2.59" to 0.87" (66 to 22 mm) 2.58" to 0.96" (66 to 24 mm)
Gravity Shear	32.50 kips (144.6 kN)
Shear Reinforcement East Column Connection Only - No Shear Reinforcement-West Column Connection	No.2 stirrups with 65.8 ksi (453.7 MPa) yield strength at 1.75" (44 mm) spacing to 14.875" (378 mm) from each column face
Comments	East column connection - Yield @ δ=0.67"(17 mm) in the first cycle of the second loading sequence; slight punching shear failure around column after 5 loading sequences. West column connection - Punching shear failure around column after 3 loading sequences.

column out to the likely region of contraflexure in the slab for a moderate earthquake and between points of contraflexure in the column.

The prototype structure assumed for development of the test specimen is shown in Fig. A.2. The structure was five stories high with columns at 20 ft. centers. For that column spacing ACI 318-71 regulations required a slab at least 6 inches (152 mm) thick and a column at least 12 inches (305 mm) square.

The dimensions for all specimens except SS-8 - SS-13 are shown in Fig. A.3(a). The slab was made 7 ft. (2.13 m) wide in one direction and 13 ft. (3.96 m) long in the other direction. The loads causing effects representing the gravity forces were applied at four points, A in Fig. A.3(a), located at equal intervals around the perimeter of a circle of approximately 3 ft. (0.91 m) radius centered on the column. The loads causing effects representing the seismic forces were applied at points B extending across the 7 ft. (2.13 m) width of the specimen on a line 6 ft. (1.82 m) from the column.

In Ref. (4) details are given of tests to destruction on four specimens without shear reinforcement (S-1, S-2, S-3, S-4) and two specimens with shear reinforcement (SS-1, SS-2). Hanna (3) tested another three specimens with shear reinforcement (SS-3, SS-4, SS-5) which he reported along with a review of SS-1 and SS-2. Symonds (5) tested five specimens subjected to high gravity loads and relatively low lateral loads (S-6, S-7, S-8 and SS-6, SS-7). Simpson (6) tested six specimens changing the proportions and aspect ratio for the column (SS-8 to SS-13). In all these tests, the influences of the percentage

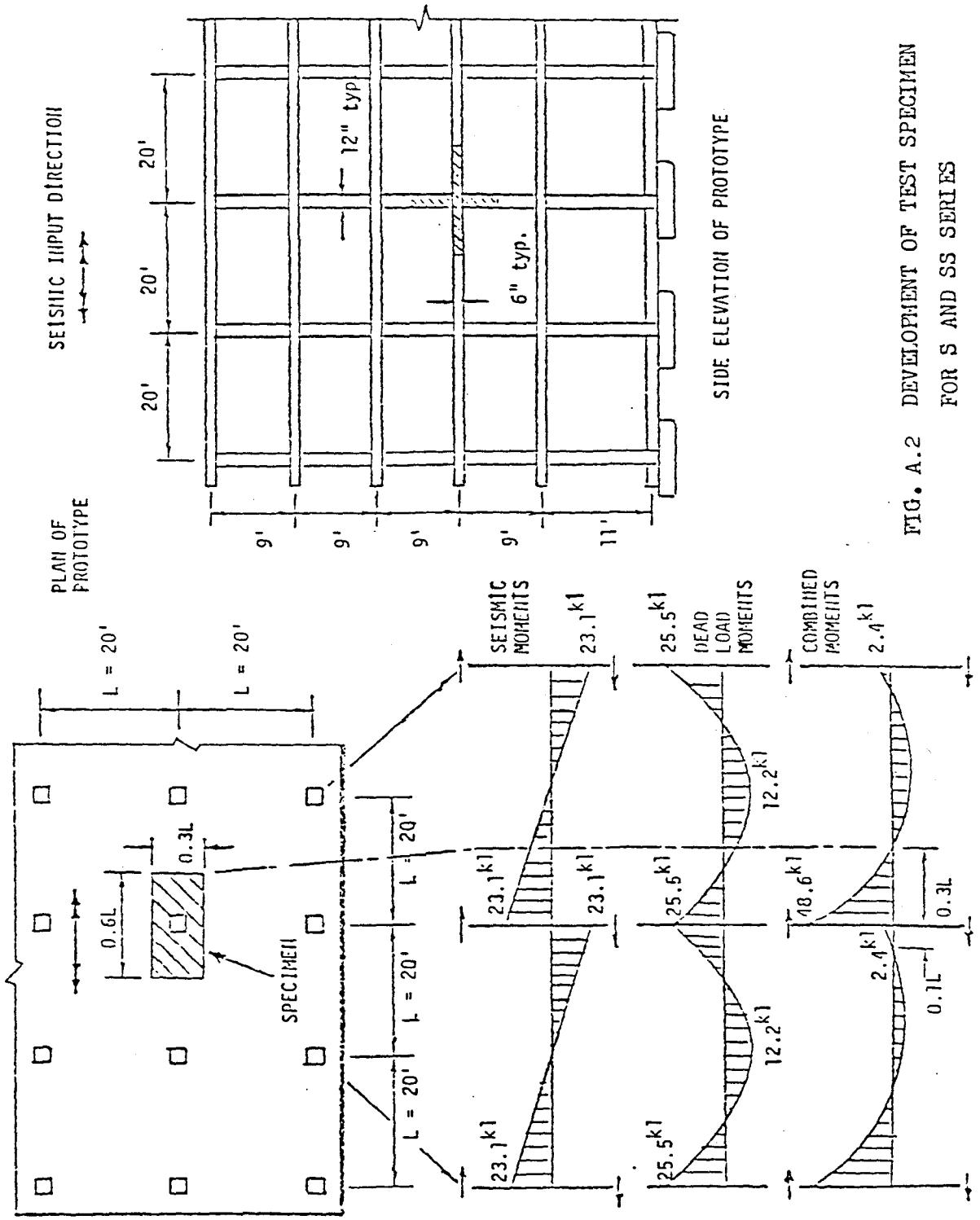

FIG. A.2 DEVELOPMENT OF TEST SPECIMEN FOR S AND SS SERIES

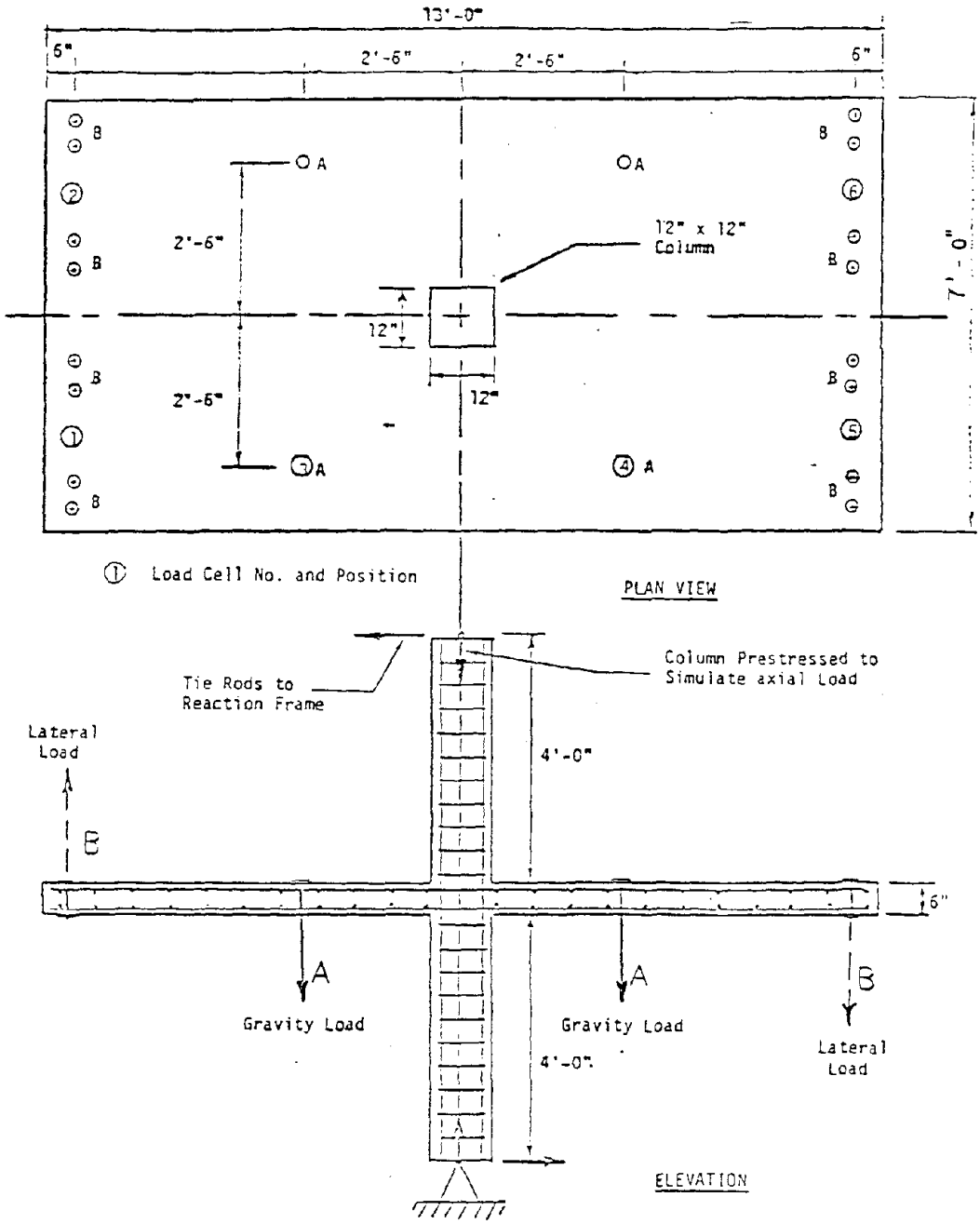

(a) INTERIOR COLUMN CONNECTION

FIG. A.3 SCHEMATIC DIAGRAM OF TEST RIG

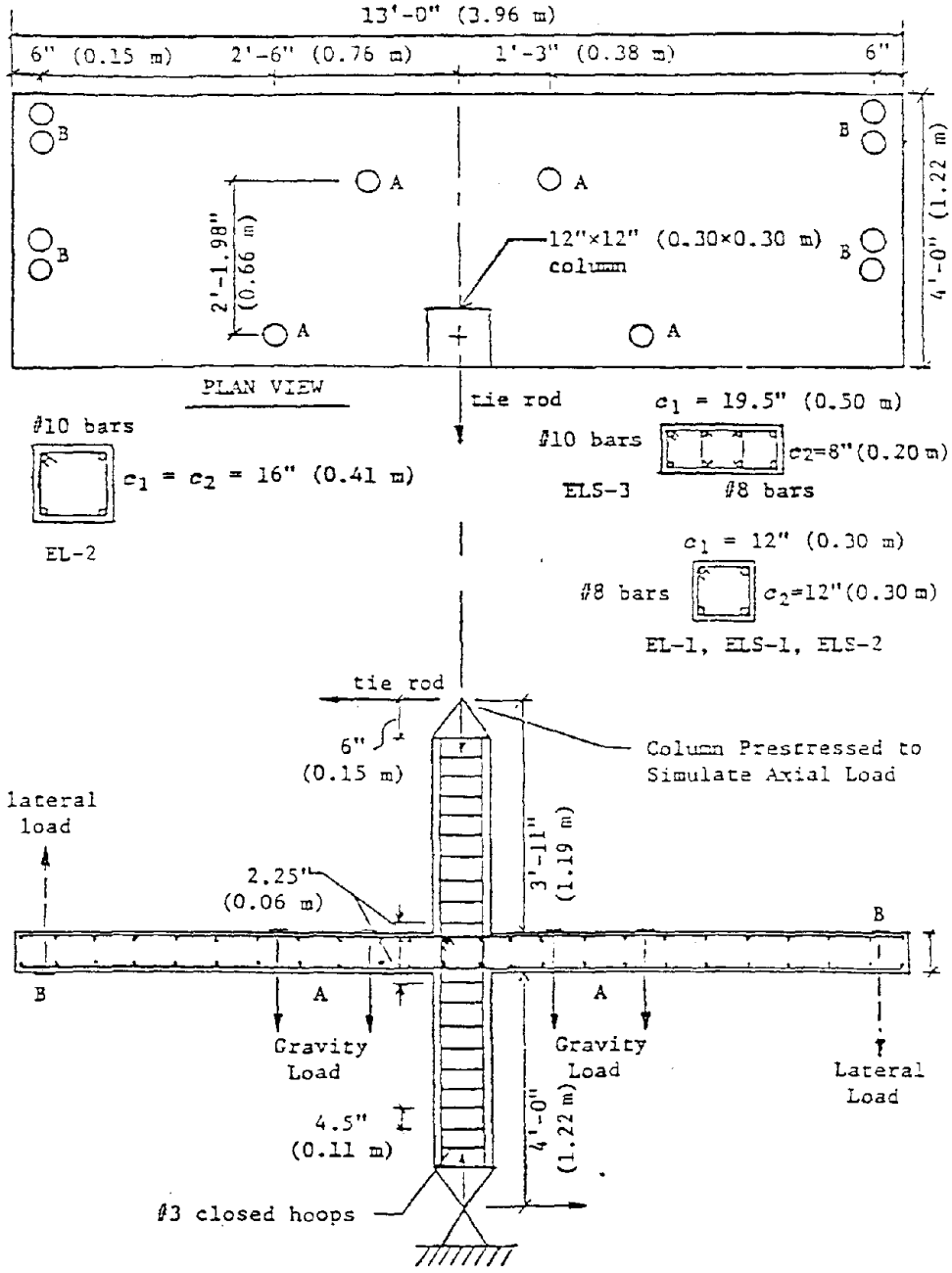

(b) EDGE COLUMN CONNECTION
MOMENT TRANSFER PARALLEL TO EDGE

FIG. A.3 SCHEMATIC DIAGRAM OF TEST RIG

Reproduced from
best available copy.

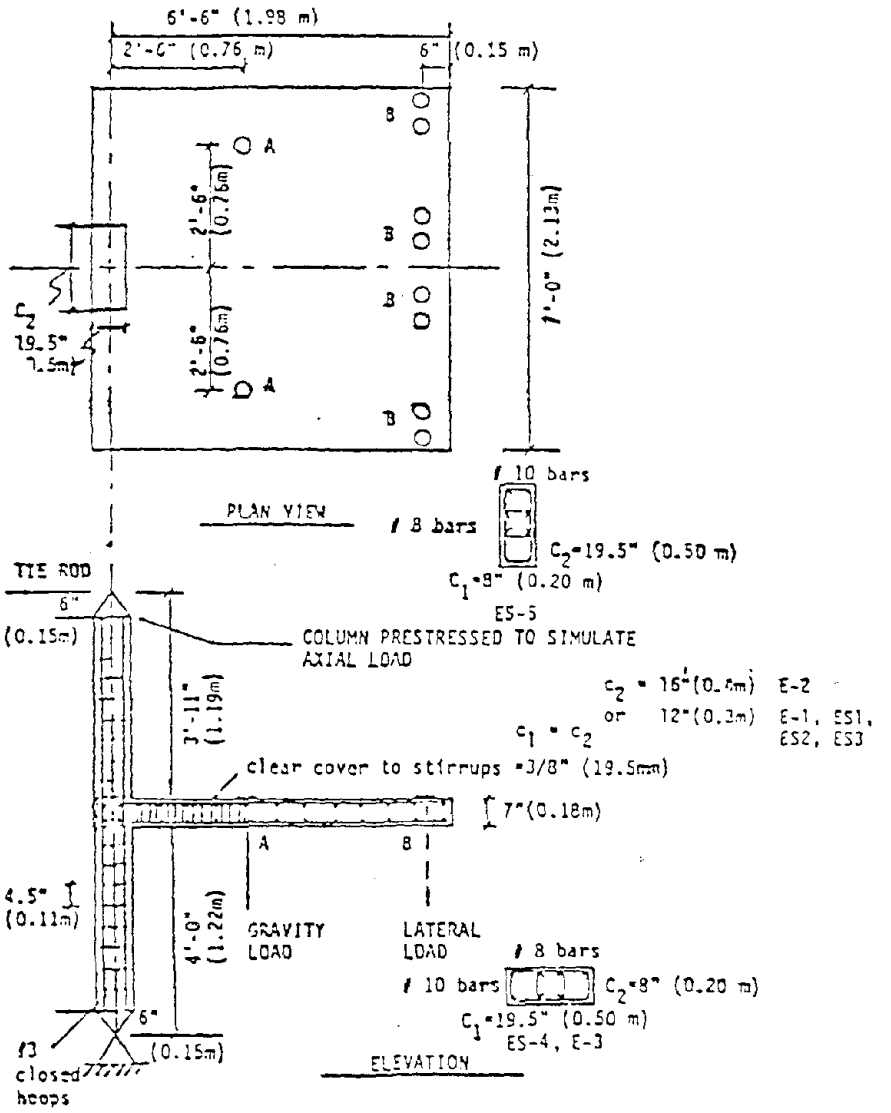

(c) EDGE COLUMN CONNECTION MOMENT TRANSFER NORMAL TO EDGE

FIG. A.3 SCHEMATIC DIAGRAM OF TEST RIG

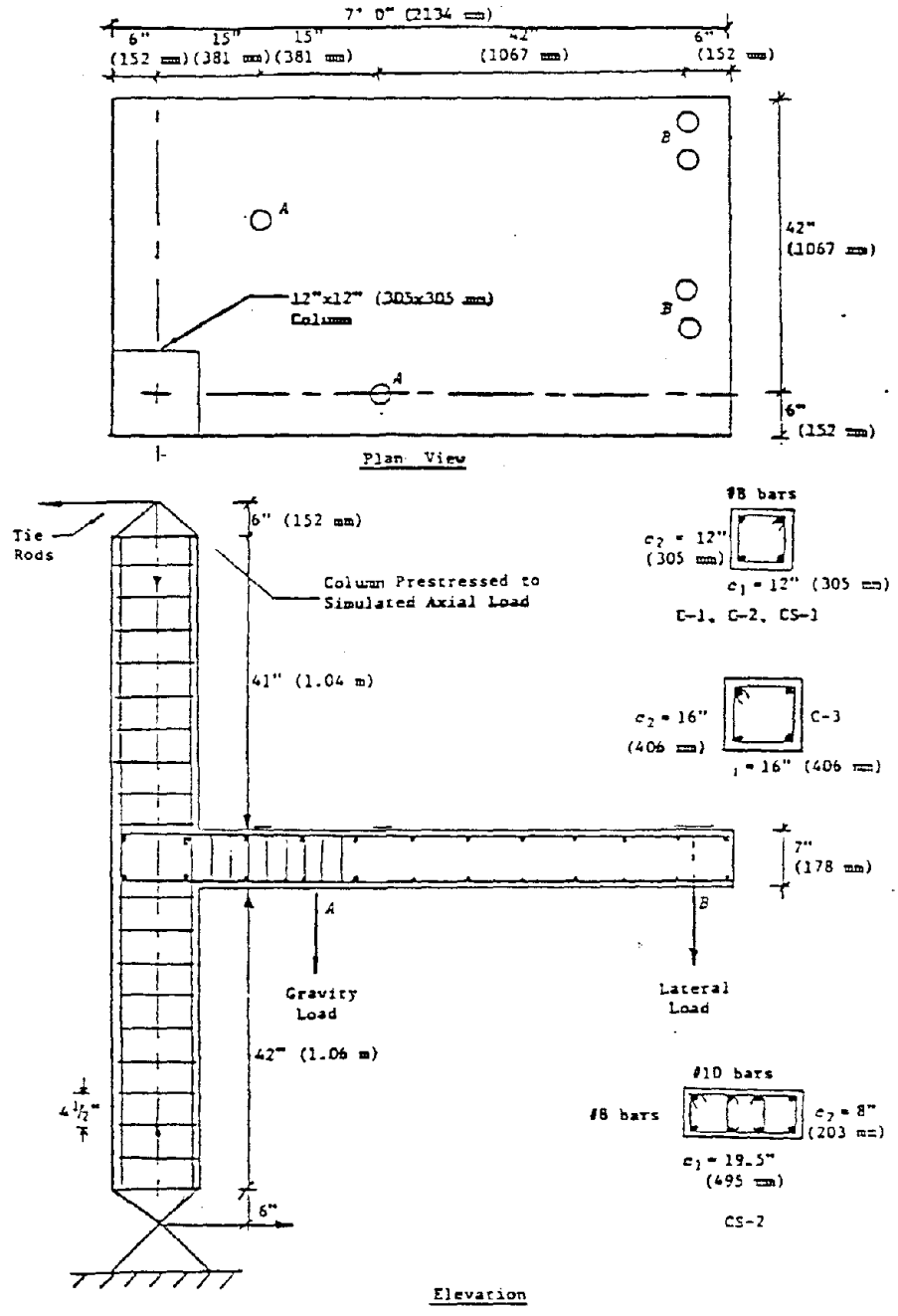

(d) CORNER COLUMN CONNECTION

FIG. A.3 SCHEMATIC DIAGRAM OF TEST RIG

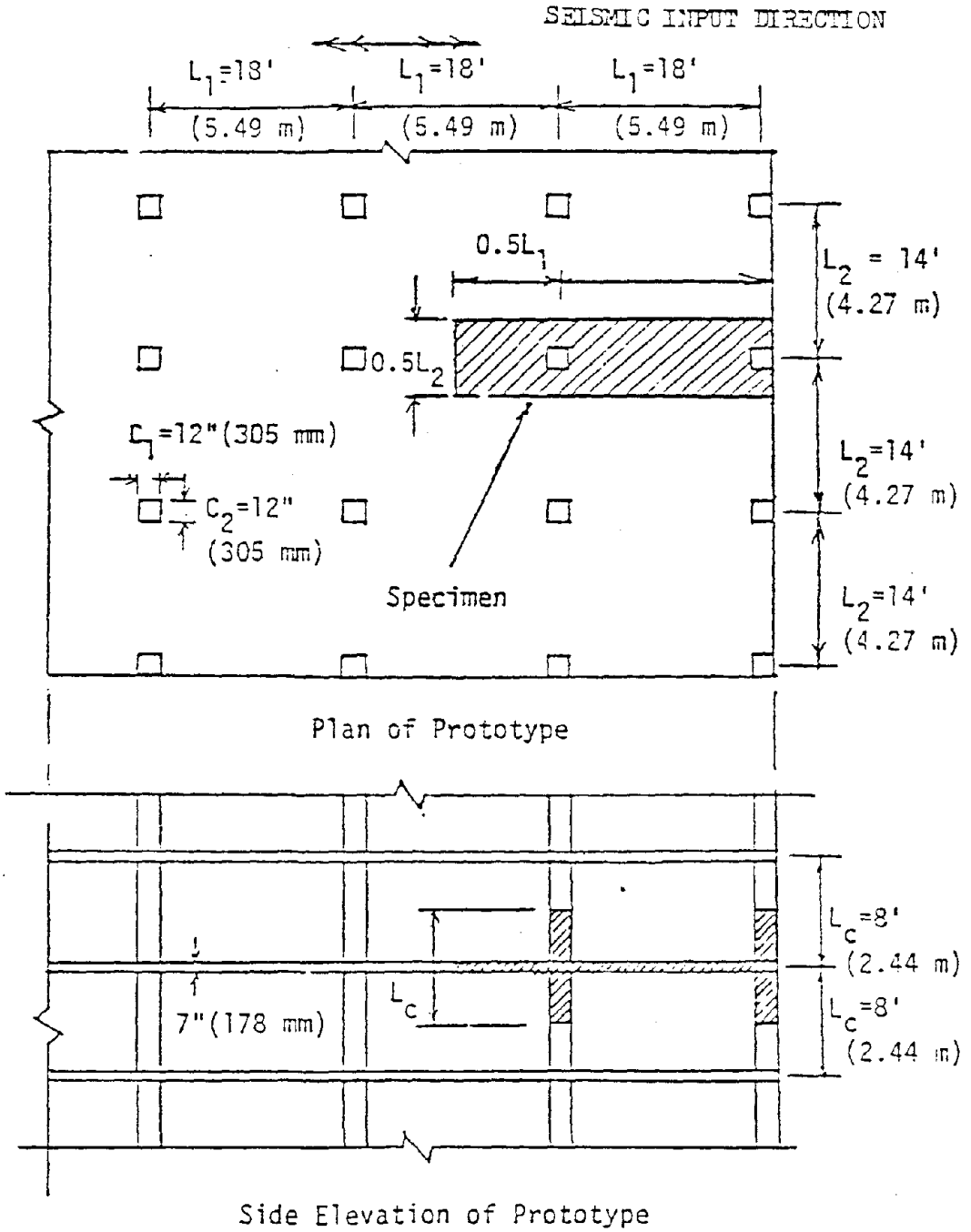

FIG. A.3(e) DEVELOPMENT OF THE TEST SPECIMEN FOR EXTERIOR FRAME
(One-bay Frame with One Interior and One Exterior Column)

Reproduced from best available copy.

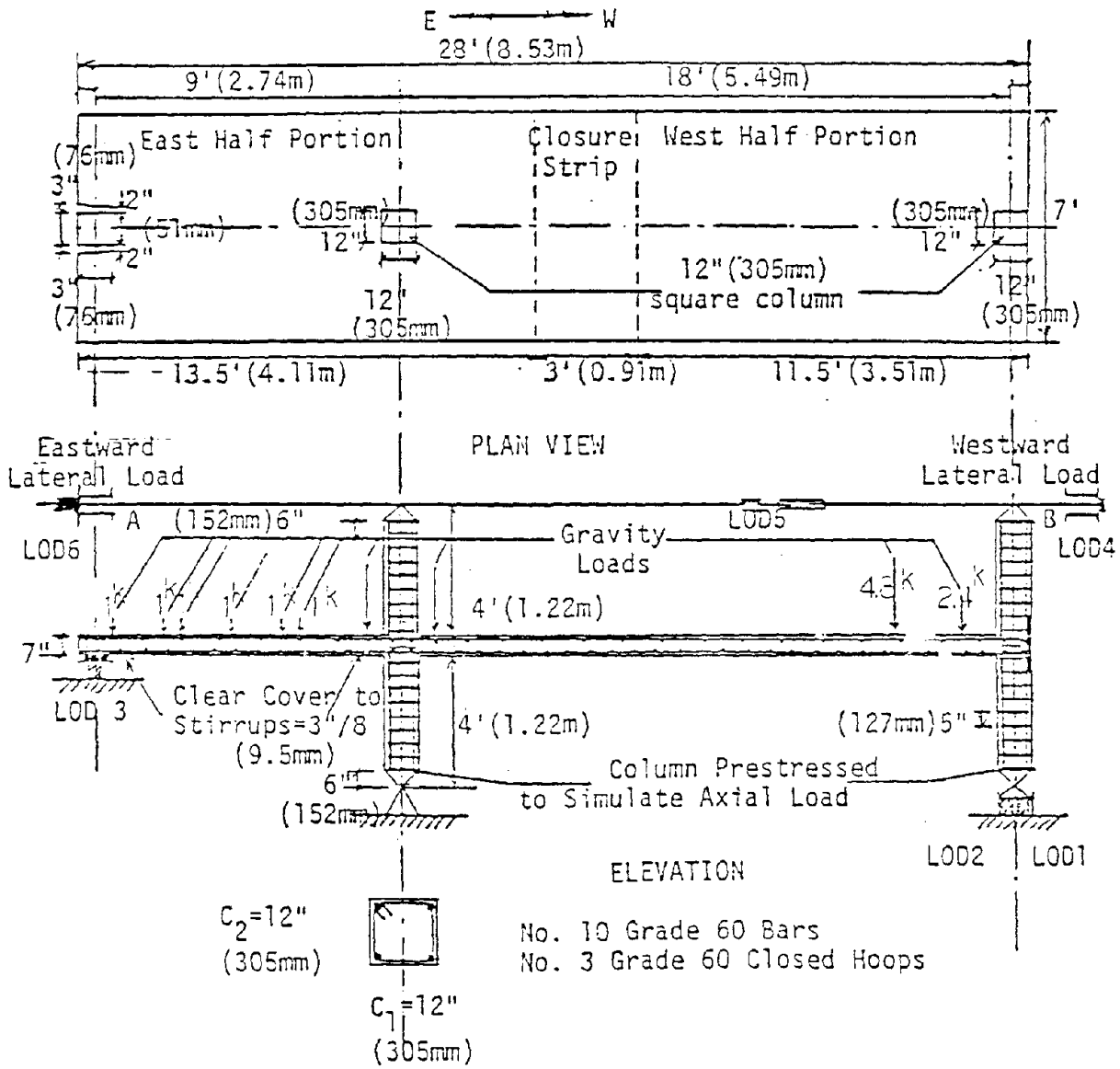

FIG. A.3(f) SCHEMATIC DIAGRAM OF TEST RIG FOR EXTERIOR FRAME

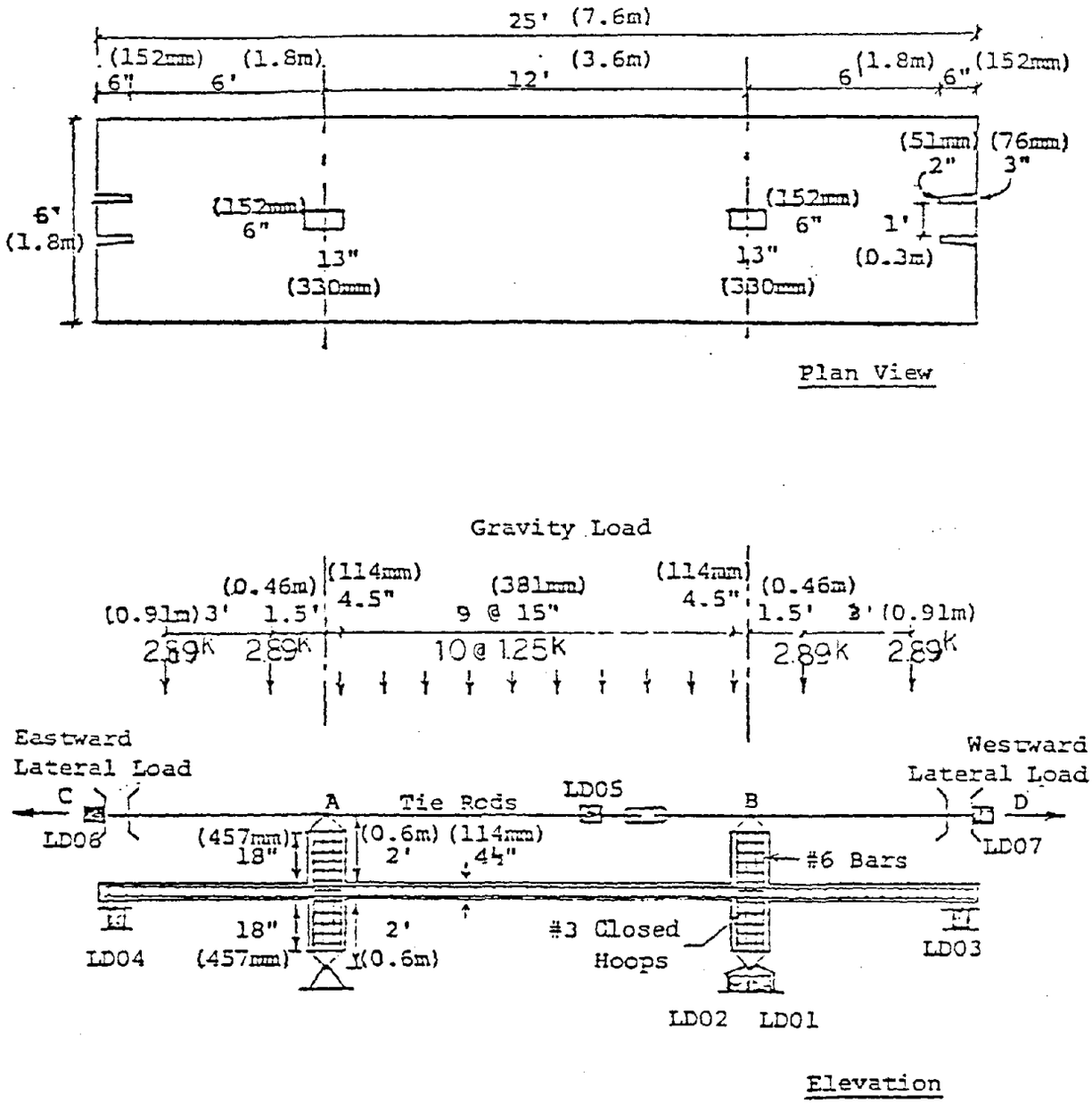

FIG. A.3(g) SCHEMATIC DIAGRAM OF TEST RIG, INTERIOR FRAME
(A One-bay Frame with Two Interior Columns)

of reinforcement as well as its distribution, the concrete strength and the loading history were studied.

A.1.2 Exterior Column-Slab Subassemblages Transferring Moment Parallel to the Edge

Thanu Chaichanavong (7) tested five specimens with two specimens without shear reinforcement (EL-1, EL-2) and three specimens with shear reinforcement (ELS-1, ELS-2, ELS-3). General properties and proportions for those test specimens are listed in Table A.1(b) and in Fig. A.3(b), respectively. In those tests, the influence of shape and size of columns was studied, in addition to the effects of loading history and reinforcement amount and distribution.

A.1.3 Exterior Column-Slab Subassemblages Transferring Moment Normal to the Edge

Wong and Yang (8) tested eight specimens, three specimens without shear reinforcement (E-1, E-2, E-3) and five specimens with shear reinforcement (ES-1, ES-2, ES-3, ES-4, ES-5). The properties of those specimens are shown in Table A.1(c) and their proportions in Fig. A.3(c).

A.1.4 Corner Column-Slab Subassemblages

Yu (9) tested five specimens. Three were without shear reinforcement (C-1, C-2, C-3) and two were with shear reinforcement (CS-1, CS-2). The proportions for the specimens are shown in Fig. A.3(d) and the properties in Table A.1(d).

A.1.5 One-Bay Frame with Interior and Exterior Columns

Hsiang (10) tested a specimen representing to full scale an exterior one-bay frame with one interior and one exterior column. The general proportions for the prototype frame and the test specimen are shown in Figs. A.3(e) and (f), and the properties in Table A.1(e).

A.1.6 One-Bay Frame with Two Interior Columns

Chang (11) tested a specimen representing to half scale a typical interior bay of a flat plate structure. The frame contained two interior columns and the slab extended out from each interior column to its likely limits of contraflexure in the slab for a severe earthquake loading. The proportions for the specimen are shown in Fig. A.3(g), and the properties in Table A.1(f).

A.2 Previous Analytical Research

The state of knowledge on the strength of column-slab connections transferring moments, that increase monotonically to failure, has been summarized by ACI-ASCE Committee 426 (2). More recently, knowledge for similar connections reversed cyclically loaded to failure has been summarized by Hawkins (12).

Available methods for predicting the ultimate strength of such connections can be divided into three groups:

1. Analyses based on a linear variation in shear stress,
2. Analyses based on thin plate theory, and
3. Beam Analogies.

The linear shear stress method is specified by the ACI Code 318-77 and

Commentary. The applicability of thin plate analysis has been examined in depth by Yamazaki and Hawkins (13). Of the three methods, the Beam Analogy method is of particular interest for this investigation and is discussed in detail in Chapter 2.

For comparison, a summary of the essential features of the three methods is presented here.

Much less research has been done on defining the stiffness of connections transferring moment than on defining their strength. Available information is limited to either elastic definitions of stiffness or the beam type model developed by Hawkins (5) and (8).

A.2.1 Strength of Column-Slab Connections

A.2.1.1 Linear Variation in Shear Stress Methods

The ACI Code 318 and Commentary specify the use of a linear variation in shear stress approach for predicting the limiting shear capacity of connections transferring moment. That type of procedure was first proposed as a working stress method by Di Stasio and Van Buren (14) in 1960. Fig. A.4 shows the model proposed by them. They divided the resisting mechanism of the connection into two parts. As shown in Fig. A.4(a), one part was a symmetric shear field that resisted the shear force applied by the gravity load. The other part was an unsymmetric shear field, Fig. A.4(b), which resisted the shear and bending moment caused by unbalanced gravity load and lateral live load. Their approach was subsequently utilized by Moe (15), and Hanson and Hanson (16). Their procedure was first incorporated into the ACI Building Code in 1963 and carried over essentially unchanged into ACI Codes 318-71, 318-77, and 318-83.

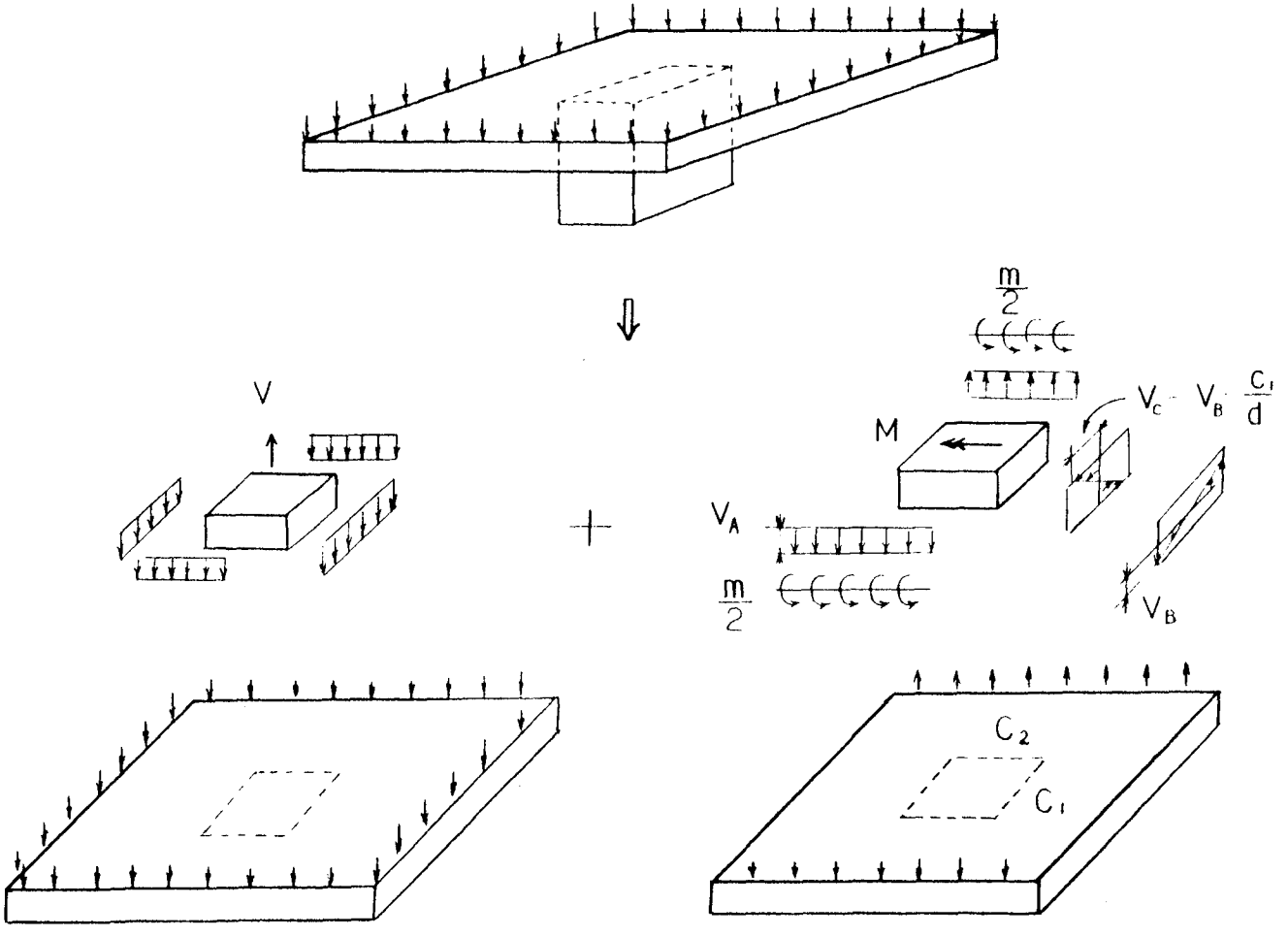

(a) symmetric shear field

(b) unsymmetric field

FIG. A.4 MODEL OF LINEAR VARIATION IN SHEAR STRESS BY DI STATIO AND VAN BUREN

For an interior slab-to-column connection, as shown in Fig. A.5, it is presumed that shear stresses on a critical perimeter located d/2 from the column perimeter vary linearly with distance from the centroidal axis of that perimeter.

ACI Code 318-83 specifies that the fraction, γ_v, of the total moment, M_T transferred by shear across the critical perimeter, be taken as:

$$\gamma_v = 1 - \frac{1}{1 + \frac{2}{3}\sqrt{\frac{c_1 + d}{c_2 + d}}} \tag{A.1}$$

The remaining fraction of the unbalanced moment $(1 - \gamma_v)\ M_T$, must be transferred by reinforcement within lines one and one-half times the slab thickness, 3h/2, either side of the column. For ACI Code 318-83 the maximum value of the shear stress is limited to

$$v_c = (2 + 4/\beta_c)\ \sqrt{f'_c}\ \text{psi} \tag{A.2}$$

but not greater than $4\sqrt{f'_c}$ psi $(0.33\sqrt{f'}\text{cMPa})$. β_c is the ratio of the long side to short side of a rectangular column.

Shown in Fig. A.6 are the moment-shear interaction relationships predicted by the ACI Code procedure for an interior column connection. Ordinates, V_u/V_o, are ratios of the direct shear transferred to the column to the capacity for shear transfer only. Abscissas, $\gamma_v M_T/M_o$, are ratios of the moment transferred by shear to the same capacity for moment transfer only. Line ab on Fig. A.6 represents the condition for which the maximum shear stress is limited to v_c. Diagrams on Fig. A.6 indicate idealized shear stress distributions for different points

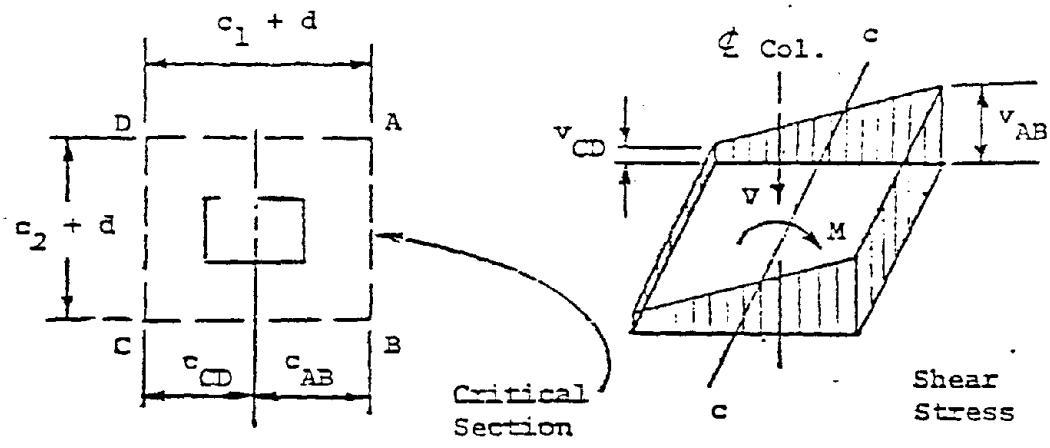

Interior Column

Critical Section Properties for ACI Code Procedure

$$A_c = 2d(c_1 + c_2 + 2d) \; ; \quad c_{AB} = c_{CD} = (c_1 + d)/2$$

$$J_c = \frac{d(c_1 + d)^3}{2} + \frac{(c_1 + d)d^3}{2} + \frac{d(c_2 + d)(c_1 + d)^2}{2}$$

$$v_{AB} = \frac{V}{Ac} + \frac{\gamma_v M \; c_{AB}}{J_c}$$

$$v_{CD} = \frac{V}{Ac} + \frac{\gamma_v M \; c_{CD}}{Jc}$$

FIG. A.5 LINEAR STRESS METHOD OF ANALYSIS

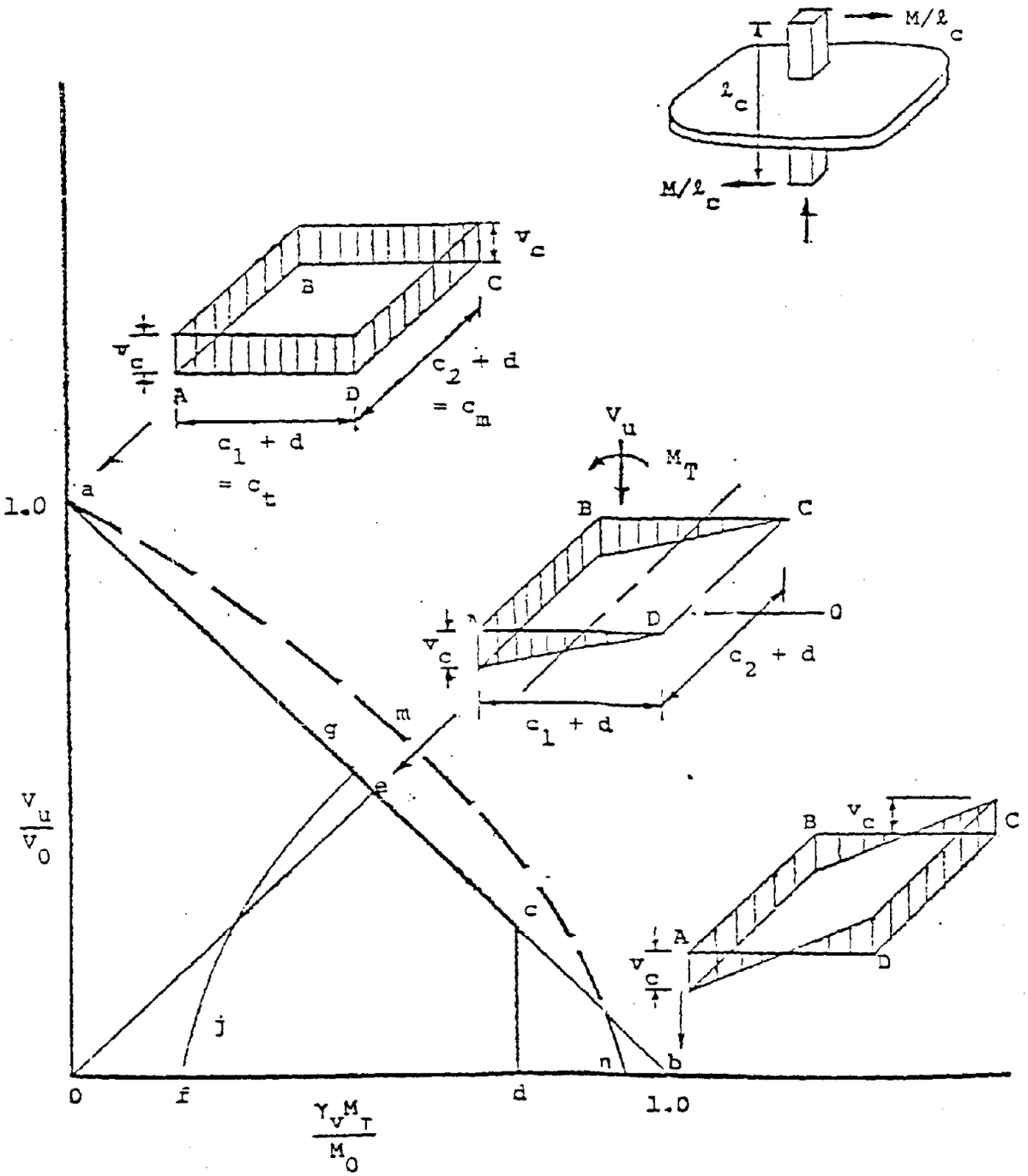

FIG. A.6 MOMENT-SHEAR INTERACTION RELATIONSHIPS FOR INTERIOR COLUMN CONNECTION

along line ab. Line cd represents the possible limitation imposed by the flexural reinforcement which must transfer the moment $(1 - \gamma_v) M_T$ not transferred by shear stress. Only reinforcement within lines one and one-half times the slab thickness, 1.5h, either side of the column is effective. That limitation on the moment can be expressed approximately as:

$$(1 - \gamma_v)M_T = (c_2 + 3h)d^2 f_y \{\rho(1 - 0.6 \frac{pf_y}{f'_c}) + \rho'(1 - 0.6\frac{pf_y}{f'_c}\} \quad (A.3)$$

where ρ, ρ' are the top and bottom reinforcement ratios for the width $(c_2 + 3h)$. The geometric properties for the connection and the concrete strength are the factors dictating the position of the line ab in Fig. A.6. The amount of reinforcement within the column region affects only the position of line cd. Test results shown in Reference (2) indicate a behavior not far from that idealization. Measured strengths lie along curves such as amn. For 3,000 psi (20.68 MPa) concrete, that curve lies progressively further outside the envelope acd as the reinforcement ratio within lines 1.5h either side of the column increases above 0.8%. The reverse is true as the ratio decreases below 0.8%.

A.2.1.2 Thin Plate Methods

Methods of analysis based on elastic thin plate theory have been proposed by Mast et al. (17), 18) and (13). While such approaches assume linear behavior, they allow also consideration of the effects of dimensions and boundary conditions for the plate as well as differing aspect ratios for the column. Mast found that, in con-

trast, to the assumptions inherent in the ACI Code 318-71 formulation, the relative participation of the torsional, flexural and shear stresses to moment transfer varied with the shape and size of the column and the dimensions and boundary conditions for the plate.

In his study, Yamazaki (13) used an incremental procedure to extend finite element plate bending analyses into the inelastic range. He concluded that capacities of slab-column connections transferring moment could not be determined by extrapolating results predicted by elastic finite element analyses, because in the inelastic range there is considerable redistribution of moments and shears between the column faces as the stiffness of each face changes with loading. He found that the ACI 318-71 procedure provides a realistic measure of the shear stress on the front column face but underestimates shear stresses on the side column face. Failure of a connection occurs when the strengths of the slab sections framing into three adjacent column faces are exhausted. He also found significant influences on ultimate capacity of the twisting moment and of bond slip of the reinforcing bars passing through the column.

A.2.1.3 Beam Analogy

The ACI Code linear shear stress method presumes that moment is transferred to a column by a combination of flexure and the shear stresses created by the column twisting with respect to the slab. The ACI method assumes no direct contribution of torsional effects that exist at the side faces of column, and completely ignores the influence of slab reinforcement at the side faces, but compensates by making the width of the slab effective for moment transfer greater than that for

shear transfer. Since the moment transferred by torsion is not small compared to that transferred by flexure, the ACI procedure is too simplistic. Kanoh (30), for example, showed with his tests that the moment which can be transferred by torsion, when converted into a torsional shear stress by the full plastic formula, equals about 1,400 psi (100 kgf/cm^2). If torsional effects are recognized, then it is apparent that the slab reinforcement at the side faces must be designed and detailed accordingly. The main difference between the ACI Code method and beam type analogies exists in the treatment of torsional effects at the side faces of column. Many investigators (2, 19, to 30) have proposed beam type analogies to predict the strength of connections tranferring moments. The accuracy of such procedures has improved as the number of test results has increased. In general, it has been found that beam analogies that account for torsion give better agreement with test data than the ACI Code method (2). Further, beam analogies predict that for all conditions, the capactiy of a connection can be increased up to a certain point, by increasing the reinforcement ratio in the region of the connection. Such an approach is very useful to a designer who might otherwise be forced to alter the geometry of his structure.

The analogy propsed by Hawkins (28) for interior column connection is shown in Fig. A.7. The slab is assumed to be attached to the column through front and back flexural beams F_1 and F_2 and side face torsional beams T_1 and T_2. The limiting strength combinations for the model are shown in Fig. 1.8. The beam analogy contains two basic elements: (a) a method for calculating the resisting capacity

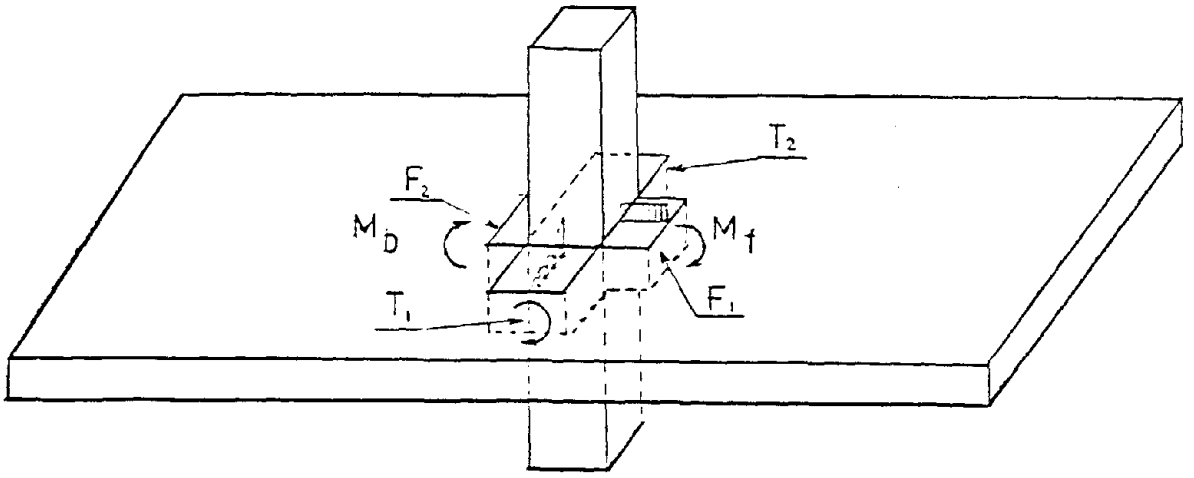

(a) general view

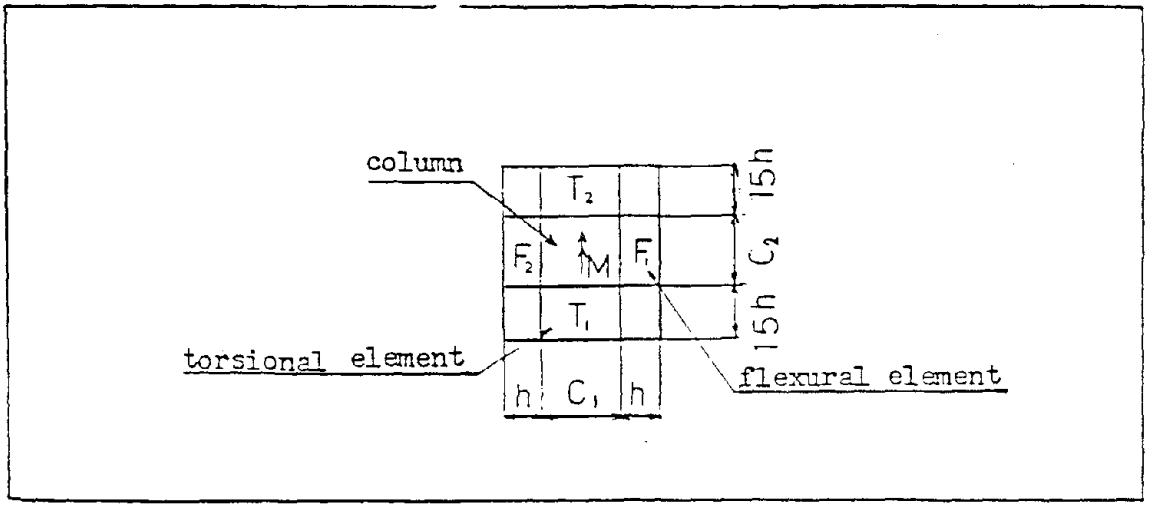

(b) plan view

FIG. A.7 STIFFNESS MODEL FOR INTERIOR COLUMN CONNECTION

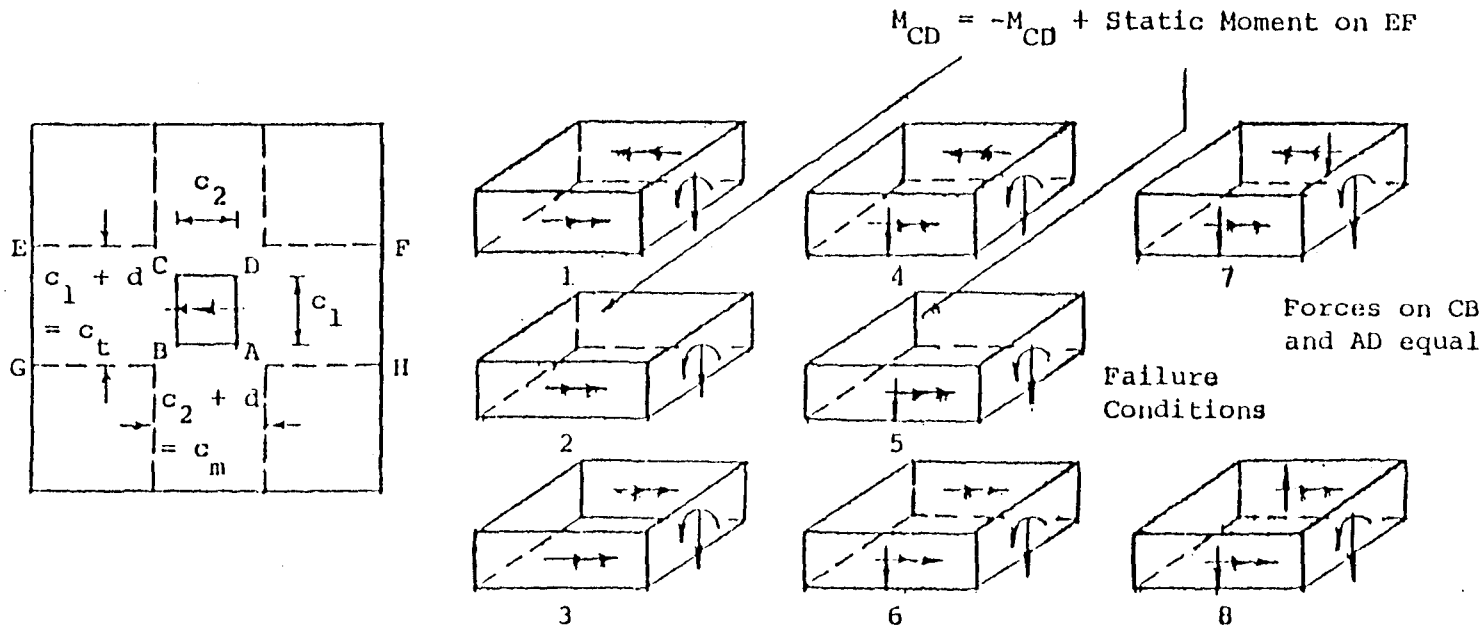

Interior Connection

Cases 1, 4, 7 low M/V ratio; Cases 3, 6, 8 high M/V ratio; Cases 1, 2, 3 likely for low ρ, high c_1/d; Cases 7, 8 likely for high ρ, low c/d

Arrows indicate development of limiting capacity; bending ⇝ ; shear ↓ ; torsion ↶
Subscript, AB, etc. indicates force assigned to critical section face AB.

FIG. A.8 LIMITING STRENGTH COMBINATIONS FOR BEAM ANALOGY FOR INTERIOR COLUMN CONNECTION

in combined shear, flexural moment and torsion of the connection faces, and (b) an iterative procedure for assigning applied forces to those faces, which is applicable to any connection transferring a known shear and moment. Without a computer program and known stiffness properties, the eight possible strength combinations of Fig. 1.8 make the application of the beam analogy difficult. Park (27) has developed an analogy that in essence assumes that case (6) of Fig. A.8 controls. That assumption provides an upper bound to the moment transfer capacity and presumes considerable ductility in shear, torsion and flexure.

In both analogies each beam section is presumed capable of developing the ultimate bending moment, torque and shear, or combinations of these quantities predicted by the accepted ultimate strength equations of the ACI Code 318-83.

The forces transferred through a connection must be distributed to the beam sections in a manner consistent with the relative deformations caused by those forces. Since for a cracked slab section, the resisting moment generated by a unit rotation is considerably greater than the resisting torque generated by an equal twist of the same section, moments are presumed transferred by flexure in preference to torsion.

Forces exceeding the capacity of the beam sections to which they are initially assigned are then redistributed to adjacent beam sections. Therefore, the unbalanced moments in excess of the flexural capacities of the transverse faces should be redistributed to the side faces as torsions. Further redistribution of excess forces should not be permitted.

To satisfy such condition, it becomes very important to evaluate the stiffness of each section with changing load stages.

A.2.2 Stiffness of Column-Slab Connections

In the University of Washington tests, accurate measurements were made of column rotations, rotations of the slab relative to the column at the four column faces, and the deflected profile of the slab.

The deflection at the slab edge has the four components shown in Fig. A.9. The quantity v_1 represents the part of the edge deflection caused by inter-story drift. The quantity v_2 represents the edge deflection caused by column rotations. The quantity v_2 was obtained by dividing the moment transferred through the connection equally between the top and bottom columns and calculating displacements by customary procedures with the column taken as cracked or uncracked as appropriate for the magnitude of the moment and axial load acting on a given section. The quantity v_4 represents the part of the edge deflection caused by bending of the slab between the column and the slab edge. For the region between one slab thickness from the column face and the edge, measured deflections were predictable using ACI Code 318-83 procedures, assuming the full width of the slab to be effective and the slab to be cracked or uncracked according to the magnitude of the moment acting on a given section of the slab.

The quantity v_3 in Fig. A.9 represents the part of the edge deflection caused by concentrated rotations occurring at the connection. In the tests the concentrated rotations occurring between the slab and column were measured by potentiometers with ends

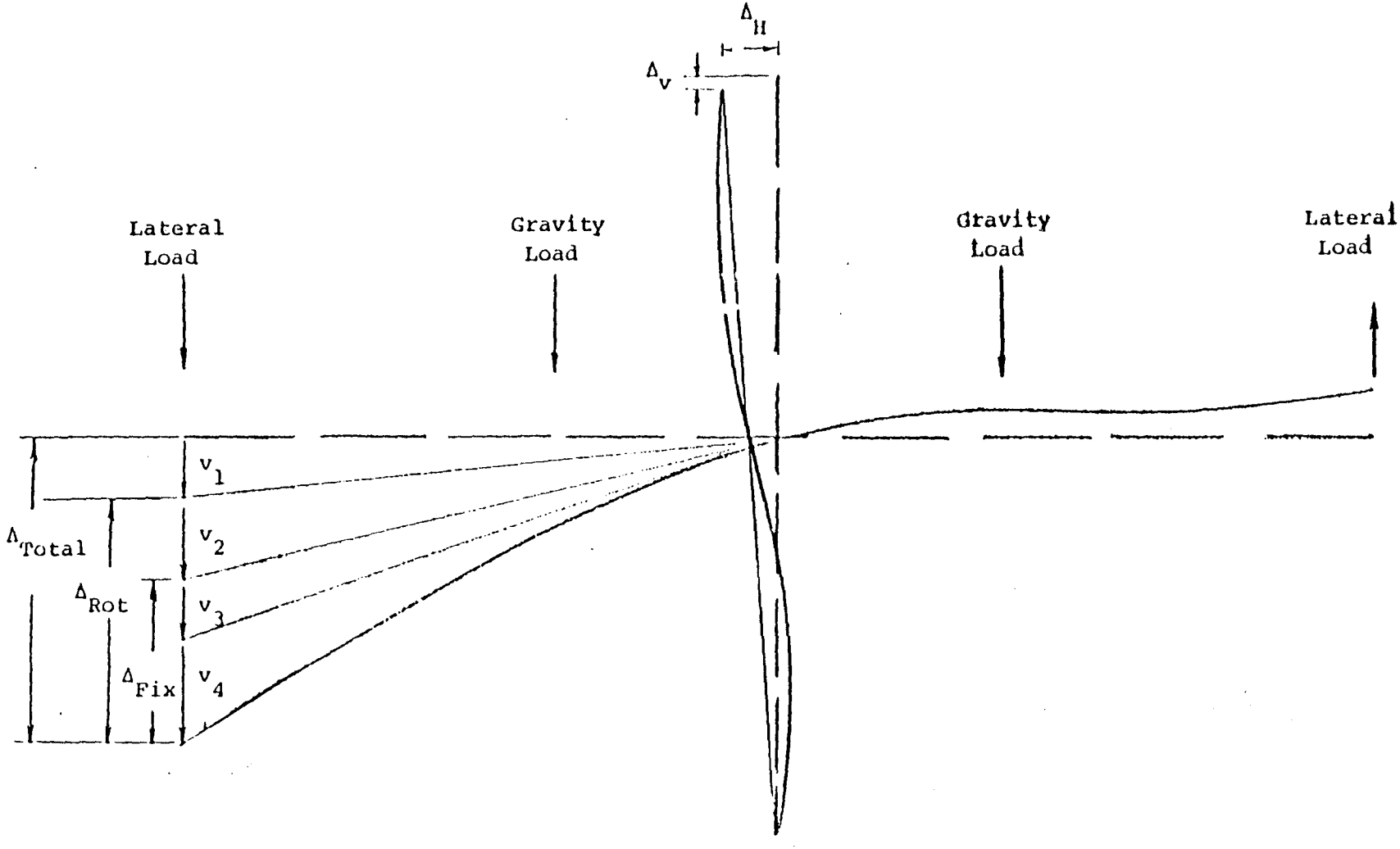

FIG. A.9 SLAB-COLUMN DEFORMATIONS

bearing centrally against the front and back faces of the column and bodies attached to the slab at one slab thickness from the column.

In the test specimens, the fraction of the total edge deflection caused by column rotations, v_2, was only about five percent even though columns were smaller than those likely in practice. Typically, connection rotations, v_3, caused considerably more than half the total edge deflection and those rotations are obviously critical for predicting the total stiffness of column-slab systems. Accurate assessment of the rotations causing v_3 is the main problem associated with predicting the lateral load stiffness of flate plate structures. The analogies outlined in Refs. (27) and (29) take no account of limitations imposed by deformation considerations and that is the main drawback to the application of those analyses.

Symonds et al. (5) found that prior to yielding of the flexural reinforcement passing through the column, the deformations measured in tests have been more than double those predicted by elastic thin plate theory and assuming a cracked concrete section. Also, Symonds, et al. showed that the measured deflections have exceeded the predicted, due in part to an overestimation of the torsional stiffness of cracked concrete, and in part to neglect of bond slip of the flexural reinforcement as it anchors itself within the column. They found that the rotations at slab-interior column connections were predictable using a model of the form shown in Fig. A.7. That form is similar to the Beam Analogy mode used for strength predictions. Its further refinement offers a potential means for overcoming the non-consideration of deformation limitations in the original Beam Analogy.

APPENDIX - B

COMPUTER PROGRAM FOR ESTIMATION OF THE PRIMARY CURVE FOR INTERIOR COLUMN - SLAB CONNECTIONS

GENERAL

The program used for determination of the load-edge deflection envelopes of Figs. 3.2 and 3.3 for interior column-slab connections is documented here. The basic principles used in that analysis have already been described in Section 2.3.2. The procedure used in that program is as follows:

1. Input the data and establish critical values for the moments and the corresponding stiffnesses of each element (Step 1 in program).
2. Set the initial values for gravity loading. Deformations are calculated by applying moments calculated as described in Section 2.3.1 to the flexural elements (Step 2 in program).
3. Build up the stiffness matrix for the model starting from the corresponding stiffnesses for the elements (Step 3 in program).
4. Solve the governing equation and calculate the moment increment for each element for a unit increment in lateral load (Step 4 in program).
5. Choose the element whose critical point is to be reached with the minimum lateral force increment (ΔP) and thus decide the increment in lateral load ΔP (Step 5 in program).
6. Calculate the moment increments and deformation increases caused by the lateral load increment ΔP (Step 6 in program).
7. Change the stiffness of the element whose critical value is reached and form a new stiffness matrix (Step 7 in program).
8. Repeat calculations until the torsional element yields.

The notation used for the input and output is shown in Table B.1 and Fig. B.1. A sample input and the corresponding output are listed at the end of the program. The output shows that the first and second steps are terminated by closing of the cracks for the back face flexural element and the bond-slip element at a lateral load of 1.65 kips. The third and fourth steps are terminated by cracking of the back face flexural element and the back bond-slip element at a lateral load of 2.18 kips. The calculation terminates at the 10th step when the torsional element crushes at a lateral load of 16.3 kips.

TABLE B.1 NOMENCLATURE FOR PROGRAM

1. Input

AH		=	overall depth of slab.
AC		=	size of column in direction of moment transfer.
AL		=	distance from column face to edge of slab in direction of moment transfer.
ALL		=	length of connecting bar.
FMI		=	moment caused by gravity load.
EIS		=	flexural stiffness of slab remote from column.
AET		=	flexural stiffness of connecting bar.
FMA	(1~4)	=	moments at front flexural element for cracking, yielding, crushing and collapse (very large value).
FMB	(1~5)	=	moments at back flexural element for zero load cracking, yielding, crushing and collapse.
FT	(1~3)	=	moments for torsional cracking, yielding and collapse.
AEIF	(1~4)	=	flexural stiffnesses of front flexural element for uncracked, cracked, yielded and crushed conditions.
AEIB	(1~5)	=	flexural stiffnesses of back flexural element for cracking for reversed loading, uncracked, cracked, yielded and crushed conditions.
AEKT	(1~3)	=	stiffnesses of torsional element for uncracked, cracked and yielded conditions.

AEBF (1~4) = stiffnesses of front bond-slip element for uncracked, cracked, yielded and final conditions.

AEBB (1~5) = stiffnesses of back bond-slip element for cracking for reversed loading, uncracked, cracked, yielded and final conditions.

FBOF (1~4) = moments at front bond-slip element for cracking, yielding, crushing and final conditions.

FBOB (1~5) = moments at back bond-slip element for zero, cracking, yielding, crushing and final conditions.

2. Output

EIF = flexural stiffness of front flexural element.

EIB = flexural stiffness of back flexural element.

EKT = stiffness of torsional element.

EBF = stiffness of front bond-slip element.

EBB = stiffness of back bond-slip element.

AET = flexural stiffness of connecting bar.

M-TOTAL = total moment transferred to column.

MF = moment at front flexural element.

MB = moment at back flexural element.

MFO = moment at front bond-slip element.

MBO = moment at back bond-slip element.

T = moment at torsional element.

DTF = inclination at end of front flexural element.

DTB = inclination at end of back flexural element.

DMF = moment at front flexural element increased by unit lateral load (P = 1).

DMB = moment at back flexural element increased by unit lateral load.

DMFO = moment at front bond-slip element increased by unit lateral load.

DMBO = moment at back bond-slip element increased by unit lateral load.

DT = moment at torsional element increased by unit lateral load.

DP = lateral load increment for given step.

DDF = deflection increment at front slab edge for given step.

DDB = deflection increment at back slab edge for given step.

DF = total deflection at front slab edge.

DB = total deflection at back slab edge.

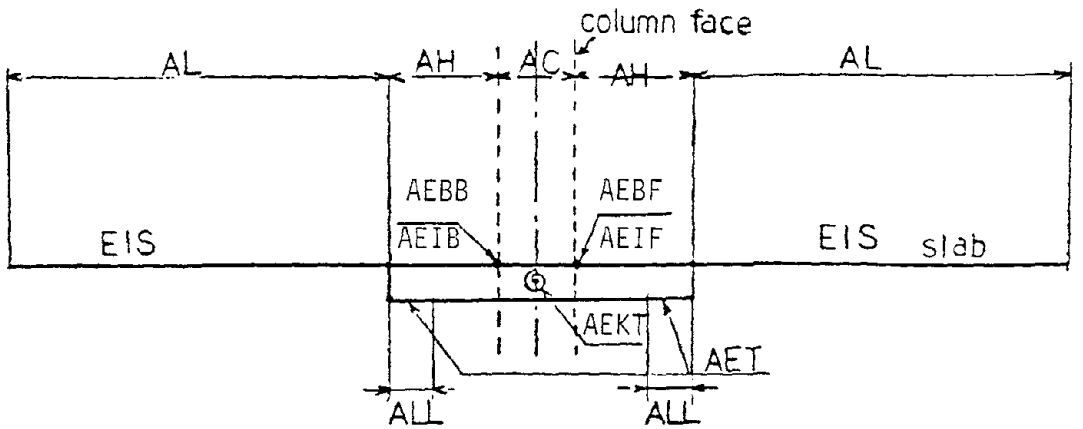

(a) Dimensions and Stiffnesses

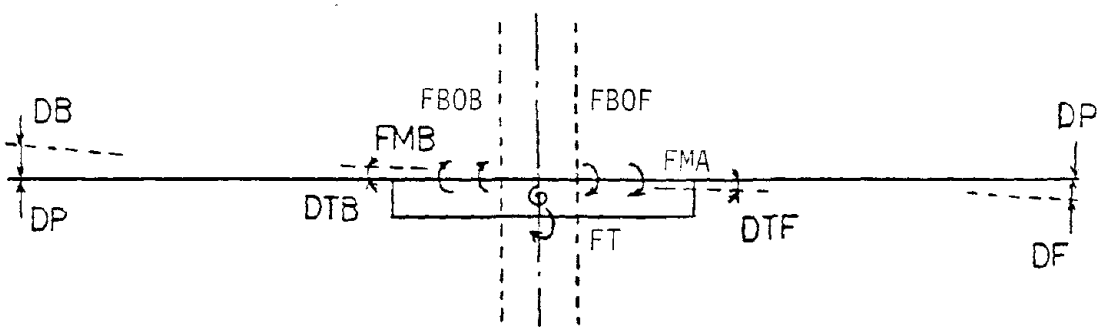

(b) Forces and Deformations

FIG. B.1 General Configuration and Notation

Reproduced from
best available copy.


```
      DIMENSION FMA(5),FMB(5),FT(5),AEIF(5),AEIB(5),AEKT(5),AEBF(5),
     1          AEBB(5),A(5,5),NANS(5),X(5),FBOF(5),FBOB(5),TITLE(6)
      READ(1,1) N
    1 FORMAT(I5)
*1    DO 999 II=1,N
      READ(1,16) (TITLE(I),I=1,6)
      WRITE(6,17) (TITLE(I),I=1,6)
   16 FORMAT(6A4)
   17 FORMAT(1H1,'*****',5X,6A4,5X,'*****')
      READ(1,10) AH,AC,AL,FMI,EIS,AET,ALL
   10 FORMAT(7F8.2)
      READ(1,15) FMA(1),FMB(1),FBOF(1),FBOB(1),AEIF(1),AEIB(1),AEBF(1),
     1           AEBB(1)
   15 FORMAT(8F8.2)
      READ(1,20) (FMA(I),I=2,4),(FMB(I),I=2,5),(FT(I),I=1,3)
      READ(1,42) (FBOF(I),I=2,4),(FBOB(I),I=2,5)
   20 FORMAT(10F8.2)
      READ(1,30) (AEIF(I),I=2,4),(AEIB(I),I=2,5),(AEKT(I),I=1,3)
   30 FORMAT(10F8.2)
      READ(1,40) (AEBF(I),I=2,4),(AEBB(I),I=2,5)
   40 FORMAT(7F8.2)
   42 FORMAT(7F8.2)
      WRITE(6,2000)
2000  FORMAT(/,10X,'***  INPUT DATA LIST  ***')
      WRITE(6,1900)
1900  FORMAT(/,'   AH   ','   AC   ','   AL   ','   ALL   ',
     1       '   FMI  ','   EIS  ','   AET  ')
      WRITE(6,10) AH,AC,AL,ALL,FMI,EIS,AET
      WRITE(6,2100)
2100  FORMAT(/,' FMA(1) ',' FMA(2) ',' FMA(3) ',' FMA(4) ',' FMB(1) ',
     1       ' FMB(2) ',' FMB(3) ',' FMB(4) ',' FMB(5) ',' FT(1) ',
     2       '  FT(2) ','  FT(3) ')
      WRITE(6,21) (FMA(I),I=1,4),(FMB(I),I=1,5),(FT(I),I=1,3)
   21 FORMAT(12F8.2)
      WRITE(6,2200)
2200  FORMAT(/,' AEIF(1)',' AEIF(2)',' AEIF(3)',' AEIF(4)',' AEIB(1)',
     1       ' AEIB(2)',' AEIB(3)',' AEIB(4)',' AEIB(5)',' AEKT(1)',
     2       ' AEKT(2)',' AEKT(3)')
      WRITE(6,21) (AEIF(I),I=1,4),(AEIB(I),I=1,5),(AEKT(I),I=1,3)
      WRITE(6,2300)
2300  FORMAT(/,' AEBF(1)',' AEBF(2)',' AEBF(3)',' AEBF(4)',
     1       ' AEBB(1)',' AEBB(2)',' AEBB(3)',' AEBB(4)',' AEBB(5)')
      WRITE(6,45) (AEBF(I),I=1,4),(AEBB(I),I=1,5)
   45 FORMAT(9F8.2)
      WRITE(6,2150) (FBOF(I),I=1,4),(FBOB(I),I=1,5)
2150  FORMAT(/,' FBOF(1)',' FBOF(2)',' FBOF(3)',' FBOF(4)',
     1       ' FBOB(1)',' FBOB(2)',' FBOB(3)',' FBOB(4)',' FBOB(5)'/9F8.2)
C       SET INITIAL VALUE
      AP=0.0
      K=0
*2    IMF=1
      IMB=2
      IKT=1
      IBF=1
      IBB=2
      HFT=0.0
      HMT=0.0
      HMF=FMI
      HMB=-FMI
      AHC=AH+AC/2.0
      HBF=FMI
```

```
*2    HBB=-FMI
      IF(HMF.GT.FMA(1)) IMF=2
      IF(HMF.GT.FMA(1)) IMB=1
      IF(HMF.GT.FMA(1)) IBF=2
      IF(HMF.GT.FMA(1)) IBB=1
      IF(HMF.GT.FMA(1)) GO TO 19
      DDF=FMA(1)**2/2.Ø/AEIF(1)
      DDF=DDF+(HMF-FMA(1))**2/2.Ø/AEIF(2)
      DDB=-DDF
      DTF=FMA(1)*AH/AEIF(1)
      DTF=DTF+(HMF-FMA(1))*AH/AEIF(2)
      DTB=-DTF
      DF=DDF+AL*DTF
      DB=DTB+AL*DTB
      GO TO 2399
   19 DDF=HMF*AH**2/2.Ø/AEIF(1)
      DDB=HMB*AH**2/2.Ø/AEIF(1)
      DTF=HMF*AH/AEIF(1)
      DTB=HMB*AH/AEIF(1)
      DF=DDF+AL*DTF
      DB=DDB+AL*DTB
 2399 WRITE(6,24ØØ)
 24ØØ FORMAT(/,'     ***************   OUT PUT   ***************     ')
      WRITE(6,25ØØ)
 25ØØ FORMAT(//,'    *******   INITIAL VALUE  *****')
      WRITE(6,41) DDF,DDB,DF,DB
   41 FORMAT('      DDF     ',',     DDB     ',',     DF     ',
     1       '      DB      ',/,4E12.5)
 1ØØ1 CONTINUE
      K=K+1
      IF(K.EQ.2Ø) GO TO 999
      FMF=FMA(IMF)
*3    FMBB=FMB(IMB)
      FTT=FT(IKT)
      FBF=FBOF(IBF)
      FBB=FBOB(IBB)
      EIF=AEIF(IMF)
      EIB=AEIB(IMB)
      EKT=AEKT(IKT)
      EBF=AEBF(IBF)
      EBB=AEBB(IBB)
      IF(EKT.EQ.Ø.ØØØØ1) GO TO 999
      A11=AH**3/3.Ø/EIF
      A12=AH**2/2.Ø/EIF
      A13=AH/EBF
      A21=ALL**3/3.Ø/AET
      A22=ALL**2/2.Ø/AET
      A23=AHC/EKT
      A31=AH**3/3.Ø/EIB
      A32=AH**2/2.Ø/EIB
      A33=AH/EBB
      A41=ALL**3/3.Ø/AET
      A42=ALL**2/2.Ø/AET
      A43=AHC/EKT
      A51=AH**2/2.Ø/EIF
      A52=AH/EIF
      A53=1.Ø/EBF
      A61=ALL**2/2.Ø/AET
      A62=ALL/AET
      A63=1.Ø/EKT
      A71=AH**2/2.Ø/EIB
      A72=AH/EIB
```

```
      A73=1.Ø/EBB
      A81=ALL**2/2.Ø/AET
*3    A82=ALL/AET
      A83=1.Ø/EKT
      A(1,1)=A11+AH*A13+A21+AHC*A23
      A(1,2)=A12+A13+A22+A23
      A(1,3)=AHC*A23
      A(1,4)=A23
      A(1,5)=A21+AL*A22+2.Ø*(AL+AHC)*A23
      A(2,1)=AHC*A43
      A(2,2)=A43
      A(2,3)=A31+AH*A33+A41+AHC*A43
      A(2,4)=A32+A33+A42+A43
      A(2,5)=A41+AL*A42+2.Ø*(AL+AHC)*A43
      A(3,1)=A51+AH*A53+A61+AHC*A63
      A(3,2)=A52+A53+A62+A63
      A(3,3)=AHC*A63
      A(3,4)=A63
      A(3,5)=A61+AL*A62+2.Ø*(AL+AHC)*A63
      A(4,1)=AHC*A83
      A(4,2)=A83
      A(4,3)=A71+AH*A73+A81+AHC*A83
      A(4,4)=A72+A73+A82+A83
      A(4,5)=A81+AL*A82+2.Ø*(AL+AHC)*A83
      CALL INV2 (A,4,1,5,5,NANS,X,DET,NSTOP,Ø)
*4    R1=A(1,5)
      R2=A(2,5)
      R3=A(3,5)
      R4=A(4,5)
      R9=R2+R1*AH/2.Ø
      R1Ø=R4+R3*AH/2.Ø
      R11=2.Ø*AL-R2-R4+(2.Ø-R1-R3)*AHC
      R12=R9+R1Ø+R11+(R1+R3)*(AC+AH)/2.Ø
      R17=R2+R1*AH
      R18=R4+R3*AH
      R13=A11*R1+A12*R2+A13*(R2+R1*AH)
      R14=A31*R3+A32*R4+A33*(R4+R3*AH)
      R15=A51*R1+A52*R2+A53*(R2+R1*AH)
      R16=A71*R3+A72*R4+A73*(R4+R3*AH)
      CA=(FMF-HBF)/R17
      CB=(FMBB-HBB)/R18
*5    CC=(FBF-HBF)/R17
      CD=(FBB-HBB)/R18
      CE=(FTT-HFT)/R11
      IF(CA.LT.Ø) CA=1ØØØØ.
      IF(CB.LT.Ø) CB=1ØØØØ.
      IF(CC.LT.Ø) CC=1ØØØØ.
      IF(CD.LT.Ø) CD=1ØØØØ.
      IF(CE.LT.Ø) CE=1ØØØØ.
      DDP=MIN(ABS(CA),ABS(CB),ABS(CC),ABS(CD),ABS(CE))
      IF(DDP.NE.ABS(CA)) GO TO 11Ø
      DP=CA
      GO TO 19Ø
11Ø   IF(DDP.NE.ABS(CB)) GO TO 12Ø
      DP=CB
      GO TO 19Ø
12Ø   IF(DDP.NE.ABS(CC)) GO TO 13Ø
      DP=CC
      GO TO 19Ø
13Ø   IF(DDP.NE.ABS(CD)) GO TO 14Ø
      DP=CD
      GO TO 19Ø
```

```
  14Ø DP=CE
  19Ø CONTINUE
      AP=AP+DP
      HMF=HMF+DP*R9
*6    HMB=HMB+DP*R1Ø
      HBF=HBF+DP*R17
      HBB=HBB+DP*R18
      HFT=HFT+DP*R11
      HMT=HMT+DP*R12
      DDF=DDF+DP*R13
      DDB=DDB+DP*R14
      DTF=DTF+DP*R15
      DTB=DTB+DP*R16
      DF=DDF+AL*DTF+AP*AL**3/3.Ø/EIS
      DB=DDB+AL*DTB+AP*AL**3/3.Ø/EIS
      WRITE(6,26ØØ) K
 26ØØ FORMAT(/,'   *****  STEP ',I2,'  *****')
      WRITE(6,1Ø1)
  1Ø1 FORMAT('    EIF     ',','     EIB     ',','     EKT     ',','     EBF     ',
     1         '     EBB     ',','     AET     ')
      WRITE(6,1ØØ) EIF,EIB,EKT,EBF,EBB,AET
  1ØØ FORMAT(6E12.4)
      WRITE(6,2Ø1)
  2Ø1 FORMAT(/,'   M-TOTAL  ',','     MF      ',','     MB      ',
     1         '     MFØ     ',','     MBØ     ',','     T       ',
     2         '     DTF     ',','     DTB     ',','     DF      ',
     3         '     DB      ')
      WRITE(6,2ØØ) HMT,HMF,HMB,HBF,HBB,HFT,DTF,DTB,DF,DB
  2ØØ FORMAT(1ØE12.4)
      WRITE(6,2Ø2)
  2Ø2 FORMAT(/,'      DMF      ',','      DMB      ',','      DMFØ     ',
     1         '     DMBØ     ',','      DT       ')
      WRITE(6,3ØØ) R9,R1Ø,R17,R18,R11
  3ØØ FORMAT(5E15.5)
      WRITE(6,5ØØ) DP,DDF,DDB,DF,DB
  5ØØ FORMAT('      DP      ',','     DDF     ',','     DDB     ',
     1       '     DF      ',','     DB      ',/,5E12.5)
      WRITE(6,5Ø1) AP
  5Ø1 FORMAT('****************************************','P=',E12.5)
      IF(DP.NE.CA) GO TO 1ØØØ
      IMF=IMF+1
*7    GO TO 1ØØ1
 1ØØØ IF(DP.NE.CB) GO TO 1Ø1Ø
      IMB=IMB+1
      GO TO 1ØØ1
 1Ø1Ø IF(DP.NE.CC) GO TO 1Ø2Ø
      IBF=IBF+1
      GO TO 1ØØ1
 1Ø2Ø IF(DP.NE.CD) GO TO 1Ø3Ø
      IBB=IBB+1
      GO TO 1ØØ1
 1Ø3Ø IKT=IKT+1
      GO TO 1ØØ1
  999 CONTINUE
      END
```

Reproduced from best available copy.

```
*****       SPECIMEN SS-8                *****

          ***  INPUT DATA LIST  ***

  AH       AC       AL       ALL       FMI      EIS      AET
   6.00    16.00    60.00     3.40   100.00 5078.00   173.00

FMA(1)  FMA(2)  FMA(3)  FMA(4)  FMB(1)  FMB(2)  FMB(3)  FMB(4)  FMB(5)   FT(1)   FT(2)   FT(3)
  42.00  525.00  553.00 5530.00    0.0    42.00  270.00  284.00 2840.00  134.00  842.00 8420.00

AEIF(1) AEIF(2) AEIF(3) AEIF(4) AEIB(1) AEIB(2) AEIB(3) AEIB(4) AEIB(5) AEKT(1) AEKT(2) AEKT(3)
 967.00  687.00   32.80    0.00 1374.00  967.00  400.00    4.90    0.00  453.00   89.00    0.00

AEBF(1) AEBF(2) AEBF(3) AEBF(4) AEBB(1) AEBB(2) AEBB(3) AEBB(4) AEBB(5)
******* 170.00    5.67    5.67  340.00******** 155.00    5.17    5.17

FBOF(1) FBOF(2) FBOF(3) FBOF(4) FBOB(1) FBOB(2) FBOB(3) FBOB(4) FBOB(5)
  42.00  395.00  553.00 3950.00    0.0    42.00  203.00  284.00 2030.00

   ***************   OUT PUT   ***************


  *******   INITIAL VALUE  *****
    DDF          DDB          DF           DB
0.18614E+01-0.18614E+01 0.39090E+02-0.39090E+02

  *****  STEP  1  *****
  EIF          EIB          EKT          EBF          EBB          AET
0.6870E+03  0.1374E+04  0.4530E+03  0.1700E+03  0.3400E+03  0.1730E+03

  M-TOTAL       MF           MB          MF0          MB0           T          DTF          DTB          DF           DB
0.2437E+03  0.1621E+03 -0.1678E+02  0.1532E+03 -0.6104E-04  0.6943E+02  0.1475E+01  0.3703E-01  0.1172E+03  0.2664E+02

     DMF          DMB          DMF0         DMB0          DT
  0.37686E+02  0.50536E+02  0.32298E+02  0.60728E+02  0.42163E+02
    DP           DDF          DDB          DF           DB
0.16467E+01 0.52870E+01 0.10667E+01 0.11715E+03 0.26636E+02
*********************************************p= 0.16467E+01

  *****  STEP  2  *****
  EIF          EIB          EKT          EBF          EBB          AET
0.6870E+03  0.9670E+03  0.4530E+03  0.1700E+03  0.3400E+03  0.1730E+03

  M-TOTAL       MF           MB          MF0          MB0           T          DTF          DTB          DF           DB
0.2437E+03  0.1621E+03 -0.1678E+02  0.1532E+03 -0.2910E-10  0.6943E+02  0.1475E+01  0.3703E-01  0.1172E+03  0.2664E+02

     DMF          DMB          DMF0         DMB0          DT
  0.37895E+02  0.47302E+02  0.33612E+02  0.56690E+02  0.44087E+02
    DP           DDF          DDB          DF           DB
0.10767E-05 0.52870E+01 0.10667E+01 0.11715E+03 0.26636E+02
*********************************************p= 0.16467E+01
```

```
  ***** STEP  3  *****
  EIF          EIB          EKT          EBF          EBB          AET
 0.6870E+03  0.9670E+03  0.4530E+03  0.1700E+03  0.1000E+08  0.1730E+03

  M-TOTAL       MF           MB          MF0          MB0           T          DTF          DTB          DF           DB
 0.3225E+03  0.1812E+03  0.1330E+02  0.1646E+03  0.4200E+02  0.8349E+02  0.1710E+01  0.2237E+00  0.1396E+03  0.4602E+02

     DMF          DMB          DMF0         DMB0          DT
  0.35976E+02  0.56518E+02  0.21536E+02  0.78894E+02  0.26408E+02
    DP           DDF          DDB          DF           DB
0.53236E+00 0.61263E+01 0.17007E+01 0.13962E+03 0.46020E+02
*********************************************p= 0.21790E+01

  ***** STEP  4  *****
  EIF          EIB          EKT          EBF          EBB          AET
 0.6870E+03  0.4000E+03  0.4530E+03  0.1700E+03  0.1000E+08  0.1730E+03

  M-TOTAL       MF           MB          MF0          MB0           T          DTF          DTB          DF           DB
 0.3225E+03  0.1812E+03  0.1330E+02  0.1646E+03  0.4200E+02  0.8349E+02  0.1710E+01  0.2237E+00  0.1396E+03  0.4602E+02

     DMF          DMB          DMF0         DMB0          DT
  0.37473E+02  0.41113E+02  0.30956E+02  0.55598E+02  0.40198E+02
    DP           DDF          DDB          DF           DB
0.27445E-06 0.61263E+01 0.17007E+01 0.13962E+03 0.46020E+02
*********************************************p= 0.21790E+01

  ***** STEP  5  *****
  EIF          EIB          EKT          EBF          EBB          AET
 0.6870E+03  0.4000E+03  0.4530E+03  0.1700E+03  0.1550E+03  0.1730E+03

  M-TOTAL       MF           MB          MF0          MB0           T          DTF          DTB          DF           DB
 0.4512E+03  0.2155E+03  0.4171E+02  0.2022E+03  0.7134E+02  0.1340E+03  0.2230E+01  0.8391E+00  0.1854E+03  0.9770E+02

     DMF          DMB          DMF0         DMB0          DT
  0.39418E+02  0.32675E+02  0.43189E+02  0.33757E+02  0.58109E+02
    DP           DDF          DDB          DF           DB
0.86928E+00 0.83778E+01 0.41289E+01 0.18541E+03 0.97697E+02
*********************************************p= 0.30483E+01

  ***** STEP  6  *****
  EIF          EIB          EKT          EBF          EBB          AET
 0.6870E+03  0.4000E+03  0.8900E+02  0.1700E+03  0.1550E+03  0.1730E+03

  M-TOTAL       MF           MB          MF0          MB0           T          DTF          DTB          DF           DB
 0.9398E+03  0.3496E+03  0.1524E+03  0.3696E+03  0.2030E+03  0.1788E+03  0.4386E+01  0.3349E+01  0.3713E+03  0.3055E+03

     DMF          DMB          DMF0         DMB0          DT
  0.40612E+02  0.33531E+02  0.50704E+02  0.39879E+02  0.13578E+02
    DP           DDF          DDB          DF           DB
0.33014E+01 0.18090E+02 0.14521E+02 0.37127E+03 0.30549E+03
*********************************************p= 0.63497E+01
```

```
  *****  STEP  7  *****
  EIF          EIB          EKT          EBF          EBB          AET
 Ø.6870E+Ø3  Ø.4000E+Ø3  Ø.8900E+Ø2  Ø.1700E+Ø3  Ø.5170E+Ø1  Ø.1730E+Ø3

  M-TOTAL       MF           MB           MFØ          MBØ           T          DTF          DTB          DF           DB
 Ø.9885E+Ø3  Ø.3643E+Ø3  Ø.1585E+Ø3  Ø.3950E+Ø3  Ø.2042E+Ø3  Ø.1858E+Ø3  Ø.4664E+Ø1  Ø.3664E+Ø1  Ø.3940E+Ø3  Ø.3306E+Ø3

     DMF           DMB          DMFØ          DMBØ           DT
  Ø.44829E+Ø2   Ø.18627E+Ø2   Ø.77231E+Ø2   Ø.34978E+Ø1   Ø.21208E+Ø2
    DP           DDF          DDB          DF           DB
Ø.32906E+ØØ Ø.19466E+Ø2 Ø.16058E+Ø2 Ø.3940ØE+Ø3 Ø.3305ØE+Ø3
**********************************************p= Ø.66788E+Ø1

  *****  STEP  8  *****
  EIF          EIB          EKT          EBF          EBB          AET
 Ø.6870E+Ø3  Ø.4000E+Ø3  Ø.8900E+Ø2  Ø.5670E+Ø1  Ø.5170E+Ø1  Ø.1730E+Ø3

  M-TOTAL       MF           MB           MFØ          MBØ           T          DTF          DTB          DF           DB
 Ø.1911E+Ø4  Ø.3623E+Ø3  Ø.1571E+Ø3  Ø.4676E+Ø3  Ø.2700E+Ø3  Ø.5914E+Ø3  Ø.1745E+Ø2  Ø.1638E+Ø2  Ø.1327E+Ø4  Ø.1259E+Ø4

     DMF           DMB          DMFØ          DMBØ           DT
  -Ø.32258E+ØØ  -Ø.22556E+ØØ   Ø.11652E+Ø2   Ø.10565E+Ø2   Ø.65078E+Ø2
    DP           DDF          DDB          DF           DB
Ø.62327E+Ø1 Ø.96913E+Ø2 Ø.93424E+Ø2 Ø.13272E+Ø4 Ø.1259ØE+Ø4
**********************************************p= Ø.12912E+Ø2

  *****  STEP  9  *****
  EIF          EIB          EKT          EBF          EBB          AET
 Ø.6870E+Ø3  Ø.4900E+Ø1  Ø.8900E+Ø2  Ø.5670E+Ø1  Ø.5170E+Ø1  Ø.1730E+Ø3

  M-TOTAL       MF           MB           MFØ          MBØ           T          DTF          DTB          DF           DB
 Ø.2346E+Ø4  Ø.3493E+Ø3  Ø.1598E+Ø3  Ø.5062E+Ø3  Ø.2840E+Ø3  Ø.8070E+Ø3  Ø.2414E+Ø2  Ø.2241E+Ø2  Ø.1811E+Ø4  Ø.1703E+Ø4

     DMF           DMB          DMFØ          DMBØ           DT
  -Ø.43983E+Ø1   Ø.92301E+ØØ   Ø.13096E+Ø2   Ø.47572E+Ø1   Ø.73270E+Ø2
    DP           DDF          DDB          DF           DB
Ø.29430E+Ø1 Ø.13781E+Ø3 Ø.13347E+Ø3 Ø.18109E+Ø4 Ø.1703ØE+Ø4
**********************************************p= Ø.15854E+Ø2

  *****  STEP 1Ø  *****
  EIF          EIB          EKT          EBF          EBB          AET
 Ø.6870E+Ø3  Ø.1000E-Ø4  Ø.8900E+Ø2  Ø.5670E+Ø1  Ø.5170E+Ø1  Ø.1730E+Ø3

  M-TOTAL       MF           MB           MFØ          MBØ           T          DTF          DTB          DF           DB
 Ø.2413E+Ø4  Ø.3463E+Ø3  Ø.1598E+Ø3  Ø.5124E+Ø3  Ø.2840E+Ø3  Ø.8420E+Ø3  Ø.2521E+Ø2  Ø.2335E+Ø2  Ø.1888E+Ø4  Ø.1772E+Ø4

     DMF           DMB          DMFØ          DMBØ           DT
  -Ø.69051E+Ø1   Ø.34875E-Ø5   Ø.13984E+Ø2   Ø.17023E-Ø4   Ø.78310E+Ø2
    DP           DDF          DDB          DF           DB
Ø.44632E+ØØ Ø.14441E+Ø3 Ø.13989E+Ø3 Ø.18883E+Ø4 Ø.17719E+Ø4
**********************************************p= Ø.16301E+Ø2
```

APPENDIX - C

DRAIN - 2D PROGRAM

GENERAL

The original Drain-2D program was developed in the University of California at Berkeley for the general dynamic response analysis of plane inelastic structures (34). That program presumes that the structure can be divided into 6 types of elements, namely: 1. Truss elements; 2. Beam-column elements; 3. Infill panel elements; 4. Semi-rigid connection elements; 5. Beam elements; and 6. Beam elements with degrading stiffness. Although these elements may be enough for ordinary structural analysis, it was necessary for this research to develop three additional elements. Since the laboratory experiments showed the response to be very sensitive to the characteristics of the slab in the connection region, it was considered vitally important to develop properties for the elements in that region which could reflect precisely the slab's properties in the same region, namely: 1. Flexural elements with different stiffnesses in positive and negative bending and with a trilinear rather than a bilinear form, so that account could be taken of both cracking and yielding effects. 2. Bond-slip elements. 3. Torsional elements which also had a trilinear form to take account of cracking and yielding. The characteristics of these elements were explained in Chapter 2.

The Drain-2D program is very large. Therefore, only the sub-routine "RESP 9" is listed here. That sub-routine shows how Drain-2D manipulates the degrading stiffness of the flexural element at varying loading stages. The input data used for the dynamic analysis of the

Holiday Inn, whose result is shown in Fig. 5.10, is listed at the end as an example. The input form is the same as explained in the Drain-2D manual (34) except for the element card E2, which should be changed as shown in Table C.1. The output format is the same as that shown in the original Drain-2D manual (34). Definitions for the new terms introduced into the Drain-2D program are shown in Table C.2.

TABLE C.1 INPUT FORMAT FOR FLEXURAL ELEMENT

CARD	COLUMN	
E2(a)	1-5	Group Type (=9)
	6-10	Number of elements in a group
	11-15	Number of different element stiffness types
	16-20	Number of different and eccentricity types
	21-25	Number of different yield moment values
	26-30	Number of different fixed end force patterns
	31-35	Number of initial element force patterns
E2(b) -1	1-5	Stiffness types number
	6-15	Initial flexural stiffness
	16-25	Axial stiffness
	26-35	Shear stiffness
	36-40	Flexural stiffness factors, K_{ii}
	41-45	Flexural stiffness factors, K_{jj}
	46-50	Flexural stiffness factors, K_{ij}
	51-60	Negative strain-hardening ratio for inelastic hinge at node i
	61-70	Negative strain-hardening ratio for inelastic hinge at node j
E2(b) -2	1-5	Stiffness type number
	6-15	Negative hinge stiffness at node i
	16-25	Negative hinge stiffness at node j
	26-35	Unloading stiffness parameter at node i, α_i
	36-45	Unloading stiffness parameter at node j, α_j
	46-55	Loading parameter at node i, β_i
	56-65	Loading parameter at node j, β_j
	66-75	Loading exponential parameter
E2(b) -3	1-10	Strain hardening ratio for inelastic hinge at node i (positive)
	11-20	Strain hardening ratio for inelastic hinge at node j (positive)
	21-30	Hinge stiffness at node i (positive)
	31-40	Hinge stiffness at node j (positive)
	41-50	Cracking moment
E2(c)		Identical to Input data for element 6 in Reference (34)
E2(d)		Identical to Input data for element 6
E2(e)		Identical to Input data for element 6
E2(f)		Identical to Input data for element 6
E2(g)		Identical to Input data for element 6

TABLE C.2 NOTATION FOR NEW TERMS INTRODUCED INTO DRAIN-2D

ROTPP	=	positive rotation of a hinge
ROTPN	=	negative rotation of a hinge
EKEPP	=	positive stiffness of a hinge
EKEP	=	negative stiffness of a hinge
EKP	=	positive stiffness of a hinge
EKN	=	negative stiffness of a hinge
BCRP	=	positive cracking moment
BCRN	=	negative cracking moment
BCRTP	=	positive rotation at cracking
BCRTN	=	negative rotation at cracking

```
 71 C
 72     30 KFAC=0
 73        ICSL=0
 74        IENDY=0
 75        DO 340 IEND=1,2
 76        FACTOR=1.-FACAC
 77        IF (DBM(IEND).EQ.0.) GO TO 340
 78        DBMAB=DABS(DBM(IEND))
 79        IF(DBMAB.LT.0.000001) GO TO 340
 80 C
 81 C      SET REVERSAL MOMENT INDICATOR
 82 C
 83        REMIND=1.
 84        IF (IND(IEND).EQ.2) REMIND=-1.
 85 C
 86 C      RULE 1. ELASTIC STAGE, GET FACTOR FOR STATUS CHANGE
 87 C      STAGE   0
 88 C
 89         IF (KODY(IEND).GT.0) GO TO 50
 90         IF (KODY(IEND).NE.0) GO TO 51
 91         IF (BMTOT(IEND).LT.BCRN) GO TO 21
 92         IF (BMTOT(IEND).GT.BCRP) GO TO 22
 93         KODY(IEND)=-1
 94         EKH(IEND)=1.E13
 95         GO TO 51
 96     21  IF (DBM(IEND).LT.0.) GO TO 2001
 97         KODY(IEND)=-5
 98         EKH(IEND)=(BCRP-BMTOT(IEND))/(BCRTP-RTOT(IEND))
 99         GO TO 51
100   2001  CONTINUE
101         KODY(IEND)=-3
102         EKH(IEND)=(BMY(IEND,2)-BMTOT(IEND))/(RY(IEND,2)-RTOT(IEND))
103         GO TO 51
104     22  IF (DBM(IEND).GT.0.) GO TO 2002
105         KODY(IEND)=-4
106         EKH(IEND)=(BCRN-BMTOT(IEND))/(BCRTN-RTOT(IEND))
107         GO TO 51
108   2002  CONTINUE
109         KODY(IEND)=-2
110         EKH(IEND)=(BMY(IEND,1)-BMTOT(IEND))/(RY(IEND,1)-RTOT(IEND))
111     51  KOD=KODY(IEND)
112         IF (KOD.EQ.-3) GO TO 55
113         IF (KOD.EQ.-2) GO TO 56
114         IF (KOD.EQ.-1) GO TO 57
115 C
116 C            CRACK   NO HAJIMARI  POINT   BETWEEN  -2  -3
117 C
118         IF(DBM(IEND).GT.0.) GO TO 2003
119         FAC=(BCRN-BMTOT(IEND))/DBM(IEND)
120         IF (FAC.GE.FACTOR) GO TO 340
121         FACTOR=FAC
122         BM=BCRN
123         ROT=BCRTN
124         KODE=-3
125         EK=(BMY(IEND,2)-BM)/(RY(IEND,2)-ROT)
126         GO TO 335
127   2003  FAC=(BCRP-BMTOT(IEND))/DBM(IEND)
128         IF (FAC.GE.FACTOR) GO TO 340
129         FACTOR=FAC
130         BM=BCRP
131         ROT=BCRTP
132         KODE=-2
133         EK=(BMY(IEND,1)-BM)/(RY(IEND,1)-ROT)
134         GO TO 335
135 C
136 C         M  IS   BELOW    MCRAK
137 C
138     55  IF (DBM(IEND).GT.0.) GO TO 2005
139         FAC=(BMY(IEND,2)-BMTOT(IEND))/DBM(IEND)
140         IF (FAC. GT.FACTOR) GO TO 340
```

```
141         FACTOR=FAC
142         BM=BMY(IEND,2)
143         ROT=RY(IEND,2)
144         KODE=2
145         EK1(IEND)=EKEP(IEND,1)
146         EKN(IEND)=EKEP(IEND,1)
147         EKH(IEND)=EKEP(IEND,1)
148         EKP(IEND)=EKEPP(IEND,1)
149         EK=EKEP(IEND,2)
150         IDK=2
151         GO TO 335
152   2005  KODY(IEND)=-4
153         ICSL=1
154         BCRN=BMTOT(IEND)
155         BCRTN=RTOT(IEND)
156         EKH(IEND)=(BCRP-BCRN)/(BCRTP-BCRTN)
157         FACTOR=0.
158         GO TO 340
159 C
160 C       M   IS   OVER   MCRK
161 C
162     56  IF (DBM(IEND).LT.0.) GO TO 2006
163         FAC=(BMY(IEND,1)-BMTOT(IEND))/DBM(IEND)
164         IF (FAC.GT.FACTOR) GO TO 340
165         FACTOR=FAC
166         BM=BMY(IEND,1)
167         ROT=RY(IEND,1)
168         KODE=1
169         EK1(IEND)=EKEPP(IEND,1)
170         EKP(IEND)=EKEPP(IEND,1)
171         EKH(IEND)=EKEPP(IEND,1)
172         EKN(IEND)=EKEP(IEND,1)
173         EK=EKEPP(IEND,2)
174         IDK=1
175         GO TO 335
176   2006  KODY(IEND)=-4
177         ICSL=1
178         BCRP=BMTOT(IEND)
179         BCRTP=RTOT(IEND)
180         EKH(IEND)=(BCRN-BCRP)/(BCRTN-BCRTP)
181         FACTOR=0.
182         GO TO 340
183     57  IF (DBM(IEND).LT.0.) GO TO 2007
184         FAC=(BCRP-BMTOT(IEND))/DBM(IEND)
185         IF (FAC.GT.FACTOR) GO TO 340
186         FACTOR=FAC
187         BM=BCRP
188         ROT=BCRTP
189         KODE=-2
190         EK=(BMY(IEND,1)-BM)/(RY(IEND,1)-ROT)
191         GO TO 335
192   2007  FAC=(BCRN-BMTOT(IEND))/DBM(IEND)
193         IF (FAC.GT.FACTOR) GO TO 340
194         FACTOR=FAC
195         BM=BCRN
196         ROT=BCRTN
197         KODE=-3
198         EK=(BMY(IEND,2)-BM)/(RY(IEND,2)-ROT)
199         GO TO 335
200 C
201 C       AFTER  THE  FIRST  YIELD
202 C
203     50 KOD=KODY(IEND)
204        GO TO (60,60,100,150,170,220,240,260,280,300,320), KOD
205 C
206 C      RULE 2. LOADING ON THE PRIMARY CURVE AFTER YIELDING
207 C    STAGE  1  AND  2
208 C
209     60 IF (REMIND*DBM(IEND).LT.0.) GO TO 70
210        MIND(IEND)=IND(IEND)
```

```
211         IMIND(IEND)=IND(IEND)
212         IF (ICH(IEND).NE.Ø) GO TO 66
213         GO TO 34Ø
214      66 IDD=IND(IEND)
215         FAC=(BMA(IEND,IDD)-BMTOT(IEND))/DBM(IEND)
216         IF(FAC.GE.FACTOR) GO TO 34Ø
217         FACTOR=FAC
218         BM=BMA(IEND,IDD)
219         ROT=RA(IEND,IDD)
22Ø         KFAC=IEND
221         KODE=IDD
222         IDK=IDD
223         ICH(IEND)=Ø
224         IF(BMTOT(IEND).LT.Ø) GO TO 67
225         EEEE=EKEPP(IEND,2)
226         GO TO 68
227      67 EEEE=EKEP(IEND,2)
228      68 CONTINUE
229         EK=EEEE
23Ø         GO TO 335
231 C     SET  THE  STIFFFESS  FOR  STARGE  3
232 C
233      7Ø KODY(IEND)=3
234         ICSL=1
235         IDD=IND(IEND)
236         BMT=BMTOT(IEND)
237         BMTEST=(BMB(IEND,IDD)-BMT)*REMIND
238         IF(KOD.EQ.2) GO TO 65
239 C
24Ø C       POSITIVE     PART
241         EKU=EKP(IEND)*2.Ø
242         EKEPP(IEND,1)=EKU
243         IF (BMTEST.GE.Ø.) GO TO 91
244         IDM=3-IDD
245 C       EKUMIN=(BMT-BMA(IEND,IDM))/(RTOT(IEND)-RA(IEND,IDM))
246 C       IF(ALPHA(IEND).LE.Ø.) G
247 C       IF(ALPHA(IEND).LE.Ø.)  GO  TO  61
248 C       IF (EKU.LT.EKUMIN) EKU=EKUMIN
249 C       GO  TO  62
25Ø C    61 CONTINUE
251 C       EKU=EKP(IEND)
252 C       IF(EKU.LT.EKUMIN)  EKU=EKUMIN
253 C    62 CONTINUE
254         BMB(IEND,IDD)=BMT
255         RB(IEND,IDD)=RTOT(IEND)
256         RA(IEND,IDD)=(1.-BETA(IEND))*RTOT(IEND)+BETA(IEND)*RY1(IEND,IDD)
257         BMA(IEND,IDD)=BMT-(RTOT(IEND)-RA(IEND,IDD))*EKEPP(IEND,2)
258         IF (BETA(IEND).GT.Ø.) GO TO 81
259         RA(IEND,IDD)=RTOT(IEND)
26Ø         BMA(IEND,IDD)=BMT
261      81 RREC(IEND,IDD)=RTOT(IEND)-BMB(IEND,IDD)/EKU
262         IDB=3-IDD
263         RREC(IEND,IDB)=RB(IEND,IDB)-BMB(IEND,IDB)/EKEP(IEND,1)
264         RCTEST=RREC(IEND,IDB)*REMIND
265         IF (RCTEST.GT.Ø.) RREC(IEND,IDB)=Ø.
266      91 EKH(IEND)=EKEPP(IEND,1)
267         REVPT(IEND)=RTOT(IEND)-BMT/EKH(IEND)
268         FACTOR=Ø.
269         KFAC=Ø
27Ø C
271 C          NEGATIVE  PART
272         GO TO 34Ø
273      65 CONTINUE
274         EKU=EKN(IEND)*2.Ø
275         EKEP(IEND,1)=EKU
276         IF (BMTEST.GE.Ø.) GO TO 9Ø
277         IDM=3-IDD
278 C       EKUMIN=(BMT-BMA(IEND,IDM))/(RTOT(IEND)-RA(IEND,IDM))
279 C       IF(ALPHA(IEND).LE.Ø.)  GO TO 71
28Ø C       IF (EKU.LT.EKUMIN) EKU=EKUMIN
```

```
C      GO TO 72
C   71 CONTINUE
C      EKU=EKN(IEND)
C      IF(EKU.LT.EKUMIN)  EKU=EKUMIN
C   72 CONTINUE
       BMB(IEND,IDD)=BMT
       RB(IEND,IDD)=RTOT(IEND)
       RA(IEND,IDD)=(1.-BETA(IEND))*RTOT(IEND)+BETA(IEND)*RY1(IEND,IDD)
       BMA(IEND,IDD)=BMT-(RTOT(IEND)-RA(IEND,IDD))*EKEP(IEND,2)
       IF (BETA(IEND).GT.0.) GO TO 80
       RA(IEND,IDD)=RTOT(IEND)
       BMA(IEND,IDD)=BMT
    80 RREC(IEND,IDD)=RTOT(IEND)-BMB(IEND,IDD)/EKEP(IEND,1)
       IDB=3-IDD
       RREC(IEND,IDB)=RB(IEND,IDB)-BMB(IEND,IDB)/EKEPP(IEND,1)
       RCTEST=RREC(IEND,IDB)*REMIND
       IF (RCTEST.GT.0.) RREC(IEND,IDB)=0.
    90 EKH(IEND)=EKEP(IEND,1)
       REVPT(IEND)=RTOT(IEND)-BMT/EKH(IEND)
       FACTOR=0.
       KFAC=0
       GO TO 340
C
C      RULE 3. UNLOADING FROM POINT 01/02 ON PRIMARY CURVE
C       STAGE  3
C
   100 IF(REMIND*DBM(IEND).LT.0.) GO TO 110
C
C     RELOAD  AGAIN   TO  PRIMARY  LINE   1  OR  2
C
       IDD=IND(IEND)
       IUD=IMIND(IEND)
       FAC=(BMY(IEND,IUD)-BMTOT(IEND))/DBM(IEND)
       IF (FAC.GE.FACTOR) GO TO 340
       FACTOR=FAC
       BM=BMY(IEND,IUD)
       ROT=RY(IEND,IUD)
       KFAC=IEND
C      KODE=IEND
       KODE=IDD
       IDK=IDD
       IF(IUD.NE.3) GO TO 929
       EEEE=EKEP(IEND,3)
       KODE=4
       IF(BMB(IEND,IDD).NE.BMA(IEND,IDD)) GO TO 3553
       BMY(IEND,IDD)=BMA(IEND,IDD)
       RY(IEND,IDD)=RA(IEND,IDD)
       GO TO 922
  3553 BMY(IEND,IDD)=GAMMA(IEND,IDD)*BMA(IEND,IDD)
       RY(IEND,IDD)=GAMMA(IEND,IDD)*RA(IEND,IDD)
       GO TO 922
   929 IF (BMTOT(IEND).LT.0.) GO TO 921
       EEEE=EKEPP(IEND,2)
       GO  TO  922
   921 EEEE=EKEP(IEND,2)
       IF(ICH(IEND).EQ.0) GO TO 922
       EEEE=BMA(IEND,IDD)/RA(IEND,IDD)
   922 CONTINUE
       EK=EEEE
       GO TO 335
C
C      CHECK   0  CROSSING
C
   110 FAC=-BMTOT(IEND)/DBM(IEND)
       IF (FAC.GE.FACTOR) GO TO 340
       FACTOR=FAC
       BM=0.
       ROT=REVPT(IEND)
       KFAC=IEND
       KODE=4
```

```
      IDK=3-IND(IEND)
      IDD=3-IDK
C
C     ESTABLISH NEW LOADING SLOPE
C     FOR  STAGE   4
C
      RTEST=(RREC(IEND,IDD)-ROT)*REMIND
      IF  (RTEST.GT.Ø.) GO TO 12Ø
      IF (BMB(IEND,IDK).EQ.BMA(IEND,IDK)) GO TO 121
      BMY(IEND,IDK)=GAMMA(IEND,IDK)*BMA(IEND,IDK)
      RY(IEND,IDK)=GAMMA(IEND,IDK)*RA(IEND,IDK)
      GO TO 13Ø
  121 BMY(IEND,IDK)=BMA(IEND,IDK)
      RY(IEND,IDK)=RA(IEND,IDK)
      GO TO 13Ø
  12Ø IF(BMA(IEND,IDK).EQ.BMB(IEND,IDK)) GO TO 4553
      RY(IEND,IDK)=GAMMA(IEND,IDK)*RA(IEND,IDK)
      BMY(IEND,IDK)=GAMMA(IEND,IDK)*BMA(IEND,IDK)
      GO TO 13Ø
 4553 BMY(IEND,IDK)=BMA(IEND,IDK)
      RY(IEND,IDK)=RA(IEND,IDK)
  13Ø IF((RY(IEND,IDK)-ROT).EQ.Ø.) GO TO 1131
      EKL=BMY(IEND,IDK)/(RY(IEND,IDK)-ROT)
      GO TO 1132
 1131 EKL=EKEPP(IEND,1)
      IF(BML(IEND).LT.Ø.) EKL=EKEP(IEND,1)
 1132 IF(BML(IEND).LT.Ø.) GO TO 181
C
C     CHECK FOR MAX SLOPE
C
      EEII=EKEPP(IEND,1)
      EEEE=EKEPP(IEND,2)
      GO  TO  182
  181 EEII=EKEP(IEND,1)
      EEEE=EKEP(IEND,2)
  182 CONTINUE
      IF(EKL.LT.Ø.) EKL=EEII*1.ØØ1
      IF(EKL.LE.EEII)  GO  TO  14Ø
      EKL=1.ØØ1*EEII
      RY(IEND,IDK)=RA(IEND,IDK)*ROT*EKL/(RA(IEND,IDK)*EKL-BMA(IEND,IDK))
      BMY(IEND,IDK)=EKL*(RY(IEND,IDK)-ROT)
  14Ø EKEP(IEND,3)=EKL
      EK=EKEP(IEND,3)
      GO TO 335
C
C     RULE 7, LOADING TOWARD POINT U1/U2 ON THE PRIMARY CURVE
C     FOR  STAGE   4
C
  15Ø IF (REMIND*DBM(IEND).LT.Ø.) GO TO 16Ø
      IDD=IND(IEND)
      MIND(IEND)=3
      IMIND(IEND)=3
      FAC=(BMY(IEND,IDD)-BMTOT(IEND))/DBM(IEND)
      IF (FAC.GE.FACTOR) GO TO 34Ø
C
C     CHECK   FOR  YIELDING  AND  RETURN  TO  PRIMARY  LINE
C
      FACTOR=FAC
      BM=BMY(IEND,IDD)
      ROT=RY(IEND,IDD)
      KFAC=IEND
      KODE=IDD
      IDK=IDD
      IF(BMB(IEND,IDD).NE.BMA(IEND,IDD)) GO TO 953
      ICH(IEND)=Ø
      IF (BMTOT(IEND).LT.Ø) GO TO 951
      EEEE=EKEPP(IEND,2)
      GO TO 952
  951 EEEE=EKEP(IEND,2)
  952 CONTINUE
```

```
421         GO TO 954
422     953 BMY(IEND,IDD)=BMA(IEND,IDD)
423         RY(IEND,IDD)=RA(IEND,IDD)
424         ICH(IEND)=1
425         EEEE=BMY(IEND,IDD)/RY(IEND,IDD)
426     954 EK=EEEE
427         GO TO 335
428 C
429 C       UNLOAD   FROM  STAGE  4  TO  STAGE  5
430 C
431     160 KODY(IEND)=3
432         ICSL=1
433         IF(BML(IEND).LT.0.)  GO  TO  183
434         EEII=EKP(IEND)*2.0
435         GO  TO  184
436     183 EEII=EKN(IEND)*2.0
437     184 CONTINUE
438         EKH(IEND)=EEII
439         REVPT(IEND)=RY(IEND,3)-BMY(IEND,3)/EKH(IEND)
440         FACTOR=0.
441         KFAC=0
442         GO TO 340
443 C
444 C       RULE 5. UNLOADING FROM POINT U3 AFTER RULE 4
445 C       STAGE    5
446 C
447     170 IF (REMIND*DBM(IEND).LT.0.) GO TO 180
448         FAC=(BMY(IEND,3)-BMTOT(IEND))/DBM(IEND)
449         IF (FAC.GE.FACTOR) GO TO 340
450 C
451 C       RETURN   FOR   STAGE4
452 C
453         FACTOR=FAC
454         BM=BMY(IEND,3)
455         ROT=RY(IEND,3)
456         KFAC=IEND
457         KODE=4
458         IDK=IND(IEND)
459         EK=EKEP(IEND,3)
460         GO TO 335
461 C
462 C       CHECK  F/R   0   CROSSING
463 C
464     180 FAC=-BMTOT(IEND)/DBM(IEND)
465         IF (FAC.GE.FACTOR) GO TO 340
466         FACTOR=FAC
467         BM=0.
468         ROT=REVPT(IEND)
469         KFAC=IEND
470         KODE=6
471         IDK=3-IND(IEND)
472         IDD=3-IDK
473 C
474 C       ESTABLISH NEW LOADING SLOPE
475 C
476         RTEST=(RREC(IEND,IDD)-ROT)*REMIND
477         IF (RTEST.GT.0.) GO TO 190
478         IF(BMB(IEND,IDK).EQ.BMA(IEND,IDK)) GO TO 195
479         BMY(IEND,IDK)=GAMMA(IEND,IDK)*BMA(IEND,IDK)
480         RY(IEND,IDK)=GAMMA(IEND,IDK)*RA(IEND,IDK)
481         GO TO 200
482     195 BMY(IEND,IDK)=BMA(IEND,IDK)
483         RY(IEND,IDK)=RA(IEND,IDK)
484         GO TO 200
485     190 CONTINUE
486         RY(IEND,IDK)=GAMMA(IEND,IDK)*RA(IEND,IDK)
487         BMY(IEND,IDK)=GAMMA(IEND,IDK)*BMA(IEND,IDK)
488     200 EKL=BMY(IEND,IDK)/(RY(IEND,IDK)-ROT)
489 C
490 C       CHECK FOR MAX SLOPE
```

```
491 C
492       IF (EKL.LT.EKEP(IEND,1)) GO TO 210
493       IF (BMTOT(IEND).LT.0.) GO TO 971
494       EEEE=EKEP(IEND,2)
495       EEII=EKEP(IEND,1)
496       GO  TO  972
497   971 EEEE=EKEPP(IEND,2)
498       EEII=EKEPP(IEND,1)
499   972 CONTINUE
500       IF (EKL.LE.EEII)  GO  TO  210
501       EKL=0.999*EEII
502       EEAC=EKL-EEEE
503       EEAB=DABS(EEAC)
504       RY(IEND,IDK)=(ROT*EKL+BMA(IEND,IDK)-RA(IEND,IDK)*EEEE)/EEAB
505       BMY(IEND,IDK)=EKL*(RY(IEND,IDK)-ROT)
506   210 EKEP(IEND,4)=EKL
507       EK=EKEP(IEND,4)
508       GO TO 335
509 C
510 C     RULE 6. LOADING TOWARD POINT U1/U2 (OPPOSITE RULE 4)
511 C
512   220 IF (REMIND*DBM(IEND).LT.0.) GO TO 230
513       IDD=IND(IEND)
514       MIND(IEND)=4
515       FAC=(BMY(IEND,IDD)-BMTOT(IEND))/DBM(IEND)
516       IF (FAC.GE.FACTOR) GO TO 340
517       FACTOR=FAC
518       BM=BMY(IEND,IDD)
519       ROT=RY(IEND,IDD)
520       KFAC=IEND
521       KODE=IDD
522       IDK=IDD
523       IF(BMB(IEND,IDD).NE.BMA(IEND,IDD)) GO TO 983
524       ICH(IEND)=0
525       IF(BMTOT(IEND).LT.0) GO TO 981
526       EEEE=EKEPP(IEND,2)
527       GO TO 982
528   981 EEEE=EKEP(IEND,2)
529   982 CONTINUE
530       GO TO 984
531   983 BMY(IEND,IDD)=BMA(IEND,IDD)
532       RY(IEND,IDD)=RA(IEND,IDD)
533       ICH(IEND)=1
534       EEEE=BMY(IEND,IDD)/RY(IEND,IDD)
535   984 EK=EEEE
536       GO TO 335
537   230 KODY(IEND)=7
538       ICSL=1
539       IF(BML(IEND).LT.0.) GO TO 186
540       EEII=EKEPP(IEND,1)
541       GO  TO  187
542   186 EEII=EKEP(IEND,1)
543   187 CONTINUE
544       EKH(IEND)=EEII
545       REVPT(IEND)=RY(IEND,4)-BMY(IEND,4)/EKH(IEND)
546       FACTOR=0.
547       KFAC=0
548       GO TO 340
549 C
550 C     RULE 7. UNLOADING FROM U4 AFTER RULE 6
551 C
552   240 IF (REMIND*DBM(IEND).LT.0.) GO TO 250
553       FAC=(BMY(IEND,4)-BMTOT(IEND))/DBM(IEND)
554       IF (FAC.GE.FACTOR) GO TO 340
555       FACTOR=FAC
556       BM=BMY(IEND,4)
557       ROT=RY(IEND,4)
558       KFAC=IEND
559       KODE=6
560       IDK=IND(IEND)
```

```
      EK=EKEP(IEND,4)
C     GO TO 340
      GO TO 335
  250 FAC=-BMTOT(IEND)/DBM(IEND)
      IF (FAC.GE.FACTOR) GO TO 340
      FACTOR=FAC
      BM=0.
      ROT=REVPT(IEND)
      KFAC=IEND
      KODE=8
      IDK=3-IND(IEND)
      EKEP(IEND,5)=BMY(IEND,3)/(RY(IEND,3)-REVPT(IEND))
      EK=EKEP(IEND,5)
C     GO TO 340
      GO TO 335
C
C     RULE 8. LOADING TOWARD POINT U3
C
  260 IF (REMIND*DBM(IEND).LT.0.) GO TO 270
      MIND(IEND)=5
      FAC=(BMY(IEND,3)-BMTOT(IEND))/DBM(IEND)
      IF (FAC.GE.FACTOR) GO TO 340
      FACTOR=FAC
      BM=BMY(IEND,3)
      ROT=RY(IEND,3)
      KFAC=IEND
      IDK=IND(IEND)
      IDD=IND(IEND)
      KODE=4
      EK=EKEP(IEND,3)
C     GO TO 340
      GO TO 335
  270 KODY(IEND)=9
      ICSL=1
      IF(BML(IEND).LT.0.) GO TO 188
      EEII=EKEPP(IEND,1)
      GO  TO  189
  188 EEII=EKEP(IEND,1)
  189 CONTINUE
      EKH(IEND)=EEII
      REVPT(IEND)=RY(IEND,5)-BMY(IEND,5)/EKH(IEND)
      FACTOR=0.
      KFAC=0
      GO TO 340
C
C     RULE 9. UNLOADING FROM POINT U5 AFTER RULE 8
C
  280 IF (REMIND*DBM(IEND).LT.0.) GO TO 290
      FAC=(BMY(IEND,5)-BMTOT(IEND))/DBM(IEND)
      IF (FAC.GE.FACTOR) GO TO 340
      FACTOR=FAC
      BM=BMY(IEND,5)
      ROT=RY(IEND,5)
      KFAC=IEND
      KODE=8
      IDK=IND(IEND)
      EK=EKEP(IEND,5)
C     GO TO 340
      GO TO 335
  290 FAC=-BMTOT(IEND)/DBM(IEND)
      IF (FAC.GE.FACTOR) GO TO 340
      FACTOR=FAC
      BM=0.
      ROT=REVPT(IEND)
      KFAC=IEND
      KODE=10
      IDK=3-IND(IEND)
      EKEP(IEND,6)=BMY(IEND,4)/(RY(IEND,4)-REVPT(IEND))
      EK=EKEP(IEND,6)
C     GO TO 340
```

```
631         GO TO 335
632 C
633 C       RULE 10. LOADING TOWARD POINT U4
634 C
635    300  IF (REMIND*DBM(IEND).LT.0.) GO TO 310
636         MIND(IEND)=6
637         FAC=(BMY(IEND,4)-BMTOT(IEND))/DBM(IEND)
638         IF (FAC.GE.FACTOR) GO TO 340.
639         FACTOR=FAC
640         BM=BMY(IEND,4)
641         ROT=RY(IEND,4)
642         KFAC=IEND
643         IDK=IND(IEND)
644         IDD=IND(IEND)
645         KODE=6
646         EK=EKEP(IEND,4)
647 C       GO TO 340
648         GO TO 335
649    310  KODY(IEND)=11
650         ICSL=1
651         IF(BML(IEND).LT.0.) GO TO 191
652         EEII=EKEPP(IEND,1)
653         GO  TO  192
654    191  EEII=EKEP(IEND,1)
655    192  CONTINUE
656         EKH(IEND)=EEII
657         REVPT(IEND)=RY(IEND,6)-BMY(IEND,6)/EKH(IEND)
658         FACTOR=0.
659         KFAC=0
660         GO TO 340
661 C
662 C       RULE 11. UNLOADING FROM U6 AFTER RULE 10
663 C
664    320  IF (REMIND*DBM(IEND).LT.0.) GO TO 330
665         FAC=(BMY(IEND,6)-BMTOT(IEND))/DBM(IEND)
666         IF (FAC.GE.FACTOR) GO TO 340
667         FACTOR=FAC
668         BM=BMY(IEND,6)
669         ROT=RY(IEND,6)
670         KFAC=IEND
671         KODE=10
672         IDK=IND(IEND)
673         EK=EKEP(IEND,6)
674 C       GO TO 340
675         GO TO 335
676    330  FAC=-BMTOT(IEND)/DBM(IEND)
677         IF (FAC.GE.FACTOR) GO TO 340
678         FACTOR=FAC
679         BM=0.
680         ROT=REVPT(IEND)
681         KFAC=IEND
682         KODE=8
683         IDK=3-IND(IEND)
684         EKEP(IEND,5)=BMY(IEND,3)/(RY(IEND,3)-REVPT(IEND))
685         EK=EKEP(IEND,5)
686    335  KODST(IEND)=KODE
687         IDKK(IEND)=IDK
688         GO  TO  331
689 C 339  KODST(IEND)=0
690 C       IDKK(IEND)=0
691    331  IENDY=IENDY+IEND
692         BMSTR(IEND)=BM
693         RTSTR(IEND)=ROT
694         EKSTR(IEND)=EK
695    340  FACTR(IEND)=FACTOR
696 C 340  CONTINUE
697         IF(KOUNT.LT.7) GO TO 355
698         FACTR(1)=1.-FACAC
699         FACTR(2)=1.-FACAC
700         GO TO 341
```

```
      355 CONTINUE
          IF(ICSL.EQ.Ø) GO TO 341
          FACTOR=Ø.
          GO TO 4Ø1
      341 IF(IENDY.LT.3) GO TO 347
          FACTOR=FACTR(1)
          ITEST=1
          IF(FACTR(1).LT.FACTR(2)) GO TO 342
          FACTOR=FACTR(2)
          ITEST=2
      342 DIF=DABS(FACTR(1)-FACTR(2))
          IF(DIF.LE.Ø.Ø1) GO TO 349
          IENDY=ITEST
      347 IF(IENDY.EQ.Ø) GO TO 349
          FACTOR=FACTR(IENDY)
      349 CONTINUE
C
C     UPDATE MOMENTS, ROTATIONS, AND YIELD DATA
C
          DO 4ØØ IEND=1,2
C         IF (IEND.EQ.KFAC) GO TO 39Ø
          IF(IENDY.EQ.3) GO TO 39Ø
          IF(IEND.EQ.IENDY) GO TO 39Ø
          BMTOT(IEND)=BMTOT(IEND)+FACTOR*DBM(IEND)
          RTOT(IEND)=RTOT(IEND)+FACTOR*DBM(IEND)/EKH(IEND)
          IF (KODY(IEND).LE.Ø) GO TO 4ØØ
          KOD=KODY(IEND)
          GO TO (35Ø,35Ø,4ØØ,35Ø,4ØØ,35Ø,4ØØ,35Ø,4ØØ,35Ø,4ØØ), KOD
      35Ø IDD=MIND(IEND)
          BMY(IEND,IDD)=BMTOT(IEND)
          RY(IEND,IDD)=RTOT(IEND)
          DROT=DBM(IEND)*FACTOR/EKH(IEND)
          IF (KOD.GT.2) GO TO 37Ø
          IF (DROT.LT.Ø.) GO TO 36Ø
          ROTPP(IEND)=ROTPP(IEND)+DROT
          GO TO 4ØØ
      36Ø ROTPN(IEND)=ROTPN(IEND)+DROT
          GO TO 4ØØ
      37Ø IF (DROT.LT.Ø.) GO TO 38Ø
          ROTSP(IEND)=ROTSP(IEND)+DROT
          GO TO 4ØØ
      38Ø ROTSN(IEND)=ROTSN(IEND)+DROT
          GO TO 4ØØ
C     39Ø BMTOT( END)=BM
C         RTOT(IEND)=ROT
C         KODY(IEND)=KODE
C         EKH(IEND)=EK
C         IND(IEND)=IDK
      39Ø BMTOT(IEND)=BMSTR(IEND)
          RTOT(IEND)=RTSTR(IEND)
          KODY(IEND)=KODST(IEND)
          EKH(IEND)=EKSTR(IEND)
          IND(IEND)=IDKK(IEND)
      4ØØ CONTINUE
C
C     CHECK FOR COMPLETION OF CYCLE
C
      4Ø1 CONTINUE
          FACAC=FACAC+FACTOR
          IF (FACAC.GT.Ø.99999) GO TO 41Ø
          CALL BMCAL9
          KBAL=1
          KOUNT=KOUNT+1
          GO TO 3Ø
C
C     TOTAL SHEAR FORCES
C
      41Ø DSF=(-BMTOT(1)+BMTOT1+BMTOT(2)-BMTOT2)/FL
          SFTOT(1)=SFTOT(1)+DSF
          SFTOT(2)=SFTOT(2)-DSF
```

```
771 C
772 C      UNBALANCED LOADS DUE TO YIELDING
773 C
774        FOUB=0.
775        IF (KBAL.EQ.0) GO TO 420
776        BMIUB=-BML(1)+BMTOT(1)
777        BMJUB=BML(2)-BMTOT(2)
778        GO TO 430
779   420  BMIUB=0.
780        BMJUB=0.
781 C
782 C      DEFORMATION RATES FOR DAMPING
783 C
784   430  IF (DFAC.EQ.0.0.AND.DELTA.EQ.0.0) GO TO 460
785        IF (TIME.EQ.0.) GO TO 470
786        KBAL=1
787        IF (EC(1).EQ.1.23456E10) GO TO 440
788        VELM(1)=VELM(1)-EC(3)*VELM(3)
789        VELM(2)=VELM(2)+EC(1)*VELM(3)
790        VELM(4)=VELM(4)-EC(4)*VELM(6)
791        VELM(5)=VELM(5)+EC(2)*VELM(6)
792   440  DVAX=COSA*(VELM(4)-VELM(1))+SINA*(VELM(5)-VELM(2))
793        ROT=(SINA*(VELM(4)-VELM(1))+COSA*(VELM(2)-VELM(5)))/FL
794        DVRI=VELM(3)+ROT
795        DVRJ=VELM(6)+ROT
796 C
797 C      BETA-O DAMPING
798 C
799        IF (DFAC.EQ.0.) GO TO 450
800        FAC=DFAC
801        CALL FSTF9 (ST,EKEP(1,1),EKEP(2,1))
802        BMIUB=BMIUB+(ST(1,1)*DVRI+ST(1,2)*DVRJ)*FAC
803        BMJUB=BMJUB+(ST(1,2)*DVRI+ST(2,2)*DVRJ)*FAC
804        FOUB=EAL*DVAX*DFAC
805 C
806 C      STRUCTURAL DAMPING LOAD
807 C
808   450  CONTINUE
809 C
810 C      SET UP UNBALANCED LOAD VECTOR
811 C
812   460  IF (KBAL.EQ.0) GO TO 470
813        SFUB=(BMIUB+BMJUB)/FL
814        DD(1)=-SFUB*SINA-FOUB*COSA
815        DD(2)=SFUB*COSA-FOUB*SINA
816        DD(3)=BMIUB
817        DD(4)=-DD(1)
818        DD(5)=-DD(2)
819        DD(6)=BMJUB
820        IF (EC(1).EQ.1.23456E10) GO TO 470
821        DD(3)=DD(3)-DD(1)*EC(3)+DD(2)*EC(1)
822        DD(6)=DD(6)-DD(4)*EC(4)+DD(5)*EC(2)
823 C
824 C      EXTRACT ENVELOPES
825   470  DO 490 I=1,8
826 C
827        S=BMTOT(I)
828        IF (S.LE.SENP(I)) GO TO 480
829        SENP(I)=S
830        TENP(I)=TIME
831   480  IF (S.GE.SENN(I)) GO TO 490
832        SENN(I)=S
833        TENN(I)=TIME
834   490  CONTINUE
835 C      SERCH FOR ABSOLUTE SHEAR AND MOMENT ENVELOPES
836 C      ENVM(NODI,2)=SENP(1)
837 C      TNVM(NODI,2)=TENP(1)
838 C      IF (-SENN(1).GT.SENP(1)) ENVM(NODI,2)=-SENN(1)
839 C      IF (-SENN(1).GT.SENP(1)) TNVM(NODI,2)=TENN(1)
840 C      ENVM(NODJ,1)=SENP(2)
```

```
C       TNVM(NODJ,1)=TENP(2)
C       IF (-SENN(2).GT.SENP(2)) ENVM(NODJ,1)=-SENN(2)
C       IF (-SENN(2).GT.SENP(2)) TNVM(NODJ,1)=TENN(2)
C
C       ENVSH(NODI,2)=SENP(3)
C       TNVSH(NODI,2)=TENP(3)
C       IF (-SENN(3).GT.SENP(3)) ENVSH(NODI,2)=-SENN(3)
C       IF (-SENN(3).GT.SENP(3)) TNVSH(NODI,2)=TENN(3)
C       ENVSH(NODJ,1)=SENP(4)
C       TNVSH(NODJ,1)=TENP(4)
C       IF (-SENN(4).GT.SENP(4)) ENVSH(NODJ,1)=-SENN(4)
C       IF (-SENN(4).GT.SENP(4)) TNVSH(NODJ,1)=TENN(4)
C
C       PRINT TIME HISTORY
C
        ISAVE=0
        IF (KPR.LT.0) GO TO 500
        IF (KPR.EQ.0.OR.KOUTDT.EQ.0) GO TO 560
        IF (ITHP.GT.1) GO TO 540
  500   IF (IHED.NE.0) GO TO 520
        KKPR=IABS(KPR)
        WRITE(6,510) KKPR,TIME
  510   FORMAT(///18H RESULTS FOR GROUP,I3,
       1        28H, R.C. BEAM ELEMENTS, TIME =,F8.3///5X,
       2        5H ELEM,4X,4HNODE,3X,5HYIELD,6X,7HBENDING,7X,5HSHEAR,
       3        7X,5HAXIAL,7X,13HCURRENT HINGE,8X,
       4        35HACCUMULATED PLASTIC HINGE ROTATIONS/5X,
       5        5H  NO.,4X,4H NO.,3X,5H CODE,6X,7H MOMENT,7X,5HFORCE,
       6        7X,5HFORCE,9X,9HROTATIONS,7X,
       7        40HPRIM POS  PRIM NEG    SECD POS  SECD NEG/)
        IHED=1
  520   WRITE(6,530) IMEM,(NOD(I),KODY(I),BMTOT(I),SFTOT(I),
       1  FTOT(I),RTOT(I), ROTPP(I),ROTPN(I),ROTSP(I),ROTSN(I),I=1,2)
  530   FORMAT(I9,I8,I7,3X,3F12.2,7X,F10.6,6X,2F10.6,2X,2F10.6/
       1        9X,I8,I7,3X,3F12.2,7X,F10.6,6X,2F10.6,2X,2F10.6)
        WRITE(6,8973) EKHIP,EKH(1),EKEPP(1,1),EKEPP(1,2),
       1    EKEP(1,1),EKEP(1,2)
 8973   FORMAT(/6E12.4)
        WRITE(6,8966) BCRN,BCRP,BCRTN,BCRTP
 8966   FORMAT(10X,4E12.4)
C
C       SET TIME HISTORY IN /THIST/
C
  540   IF (ITHP.LT.1.OR.KOUTDT.EQ.0) GO TO 560
        KKPR=IABS(KPR)
        ITHOUT(1)=KKPR
        ITHOUT(2)=9
        ITHOUT(3)=IMEM
        ITHOUT(4)=KODY(1)
        ITHOUT(5)=KODY(2)
        ITHOUT(6)=NODI
        ITHOUT(7)=NODJ
        DO 550 I=1,16
  550   THOUT(I)=BMTOT(I)
        THOUT(17)=TIME
        ISAVE=1
C
C       SET INDICATOR FOR SIFFNESS CHANGE
  560   KST=0
        IF (KODYX(1).NE.KODY(1).OR.KODYX(2).NE.KODY(2)) KST=1
C
        IF (EKH(1).NE.EKHIP.OR.EKH(2).NE.EKHJP) KST=1
C
C       UPDATE INFORMATION IN COMS
C
        DO 570 J=35,177
  570   COMS(J)=COM(J)
        COMS(2)=COM(2)
C
        RETURN
        END
```

```
 1 START     83.12.02 RESPONSE OF HOLIDAY INN BUILDING BY SAN FERNAND
 2    53   53     0     1   11   28    2                60000
 3     1    0.0       0.0
 4     2  241.0       0.0
 5     3  491.0       0.0
 6     4  732.0       0.0
 7     5    0.0     157.0
 8     6  241.0     157.0
 9     7  491.0     157.0
10     8  732.0     157.0
11     9    0.0     262.25
12    10  241.0     262.25
13    11  491.0     262.25
14    12  732.0     262.25
15    13    0.0     366.75
16    14  241.0     366.75
17    15  491.0     366.75
18    16  732.0     366.75
19    17    0.0     471.25
20    18  241.0     471.25
21    19  491.0     471.25
22    20  732.0     471.25
23    21    0.0     575.75
24    22  241.0     575.75
25    23  491.0     575.75
26    24  732.0     575.75
27    25    0.0     680.25
28    26  241.0     680.25
29    27  491.0     680.25
30    28  732.0     680.25
31    29    0.0     784.5
32    30  241.0     784.5
33    31  491.0     784.5
34    32  732.0     784.5
35    33  120.5     157.0
36    34  611.5     157.0
37    35  120.5     262.25
38    36  611.5     262.25
39    37  120.5     366.75
40    38  611.5     366.75
41    39  120.5     471.25
42    40  611.5     471.25
43    41  120.5     575.75
44    42  611.5     575.75
45    43  120.5     680.25
46    44  611.5     680.25
47    45  120.5     784.5
48    46  611.5     784.5
49    47  366.0     157.0
50    48  366.0     262.25
51    49  366.0     366.75
52    50  366.0     471.25
53    51  366.0     575.75
54    52  366.0     680.25
55    53  366.0     784.5
56     1    1     1     1     4
57     2    7     5     9    13    17    21    25    29
58     2    7     6    10    14    18    22    26    30
59     2    7     7    11    15    19    23    27    31
60     2    7     8    12    16    20    24    28    32
61     1    7     5     6     7     8    33    34    47
62     1    7     9    10    11    12    35    36    48
63     1    7    13    14    15    16    37    38    49
64     1    7    17    18    19    20    39    40    50
65     1    7    21    22    23    24    41    42    51
66     1    7    25    26    27    28    43    44    52
67     1    7    29    30    31    32    45    46    53
68     5   43.50                                        386.4
69     6   87.30                                        386.4
70     7   87.30                                        386.4
71     8   43.50                                        386.4
72     9   36.96                                        386.4
73    10   74.26                                        386.4
74    11   74.26                                        386.4
75    12   36.96                                        386.4
76    13   36.96                                        386.4
77    14   74.26                                        386.4
78    15   74.26                                        386.4
79    16   36.96                                        386.4
80    17   36.96                                        386.4
81    18   74.26                                        386.4
82    19   74.26                                        386.4
```

```
 83    20  36.96                                                  386.4
 84    21  36.96                                                  386.4
 85    22  74.25                                                  386.4
 86    23  74.26                                                  386.4
 87    24  36.96                                                  386.4
 88    25  36.96                                                  386.4
 89    26  74.26                                                  386.4
 90    27  74.26                                                  386.4
 91    28  36.96                                                  386.4
 92    29  34.72                                                  386.4
 93    30  69.74                                                  386.4
 94    31  69.74                                                  386.4
 95    32  34.72                                                  386.4
 96     0    0 2998  0.01       0.394       1.0                        1.0
 97  1500    0    0    0  SAN FERNAND EARTHQUAKE RECORDS AT HOLIDAY INN
 98   0.0    0.0  0.02   2.3  0.04  -1.1  0.06   0.4  0.08  -4.5  0.10  -7.2
 99   0.12   4.4  0.14   5.3  0.16   2.7  0.18   9.8  0.20  20.5  0.22  25.8
100  0.24  19.1  0.26   0.2  0.28 -11.0  0.30 -11.9  0.32  -7.7  0.34 -10.1
101  0.36  -2.4  0.38   6.4  0.40  12.8  0.42  16.7  0.44  21.4  0.46  21.3
102  0.48  16.6  0.50  11.8  0.52   7.2  0.54   0.5  0.56  -8.7  0.58 -11.1
103  0.60   1.7  0.62  11.2  0.64   7.7  0.66  -7.0  0.68 -12.2  0.70   0.4
104  0.72   6.5  0.74  -1.8  0.76  -7.9  0.78  -3.7  0.80  15.0  0.82  19.4
105  0.84   6.5  0.86  -8.8  0.88 -17.3  0.90  -4.4  0.92  16.5  0.94  10.0
106  0.96   0.8  0.98  -4.6  1.00 -10.7  1.02 -17.0  1.04 -14.0  1.06   5.8
107  1.08  15.4  1.10   7.2  1.12   9.7  1.14  15.2  1.16  15.3  1.18  14.1
108  1.20  -1.5  1.22  -4.6  1.24   5.2  1.26   2.5  1.28   3.5  1.30   8.5
109  1.32  14.2  1.34  23.0  1.36  20.3  1.38   4.6  1.40  -2.7  1.42   3.0
110  1.44   3.8  1.46  -8.3  1.48 -17.3  1.50   0.6  1.52  18.4  1.54  13.5

345 29.64  13.3 29.66  13.7 29.68  13.0 29.70  11.9 29.72   9.0 29.74   4.5
346 29.76  -0.7 29.78  -5.1 29.80  -6.6 29.82  -4.8 29.84  -4.0 29.86  -3.9
347 29.88  -4.1 29.90  -6.2 29.92  -8.5 29.94 -10.6 29.96 -12.1 29.98 -14.0
348      0.0       0.02       0.0
349     2    2 2998    7    0    7    0    0    2    2    2   10   10
350     5    9   13   17   21   25   29
351     5    9   13   17   21   25   29
352     6   28    2    0    1    0    0
353     1 0.2890+00 0.1070+07    0.0      4.0  4.0  2.0    1.0       1.0
354     1 0.2890+00 0.2890+00    0.5        0.5       0.5       0.5       1.0
355     2 0.3080+00 0.9240+6     0.0      4.0  4.0  2.0    1.0       1.0
356     2 0.3080+00 0.3080+00    0.5        0.5       0.5       0.5       1.0
357     1       100000.  -100000.
358     1    1    5    4    2         1    1
359     8    2    6    4    1         1    1
360    15    3    7    4    1         1    1
361    22    4    8    4    2         1    1
362    28   28   32         2         1    1
363     9   42   10    4   11
364     1 3168000.  594000.     0.0      4.0  4.0  2.0 0.617000    1.0
365     1    70000.1000000000.     0.2        0.2       0.3       0.3       1.0
366 0.723000    1.0          70000.1000000000.    1.0
367     2 3168000.  594000.     0.0      4.0  4.0  2.0 0.393000    1.0
368     2    80000.1000000000.     0.2        0.2       0.3       0.3       1.0
369 0.147000    1.0          140000.1000000000.    1.0
370     3 3168000.  594000.     0.0      4.0  4.0  2.0 0.449000    1.0
371     3    90000.1000000000.     0.2        0.2       0.3       0.3       1.0
372 0.468000    1.0          100000.1000000000.    1.0
373     4 3168000.  594000.     0.0      4.0  4.0  2.0 0.444000    1.0
374     4    90000.1000000000.     0.2        0.2       0.3       0.3       1.0
375 0.179000    1.0          150000.1000000000.    1.0
376     5 3168000.  594000.     0.0      4.0  4.0  2.0 0.652000    1.0
377     5    90000.1000000000.     0.2        0.2       0.3       0.3       1.0
378 0.567000    1.0          110000.1000000000.    1.0
379     6 3168000.  594000.     0.0      4.0  4.0  2.0 0.556000    1.0
380     6    90000.1000000000.     0.2        0.2       0.3       0.3       1.0
381 0.162000    1.0          160000.1000000000.    1.0
382     7 3800000.  630000.     0.0      4.0  4.0  2.0 0.759000    1.0
383     7    90000.1000000000.     0.2        0.2       0.3       0.3       1.0
384 0.388000    1.0          140000.1000000000.    1.0
385     8 3800000.  630000.     0.0      4.0  4.0  2.0 0.577000    1.0
386     8    90000.1000000000.     0.2        0.2       0.3       0.3       1.0
387 0.153000    1.0          170000.1000000000.    1.0
388     9 6900000.  832500.     0.0      4.0  4.0  2.0 0.455000    1.0
389     9   140000.1000000000.     0.2        0.2       0.3       0.3       1.0
390 0.217000    1.0          220000.1000000000.    1.0
391    10 6900000.  832500.     0.0      4.0  4.0  2.0 0.504000    1.0
392    10   140000.1000000000.     0.2        0.2       0.3       0.3       1.0
393 0.133000    1.0          280000.1000000000.    1.0
394          0.5        0.5        0.5        0.5
395     1   10.0       0.0
396     2   -9.0       0.0
397     3    9.0       0.0
398     4  -10.0       0.0
399     1          435.     -915.
400     2          310.     -275.0
```

```
401      3          465.     -1000.
402      4          320.      -285.
403      5          520.     -1000.
404      6          395.      -285.
405      7          550.     -1000.
406      8          425.      -285.
407      9          900.     -1300.
408     10          575.      -370.
409     11       100000.   -100000.
410      1     5    33         9     1    9    11          1
411      2     9    35         7     1    7    11
412      3    13    37         5     1    5    11          1
413      4    17    39         5     1    5    11
414      5    21    41         5     1    5    11
415      6    25    43         3     1    3    11
416      7    29    45         1     1    1    11          1
417      8     6    33        10     2   10    11          1
418      9    10    35         8     2    8    11
419     10    14    37         6     2    6    11          1
420     11    18    39         6     2    6    11
421     12    22    41         6     2    6    11
422     13    26    43         4     2    4    11
423     14    30    45         2     2    2    11          1
424     15     6    47        10     3   10    11
425     16    10    48         8     3   10    11
426     17    14    49         6     3    6    11
427     18    18    50         6     3    6    11
428     19    22    51         6     3    6    11
429     20    26    52         4     3    4    11
430     21    30    53         2     3    2    11          1
431     22     7    47        10     2   10    11
432     23    11    48         8     2    8    11
433     24    15    49         6     2    6    11          1
434     25    19    50         6     2    6    11
435     26    23    51         6     2    6    11
436     27    27    52         4     2    4    11
437     28    31    53         2     2    2    11          1
438     29     7    34        10     3   10    11
439     30    11    36         8     3    8    11
440     31    15    38         6     3    6    11          1
441     32    19    40         6     3    6    11
442     33    23    42         6     3    6    11
443     34    27    44         4     3    4    11
444     35    31    46         2     3    2    11
445     36     8    34         9     4    9    11
446     37    12    36         7     4    7    11
447     38    16    38         5     4    5    11          1
448     39    20    40         5     4    5    11
449     40    24    42         5     4    5    11
450     41    28    44         3     4    3    11
451     42    32    46         1     4    1    11          1
452 STOP
```

APPENDIX D

PREDICTION OF ULTIMATE CAPACITIES OF TEST SPECIMENS IN ACCORDANCE WITH MOMENT TRANSFER PROVISIONS OF ACI CODES 318-77 AND 318-83

Section		Page
D.1	Code-Provisions	
1.1	Shear Stresses	2
1.2	Unbalanced Moment	2
D.2	Committee 426 Recommendations	
2.1	General	3
2.2	Interior Column Connection	6
2.3	Exterior Column Connection	7
2.4	Corner Column Connection	9
D.3	Comparison of Measured and Predicted Behavior and Strength	
3.1	Interior Column Connections	10
3.2	Edge Column Connections Transferring Moments Normal to Edge	13
3.3	Edge Column Connections Transferring Moments Parallel to Edge	22
3.4	Corner Column Connections	30
D.4	Conclusions	34

PREDICTION OF ULTIMATE CAPACITIES OF TEST SPECIMENS IN ACCORDANCE WITH MOMENT TRANSFER PROVISIONS OF ACI CODES 318-77 AND 318-83

D.1 Code Provisions

D.1.1 Shear Stresses

In ACI Codes 318-77 and 318-83, Sec. 11.12.1.4, it is specified that shear stresses shall be taken as varying linearly about the centroid of the critical section and that the maximum shear stress, v_c, due to factored shear forces and moments shall not exceed $\phi(2 + 4/\beta_c)\sqrt{f'_c}$ and be not greater than $\phi 4\sqrt{f'_c}$.

ACI Code 318-77 did not specify procedures for connections with shear reinforcement and the Commentary showed expressions, and appropriate dimensions, for interior column-to-slab connections only. Thus, there was considerable ambiguity as to the procedures appropriate for connections with shear reinforcement and the expressions (and critical sections) that should be used for exterior and corner column-to-slab connections. ACI Code 318-83 does specify a procedure for connections with shear reinforcement. The shear strength V_n is taken as V_c plus V_s where v_c is limited to $2\sqrt{f'_c}$ and V_n to $6\sqrt{f'_c}\, b_o d$.

D.1.2 Unbalanced Moment

Section 13.2.4.2 of ACI Code 318-77 and 13.3.3.2 of ACI 318-83 specified that the fraction of the unbalanced moment given by:

$$\gamma_t = \frac{1}{1 + 2/3\sqrt{(c_1 + d)/(c_2 + d)}} \qquad \text{D.1}$$

should be considered transferred by flexure over an effective slab width between lines that are one and one-half slab or drop

panel thickness (1.5h) outside opposite faces of the column or capital. Concentration of reinforcement within that width could be used to resist that moment. The fraction of the unbalanced moment not transferred by flexure had to be transferred by shear according to Section 11.12.1.4.

D.2 Committee 426 Recommendations (29)

D.2.1 General

Because of the ambiguity in ACI 318-77 provisions, Committee 426 made extensive recommendations (29) for interpretation of the ACI Code and Commentary. Those recommendations are elaborated here. A similar elaboration is presented in Park and Gamble's text Reinforced Concrete Slabs (27).

Shown in Figs. D.1, D.2, and D.3 are the manner in which the shear-moment interaction relationships for ACI Code 318-77 are interpreted in this report for interior, exterior, and corner column connections, respectively. The notation used is that of Reference 29.

In each diagram, ordinates V_u/V_o are ratios of the shear transferred to the column, V_u, to the shear capacity, V_o, for shear transfer only. Abscissas M_{ub}/M_o are ratios of the moment transferred by shear, $(1 - \gamma_t) M_{ub}$, to the moment transfer capacity $(1 - \gamma_t) M_o$ when there is no simultaneous shear transfer. Thus, a fraction $(1 - \gamma_t)$ of M_{ub} is assumed to be transferred by eccentricity of the shear stresses. The remaining fraction γ_t of M_{ub} must be transferred by reinforcement within lines one and one-half times the slab thickness, 3h/2 or c_t whichever is less, either side of the column.

The maximum shear stress, v_{AB}, in the direction in which the shear stress due to shear transfer is additive with the shear stress due to moment transfer is given by:

$$v_{AB} = \frac{V_u}{A_c} + \frac{(1 - \gamma_t) M_{ub} c_{AB}}{J_c} \qquad D.2$$

where M_{ub} = design moment acting about centroid of critical section and to be transferred to the column.

c_{AB} = distance of face AB from centroid of critical section.

J_c = polar moment of inertia for critical section.

A_c = area of critical section.

The maximum shear stress, v_{CD}, in the direction in which the shear stress due to moment transfer acts in the opposite direction to that due to shear transfer is given by:

$$v_{CD} = \frac{V_u}{A_c} - \frac{(1 - \gamma_t) M_{ub} c_{cp}}{J_c} \qquad D.3$$

The expressions proposed by Committee 426 for A_c, J_c, C_{AB}, C_{CD} and γ_t for interior, exterior and corner column connections are shown on Figs. D.1, D.2, and D.3, respectively. From Figs. D.2 and D.3, it can be seen that where the centroids of the critical section and the column do not coincide M_{ub} is given by:

$$M_{ub} = M_u - V_u g \qquad D.4$$

where M_u = factored design moment transferred to column.

g = eccentricity of centroid of column from centroid of critical section.

For slabs without shear reinforcement, Committee 426 recommended that the shear stress calculated from Eqs. D.2 and D.3 must not exceed a limiting shear stress, v_c, for normal weight concrete given by:

$$v_c = (2 + 4/\beta_c)\sqrt{f'_c} \leq 4\sqrt{f'_c} \qquad \text{D.5}$$

For slabs with shear reinforcement Committee 426 recommended that the shear stress, v_u, on any column face must not exceed the larger of the values given by Eqs. D.5 and D.6.

$$v_u = \frac{v_c}{2} + A_v f_y / b_o s \qquad \text{D.6}$$

where $A_v f_y$ = yield strength of stirrups crossing a potential inclined crack extending at 45 degrees from the compressive surface of the slab and a perimeter located d/2 closer to the loaded area than the critical section under consideration.

b_o = perimeter of critical section under consideration.

s = spacing of stirrups in direction perpendicular to perimeter of critical section.

It can be seen that if Eq. D.2 is divided by Eq. D.5, then:

$$v_{AB}/v_c = \frac{V_u}{V_o} + \frac{M_{ub}}{M_o} \qquad \text{D.7}$$

where $V_o = \phi v_c A_c$

and $M_o = \phi \frac{v_c J_c}{C_{AB}}$

Thus, in each of Figs. D.1, D.2 and D.3 ordinates are the first terms of Eqs. D.2 or D.3 divided by ϕv_c or ϕv_u as appropriate and abscissas are the second term also divided by ϕv_c or ϕv_u.

D.2.2 Interior Column Connection

In Fig. D.1 line ab represents the condition where maximum shear stresses are limited according to Eq. D.2 divided by ϕv_c. Appropriate shear stress distributions are shown for three positions along ab. Line cd represents the cut-off on the moment transfer capacity that is imposed when there is insufficient reinforcement within lines 1.5h either side of the column to resist the moment not transferred by shear. As illustrated in Fig. D.1(a), that moment cut-off equals the sum of the flexural capacities of the top and bottom reinforcement between lines 1.5h either side of the column provided there is adequate distance between opposite faces of the column to develop through bond the yield strength of that reinforcement (13, 42, 43).

The geometric proportions for the connection and the concrete strength are the sole factors dictating the position of the line ab in Fig. D.1. The amount of reinforcement within the column region affects only the position of line cd. Test results (2, 43) indicate a behavior not far from that idealization. Measured strengths lie along curves such an amn. For a 3,000 psi concrete (21 Mn/m^2) that curve lies progressively further outside the envelope acd as the reinforcement ratio within lines 1.5h either side of the column increases above 0.8%. The reverse is true as ratios decrease below 0.8%.

For combinations of shear and moment lying to the right of line oe in Fig. D.1, Eq. D3 predicts a shear stress on face CD opposite in sign to that on face AB. Those shears create tensions at the intersection of the bottom surface of the slab and the column, and in tests (43, 44) cracking develops at that intersection for V and M combinations to the right of a curve such as fjg. Shear stresses for cracking range from 0.2 to 0.8 $\sqrt{f'_c}$ since tensile stresses at CD increase rapidly once yielding occurs in the top reinforcement passing through face AB. Thus, to control cracking, the Suggested Revisions required bonded bottom reinforcement within lines 1.5h either side of the column at least equal to the amount for shrinkage and temperature effects.

For V and M combinations to the right of curve fjg, the bottom reinforcement through the face CD and the top reinforcement through the face AB are stressed in tension. If, as shown in Fig. D.1(a), the top bars have development lengths, ℓ_d, greater than the column dimension c in the direction of that reinforcement, then tensile forces, T_3 and T_2, develop in both top and bottom bars, respectively, at face CD. Consequently, to avoid an over-reinforced condition, the Suggested Revisions required that the sum of the ratios for the top and bottom reinforcement considered effective for moment transfer should not exceed $0.75p_b$.

D.2.3 Exterior Column Connection

Interaction relationships for a slab connected to a protruding exterior column with moments transferred normal to the discontinuous edge are shown in Fig. D.2. The moment acting

about the centroid of the critical section equals the moment transferred to the column M, less a moment equal to the shear, V, times the eccentricity, g, of the centroid of the critical section from the centroid of the column. For line ab the maximum shear stress is limited by Eq. D.2 to v_c, while line cd indicates the capacity of the reinforcement within lines 1.5h or c_t, either side of the column. That reinforcement must transfer the moment $\gamma_t(M-V_u g)/\phi$ not transferred by shear stresses. The line ef represents the limitation imposed by Eq. D.3 for v_{CD} equal to v_c. The value of V_u/V_o at which that limitation control depends on the geometry of the connection. For a square column having its exterior edge coincident with the discontinuous edge of the slab, Eq. D.3 controls for $2\sqrt{f'_c}$ values less than 0.28. Strengths measured in tests lie along a curve such as amn. Measured strengths have increased with increasing reinforcement ratios within lines 1.5h either side of the colum and have been greater than the predicted strengths for ratios as low as 0.5% (2).

Limitation of the shear stresses according to Eqs. D.2 and D.3 ensures adequate ultimate strength only. Shear or torsional cracks develop, as indicated in Figs. 5(a) and (b), at shear stresses less than those for failure. Torsional cracks occur for conditions to the right of a line such as gh in Fig. D.2 when the upward shear stress at the discontinuous edge, calculated according to Eq. D.3, reaches about $1.5\sqrt{f'_c}$ for both reinforced and prestressed concrete (8). Shear cracks occur for conditions to the left of a line such as jk when the downward shear stress at the discontinuous edge reaches about $2\sqrt{f'_c}$.

The procedures detailed in Fig. D.2 are for slabs without edge beams. Section 7.9.6 of the Suggested Revisions provides additional information for slabs with edge beams. If the edge beam has a torsional capacity greater than the exterior negative moment assigned to the slab strip framing into that beam, then all shear can be assumed to flow to the column through the edge beam. If that condition does not exist, then the reinforcement at the slab edge and adjacent to the column must be detailed so that it can control the opening of the torsional cracks shown in Fig. D.2(d). For slabs with shallow or no edge beams such cracks are possible at service loads. Reinforcement details satisfying Section 7.9.6 are shown in Fig. D.2(d).

Where moments are transferred parallel to the discontinuous edge, analyses according to procedures similar to those for interior connections, yield conservative estimates of measured strengths (2, 7).

D.2.4 Corner Column Connection

Interaction relationships for a slab-corner column connection are shown in Fig. D.3. Such a connection usually transfers biaxial moments and therefore abscissas are expressed as the sum of the two moment components, $(M_x - V_u g_x)/M_{ox}$ and $(M_y - V_u g_y)/M_{oy}$, where subscripts x and y refer to properties in the x and y directions. Shear stresses are assumed to vary linearly across each column face. The maximum stress occurs at point A on the critical section, and stresses at A, B, and D are given by Eqs. (Ca), (Cb), and (Cc) shown on Fig. D.3. Those equations are biaxial forms of Eqs. D.2 and D.3. For line ab on Fig. D.3 the stress at A is limited according to Eq. (Ca) to v_c. For biaxial

bending there is seldom difficulty in transferring the portion of the moment not transferred by shear and therefore no cut-off line appears on Fig. D.3. However, for predominately single axis bending, that cut-off can govern and the corresponding capacity should be checked. Line ef is the limitation imposed by Eq. (Cb) or (Cc) when the stress at B or D equals v_c. That likelihood increases as the moment transfer becomes increasingly uniaxial. Limitation of the downward shear stress at the edge to about $2\sqrt{f'_c}$, line jk, or the upward shear stress to $1.4\sqrt{f'_c}$, line gh, is necessary to avoid shear and torsional cracking, respectively, at the slab edge. Strengths measured in tests lie along a curve such as amn. As is also the case for interior and exterior connections, measured strengths have increased with increasing reinforcement ratios within the column region. Measured strengths have been greater than the predicted for all reinforcement ratios test to date (2).

D.3 Comparison of Measured and Predicted Behavior and Strength

D.3.1 Interior Column Connections

The properties of the 21 interior volumn-slab subassemblages tested in this investigation are shown in Table A.1(a), and the results of applying the ACI Code 318-77 and 83 provisions to predictions of the measured strengths of those specimens are summarized in Table D1. ϕ values are taken as unity in those predictions. Eight (8) of the specimens contained no shear reinforcement and thirteen (13) contained integral beam stirrup reinforcements. Moment transfer strengths, as limited by shear stresses in the slab, are examined as if all specimens were

without shear reinforcement. In all specimens, the shear reinforcement was such as to provide a V_n value greater than the limiting value of $6\sqrt{f'_c}$ in ACI 318.

In Table D.1, Col. (1) lists the specimen, Col. (2) the dimensions c_1 x c_2 of the column, and Col. (3) lists the reinforcment ratio ρ_t for the top slab steel within lines 3h/2 either side of the column.

Columns (4) and (5) list the shear and moment transfer to the column at the maximum load achieved in the test. Columns (6) and (7) list the ratios of those values to the quantities V_o and M_o which are defined in Eq. D.7. Specimens S1 through S7 all failed due to shear punching adjacent to the most heavily loaded face of the column. For all specimens except S3, the sum of the quantities V_{TEST}/V_o and M_{TEST}/M_o exceeds 1.0 for specimens without shear reinforcement, and thus the ACI 318 provisions for shear limitations on the moment transfer capacity are conservative for those specimens. Further, the quantity listed in Col. (8) increases as the reinforcement ratio for the slab, Col. (3), in the vicinity of the column increases. Specimens S3 and S8 had the lowest reinforcment ratio with only 0.55% top steel in the column vicinity, S8, failed with the development of a yield line extending across the full width of the slab at the column face. Specimen S3, however, failed in shear. Apparently the shear capacity can decrease with reversed cyclic loading when the slab steel in the column vicinity is stressed well into its inelastic range. For the specimens with shear reinforcement, values in Col. 8 exceed 1.5, (corresponding to a limiting shear stress of

6 $\sqrt{f'_c}$), for all specimens except SS2, SS5 and SS6 which had the lowest ρ_t values.

Column (9) lists the moment resisting capacities of the top and bottom reinforcement, M_{RES}, within lines one and one-half times the slab thickness (3h/2) either side of the column. As indicated by the footnote, that capacity is limited to the capacity for ρ_{bal} if the column dimension in the direction of moment transfer is less than the development length for the larger bar passing through the column. That condition controlled for specimens with large amounts of reinforcement concentrated in the column vicinity (S5, SS3, and SS4) and for specimens with small column dimensions (8 in.) in the direction of moment transfer. Ratios of the fraction of the moment presumed to be transferred by flexure to M_{RES} are listed in Col (10). Values equal or exceed unity for three specimens SS1, SS2, SS3, SS5, and SS12. All of those specimens, except SS2, failed due to excessive twisting actions centered on the column, but did not punch at the column; SS2 punched at the column.

Column (11) lists the moment, M_s, of all forces acting to one side of a line extending across the width of the slab at the column face. That line was the predicted yield line location for a flexural failure of one half of the slab. Ratios of M_s to the flexural capacity, M_{FLEX}, in negative bending of the reinforcement crossing that line are listed in Col. (12). Ratios exceed unity for specimens S8 and SS8 through SS13, all of which exhibited flexural failures.

Observed failure modes are listed in Col. (13). Three specimens, SS4, SS6, and SS7, had premature shear failures

associated with investigation of the criteria governing the appropriate amount and extent of the stirrup reinforcement. It is apparent that the ACI Code procedures, interpreted as indicated in the foregoing section, are likely to predict correctly the mode of failure. Average values of measured to computed capacity are 1.30 for a punching failure for specimens without shear reinforcement; 1.12 for a moment cut-off failure; and 1.12 for a flexural failure. Ranges about those means are +0.25 to -0.41 for a punching failure; +0.14 to -0.12 for a moment cut-off failure; and +0.07 to -0.08 for a flexural failure. Those ranges suggest that reasonable confidence can be associated with the moment cut-off and flexural limitation calculations, but not with the shear calculations. Obviously, in the latter case the shear resistance needs to be made dependent on the reinforcement ratio within the immediate region of the column.

D.3.2 Edge Columns Connections Transferring Moments Normal to Edge

D.3.2.1 Detailed Analyses

The properties of the 8 test specimens are shown in Table A.1(c). The results of applying the ACI Code 318-77 and 83 provisions to predictions of the measured strengths of those specimens are summarized in Table D.2. ϕ values are taken as unity in the analyses.

Lines 1 through 8 list geometric properties of the critical section. Lines 9 through 17 list relevant forces, stresses, and moments. Lines 20 through 28 list relevant measured strengths and ultimate strength ratios. The quantity V_{TEST}, line 20, is

the total shear applied to the slab at the time M_{TEST}, line 21, was achieved. M_{TEST} is the maximum moment transferred to the column in the test. For these specimens, V_{TEST} equals the sum of the slab's dead weight, line 9; the gravity load shear, line 10; and the lateral load shear, line 11. M_{TEST} equals the moment about the column center of the slab's self-weight, the weight of the loading apparatus, the gravity load force, and the lateral load force.

The quantity M_{FLEX}, line 22, is the theoretical flexural capacity for a line extending across the full width of the slab at the front column face. M_{FLEX} was calculated from the known properties of the section, the concrete, and the reinforcing steel.

The quantity M_s, line 23, is the maximum moment caused by the gravity and lateral loads acting on one side of the line on which M_{FLEX} is calculated. Equilibrium analyses predict failure on that line for attainment of the theoretical flexural capacity of the specimens. The quantity M_s/M_{FLEX} is less than unity for all specimens, and therefore a flexural failure was not predicted for any of the specimens. Steel strains, measured in the tests, showed that in every case, yielding did not occur in all of the top bars across the width of the specimen prior to collapse. For specimen ES-4, however, only the outermost bars did not yield. That result is consistent with the M_s/M_{FLEX} value of 0.87 for that specimen.

In line 24 of Table D.2, the quantity V_{TEST} is compared with the shear strength, V_o, for a connection transferring zero moment, and containing no shear reinforcement. Thus, V_o equals

v_c, line 15, multiplied by A_c, line 4. In accordance with Eq. D.5, the quantity v_c equals $4\sqrt{f'_c}$ for the specimens with square columns, and $3.64\sqrt{f'_c}$ for those with rectangular columns. When the value of v_u for the specimens with shear reinforcement is evaluated according to Eq. D.6, then v_u equals about $8\sqrt{f'_c}$ at the front face of ES-2 and ES-4 and about $5.5\sqrt{f'_c}$ at the exterior edge of ES-1, ES-3, and ES-5. None of the values of V_{TEST}/V_o exceed 0.5 and it is to be expected that torsional rather than shear effects would control the behavior of these specimens.

On line 25, the moment M_R, acting about the centroid of the critical section for shear at M_{TEST} is listed, and on line 26 the ratio of M_R to M_{OFS} is listed, where M_{OFS} is the moment transfer capacity for zero shear transfer and a shear stress at the front face of the critical section limited to v_c (the quantity M_{OFS} equals $v_c J_c/C_{AB}$). On line 27, the ratio of M_R/M_{OBS} is listed where M_{OBS} is $v_c J_c/C_{CD}$.

On line 28 the ratio $\alpha_b M_R/M_{RES}$ is listed. The quantity $\alpha_b M_R$ is listed on line 16 and is the fraction of M_{TEST} to be transferred by flexure. The quantity M_{RES} is listed on line 17. It is the capacity in flexure of the reinforcement within lines 1.5h either side of the column.

On line 13, the shear stress at the front face, v_{AB}, calculated according to Eq. D.2 is listed, and on line 14, the shear stress at the back face v_{CD}, calculated according to Eq. D.3 is listed. The ratio v_{AB}/v_c is the same as the sum of the ratios on lines 24 and 26; and the ratio v_{CD}/v_c is the same as the sum of the ratio on line 27 less that on lines 24.

Listed on line 19 of Table D.2 for ES-2 and ES-4 are the resisting capacities, v_{STIRF} equal to v_u, Eq. D.5, taking into account the integral beam stirrups extending out from the front column face. The quantities v_{STIRB} on line 18 is the corresponding condition for the edge of the slab. In that case quantities are also listed for ES-1, ES-3, and ES-5, since the hairpins, placed at the edge for the specimens, had one leg effective as shear reinforcement.

For specimen E-1, torsional cracking developed at the back edge of the slab when about 80% of the gravity load had been applied. For that latter condition, V_{TEST}/V_o equalled 0.20 and M_R/M_{OFS} equalled 0.4. For a shear stress of $2\sqrt{f'_c}$ at the back edge, cracking was predicted at V_{TEST}/V_o of 0.15 and M_R/M_{OFS} of 0.3. The development of torsional cracking at the back edge did not lead immediately to failure. Failure occurred due to punching at the front column face. At failure the ratios of measured-to-predicted capacities were as follows:

1) shear failure at front column face, v_{AB}/v_c, 0.99
2) torsion at back edge, v_{CD}/v_c, 1.27
3) flexural failure across width of slab, M_x/M_{FLEX}, 0.41
4) flexural component of moment transfer in column head region, $\gamma_t M_R/M_{RES}$, 0.79

Thus, although a torsional failure at the edge was predicted, a capacity was reached very close to that predicted for a punching shear failure at the front face.

For specimen E-2, the column was larger than for E-1 and reinforcement was concentrated in the column head region.

Torsional cracking developed at the back edge when V_{TEST}/V_o equalled 0.24 and M_R/M_{OFS} equalled 0.32. Cracking at a shear stress of $2\sqrt{f'_c}$ was predicted at V_{TEST}/V_o equal to 0.23 and M_R/M_{OFS} equal to 0.30. Failure occurred due to punching at the front column face. For failure, the ratios of measured-to-predicted capacities were as follows:

1) shear failure at front column face, v_{AB}/v_C, 1.13
2) torsion at back edge, v_{CD}/v_C, 1.42
3) flexural failure, M_S/M_{FLEX}, 0.75
4) flexural component of moment transfer, $\gamma_t M_R/M_{RES}$, 0.99

Thus, although a torsional failure at the edge was predicted, a capacity was reached exceeding that for a shear failure at the front column face.

Specimen ES-1 had the same column size at E-1, flexural reinforcement concentrated in the column head region, and hairpin stirrups at the discontinuous edge. Failure occurred due to punching at the front column face. The hairpin stirrups restrained the opening of the torsion cracks at the back edge. For failure, ratios of measured-to-predicted capacities were as follows:

1) shear failure at front column face, v_{AB}/v_C, 1.30
2) torsion failure at edge, 1.24
   $(M_R/M_{OBS} - V_{TEST}/V_o)$, v_c/v_{STIRB},
3) flexural failure M_S/M_{FLEX}, 0.54
4) flexural component of moment transfer, $\gamma_t M_R/M_{RES}$, 0.66

Thus, failure in punching shear at the front column face was both predicted and observed.

For ES-2 Proportions, flexural reinforcement, and gravity loading were similar to those for ES-1. However, integral beam stirrup reinforcement, rather than hairpin hoops were used for ES-2. Failure could not be induced in the specimen within the limits of the testing equipment. It was found that the ultimate load capacity could still be maintained for edge deflections varying between 8 in. down for a lateral down load of 8 kips, and 1.5 in. down for an upward lateral load of 13 kips. For failure, ratios of measured-to-predicted capacities were as follows for downward lateral loading:

1) shear failure at front column face, $(M_R/M_{OFS} + V_{TEST}/V_o)\ v_c/v_{STIRF}$, 0.78
2) torsion failure at edge, $(M_R/M_{OBS} - V_{TEST}/V_o)\ v_c/v_{STIRB}$, 1.04
3) flexural failure, M_S/M_{FLEX}, 0.66
4) flexural component of moment transfer, $\gamma_t\ M_R/M_{RES}$, 0.80

Thus, a torsional failure was predicted at the edge, following yielding of the stirrup reinforcement. Large local deformations were to be expected and were observed.

For ES-3 Proportions, and flexural and shear reinforcement, were the same as for ES-1. However, the gravity load for ES-3 was made about two-thirds of that for ES-1. Failure was in punching around the column face, and large ductilities did not develop as was the case for ES-2. For failure ratios of measured-to-predicted capacities were as follows for downward lateral loading:

1) shear failure at front column face, v_{AB}/v_C, 1.27

2) torsion failure at edge, $(M_R/M_{OBS}-V_{TEST}/V_o)\ v_c/v_{STIRB}$, 1.37

3) flexural failure, M_S/M_{FLEX}, 0.58

4) flexural component of moment transfer, $\gamma_t\ M_R/M_{RES}$, 0.80

Thus, a punching shear failure was predicted starting at the edge and spreading around the column. That prediction was consistent with the observed behavior.

Specimen E-3 had a rectangular column with a front face 8 in. wide and torsional faces 19-1/2 in. deep. Reinforcement was concentrated in the column head region. Failure was in punching shear at the front column face. Torsional cracking developed at the back edge when V_{TEST}/V_o equalled 0.30 and M_R/M_{OFS} equalled 0.55. Cracking at a shear stress of $2\sqrt{f'_c}$ was predicted at V_{TEST}/V_o equal to 0.27 and M_R/M_{OFS} equal to 0.50. For failure ratios of measured-to-predicted capacities were as follows:

1) shear failure at front face, v_{AB}/v_C, 1.49

2) torsion failure at edge, v_{CD}/v_C, 1.40

3) flexural failure, M_X/M_{FLEX}, 0.59

4) flexural component of moment transfer, $\gamma_t\ M_R/M_{RES}$, 0.83

Thus, a punching shear failure at the front face was predicted and observed. However, the capacity reached was almost 50% greater than that predicted.

Specimen ES-4 was the same as E-3 except for the use of integral beam shear reinforcement. Failure could not be induced within the limits of the test equipment. Crushing of the concrete occurred at the front column face on the compression side of the slab for downward loading. Large rotations developed

that were concentrated on the column. The ultimate load capacity could still be maintained for edge deflections varying between 5.5 in. down for a lateral down load of 14 kips, and 0.8 in. down for an upward lateral load of 15 kips. For the maximum load, ratios of measured to predicted capacities were as follows for downward loading:

1) shear failure at front column face, $(M_R/M_{OFS} + V_{TEST}V_o)$, v_c/v_{STIRF}, 0.72
2) torsion failure at edge, $(M_R/M_{OBS} - V_{TEST}/V_o)$, v_c/v_{STIRB}, 0.73
3) flexural failure, M_S/M_{FLEX}, 0.87
4) flexural component of moment transfer, $\gamma_t M_R/M_{RES}$, 1.22

For ES-4 a failure due to inadequate flexural reinforcement, within line 1.5h either side of the column, to transfer the portion of the moment not transferred by shear was predicted. That prediction was consistent with the observed behavior and demonstrates clearly the need for adequate flexural reinforcement in the column head region.

Specimen ES-5 had a 19-1/2 by 8 in. column but with the 8 in. dimension as the torsional face. Hairpin stirrups were also provided at the back edge. Failure occurred following excessive deflections and crushing at the front column face. Torsional cracking at the back edge did not develop until V_{TEST}/V_o and M_R/M_{OFS} values double those predicted for a shear of $2\sqrt{f'_c}$. For the maximum load, ratios of measured-to-predicted capacities were as follows for downward lateral loading:

1) shear failure at front column face, v_{AB}/v_C, 1.43

2) torsion failure at edge, 1.91

$(M_R/M_{OBS} - V_{TEST}/V_o)$, v_c/v_{STIRB},

3) flexural failure, M_S/M_{FLEX}, 0.67

4) flexural component of moment transfer, $\gamma_t M_R/M_{RES}$, 0.66

The maximum upward lateral load applied to the specimen was 12 kips achieved at an upward deflection of 0.2 in.

The behavior of ES-5 was not in agreement with ACI Code predictions. The capacity that was achieved was almost double that predicted, and a ductile rather than the predicted brittle failure developed.

D.3.2.2 Summary

Measured and predicted capacities are summarized in Table D.3. Except for specimen ES-5, measured-and-predicted failure modes are in reasonable agreement. Five specimens were observed to have failed due to punching shear at the front column face. In three of those cases, shear failures were predicted to occur first at the edge. However, the use of a limiting shear stress of $4\sqrt{f'_c}$ at the front face, and neglect of conditions at the edge would still be safe. Nevertheless, it is also apparent that the use of hairpins increases the capacity for punching shear at the front face even though such stirrups do not provide any shear reinforcement at that face. For the five specimens failing in shear at the front face, measured-to-predicted capacities average 1.24 and the range about that mean is +0.24 to -0.25. Again, it is apparent that the shear capacity increases with increasing slab reinforcement anchored in the column vicinity.

The results for ES-2, ES-4, and ES-5 suggest that a limiting capacity based on a bending failure at the front face combined with a twisting failure at the side faces is needed. The use of a capacity based on the flexural capacity of the reinforcement within line 3h/2 either side of the column is not an adequate criterion.

D.3.3 Edge Column Connections Transferring Moments Parallel to Edge

D.3.3.1 Detailed Analyses

Properties for the five test specimens modeling the transfer of moments parallel to a slab's edge are shown in Table A.1(b). The measured and predicted capacities for those specimens, evaluated according to ACI Code 318-77 and 83 procedures, are summarized in Table D.4. Again, ϕ values are taken as unity for those evaluations. The arrangement for Table D.4 is similar to that for Table D.2. Lines 1 through 8 list geometric properties for the critical section which is assumed to have the form shown in Fig. D.4. The quantity d_{AB} is the effective depth for the front column face AB; c_m and c_t are the effective lengths of the critical section for shear at the front face AB and the torsion face AD, respectively, and J_{c1} and J_{c2} are the polar moments of inertia for moment transfer parallel and perpendicular to the discontinuous edge of the slab, respectively. The quantities γ_{t1} and γ_{t2} are the fraction of the moment acting about the centroid of the critical section that is assumed to be transferred from the slab to the column by flexure for directions parallel and perpendicular to the discontinuous edge, respectively.

The complete interaction diagram for the loading conditions on these connections would be a three-dimensional figure for which the diagram for a cut along one axis would be similar to the diagram for an interior column connection, Fig. D.1, less one torsion face, and for a cut along the other axis would be similar to the diagram for an exterior column transferring moment normal to the discontinuous edge, Fig. D.2. Thus, values of the shear stress are different for all four corners of the critical section and vary linearly between those locations. If M_1 is the moment transferred to the column parallel to the discontinuous edge, M_2 is the moment transferred perpendicular to that edge, and AB is the front face of the column, then the shear stress values at each corner of the critical section are:

$$v_A = \frac{V}{A_c} + (1-\gamma_{t1})\frac{M_1 (c_1+d)}{2J_{c1}} + (1-\gamma_{t2})\frac{(M_2-Vg)\, c_{AD}}{J_{c2}} \qquad D.8$$

$$v_B = \frac{V}{A_c} + (1-\gamma_{t1})\frac{M_1 (c_1+d)}{2J_{c1}} - (1-\gamma_{t2})\frac{(M_2-Vg)\, c_{BC}}{J_{c2}} \qquad D.9$$

$$v_C \quad \frac{V}{A_c} - (1-\gamma_{t1})\frac{M_1 (c_1+d)}{2J_{c1}} + (1-\gamma_{t2})\frac{(M_2-Vg)\, c_{AD}}{J_{c2}} \qquad D.10$$

$$v_D \quad \frac{V}{A_c} - (1-\gamma_{t1})\frac{M_1 (c_1+d)}{2J_{c1}} - (1-\gamma_{t2})\frac{(M_2-Vg)\, c_{BC}}{J_{c2}} \qquad D.11$$

The absolute value of each of those quantities would have to be limited to v_c as defined by Eq. D.5 or v_u as defined by Eq. D.6 for dense aggregate concrete connection without and with shear reinforcement, respectively.

Sufficient reinforcement would have to be placed within lines 1.5h either side of the column, for both the M_1 and M_2

directions to transfer the fraction of the moments $\gamma_{t1} M_1$ and $\gamma_{t2} (M_2 - Vg)$, respectively, that must be transferred by flexure.

Lines 9 through 17 list relevant forces, stresses, and moments. The shear stresses due to shear, line 12, equals the sum of the shear forces, lines 9 through 11, divided by the area of the critical section A_c. The shear stress at the inside corner v_A, line 13, is the maximum shear stress for moment transfer and is given by Eq. D.8. The shear stress at the outside corner, v_B, line 14, is the shear stress given by Eq. D.9. The minimum shear stress value, v_C, line 15, is the shear stress given by Eq. D.10.

The quantity $\gamma_{t1} M_{TEST}$, line 18, is the fraction of the moment M_{TEST} for the direction M_1 (Fig. D.4), assumed to be transferred to the column by flexure. The moment M_{RES}, line 19, is the capacity of the reinforcement top and bottom passing through the column head region for the M_1 direction and located between the specimen's edge and a line 1.5h outside the column face opposite that edge.

The quantities V_{TEST}, line 20, and M_{TEST}, line 21, have the same meaning as for Table D.2. The quantity M_2, line 22, is the moment transferred to the column in the M_2 direction (Fig. D.4). M_{FLEX}, line 23, is the theoretical flexural capacity for a line extending across the full width of the slab at face AB, Fig. D.4. The quantity M_s is the maximum moment caused by the gravity and lateral load acting about the line on which M_{FLEX} is calculated. Hence, the ratio M_s/M_{FLEX}, line 24, indicates the probability of the failure having been theoretically a flexural failure. Since

M_s/M_{FLEX} is less than unity for all specimens, a flexural failure is not predicted for any of the specimens.

The quantity V_o, line 25, is the limiting shear stress v_c, line 16, multiplied by the area of the critical section A_c, line 4. The ratio V_{TEST}/V_{FLEX} indicates the severity of the loading due to shear transfer on the connection. The largest ratio is 0.32. Thus, moment transfer rather than shear transfer effects, should have dominated the behavior of the test specimens.

On line 26 the moment M_{OFS1} is the moment transfer capacity for zero shear transfer and a shear stress on length AB, Fig. D.4 of the critical section, equal to v_c. M_{OFS1} equals $2\ v_c\ J_{c1}/(c_1 + d)$.

On line 27 $(M_2 - Vg)$ is the moment acting about the centroid of the critical section for shear for the M_2 direction, Fig. D.4, when M_{TEST} was acting in the M_1 direction. The moment M_{OFS2} is the moment transfer capacity for zero shear transfer and a shear stress on length AD, Fig. D.4, equal to v_c. M_{OFS2} equals $v_c\ J_{c2}/C_{AD}$. Similarly on line 28, the moment M_{OBS2} is the moment transfer capacity for an upward shear stress at edge BC, Fig. D.4 equal to v_c. M_{OBS2} equals $v_c\ J_{c2}/c_{BC}$.

For the discontinuous edge of the slabs, cracking through the depth of the slab adjacent to the column was plainly visible. The downward shear stress at B at failure, v_B, and the upward shear stress at C, Fig. D.4, at failure, v_C, are shown on lines 14 and 15, respectively, of Table D.2. Both those values exceed half the critical shear stress for the concrete, $v_{c/2}$, line 16, and therefore cracking was to be expected in shear at B and in

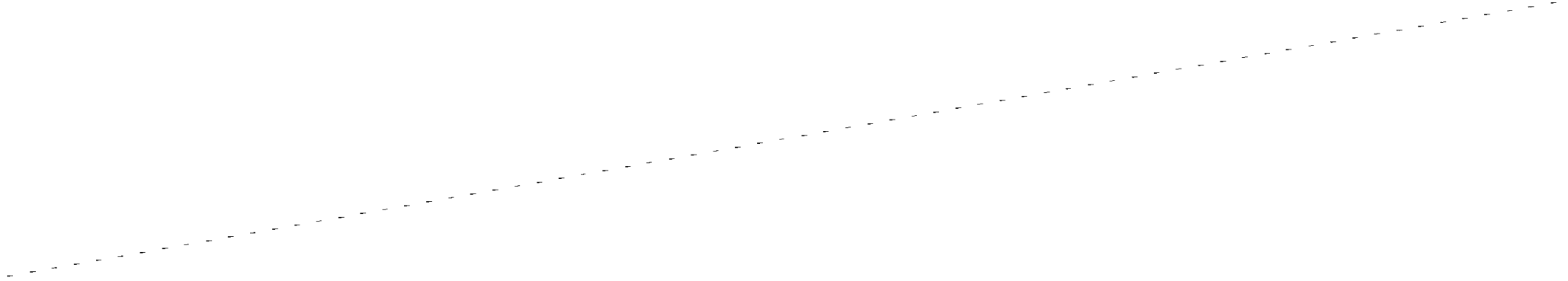

torsion at C. Cracking had occurred in that manner at both locations prior to failure.

Specimen EL-1 had a 12-in. square column, flexural reinforcement distributed evenly across the width of the slab and no shear reinforcement. Failure occurred due to punching that extended back from corner A, Fig. D.4, along faces AB and AD. At failure the ratios of measured to predicted capacities were as follows:

(1) shear failure at corner A, v_A/v_c, 1.17
or $V_{TEST}/V_o + M_{TEST}/M_{OFS1} + (M_2 - Vg)/M_{OFS2}$,

(2) torsion failure at corner C v_C/v_c, 0.83
or $V_{TEST}/V_o - M_{TEST}/M_{OFS1} - (M_2 - Vg)/M_{OBS2}$,

(3) flexural failure M_s/M_{FLEX}, 0.72

(4) flexural component of moment transfer, 0.87
$\gamma_{t1} M_{TEST}/M_{RES}$,

Thus, a punching failure is predicted at A and was observed. However, it should also be noted that the quantity $V_{TEST}/V_o + M_{TEST}/M_{OFS1}$ equals 1.00 so that the connection "carried free" the moment $(1 - \gamma_{t2}) M_B$ transferred by shear in the M_2 direction.

Specimen EL-2 had a 16-in. square column, flexural reinforcement concentrated in the column head region and no shear reinforcement. Failure occurred due to punching that extended back from corner A, Fig. D.4, along face AD and the entire length of AB. At failure ratios of measured to predicted capacities were as follows:

(1) shear failure at corner A, v_A/v_c, 1.09

(2) torsion failure at corner C, v_C/v_c, 0.72

(3) flexural failure, M_S/M_{FLEX}, 0.74

(4) flexural component of moment transfer, 0.99

$\gamma_{t1} M_{TEST}/M_{RES}$,

Thus, a punching failure at A was both predicted and observed. Again, it should be noted that the quantity $V_{TEST}/V_o + M_{TEST}/M_{OFS1}$ equalled 0.97 so that in essence the connection "carried free" the moment $\gamma_{t2} M_B$ transferred by shear in the M_2 direction.

Specimen ELS-1 had a 12-in. square column, a slightly thicker slab than EL-1, flexural reinforcement concentrated in the column head region, and hairpin stirrups at the discontinuous edge. Failure occurred due to punching on a line extending across the width of the slab and column face AB, Fig. D.4. However, that failure occurred only after the moment transfer capacity had started to decrease with reversed cycling and yielding had been observed in the vertical leg of the hairpin stirrup adjacent to face AB. At failure ratios of measured to predicted capacities were:

(1) shear failure at corner A, v_A/v_c, 1.52

(2) shear failure at corner B, v_B/v_U, 0.86

(3) torsion failure at corner C, v_C/v_u, 1.01

(4) flexural failure, M_s/M_{FLEX}, 0.68

(5) flexural component of moment transfer, 0.69

$\gamma_{t1} M_{TEST}/M_{RES}$,

Thus, a punching failure is predicted at A but not at B. Further, because of the location of the single stirrup at B, it is reasonable to expect punching to extend outwards from A over

a wide area. Thus, the observed failure was in essence consistent with the predicted failure, although the hairpin stirrups provided a greater increase in capacity than predicted with the use of ACI Code 318 procedures. Again, it should be noted that the quantity $V_{TEST}/V_o + M_{TEST}/M_{OFS1}$, equals 1.33 so that the transfer of moment in the M_2 direction, in essence, did not decrease the capacity for transfer of moment in the M_1 direction.

Specimen ELS-2 was essentially the same as ELS-1 except for the use of integral beam stirrups extending out from each column face rather than hairpin stirrups. No shear failure occurred for this specimen. There was, however, extensive crushing on the compression face of the slab at column face AD, Fig. D.4. Once crushing initiated, the capacity decreased with cycling, the crushing extended out from the column along the line of the integral beam stirrups, and the stiffness of the connection dropped markedly. At failure, ratios of measured-to-predicted capacities were:

(1) shear failure at corner A, v_A/v_u, 0.62

(2) shear failure at corner B, v_B/v_u, 0.40

(3) torsion failure at corner C, v_C/v_u, 0.46

(4) flexural failure, M_s/M_{FLEX}, 0.74

(5) flexural component of moment transfer, 0.75

$\gamma_{t1} M_{TEST}/M_{RES}$,

The ACI Code procedure does not predict failure in shear. Therefore, it is reasonable to expect that it should have predicted failure in some flexural mode (i.e., as a wide beam (4)

or as a local mechanism at the column, (5)). In this case no flexural failure is predicted, even though large twists and crushing, normally associated with a local flexural failure, occurred for the specimen.

Specimen ELS-3 had a rectangular 19-1/2 x 8 in. column with the longer dimension paralleling the discontinuous edge. Reinforcement was concentrated in the column head region and hairpin stirrups were provided perpendicular to the discontinuous edge. Failure occurred due to punching on a line that extended across the width of the slab and column face, AB, Fig. D.4. At failure ratios of measured-to-predicted capacities were:

(1) shear failure at corner A, v_A/v_c, 1.56

(2) shear failure at corner B, v_B/v_u, 0.89

(3) torsion failure at corner C, v_C/v_u, 1.15

(4) flexural failure, M_s/M_{FLEX}, 0.82

(5) flexural component of moment transfer, $\gamma_{t1} M_{TEST}/M_{RES}$, 0.66

Thus, a punching failure is predicted at A but not at B. Further, because of the location of the single stirrup at B, it is reasonable to expect the punching to extend from A over a wide area. Thus, the observed failure is, in essence, consistent with the predicted failure, although the hairpin stirrups provided a greater increase in capacity than that predicted with the use of ACI Code 318 procedure. Again, it can be noted that the moment in the M_2 direction had, in essence, no effect on the slab's shear capacity.

D.3.3.2 Summary

Measured and predicted capacities are summarized in Table D.5. Measured and predicted failure modes are in reasonable agreement except for specimen ELS-3 where the hairpins considerably increased the capacity but a wide beam shear failure resulted at an average shear stress on the failure line of 1.35 $\sqrt{f'_c}$. The results in row 4 show clearly that for these specimens, the biaxial moment transfer condition can be ignored and design based on the greater moment only. For these specimens, values of M_2/M_1, Fig. D.4, ranged from a high of 0.32 for EL1 to a low of 0.23 for EL2 and ELS2. Corresponding values of $(M_2 - Vg)/M_1$ range from 0.23 to 0.16. Those values suggest that for biaxial moment transfer the effects of the lesser moment can be ignored if the value of $(M_2 - Vg_2)/(M_1 - Vg_1)$ is less than 0.20. For that ratio, g_1 and g_2 are the distances between the centroids of the column and the critical section for shear for the M_1 and M_2 directions, respectively.

D.3.4 Corner Column Connections

D.3.4.1 Detailed Analyses

Properties for the five test specimens modeling the transfer of moments from a slab to a corner column are shown in Table A.1(c). The measured and predicted capacities for those specimens, evaluated according to ACI Code 318 procedures, are summarized in Table D.6. Again ø values are taken as unity for those evaluations. The arrangement for Table D.6 is similar to that for Tables D2 and D4. Lines 2 through 12, list geometric properties for the critical section, which is assumed to have the form shown in Fig. D.3. The quantity d_{AD}, line 2, is the

effective depth for the front column face AD. That face was transverse to the direction of maximum moment transfer in the tests. Line 3 lists the effective depth d_{AB} for the adjacent column face. The quantities C_{AD} and C_{AB}, and g_x and g_y have the significance shown in Fig. D.3. C_{AD} is the distance from the critical section perimeter AB to the centroid of the critical section, and g_y is the distance from that centroid to the column centroid. J_{cx} and J_{cy}, lines 7 and 8, are the polar moments of inertia for the x and y directions, respectively (Fig. D.3). The quantities γ_{tx} and γ_{ty} are the fractions of the moment acting about the centroid of the critical section that are assumed to be transferred from the slab to the column by flexure for the x and y directions, respectively.

The shear force, V_{TEST}, listed on Line 13, is the total shear acting on the slab when the maximum biaxial moments M_x and M_y for the x and y directions, respectively, were transferred to the column. M_x and M_y are the moments in the x and y directions about the column center caused by all loads acting on the slab. For all five test specimens, M_x was the major moment transferred to the column and M_y was the minor. Ratios of M_y to M_x ranged from 0.39 to 0.47. The limiting shear capacity, v_c, according to ACI Code 318-77 or 83 is listed in line 16. That quantity neglects the effects of shear reinforcement. Listed in lines 17, 18, and 19 are the calculated shear stresses at the junction of the three corners of the column and the slab.

On lines 20 and 21 are listed the moments $M_{CR,x}$ and $M_{CR,y}$ which equal the moments acting about the centroid of the critical

section at failure for the x and y directions, respectively. As noted in Table D3, $M_{CR,x}$ equals $(M_x - V_{TEST}\, g_x)$ and $M_{CR,y}$ equals $(M_y - V_{TEST}\, g_y)$. The quantities $M_{o,xf}$ and $M_{o,yf}$ listed on lines 22 and 23 are the moment capacities according to ACI 318-77 or 83 when the shear strength of the concrete limits the capacity of the connection at the front of the critical section, but shear stresses are caused by moment transfer only and there is no simultaneous shear transfer. The sum of the ratios V_{TEST}/V_o, $\frac{M_{CR,X}}{M_{OXF}}$ and $\frac{M_{CR,Y}}{M_{OYF}}$ gives the same value as the ratio v_A/v_c. However, the value of v_D/v_c cannot be calculated similarly since the value of $M_{CR,y}/M_{oyb}$ must be utilized instead of $M_{CR,y}/M_{oyf}$. The quantity M_{oyB} equals M_{oyf} times $C_{AD}/(C_y + d/2 - C_{AD})$ (Fig. D3).

The capacities $M_{RES,x}$ and $M_{RES,y}$ listed on Lines 27 and 28 are the flexural capacities of the reinforcement within lines one and one-half times the slab thickness to one side of the column for the x and y directions, respectively. The direction for which the greater moment had to be transferred to the column was the x direction. Listed on line 29 are ratios of the fraction of that moment to be transferred by flexure to the capacity of the reinforcement $M_{RES,x}$ in that direction. Line 30 lists the corresponding values for the y direction.

Limiting flexural capacities predicted for the five test specimens are listed on lines 32 through 36. The quantity, θ, listed on line 32, is the angle between a line passing through the inner column corner and the x-axis that gives the minimum ratio of the moment, M_s, caused in the test by the applied dead

load, slab weight, and lateral load acting to one side of that line, to the flexural capacity, M_{flex}, across that line as calculated from the known properties of the sections, the concrete and the steel. Values for M_s and M_{flex} are listed on lines 33 and 34, respectively, and ratios of M_s to M_{flex} on line 35. The value of M_{flex}, calculated in that manner overestimates the flexural capacity and leads to unrealistically low values of M_s/M_{flex}. Consider the situation illustrated in Fig. D.5. The line AB represents the theoretical position of the yield line which for simplicity in this discussion is shown as 45 degrees. Bars located outside the column DECF are indicated by broken lines. Although all those bars were provided in the tests with 180-degree hooks on their ends, it is obvious that bars located some distance from the column and crossed by the theoretical yield line may not have been able to develop their yield strengths. Calculations showed that more realistic values for M_{flex} taking into account development length requirements would be those listed on line 36 as $M_{flex,r}$. Ratios of M_s to $M_{flex,r}$ are listed on line 36 and those values are probably the most realistic indicators of the potential for a flexural failure.

D.3.4.2 Summary

Table D.7 summarizes measured-to-predicted failure ratios and failure modes for these corner column specimens. It is apparent that use of the ACI expressions with the strength limited according to conditions at position A yields satisfactory results for predictions of shear strength. For the specimens without shear reinforcement, the ratios of measured-to-computed capacities then average 1.18 with a range from +0.26 to -0.19

about that average. The results for CS1 and CS2, however, show clearly that hairpins, although providing no shear reinforcement at A, can dramatically increase the shear strength. The smallest ratios of M_y/M_x or $M_{CR,y}/M_{CR,x}$ are 0.39 and 0.33, respectively. Those values are considerably larger than the corresponding ratios for the ELS series and add further evidence that the lesser moment effect should be ignored only if $M_{CR,y}/M_{CR,x}$ is less than 0.20. The need to consider biaxial effects for this corner column series is not inconsistent with the results for the ELS series. The flexural failure ratios listed in row 6 are based on $M_{flex,r}$ values (line 35 of Table D.6). In this regard, it will be recognized that the reasons advanced previously for reducing M_{flex} to $M_{flex,r}$ are equally applicable to $M_{RES,x}$ values. Hence, row 7 lists twisting failure ratios as reported on line 30 of Table D.6 while row 8 lists the similar ratio reduced appropriately for bar anchorage limitations. Recognition of that effect changes the twisting failure ratio prediction for CS2 to a value consistent with the observed failure mode.

D.4 Conclusions

From the foregoing comparisons of the measured capacities of the specimens and those predicted by ACI Code 318-77 and 318-83 provisions for moment transfer, interpreted as described in Section D.2, the following conclusions can be drawn:

1) ACI Code procedures will, in general, predict correctly and conservatively (provided ρ within lines 3h/2 either side of the column exceeds 0.8%) the mode of failure. Several limitations, however, need to be observed:

i) the sum of the amounts of top and bottom reinforcement continuous through the column and assumed effective for moment transfer must be limited to ρ_b unless the development length for that reinforcement is less than the column dimensions in the direction of moment transfer (See also conclusion 6).

ii) if the development length for the reinforcement on either side of the potential yield line for a flexural or twisting failure, and in the direction of moment transfer, is less than that for yielding of the bar, then the flexural and twisting (portion of the moment not transferred by shear) capacity must be reduced appropriately. This condition needs to be evaluated carefully for a corner column connection (where the yield line is likely to be on a diagonal passing through the inner corner of the column) and for an edge column transferring moment normal to the edge (where the yield line passes through the front face of the column and especially where the column dimension in the direction of moment transfer is a minimum); and

iii) if the length of the potential yield line is relatively short and the lateral load reverses sufficiently that the slab is cracked through its depth, then the shear stress on that yield line for the slab acting as a wide beam should be limited to $1.4\sqrt{f'_c}$.

2) The variation in the ratio of the measured-to-predicted capacities for the three possible modes of failure recognized by the ACI Code (shear failure, flexural failure,

and twisting failure) is more for a shear failure than for the other two failure modes. The ratio of the measured-to-predicted capacity for a shear failure increases as the reinforcement ratio within lines 3h/2 either side of the column increases. The ratio of the measured-to-predicted capacity for a shear failure will be about 1.00 if the procedures described in these conclusions are utilized and ρ equals 0.8%.

3) For shear failure predictions, it is adequate to consider stress conditions at the front face of the column only (Eq. D.2) and limit that stress to $4\sqrt{f'_c}$. It is not necessary to consider shear stress conditions at the back face of the column (Eq. D.3) unless there is a serviceability concern with the development of large torsional cracks at the discontinuous edge of the slab for an exterior or corner column.

4) Notwithstanding the foregoing conclusion (3), when hairpin stirrups are inserted at the exterior edge to control torsion cracking, the shear capacity is increased.

5) For biaxial moment transfer conditions the effect of the minor moment on shear stresses can be ignored if the ratio $(M_2 - Vg_2)/(M_1 - Vg_1)$ is less than 0.2, where $(M_2 - Vg_2)$ is the moment acting about the centroid of the critical section for shear in the minor moment direction and and $(M_1 - Vg_1)$ is the corresponding moment for the major moment direction.

6) For development of the fraction of the moment not

transferred by shear at a discontinuous edge (i.e., for moment transfer normal to the edge at an exterior column or a corner column), it should be recognized that a portion of that moment is developed in flexure at the front face of the column and the remainder in torsion at the side faces of the column. The amount of reinforcement that can be effective for moment transfer at the front face need be limited only by ρ_b since flexural conditions control at that face. However, at the side faces the amount of reinforcement considered effective for moment transfer must be limited by about $\rho_b/2$ since balanced reinforcement ratios for torsion, rather than flexure, control at those faces.

TABLE D1 INTERIOR COLUMN SPECIMENS

Spec	$c_1 \times c_2$	ρ_t	V_{TEST}	M_{TEST}	V_{TEST}/V_o	M_{TEST}/M_o	(6)+(7)	M_{RES}	$\gamma_t M_{TEST}/M_{RES}$	M_s	M_s/M_{FLEX}	FAILURE MODE
	in.xin.	%	kips	kip-in				kip-in		kip-in		
	(2)	(3)	(4)	(5)	(6)	(7)	(8)	(9)	(10)	(11)	(12)	(13)
S1	12x12	1.20	28.8	1280	0.34	1.08	1.42	778	0.99	977	0.63	S
S2	12x12	1.84	32.0	778	0.45	0.77	1.22	629	0.74	783	0.70	S
S3	12x12	0.55	31.2	475	0.43	0.46	0.89	402	0.71	640	0.71	S
S4	12x12	1.20	33.7	1110	0.42	0.97	1.39	778	0.85	961	0.62	S
S5	12x12	1.50	29.0	1210	0.38	1.13	1.51	949*	0.77	966	0.72	S
S6	12x12	1.81	60.2	644	0.88	0.67	1.55	1033	0.66	1099	0.83	S
S7	12x12	0.84	60.8	376	0.80	0.35	1.15	633	0.21	985	0.88	S
S8	12x12	0.55	52.8	289	0.62	0.24	0.86	416	0.66	836	1.11	F
SS1	12x12	1.20	30.8	1426	0.41	1.37	1.78	778	1.11	1039	0.67	M
SS2	12x12	0.84	29.0	1120	0.39	1.06	1.45	629	1.07	839	0.75	S
SS3	12x12	1.81	29.0	1570	0.40	1.54	1.94	947*	1.00	1080	0.80	M
SS4	12x12	1.81	23.7	1339	0.38	1.27	1.65	947*	0.85	999	0.74	W
SS5	12x12	0.84	28.3	1353	0.34	1.13	1.47	737	1.26	998	0.88	M
SS6	12x12	0.84	59.7	605	0.82	0.59	1.41	628	0.65	1065	0.96	A
SS7	12x12	1.81	60.4	942	0.81	0.91	1.72	1073	0.39	1230	0.91	A
SS8	16x16	2.04	29.3	1995	0.33	1.32	1.65	1251	0.96	1267	1.05	F
SS9	16x16	2.04	60.5	1592	0.66	1.02	1.68	1278	0.75	1430	1.17	F
SS10	19½x8	1.75	61.6	1463	0.81	1.38	2.19	1014	0.74	1314	1.19	F
SS11	19½x8	1.75	27.1	1981	0.31	1.65	1.96	1067	0.95	1186	1.04	F
SS12	8x19½	2.05	29.6	1732	0.36	1.42	1.78	1055*	1.10	1260	1.12	M,F
SS13	8x19½	2.42	60.4	793	0.74	0.61	1.35	843*	0.64	1219	1.17	F

* Limited by $\rho_{top} + \rho_{bottom} \leq \rho_{bal}$ if $c_1 < \ell_{dh}$

Modes of Failure: S = Punching; F = Flexure; M = Local Twisting;
A = Punching Outside Stirrups; W = Wide Beam Shear Failure.

TABLE D2 QUANTITIES FOR ACI 318 MOMENT TRANSFER CALCULATIONS
EDGE COLUMNS WITH MOMENTS TRANSFERRED PARALLEL TO THE EDGE

	Specimen	E-1	E-2	ES-1	ES-2	ES-3	ES-4	E-3	ES-5
					Critical Section Properties				
1.	d_{AB}, in. (mm)	5.44 (138.2)	5.88 (149.4)	5.88 (149.4)	5.88 (149.4)	5.88 (149.4)	5.88 (149.4)	5.88 (149.4)	5.88 (149.4)
2.	c_m, in. (mm)	16.82 (427.4)	21.13 (536.9)	17.13 (435.2)	17.13 (435.2)	17.13 (435.2)	13.13 (333.5)	13.13 (333.5)	24.63 (625.6)
3.	c_t, in. (mm)	14.72 (374.0)	18.94 (481.2)	14.94 (379.6)	14.94 (379.6)	14.94 (379.6)	22.44 (570.0)	22.44 (570.0)	10.94 (570.0)
4.	A_c, $in.^2$ (m^2)	233.4 (0.15)	318.6 (0.21)	254.0 (0.17)	254.0 (0.17)	254.0 (0.17)	307.1 (0.20)	307.1 (0.20)	256.8 (0.17)
5.	c_{AB}, in. (mm)	4.47 (113.6)	5.78 (146.9)	4.51 (114.6)	4.51 (114.6)	4.51 (114.6)	8.40 (213.4)	8.40 (213.4)	2.39 (60.7)
6.	g, in. (mm)	4.25 (108.0)	5.16 (131.1)	4.43 (112.6)	4.43 (112.6)	4.43 (112.6)	4.29 (109.0)	4.29 (109.0)	4.55 (115.6)
7.	J_c, $in.^4$	5,850	13,020	6,579	6,579	6,579	17,420	17,420	3,252
8.	$(1-\gamma_t)$	0.384	0.387	0.384	0.384	0.384	0.466	0.466	0.308
					Shear Strength Properties				
9.	Slab Self Weight kips, (kN)	4.0 (17.8)	4.3 (19.1)	4.3 (19.1)	4.3 (19.1)	4.3 (19.1)	4.5 (20.0)	4.5 (20.0)	4.2 (18.7)
10.	Gravity Shear kips, (kN)	8.8 (39.1)	13.9 (61.8)	14.2 (63.1)	13.9 (61.8)	6.6 (29.3)	14.0 (62.3	14.0 (62.3)	14.0 (62.3)
11.	Lateral Load Shear kips, (kN)	2.65 (11.8)	10.61 (47.1)	5.87 (26.1)	8.94 (39.8)	9.6 (42.7)	14.64 (65.1)	7.54 (33.5)	7.21 (32.1)
12.	Shear Stress Due to Shear, psi, (mN/m^2)	66.1 (0.45)	90.5 (0.62)	96.0 (0.66)	106.7 (0.73)	80.5 (0.55)	107.9 (0.74)	84.8 (0.58)	99.0 (0.58)
13.	Shear Stress at Front,	221.5	293.7	331.8	394.7	330.7	441.7	310.8	320.6

TABLE D2 (Continued)

14. Shear Stress at Back, v_{CD}, psi, (mN/m^2)	290.1 (1.99)	372.2 (2.55)	449.3 (3.08)	559.3 (3.84)	498.1 (3.42)	449.9 (3.10)	292.9 (2.02)	693.5 (4.78)
15. v_c, psi, (mN/m^2)	228.7 (1.57)	262.0 (1.80)	255.5 (1.75)	259.0 (1.78)	261.4 (1.79)	217.6 (1.50)	208.5 (1.44)	224.2 (1.55)
16. M_R γ_t kip-in. (N-m)	326.2 (3,635.0)	725.3 (8,194.0)	551.8 (6,232.0)	674.0 (7,615.0)	585.6 (6,616.0)	793.5 (8,965.0)	536.6 (6,062.0)	677.5 (7,654.0)
17. M_{RES}, kip-in. (N-m)	413.1 (4,667.0)	729.7 (8,244.0)	841.3 (9.505.0)	845.4 (9,551.0)	846.2 (9,560.0)	651.5 (7,360.6)	643.9 (7,274.7)	1,023.0 (11,557.9)
18. v_{STIRB}, psi, (mN/m^2)	0	0	359.8 (2.47)	527.0 (3.61)	363.0 (2.49)	615.5 (4.24)	-	363.0 (2.49)
19. v_{STIRF}, psi, (mN/m^2)	0	0	0	527.0 (3.61)	0	615.6 (4.24)	-	0
20. V_{TEST}, kips (kN)	15.43 (68.6)	28.83 (128.2)	24.38 (108.4)	27.10 (120.5)	20.45 (91.0)	33.14 (147.4)	26.04 (115.8)	25.40 (113.0)
21. M_{TEST}, kip-in. (Nm)	598.5 (6,762.0)	1,332.0 (15,049.0)	1,003.7 (11,340.0)	1,214.0 (13,719.0)	1,041.0 (11,763.0)	1,628.0 (18,400.0)	1,116.0 (12,600.0)	1,095.0 (12,400.0)
22. M_{FLEX}, kip-in. (Nm)	1,224.0 (13,832.0)	1,461.0 (16,508.0)	1,582.0 (17,875.0)	1,596.0 (17,919.0)	1,588.0 (17,941.0)	1,506.0 (17,000.0)	1,464.0 (16,500.0)	1,486.0 (16,800.0)
23. M_S/M_{FLEX}	0.41	0.75	0.54	0.66	0.58	0.87	0.59	0.67
24. V_{TEST}/V_o	0.29	0.35	0.38	0.41	0.31	0.50	0.41	0.44
25. M_R, kip-in. (Nm)	529.5 (6,004.0)	1,183.0 (13,416.0)	896.0 (10,156.0)	1,094.0 (12,406.0)	950.6 (10,780.0)	1,486.0 (16,800.0)	1,005.0 (11,400.0)	979.0 (11,100.0)
26. $(1-\gamma_t)$ $M_R/(1-\gamma_t)$ M_{OFS}	0.70	0.78	0.92	1.11	0.96	1.53	1.08	0.99
27. $(1-\gamma_t)$ $M_R/(1-\gamma_t)$ M_{OBS}	1.56	1.77	2.13	2.57	2.21	2.56	1.81	3.53
28. γ_t M_R/M_{RES}	0.79	0.99	0.66	0.80	0.69	1.22	0.83	0.66

TABLE D.3 COMPARISON OF MEASURED AND COMPUTED ACI 318 CAPACITIES EDGE COLUMNS WITH MOMENTS TRANSFERRED NORMAL TO THE EDGE

Measured Capacity/Predicted Capacity

Spec.	ρ %	Shear at Front	Failures at Edge	Flexural Failure	Twisting	Observed Mode*	Comments
E 1	0.76	0.99	1.27	0.41	0.79	SF	
E 2	1.06	1.13	1.42	0.75	0.99	SF	
ES 1	1.36	1.30	1.24	0.54	0.66	SF	Hairpins
ES 2	1.36	0.78	1.04	0.66	0.80	ED	Integral Beams
ES 3	1.36	1.27	1.37	0.58	0.80	SF	Hairpins
E 3	1.00	1.49	1.40	0.59	0.83	SF	
ES 4	1.00	0.72	0.73	0.87	1.22	M	Integral Beams
ES 5	1.00	1.43	1.91	0.67	0.66	ED	Hairpins

* Modes of Failure: SF = Punching at Front Column Face.

ED = Excessive Deflections.

M = Local Twisting.

TABLE D.4 EDGE COLUMN SPECIMENS WITH MOMENTS TRANSFERRED PARALLEL TO THE EDGE

	Specimen	Shear Strength Properties				
		EL-1	EL-2	ELS-1	ELS-2	ELS-3
1.	d_{AB}, in. (mm)	5.44 (138.2)	5.88 (149.4)	5.88 (149.4)	5.88 (149.4)	5.88 (149.4)
2.	c_m, in. (mm)	14.41 (366.0)	18.57 (471.7)	14.57 (370.1)	14.57 (370.1)	10.57 (268.49)
3.	c_t, in. (mm)	17.44 (443.0)	21.88 (555.8)	17.88 (454.2)	17.88 (454.2)	25.38 (644.7)
4.	A_c, $in.^2$ (m^2)	240.67 (0.16)	330.63 (0.21)	263.07 (0.17)	263.07 (0.17)	254.50 (0.16)
5.	c_{AD}, in. (mm)	4.69 (119.1)	6.13 (155.7)	4.74 (120.4)	4.74 (120.4)	2.55 (64.8)
6.	g, in. (mm)	3.72 (94.5)	4.44 (112.8)	3.83 (97.3)	3.83 (97.3)	3.99 (101.3)
7.	J_{c1} $in.^4$ J_{c2} $in.^4$	14,209 7,114	30,861 15,428	16,339 8,099	16,339 8,099	27,292 4,361
8.	$(1-\gamma_{t1})$ $(1-\gamma_{t2})$	0.423 0.377	0.420 0.380	0.425 0.375	0.425 0.375	0.508 0.301
9.	Slab Self Weight kips (kN)	4.23 (18.8)	4.74 (21.1)	4.55 (20.2)	4.55 (20.2)	4.36 (19.4)
10.	Gravity Shear kips (kN)	12.02 (53.5)	13.14 (58.5)	13.98 (62.2)	12.92 (57.5)	14.06 (62.6)
11.	Lateral Load Shear, kips (kN)	4.76 (21.2)	7.73 (34.4)	6.42 (28.6)	7.56 (33.6)	7.88 (35.1)
12.	Shear Stress Due to Shear, psi (mN/m^2)	70.43 (0.48)	56.20 (0.38)	73.10 (0.50)	42.61 (0.29)	75.13 (0.51)
13.	Shear Stress at Inside Corner of Column, v_A, psi	318.14 (2.17)	257.07 (1.75)	349.30 (2.38)	374.58 (2.55)	387.43 (2.64)
14.	Shear Stress at Outside Edge, v_B, psi (mN/m^2)	178.62 (1.22)	171.54 (1.17)	211.70 (1.44)	243.65 (1.66)	238.25 (1.62)

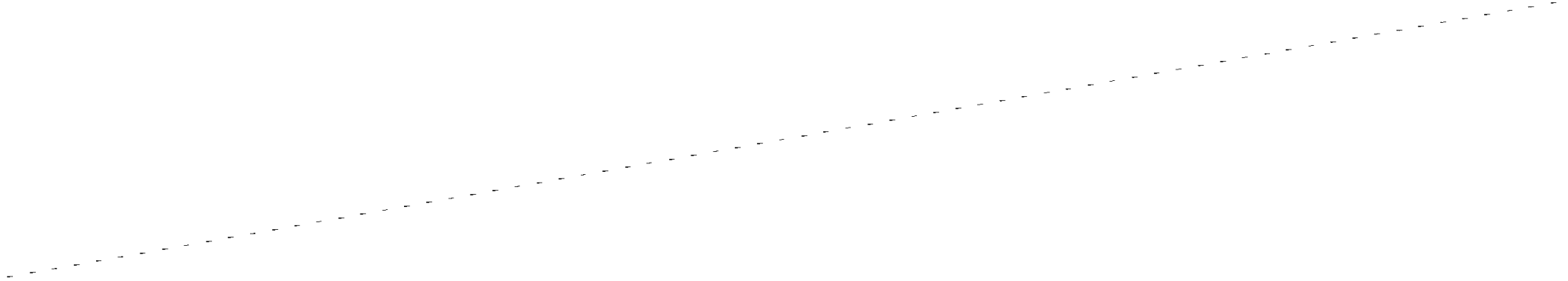

TABLE D.4 (Continued)

15.	Shear Stress at Outside Edge, v_c,	-225.7 (1.54)	-171.5 (1.17)	-249.4 (1.70)	-281.8 (1.92)	-308.1 (2.09)
16.	v_c, psi (mN/m^2)	271.91 (1.85)	237.32 (1.62)	228.81 (1.56)	242.92 (1.65)	248.50 (1.69)
17.	v_U, psi (mN/m^2)	-	-	245.8 (1.68)	607.3 (4.13)	267.8 (1.82)
18.	γ_{t1}, M_{TEST} kip-in. (Nm)	449.7 (5,080.0)	672.5 (7,598.0)	672.1 (6,464.0)	650.1 (7,345.0)	575.3 (6,500.0)
19.	M_{RES}, kip-in. (Nm)	518.4 (5,857.0)	680.8 (7,692.0)	851.8 (9,624.0)	866.3 (9,787.0)	870.5 (9,834.0)
20.	V_{TEST}, kips (kN)	16.95 (75.4)	18.58 (82.6)	19.23 (85.5)	18.17 (80.8)	19.12 (85.0)
21.	M_{TEST}, kip-in. (Nm)	779.3 (8,829.0)	1,159.3 (13,136.0)	995.0 (11,273.0)	1,130.6 (12,809.0)	1,169.4 (13,248.0)
22.	M_2, kip-in. (Nm)	245.8 (2,776.0)	269.5 (3,053.0)	277.0 (3,138.0)	263.2 (2,982.0)	279.0 (3,161.0)
23.	M_{FLEX}, kip-in. (Nm)	737.5 (8,355.0)	952.0 (10,785.0)	943.4 (10,688.0)	957.3 (10,846.0)	898.4 (10,178.0)
24.	M_S/M_{FLEX}	0.72	0.74	0.68	0.74	0.82
25.	V_{TEST}/V_o	0.26	0.24	0.32	0.28	0.30
26.	M_{TEST}/M_{OFS1}	0.74	0.73	1.01	1.08	1.11
27.	$(M_2-Vg)/M_{OFS2}$	0.17	0.12	0.19	0.17	0.14
28.	$(M_2-Vg)/M_{OBS2}$	0.35	0.24	0.40	0.36	0.45
29.	$\gamma_{t1}\ M_{TEST}/M_{RES}$	0.87	0.99	0.69	0.75	0.66

TABLE D5 COMPARISON OF MEASURED AND COMPUTED ACI 318 CAPACITIES - EDGE COLUMNS WITH MOMENTS TRANSFERRED PARALLEL TO EDGE

		EL-1	EL-2	ELS-1	ELS-2	ELS-3
Shear Failures	At Position A	1.17	1.09	1.52	1.55	1.56
	At Position C	0.83	0.72	1.09	1.15	1.24
	For Length AB	1.00	0.97	1.43	1.36	1.41
Flexural Failure		0.72	0.74	0.68	0.74	0.82
Twisting Failure		0.87	0.99	0.69	0.75	0.66
Observed Mode *		SF	SF	SF	ED	W
Shear Reinforcement				Hairpins	Integral Beams	Hairpins

Modes of Failure: SF = Punching at Front Column Face.

ED = Excessive Deflections.

W = Wide Beam Shear Failure.

TABLE D6 CORNER COLUMN CONNECTIONS - QUANTITIES FOR ACI CODE 318 MOMENT TRANSFER CALCULATIONS

Line		Specimen	C-1	C-2	C-3	CS-1	CS-2
1			Critical Section Properties				
2	d_{AD}	in. (mm)	5.44 (138.0)	5.44 (138.0)	5.875 (149.2)	5.875 (149.2)	5.875 (149.2)
3	d_{AB}	in. (mm)	4.81 (122.2)	4.81 (122.2)	5.125 (130.2)	5.125 (130.2)	5.125 (130.2)
4	A_c	in. (mm)	149.20 (0.10)	149.20 (0.10)	206.11 (0.13)	162.11 (0.11)	177.05 (0.12)
5	c_{AD}	in. (mm)	3.79 (96.2)	3.79 (96.2)	4.91 (124.7)	3.84 (97.5)	1.85 (50.0)
6	c_{AB}	in. (mm)	3.49 (88.6)	3.49 (88.6)	4.46 (113.3)	3.53 (89.7)	7.29 (185.2)
7	J_{cx}	$in.^4$	3,430.18	3,430.18	7,719.55	3.846.28	10,150.96
8	J_{cy}	$in.^4$	3,481.02	3,481.02	7,866.19	3,898.45	1,878.47
9	g_x	in. (mm)	5.23 (132.8)	5.23 (132.8)	6.48 (164.6)	5.41 (137.4)	5.40 (137.2)
10	g_y	in. (mm)	4.62 (117.3)	4.62 (117.3)	5.65 (143.5)	4.72 (120.0)	4.71 (120.0)
11	γ_{tx}		0.60	0.60	0.598	0.597	0.507
12	γ_{ty}		0.60	0.60	0.602	0.603	0.656
			Shear Stress Properties				
13	V_{TEST}	kips (Kn)	10.83 (48.17)	9.79 (43.54)	24.56 (109.2)	13.92 (61.92)	17.67 (78.70)
14	M_x	k-in. (Kn-m)	452.30 (51.10)	384.84 (43.50)	950.04 (107.33)	689.18 (77.84)	955.83 (108.0)
15	M_y	k-in. (Kn-m)	202.62 (22.90)	179.31 (20.22)	427.36 (48.24)	281.15 (31.75)	369.04 (41.70)
16	v_c	psi (10^{-3}MPa)	303.2 (2,091.0)	234.2 (1,615.0)	256.1 (1,766.0)	244.1 (1,683.0)	231.9 (1,599.0)

TABLE D6 (Continued)

Line			C-1	C-2	C-3	CS-1	CS-2
17	Shear Stress at x Direction Edge v_D, psi		58.7	37.7	103.5	77.6	7.2
18	Shear Stress at Inside Corner v_A, psi		299.3	260.0	374.4	397.3	492.8
19	Shear Stress at y Direction Edge v_B, psi		-376.3	-312.9	-405.4	-563.9	-445.0
20	$M_{CR,x}$	k-in. (Kn-m)	395.66 (44.70)	333.64 (37.62)	790.89 (89.25)	613.87 (69.26)	860.41 (97.21)
21	$M_{CR,x}$	k-in. (Kn-m)	152.58 (17.17)	134.08 (15.14)	288.60 (32.54)	215.45 (24.30)	285.81 (32.29)
22	$M_{0,xF}$	k-in. (Kn-m)	745.29 (84.17)	575.62 (65.07)	1,102.76 (124.50)	990.10 (111.85)	1,079.8 (122.0)
23	$M_{0,yF}$	k-in.	696.47 (78.63)	537.92 (60.70)	1,030.98 (116.37)	936.46 (105.75)	1,236.3 (139.63)
24	V_{TEST}/V_o		0.240	0.278	0.465	0.353	0.406
25	$\frac{M_{CR,x}}{M_{0xF}}$		0.531	0.580	0.717	0.984	1.315
26	$\frac{M_{CR,y}}{M_{0yF}}$		0.219	0.249	0.280	0.345	0.381
27	$M_{RES,x}$	k-in. (Kn-m)	320.79 (36.26)	308.15 (34.80)	599.01 (67.67)	585.84 (66.20)	512.43 (57.84)
28	$M_{RES,y}$	k-in. (Kn-m)	281.50 (31.75)	268.85 (30.28)	513.34 (57.96)	498.72 (56.34)	640.29 (72.31)
29	$\frac{\gamma_{t1} M_{CR,x}}{M_{RES,x}}$		0.74	0.65	0.79	0.63	0.85
30	$\frac{\gamma_{t2} M_{CR,y}}{M_{RES,y}}$		0.33	0.30	0.34	0.26	0.31
31	$\sqrt{(\text{line } 29)^2+(\text{line } 30)^2}$		0.81	0.72	0.86	0.68	0.90

TABLE D6 (Continued)

			C-1	C-2	C-3	CS-1	CS-2
32		degree	46	50	48	50	43
33	M_s	k-in. (Kn-m)	355.94 (40.21)	307.04 (34.70)	696.67 (78.71)	568.23 (64.20)	516.78 (58.40)
34	M_{flex}	k-in. (Kn-m)	456.75 (51.60)	465.94 (52.64)	990.63 (111.92)	840.69 (95.00)	880.12 (99.44)
35	$\frac{M_s}{M_{flex}}$		0.78	0.66	0.70	0.68	0.59
36	$\frac{M_s}{M_{flex,r}}$		0.78	0.66	0.88	0.85	0.84

$M_{flex,r}$ = Value of M_{flex} reduced by effects of inadequate bar end anchorage (see text).

TABLE D7 COMPARISON OF MEASURED AND PREDICTED ACI 318 CAPACITIES - CORNER COLUMN SUBASSEMBLAGES

		C1	C2	C3	CS1	CS2
Shear Failures v_{TEST}/v_C	At Position A	0.99	1.11	1.46	1.63	2.13
	At Position B	1.24	1.34	1.58	2.31	1.92
M_Y/M_X		0.45	0.47	0.45	0.41	0.39
$M_{CR,Y}/M_{CR,Y}$		0.39	0.40	0.36	0.35	0.33
Flexural Failure		0.78	0.66	0.88	0.85	0.98
Twisting Failure 1		0.74	0.65	0.79	0.63	0.85
Twisting Failure 2		0.74	0.65	0.99	0.79	1.21
Observed Failure Mode		SFC	SFC	SFC	ED	M
Shear Reinforcement		-	-	-	Hairpins	Hairpins

Modes of Failure: SF = Punching at Corner A.

ED = Excessive Deflections.

M = Local Twisting.

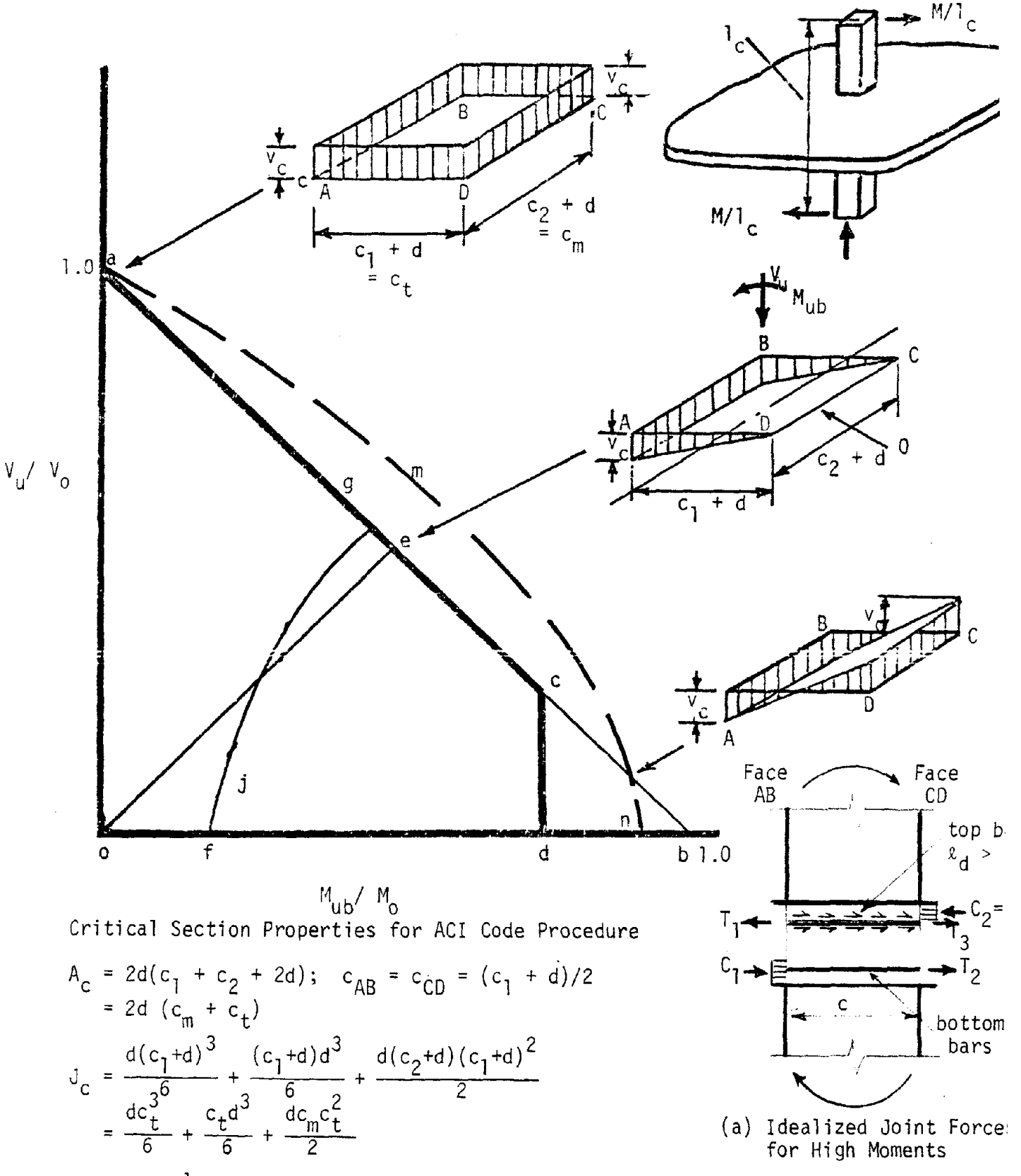

Critical Section Properties for ACI Code Procedure

(a) Idealized Joint Force for High Moments

$$A_c = 2d(c_1 + c_2 + 2d); \quad c_{AB} = c_{CD} = (c_1 + d)/2$$
$$= 2d\,(c_m + c_t)$$

$$J_c = \frac{d(c_1+d)^3}{6} + \frac{(c_1+d)d^3}{6} + \frac{d(c_2+d)(c_1+d)^2}{2}$$
$$= \frac{dc_t^3}{6} + \frac{c_t d^3}{6} + \frac{dc_m c_t^2}{2}$$

$$\gamma_t = \frac{1}{1+2/3\sqrt{c_t/c_m}}$$

FIG. D.1 MOMENT-SHEAR INTERACTION RELATIONSHIPS FOR INTERIOR COLUMN CONNECTION

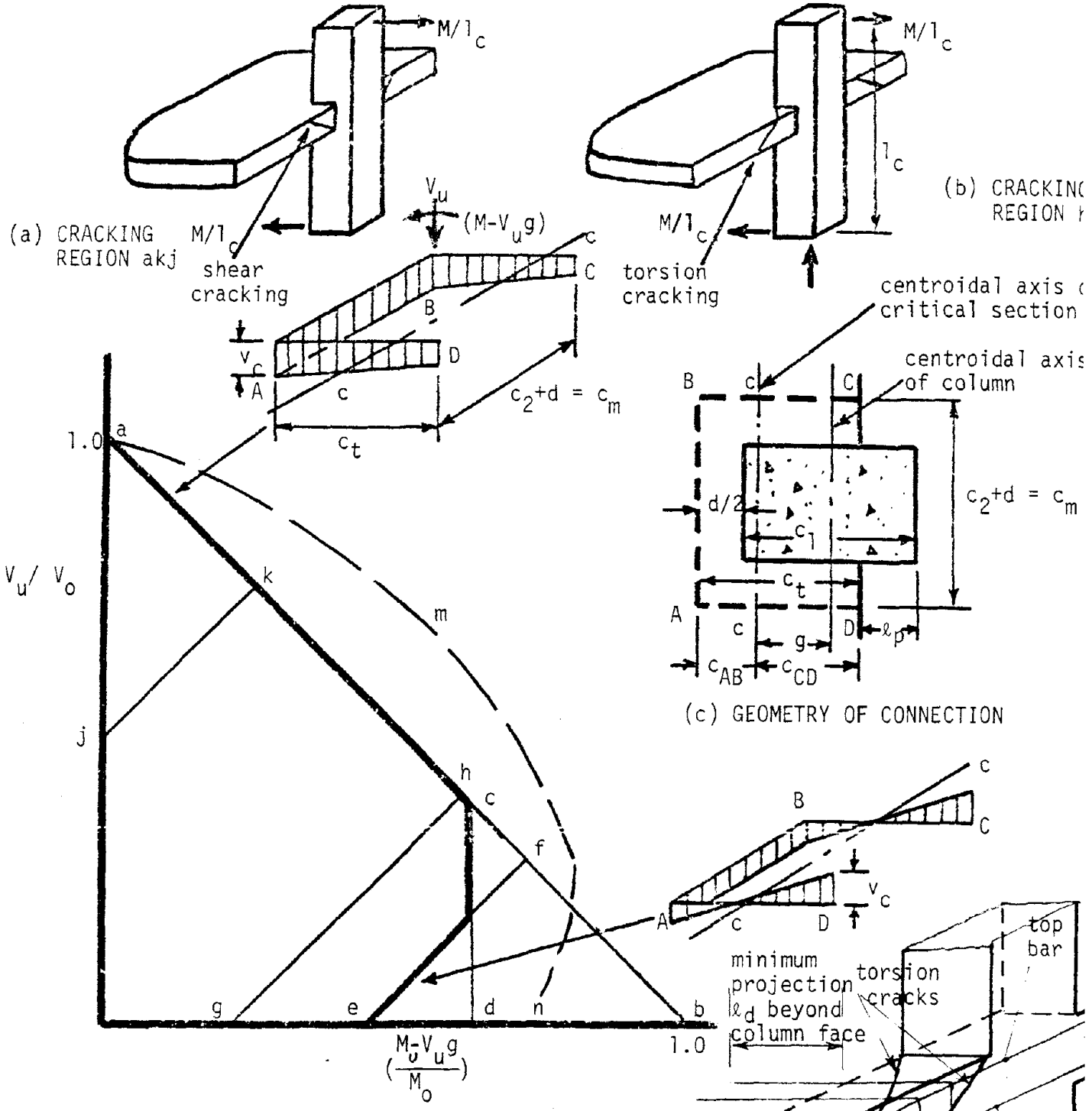

Critical Section Properties for ACI Code Procedure

$$A_c = d(c_2 + d + 2c_t);\quad c_{AB} = \frac{c_t^2 d}{A_c};\quad c_{CD} = c_t - c_{AB};$$

$$J_c = \frac{dc_t^3}{6} + \frac{c_t d^3}{6} + (c_2 + d)\, d\, c_{AB}^2 + 2c_t d\left(\frac{c_t}{2} - c_{AB}\right)^2$$

$$\gamma_t = 1/(1 + 2/3\sqrt{c_t/(c_2 + d)}) = 1/(1 + 2/3\sqrt{c_t/c_m})$$

FIG. D.2 MOMENT-SHEAR INTERACTION RELATIONSHIPS FOR PROTRUDING EDGE COLUMN CONNECTION

Shear Stresses

$$= \frac{V_u}{A_c} + \frac{(1-\gamma_{bx})(M_x - V_u g_x)c_{AB}}{J_{cx}} + \frac{(1-\gamma_{by})(M_y - V_u g_y)c_{CD}}{J_{cy}} \leq \phi v_c \quad \text{(Ca)}$$

$$= + \frac{V_u}{A_c} + \frac{(1-\gamma_{bx})(M_x - V_u g_x)c_{AB}}{J_{cx}} - \frac{(1-\gamma_{by})(M_y - V_u g_y)(c_y + d/2 - c_{CD})}{J_{cy}} \geq -\phi v_c \quad \text{(Cb)}$$

$$= + \frac{V_u}{A_c} - \frac{(1-\gamma_{bx})(M_x - V_u g_x)c_x + d/2 - c_{AB})}{J_{cx}} + \frac{(1-\gamma_{by})(M_y - V_u g_y)d_{CD}}{J_{cy}} \geq -\phi v_c \quad \text{(Cc)}$$

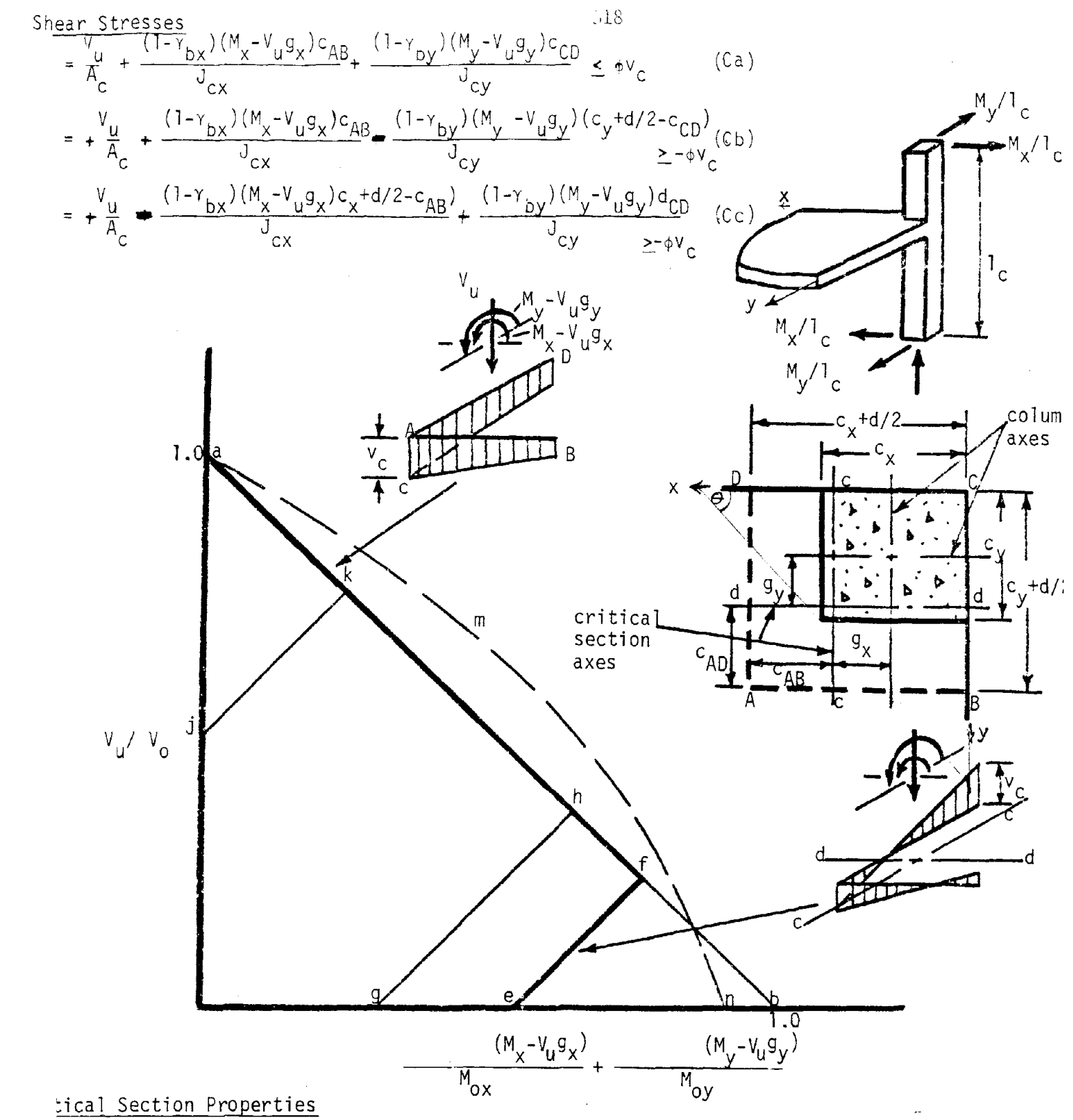

Critical Section Properties

$\gamma_{tx} = 1/(1+(2/3)\sqrt{(c_x+d/2)/(c_y+d/2)})$; $\gamma_{ty} = 1/(1+(2/3)\sqrt{(c_y+d/2)/(c_x+d/2)})$ $A_c = (c_x + c_y + d)d$

$$= \frac{(c_x+d/2)^2 d}{2A_c} \quad ; \quad c_{AD} = \frac{(c_y+d/2)^2 d}{2A_c}; \quad J_{cx} = \left[\frac{d(c_x+d/2)^3}{12} + \frac{(c_x+d/2)d^3}{12} + (c_y+d/2)dc_{AB}^2 - \right.$$

$$= \left[\frac{d(c_y+d/2)^3}{12} + \frac{(c_y+d/2)d^3}{12} + (c_x+d/2)dc_{AD}^2 + (c_y+d/2)d\left(\frac{c_y+d/2}{2} - c_{AD}\right)^2\right] \quad \left. + (c_x+d/2)d\left(\frac{c_x+d/2}{2} - c_{AB}\right)^2\right]$$

3. D.3 MOMENT-SHEAR INTERACTION RELATIONSHIPS FOR CORNER COLUMN CONNECTION

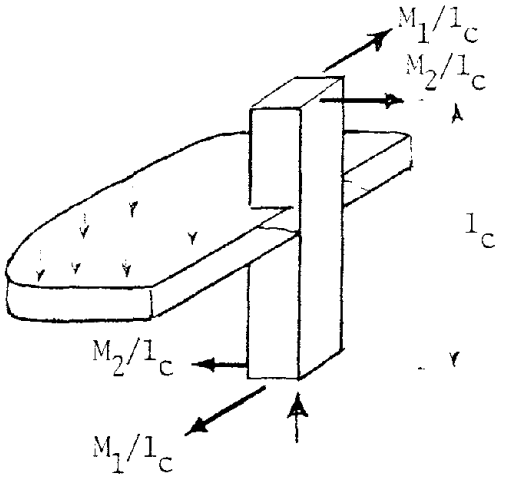

(a) Moments and Shears Acting on Column

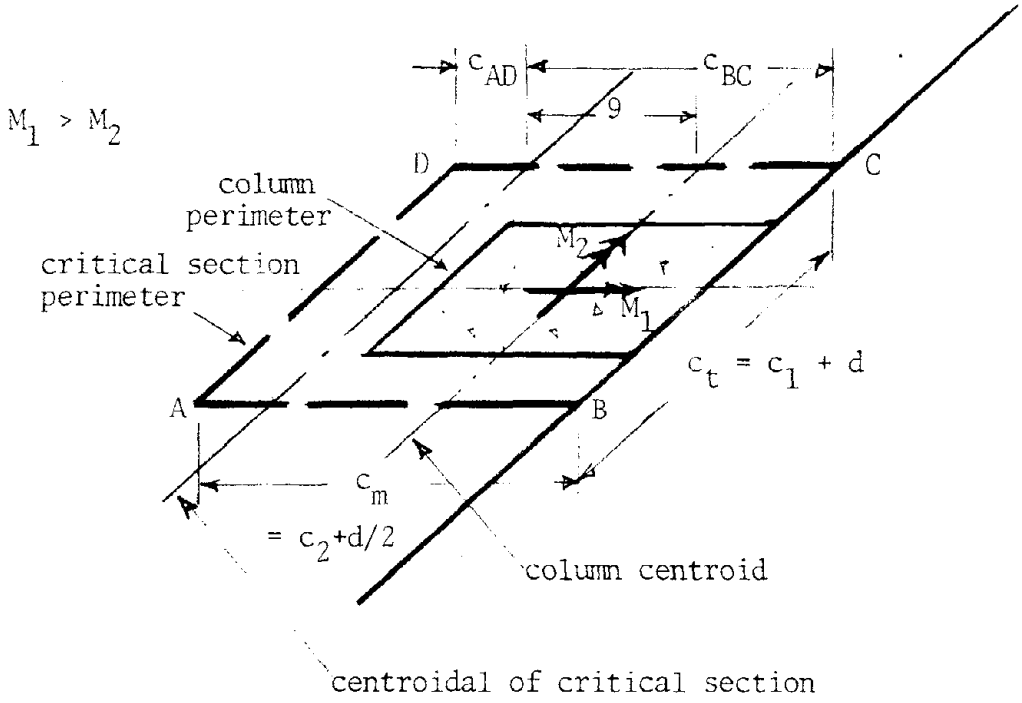

(b) Critical Section Geometry

FIG. D.4 EXTERIOR COLUMN CONNECTION TRANSFERRING MAJOR MOMENT PARALLEL TO EDGE

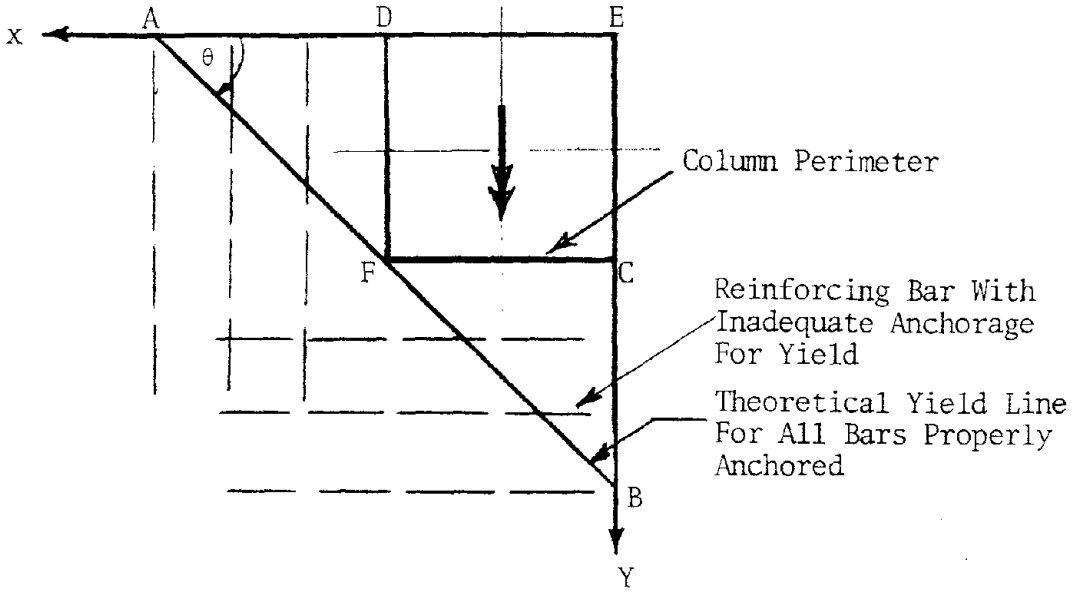

FIG. D.5 PRACTICAL LIMITATIONS OF BAR ANCHORAGE ON YIELD CAPACITY